Beyond the Standard Model Phenomenology at Next-to-Leading Order at the LHC

FRIDMAN-ROJAS, ILAN

Beyond the Standard Model Phenomenology at Next-to-Leading Order at the LHC

by

Ilán Fridman Rojas

Submitted in conformity with the requirements
for the degree of Doctor of Philosophy
Institute for Particle Physics Phenomenology (IPPP)
University of Durham

Abstract

Beyond the Standard Model Phenomenology at Next-to-Leading Order at the LHC

Ilán Fridman Rojas

The methods by which modern event generators incorporate matrix elements accurate to next-to-leading order in the strong coupling for inclusive observables, as well as how such amplitudes are combined with the parton shower algorithms are overviewed and a novel implementation of both to Beyond-the-Standard-Model constructions for processes with non-coloured final states is presented.

This implementation is applied to Z' models inspired on E_6 grand unified theories as well as to supersymmetric scenarios involving pair production of the supersymmetric partners to the Standard Model leptons and gauge bosons/Higgs. Total cross sections are verified to be in agreement with results from pre-existing software packages and observables inclusive in jets are presented at novel NLO accuracy with local increases in cross section properly accounted for and scale variation reduced.

The modest increases in cross section and reduction in theoretical uncertainty make the use of the present implementation for searches at the Large Hadron Collider highly desirable.

Dedication

To Boris, Paula, Joel, Natán, and Ieva Kaminskaitė.

For all the love and support you have unconditionally given me, through the good times and the bad.

In loving memory of Porfirio Díaz Rojas.

Acknowledgements

Many people have supported me in completing this work and deserve my gratitude. First and foremost I am grateful to Peter Richardson for his constant support, encouragement and guidance without which this project would not have been possible.

For their encouragement and helpful discussions I am indebted to Frank Krauss, Marek Schönherr, Andrew Papanastasiou, James Currie and Chris Wallace, as well as David Grellscheid for much computing and technical assistance. And for their unwavering support I thank Mike Seymour, Adrian Signer and Keith Hamilton.

I am particularly indebted to Frank Krauss for his encouragement and support throughout my PhD, and to Keith Hamilton and Marek Schönherr for reading parts of the manuscript.

For their constant moral support through the ups and downs there are more people than I can reasonably name here, but I thank Christian Schneider, Jean Fernand Castañon Darsky, Mauricio Castañeda Martínez, Walter Carrillo Herrera, Luis David Fernández del Campo, David Romero Álvarez and Gurdeep Sehmbi for helping me shoulder the burden and ride out the difficult parts.

But above all I thank my family, Boris, Paula, Natán, Joel, and my dearest Ieva, without whose love and unconditional support I could not have done without. To them I owe this.

Declaration

The material contained within this thesis has not previously been submitted for a degree at the University of Durham or any other university. The research reported within this thesis has been conducted by the author unless indicated otherwise.

Copyright Notice

Contents

1 Introduction **18**

2 The Standard Model and Beyond **20**
2.1 The Standard Model . . . 20
2.1.1 The QCD Sector . . . 24
Collinear Factorisation . . . 26
Factorisation Theorem . . . 26
2.1.2 The Electroweak Sector of the Standard Model . . . 27
Electroweak Symmetry Breaking . . . 28
The Discovery of the Higgs . . . 30
The Hierarchy Problem . . . 32
2.1.3 The Neutral Current in the Standard Model . . . 32
2.1.4 Current Status of the SM . . . 33
2.2 $U(1)'$ Extensions of the Electroweak Sector . . . 36
2.2.1 Grand Unified Theories . . . 36
The Minimal GUT: The Georgi-Glashow $SU(5)$ Model . . . 37
Anomaly Cancellation . . . 40
Symmetry Breaking and the Extended Gauge Sector . . . 40
Extended GUTs: $SO(10)$ and E_6 . . . 42
Anomalies . . . 45
Exotics . . . 47
Mass Generation for the Z' . . . 48
2.2.2 E_6 and Effective Rank 5 Models . . . 48
Kinetic Mixing . . . 50
Mass Mixing . . . 51
Z' Width . . . 52
γ-Z-Z' Interference . . . 53
Current Z' Limits . . . 53
Theory Assumptions . . . 54
2.3 Supersymmetry . . . 56
2.3.1 Motivation . . . 56
The Super-Poincarè Group . . . 57
Dark Matter Candidate . . . 59
Gauge Coupling Unification . . . 60
Radiative Electroweak Symmetry Breaking . . . 60
Solution to the Hierarchy Problem . . . 61
2.3.2 Ingredients for the Construction of SUSY-invariant Lagrangians . . . 65
Superfields . . . 65
Grassmann Calculus . . . 67
Chiral Superfields . . . 68

Vector Superfields . . . 69
Supersymmetric Field Strength . . . 69
Abelian Supersymmetric Field Strength . . . 69
Non-Abelian Supersymmetric Field Strength . . . 70
The Superpotential . . . 71
2.3.3 The Supersymmetric Standard Model (SSM) . . . 72
The Supersymmetric Quantum Electrodynamics Lagrangian . . . 73
The Supersymmetric Quantum Chromodynamics Lagrangian . . . 73
The Supersymmetric Standard Model Field Content . . . 73
The Supersymmetric Standard Model Superpotential . . . 75
R-Parity . . . 75
2.3.4 Soft SUSY-breaking . . . 76
2.3.5 The MSSM . . . 78
Minimal models: The CMSSM . . . 79
Current Experimental Constraints on the CMSSM . . . 80
The pMSSM . . . 81
Simplified Models . . . 83
2.3.6 Sleptons: Mixing and Mass Eigenstates . . . 84
2.3.7 Gauginos: Gaugino-Higgsino Mixing and the Chargino(Neutralino) Mass Eigenstates . . . 86
Chargino Masses . . . 86
Neutralino Masses . . . 88
2.3.8 Naturalness . . . 89
2.3.9 Status of Current SUSY Searches . . . 90

3 The Anatomy of Next-to-Leading Order Calculations 93
3.1 Drell-Yan Production . . . 94
3.2 The Born Contribution . . . 96
3.3 Next-to-leading Order Contributions . . . 98
3.3.1 Real Emission . . . 99
3.3.2 Virtual Contribution . . . 106
Quark Self-energy Corrections . . . 107
Vertex Correction . . . 109
3.3.3 Mass Factorisation . . . 109
3.3.4 The Full NLO Cross Section . . . 113
3.3.5 The Running Strong Coupling . . . 114
3.4 Notation . . . 115
3.5 Numerical Calculation of NLO Amplitudes . . . 116
3.5.1 Plus-Prescription Subtraction . . . 117
3.5.2 Subtraction Methods . . . 118
3.5.3 The Implementation of Dipole Subtraction . . . 121
The Dipoles . . . 122
The Insertion Operator . . . 124
The Collinear Remnants . . . 125

4 Parton Showers and Resummation 131
4.1 Logarithms from Fixed Order Calculations . . . 132
4.1.1 Proof of DGLAP Resummation . . . 133
4.2 Origin, Argument and Size of Logarithmic Contributions . . . 135
4.3 The Logarithms of Perturbative QCD . . . 136
4.4 Single Emission . . . 137
4.5 Coherence and Angular Ordering . . . 138
4.5.1 Choice of Ordering Variable and Type of Logarithm Resummed . . . 141

4.6 Multiple Emissions . . . 143
4.7 Motivation and Properties of the Sudakov Form Factor . . . 146
4.8 The Parton Shower . . . 147
4.9 The Logarithmic Accuracy of the Parton Shower . . . 148

5 Matching Next-to-Leading Order Calculations with Parton Showers 150
5.1 Generalities of Resummation and Matching . . . 151
5.2 Leading Order + Leading Logarithmic Matching . . . 154
5.2.1 Shower Unitarity . . . 156
5.3 Next-to-Leading-Order + Leading Logarithmic Matching . . . 157
5.3.1 The MC@NLO Method . . . 158
5.3.2 The POWHEG Method . . . 160
Shower Reorganisation . . . 161
Generation of the Hardest Emission . . . 164

6 POWHEG Implementations 168
6.1 Z' POWHEG Implementation . . . 168
6.1.1 Generation of the $\overline{B}$ Function . . . 169
6.1.2 Generation of the Hardest Emission . . . 172
6.2 Slepton Pair Production POWHEG Implementation . . . 173
6.2.1 Next-to-Leading Order Supersymmetric Quantum Chromodynamics Corrections . . . 174
6.2.2 POWHEG Implementation . . . 175
Generation of the $\overline{B}$ Function . . . 175
Generation of the Hardest Emission . . . 178
6.3 Gaugino Pair Production POWHEG Implementation . . . 182
6.3.1 Next-to-Leading Order Supersymmetric Quantum Chromodynamics Corrections . . . 182
6.3.2 The Treatment of Resonant Diagrams . . . 184
6.3.3 The Introduction of Width . . . 186
Gauge Invariance . . . 186
6.3.4 Treatment of On-shell Contributions . . . 189
The On-shell Subtraction Terms . . . 191
Construction of the On-shell Subtraction Terms . . . 191
The On-shell Kinematic Projection . . . 193
6.3.5 POWHEG Implementation . . . 194
Generation of the On-shell Subtraction Term . . . 194

7 Results 197
7.1 NLO Z' Results . . . 197
7.1.1 NLO-accurate Differential Distributions . . . 197
7.1.2 Discussion . . . 204
7.2 NLO Slepton Pair Production Results . . . 205
7.2.1 Validation of NLO Slepton Pair Total Cross Sections . . . 205
7.2.2 NLO-accurate Differential Distributions . . . 206
7.2.3 Suppression Scale Dependence of Observables . . . 208
7.2.4 Discussion . . . 212
7.3 NLO Gaugino Pair Production Results . . . 214
7.3.1 Validation of NLO Gaugino Pair Total Cross Sections . . . 214
Validation Using SPS1a . . . 214
Validation Using the Parameter Point $m_0 = 500\ \mathrm{GeV}$, $m_{1/2} = 200\ \mathrm{GeV}$ . . . 216
7.3.2 NLO-accurate Differential Distributions . . . 217
7.3.3 Width-Dependence of the Total Cross Sections . . . 220
7.3.4 Discussion . . . 221

8 Summary and Outlook **227**

A Monte Carlo Integration **229**
A.1 Selection from a Distribution 230
A.2 Hit-or-Miss Method 231
A.3 Importance Sampling 232
A.4 Multi-channel Integration 232
A.5 Variable Transformation 233
A.6 The Veto Algorithm 235

B Technical Remarks **238**
B.1 The Definition of Width 238
B.2 Renormalisation of SUSY Radiative Corrections 242

List of Figures

2.1 Current signal strength fits for the Higgs, as measured by both CMS and ATLAS collaborations. 30
2.2 The CMS Higgs signal strengths to fermions and bosons, and as a function of mass. 31
2.3 The status of SM predictions versus measurements. 35
2.4 The $SU(5)$ proton decay modes. 41
2.5 A triangle diagram from which the anomaly condition can be calculated. 45
2.6 The running of the SM gauge couplings within the SM (dashed), and within the MSSM (solid), taken from [1]. 61
2.7 Fermionic loop correction to the Higgs self-energy. Given that the Higgs couplings to fermions are proportional to m_f the top quark contribution is strongly dominant. 63
2.8 Loop corrections from BSM scalar fields to the Higgs self-energy. The fields in the loop are assumed to be new scalar fields. 64
2.9 Running of the parameters of the CMSSM taken from [1]. Note that $m_2 = m_{H_u}$ runs to negative values at roughly the electroweak scale, as required for radiative EWSB. 81
2.10 Current ATLAS exclusion of CMSSM parameters in the $(m_0, m_{1/2})$ parameter plane, with the other parameters fixed as indicated in the top margin of the plot. This exclusion is fairly independent of the values of the fixed parameters, within currently viable and reasonable ranges. The current CMS result is virtually identical. Taken from the ATLAS Supersymmetry Public Results webpage. 82
2.11 The current ATLAS (a) and CMS (b) mass exclusion limits for R-parity conserving models. . . 92

3.1 The leading order Drell-Yan process. 95
3.2 The next-to-leading order corrections to Drell-Yan lepton pair production. 98
3.3 The real emission contributions to Drell-Yan at NLO. 99
3.4 QCD self-energy corrections to the incoming (anti)quark propagator. 107

4.1 The one-loop regularised Altarelli-Parisi splitting functions. 134
4.2 Collinear splitting of a gluon off a hard quark. 138
4.3 Parton shower evolution as a function of the ordering variable and momentum fractions. . . . 144

6.1 The NLO SQCD corrections to Drell-Yan slepton pair production. 174
6.2 The leading-order contributions to gaugino pair production. 182
6.3 The virtual one-loop radiative corrections to gaugino pair production. 183
6.4 The real emission contribution to NLO gaugino pair production. 183
6.5 The $q(\bar{q})g$ initial-state contributions to real emission. This subset of diagrams includes two diagrams with resonant regions, (a) and (b), as well as a non-resonant contribution, (c), which will not necessarily be negligible in the resonant regions. 185
6.6 Diagrams for on-shell squark-gaugino pair production. 192
6.7 Diagram for on-shell squark decay. 193

7.1 Comparison of the invariant mass of electron and muon produced by LO and NLO event generation for a Z'_χ with $m_{Z'} = 500\ \mathrm{GeV}$ (at the LHC for a centre-of-mass energy of $\sqrt{s} = 13\ \mathrm{TeV}$) both up to, and focussed on, the Z' resonance. 198
7.2 Comparison of leading and sub-leading lepton transverse momenta produced by LO and NLO event generation for a Z'_χ with $m_{Z'} = 500\ \mathrm{GeV}$ at the LHC for a centre-of-mass energy of $\sqrt{s} = 13\ \mathrm{TeV}$. 199
7.3 Comparison of the invariant mass of electron and muon produced by LO and NLO event generation for the χ, ψ and the SSM models with a Z'_χ with $m_{Z'} = 500\ \mathrm{GeV}$ (at the LHC for a centre-of-mass energy of $\sqrt{s} = 13\ \mathrm{TeV}$) both up to, and focussed on, the Z' resonance. . . 200
7.4 Comparison of leading and sub-leading lepton transverse momenta produced by LO and NLO event generation for the χ, ψ and the SSM models with $m_{Z'} = 500\ \mathrm{GeV}$ at the LHC for a centre-of-mass energy of $\sqrt{s} = 13\ \mathrm{TeV}$. 201
7.5 The invariant mass distributions of electron and muon produced at NLO under the scale variation $\frac{1}{2}\,\mu \leftrightarrow \mu \leftrightarrow 2\,\mu$ (where $\mu := \mu_F = \mu_R = \sqrt{s}$) for the SSM model with a Z'_{SSM} with $m_{Z'} = 500\ \mathrm{GeV}$ (at the LHC for a centre-of-mass energy of $\sqrt{s} = 13\ \mathrm{TeV}$). 202
7.6 The leading and sub-leading lepton transverse momentum distributions for NLO event generation under the scale variation $\frac{1}{2}\,\mu \leftrightarrow \mu \leftrightarrow 2\,\mu$ (where $\mu := \mu_F = \mu_R = \sqrt{s}$) for the SSM model with $m_{Z'} = 500\ \mathrm{GeV}$ at the LHC for a centre-of-mass energy of $\sqrt{s} = 13\ \mathrm{TeV}$. 203
7.7 The LO+PS and NLO+PS invariant mass and transverse momentum distributions of the slepton pair, $\tilde{e}_L\tilde{e}_L$, for a $\sqrt{s} = 14\,\mathrm{TeV}$ LHC, with masses $m_{\tilde{e}_L} = 350\,\mathrm{GeV}$ and $m_{\widetilde{N}_1} = 150\,\mathrm{GeV}$. . 206
7.8 The LO+PS and NLO+PS stransverse mass and missing transverse momentum distributions produced by the decay of the $\tilde{e}_L\tilde{e}_L$ slepton pairs, for a $\sqrt{s} = 14\,\mathrm{TeV}$ LHC, with masses $m_{\tilde{e}_L} = 350\,\mathrm{GeV}$ and $m_{\widetilde{N}_1} = 150\,\mathrm{GeV}$. The actual neutralino mass, $m_{\widetilde{N}_1} = 150\,\mathrm{GeV}$ was used as the trial mass in the stransverse momentum computation. 207
7.9 The LO+PS and NLO+PS leading slepton and electron transverse momentum distributions for $\tilde{e}_L\tilde{e}_L$ production, for a $\sqrt{s} = 14\,\mathrm{TeV}$ LHC, with masses $m_{\tilde{e}_L} = 350\,\mathrm{GeV}$ and $m_{\widetilde{N}_1} = 150\,\mathrm{GeV}$. 208
7.10 The invariant mass and transverse momentum distributions of the slepton pair, $\tilde{e}_L\tilde{e}_L$, as a function of varying suppression scale, Λ^2, for a $\sqrt{s} = 14\,\mathrm{TeV}$ LHC, with masses $m_{\tilde{e}_L} = 350\,\mathrm{GeV}$ and $m_{\widetilde{N}_1} = 150\,\mathrm{GeV}$. 209
7.11 The stransverse mass and missing transverse momentum distributions produced by the decay of the $\tilde{e}_L\tilde{e}_L$ slepton pairs, as a function of varying suppression scale, Λ^2, for a $\sqrt{s} = 14\,\mathrm{TeV}$ LHC, with masses $m_{\tilde{e}_L} = 350\,\mathrm{GeV}$ and $m_{\widetilde{N}_1} = 150\,\mathrm{GeV}$. The actual neutralino mass, $m_{\widetilde{N}_1} = 150\,\mathrm{GeV}$ was used as the trial mass in the stransverse momentum computation. 210
7.12 The leading slepton and electron transverse momentum distributions for $\tilde{e}_L\tilde{e}_L$ production, as a function of varying suppression scale, Λ^2, for a $\sqrt{s} = 14\,\mathrm{TeV}$ LHC, with masses $m_{\tilde{e}_L} = 350\,\mathrm{GeV}$ and $m_{\widetilde{N}_1} = 150\,\mathrm{GeV}$. 211
7.13 Sample transversve momentum distributions for LO and NLO-accurate leptonic observables, as produced by our implementation, for an arbitrary point in the SUSY parameter space in the channel $\widetilde{C}_1^+\widetilde{N}_2$ with W- and Z-mediated decays with branching fraction 1. 218
7.14 Sample invariant mass distributions for LO and NLO-accurate leptonic observables, as produced by our implementation, for an arbitrary point in the SUSY parameter space in the channel $\widetilde{C}_1^+\widetilde{N}_2$ with W- and Z-mediated decays with branching fraction 1. The stransverse mass trial mass is set exactly to $m_{\widetilde{N}_1}$. 219
7.15 Sample stransverse mass distributions for LO and NLO-accurate leptonic observables, as produced by our implementation, for an arbitrary point in the SUSY parameter space in the channel $\widetilde{C}_1^+\widetilde{N}_2$ with W- and Z-mediated decays with branching fraction 1. The stransverse mass trial mass is set exactly to $m_{\widetilde{N}_1}$. 220
7.16 Proof of the relative independence of the total cross section on the squark width, for spectra where on-shell subtraction is relevant. 222

Nomenclature

2HDM Two Higgs Doublet Models, page 32

BSM Beyond-the-Standard-Model, page 18

C.L. Confidence Level, page 54

CC Charged Current, page 32

CKM Cabibbo-Kobayashi-Maskawa, page 36

CM Centre of Mass, page 102

CMSSM Constrained Minimal Supersymmetric Standard Model, page 79

DGLAP Dokshitzer-Gribov-Lipatov-Altarelli-Parisi, page 133

DIS Deep Inelastic Scattering, page 110

DLL Double Leading Logarithm(ic), page 153

DRED Dimensional Reduction, page 243

E6SSM E_6 Supersymmetric Standard Model, page 51

ER5M Effective rank-5 Models, page 44

EW Electroweak, page 20

EWPD Electroweak Precision Data, page 54

EWSB Electroweak Symmetry Breaking, page 28

FCNC Flavour Changing Neutral Current, page 55

GUT Grand Unified Theory, page 37

IR Infrared, page 96

ISR Initial-state Radiation, page 116

KLN Kinoshita-Lee-Nauenberg, page 114

LFV Lepton Flavour Violation, page 84

LHCSF Left-Handed Chiral Superfield, page 68

LL Leading Logarithm(ic), page 141

LL Leading Logarithm, page 153

LO Leading Order, page 52

LSP Lightest Supersymmetric Particle, page 59

LSZ Lehmann-Symanzik-Zimmermann, page 186

MPI Multi-parton interactions, page 131

MSSM Minimal Supersymmetric Standard Model, page 64

MSSM Minimal Supersymmetric Standard Model, page 72

MSSM Minimal Supersymmetric Standard Model, page 95

mSUGRA minimal Supergravity, page 79

NC Neutral Current, page 32

NLL Next-to-Leading Logarithm(ic), page 153

NMSSM Next-to-Minimal Supersymmetric Standard Model, page 80

NNLL Next-to-Next-to-Leading Logarithm, page 95

NWA Narrow Width Approximation, page 52

OS On-shell, page 191

PDF Parton Distribution Function, page 27

PDG Particle Data Group, page 241

PMNS Pontecorvo-Maki-Nakagawa-Sakata, page 36

pMSSM Phenomenological Minimal Supersymmetric Standard Model, page 81

POWHEG Positive Weight Hardest Emission Generator, page 160

pQCD perturbative Quantum Chromodynamics, page 143

QCD Quantum Chromodynamics, page 20

QED Quantum Electrodynamics, page 20

QFT Quantum Field Theory, page 20

RG Renormalisation Group, page 39

RG Renormalisation Group, page 50

RHCSF Right-Handed Chiral Superfield, page 68

RPV R-Parity Violating, page 76

SLHA SUSY Les Houches Accord, page 89

SM Standard Model, page 18

SQCD Supersymmetric Quantum Chromodynamics, page 73

SQED Supersymmetric Quantum Electrodynamics, page 72

SSB Spontaneous Symmetry Breaking, page 37

SSM Supersymmetric Standard Model, page 72

SUGRA Supergravity, page 66

SUSY Supersymmetry(ic), page 18

UE Underlying Event, page 131

UV Ultraviolet, page 43

VBF Vector Boson Fusion, page 175

vev vacuum expectation value, page 28

VSF Vector Superfield, page 69

WIMP Weakly Interacting Massive Particle, page 59

WIMP Weakly-interacting Massive Particle, page 56

Chapter 1

Introduction

With the advent of the Large Hadron Collider (LHC) which came online in 2009 (with Run 1 lasting from 2009 to 2013) the high energy limit of the physics which can be directly probed under laboratory conditions has been increased four-fold relative to the previous high energy frontier (set by the Tevatron with a centre-of-mass energy of $1.96\ \mathrm{TeV}$), with an up to seven-fold increase currently being prepared for and to be delivered in the near future (Run 2 of the LHC is scheduled to start in 2015). The previously unexplored phase space this opens up promises new discoveries, both those which were expected within the framework of the Standard Model (SM) such as the Higgs boson –expected both from the known masses of the electroweak bosons and from unitarity considerations in WW scattering– to those originating from physics beyond the SM, whether in the guise of well studied beyond-the-Standard-Model (BSM) frameworks such as Supersymmetry (SUSY), or something else and entirely unexpected.

As such the error in the theoretical predictions for the known potential signal processes must be ensured to be at least comparable to –or smaller than– the experimental errors expected to be attainable at the LHC, as no potential discovery can be reliably claimed otherwise, or alternatively, exclusion bounds cannot be set with any confidence.

Therefore the theoretical certainty of the signal processes must be implemented to the best of our ability, not just in fully-inclusive, total (and therefore directly unmeasurable) cross sections, but rather in the observables that can be measured at the LHC, with all the experimental cuts, acceptances and efficiencies this involves. The only way to obtain such predictions is via event generation, using Monte Carlo methods. Improvements in theory predictions must therefore be implemented within the framework of Monte Carlo event generators for their impact on measurable signal cross sections and differential distributions to be fully accounted for.

The theory predictions for the signal contribution to observables can be improved in two disjoint regimes (keeping these two disjoint and preventing overlap and double-counting between them being crucial, a point which we will elaborate on later): the soft and collinear phase space regions, and the phase space region appropriately described by the hard interaction and hard, non-collinear radiation from it.

In this work we will focus on improving the latter by incorporating known radiative corrections to it to improve its accuracy and reduce the uncertainty of predictions produced from it, while preserving the existing Monte Carlo accuracy for the former –within the HERWIG++ event generator– and ensuring no overlap between the two regions is induced in the process. We will perform this via the well known POWHEG matching method, for a selection of leptonic final states of well studied and strongly motivated BSM models, presenting the results obtained from this in some generic observables accessible at the LHC. The tools here developed therefore represent an improvement over existing predictions in LHC searches using observables exclusive in the corresponding final-state leptons, but inclusive in jets.

Similar implementations already exist for all basic SM processes, both for colour-singlet final states (Drell-Yan, diboson and Higgs production with varying numbers of jet multiplicities at leading order), and dijet, trijet, single top and heavy quark pair production. A subset of these can be found in either handmade implementations in the POWHEG-BOX package or HERWIG++, with automated implementations (requiring only the virtual matrix element to be inserted) exist in both the Sherpa and HERWIG++ packages.

For BSM processes the first processes have begun to be implemented to this higher level of event generation accuracy, with novel results presented in this work. Handmade implementations for several BSM processes have been implemented in HERWIG++ (namely the processes presented in this work, as well as a previous W' implementation [2]) and in the POWHEG-BOX package (notably slepton pair production [3], slepton pair + jet [4], and squark pair production [5], see the POWHEG-BOX webpage[1] for an up-to-date list).

[1] `http://powhegbox.mib.infn.it/`

Chapter 2

The Standard Model and Beyond

In this chapter we will introduce both the Standard Model and the Beyond-the-Standard-Model frameworks which we will deal with in this work.

2.1 The Standard Model

The Standard Model is the agglomeration of Quantum Electrodynamics (QED) as formulated in the early twentieth century, its embedding in the Electroweak (EW) model of Salam, Glashow and Weinberg, the parton model and Quantum Chromodynamics (QCD) as developed in the 1970s, and the Anderson-Brout-Englert-Higgs mechanism required to provide the bosons and fermions with masses. All together these comprise a model whose success in describing all known physics (bar gravity) from scales of neutrino physics $\mathcal{O}(0.1\ \mathrm{eV})$ to the $\mathcal{O}(1\ \mathrm{TeV})$ energies now being probed at the Large Hadron Collider (LHC) [1] is unrivalled, though not complete[2].

The Standard Model can be defined as a Quantum Field Theory (QFT) on a four-dimensional Minkowski metric which includes all the renormalisable operators invariant under the following local symmetries (gauge groups)

$$G_{\mathrm{SM}} = SU(3)_C \otimes SU(2)_L \otimes U(1)_Y \,, \tag{2.1}$$

[1] And indeed even up to energies of $\mathcal{O}(10^{19}\ \mathrm{eV})$ where the Greisen-Zatsepin-Kuzmin suppression in the flux of cosmic rays has been observed [6]. With the recent detection of $1\ \mathrm{PeV}$ astrophysical neutrinos by the IceCube collaboration [7] some intermediate energies between collider searches and cosmic rays are now also being directly probed.

[2] With issues such as the Dirac or Majorana nature of neutrinos still remaining to be settled.

under which the following fermionic field content is posited, in the following representations[3]

$$\begin{aligned} u_L &: \left(\mathbf{3},\mathbf{2},\frac{1}{3}\right), \qquad u_R : \left(\mathbf{3},\mathbf{1},\frac{4}{3}\right), \\ d_L &: \left(\mathbf{3},\mathbf{2},\frac{1}{3}\right), \qquad d_R : \left(\mathbf{3},\mathbf{1},-\frac{2}{3}\right), \\ \nu_L &: (\mathbf{1},\mathbf{2},-1), \qquad \nu_R : (\mathbf{1},\mathbf{1},0), \\ e_L &: (\mathbf{1},\mathbf{2},-1), \qquad e_R : (\mathbf{1},\mathbf{1},-2), \end{aligned} \tag{2.2}$$

and a scalar Higgs sector is added as

$$\begin{aligned} \phi = \begin{pmatrix} \phi^+ \\ \phi^0 \end{pmatrix} &: (\mathbf{1},\mathbf{2},1), \\ \tilde{\phi} = i\sigma_2\phi^* &: (\mathbf{1},\bar{\mathbf{2}},-1). \end{aligned} \tag{2.3}$$

The third component of the isospin doublets, t_3, are assigned as follows

$$t_3(u_L) = t_3(\nu_L) = \frac{1}{2}, \tag{2.4a}$$

$$t_3(d_L) = t_3(e_L) = -\frac{1}{2}, \tag{2.4b}$$

It is clear from these charges that the SM is a chiral theory in the EW sector, which in turn forbids explicit mass terms, i.e. Dirac masses are forbidden because none of the fermions has left- and right-handed fields which transform under the complex-conjugate representations of each other, and Majorana masses are forbidden for all fermions except the neutrinos as they carry no unbroken global or local $U(1)$ charge, i.e. no electric charge. Gauge boson masses are forbidden by the gauge symmetry itself.

These models together form a structure which can fall under four types of terms which can be added to form the Lagrangian density of the SM

$$\mathcal{L}_{\text{SM}} = \mathcal{L}_{\text{Gauge}} + \mathcal{L}_{\text{Dirac}} + \mathcal{L}_{\text{Higgs}} + \mathcal{L}_{\text{Yukawa}}. \tag{2.5}$$

[3]We have written the charges for both the left- and right-handed Weyl spinors, by convention these may be written in terms of left-handed spinors only by noting that $\psi = \mathcal{C}^{-1}(\gamma^0)^T(\psi^c)^*$ such that the right-handed fields can be written in terms of charge conjugated left-handed fields $\psi_R = P_R\psi = \mathcal{C}^{-1}(\gamma^0)^T((\psi^c)_L)^* := \mathcal{C}^{-1}(\gamma^0)^T(\psi^c_L)^*$, with the hypercharge multiplied by a factor of -1 and the colour and isospin representations conjugated (e.g. $\mathbf{3},\mathbf{2} \to \bar{\mathbf{3}},\bar{\mathbf{2}}$) with respect to the ones shown here. The relations $\mathcal{C}\gamma^5\mathcal{C}^{-1} = (\gamma^5)^T$, $\{\gamma^\mu,\gamma^5\} = 0$ and $(\gamma^5)^\dagger = \gamma^5 \implies P_L^T = P_L^*$ have been used.

Each of these terms is given by

$$\mathcal{L}_{\text{Gauge}} = -\frac{1}{4}G^{a\,\mu\nu}G_{a\,\mu\nu} - \frac{1}{4}W^{a\,\mu\nu}W_{a\,\mu\nu} - \frac{1}{4}B^{\mu\nu}B_{\mu\nu}\,, \tag{2.6a}$$

$$\mathcal{L}_{\text{Dirac}} = -\sum_{\text{fermions}} i\bar{f}_i \not{D} f_i\,, \tag{2.6b}$$

$$\mathcal{L}_{\text{Higgs}} = (D_\mu\phi)^\dagger(D^\mu\phi) - V(\phi^\dagger\phi) = (D_\mu\phi)^\dagger(D^\mu\phi) - \mu^2(\phi^\dagger\phi) + \lambda(\phi^\dagger\phi)^2\,, \tag{2.6c}$$

$$\mathcal{L}_{\text{Yukawa}} = \left(y_i\bar{Q}\tilde{\phi}u_R + y_i\bar{Q}\phi d_R + y_i\bar{L}\phi l_R\right) + \text{h.c.} + \mathcal{L}_{\text{Neutrino mass}}\,, \tag{2.6d}$$

where

$$Q = \begin{pmatrix} u_L \\ d_L \end{pmatrix} \qquad \text{and} \qquad L = \begin{pmatrix} \nu_L \\ e_L \end{pmatrix} \tag{2.7}$$

are isospin doublets[4] and the Higgs self-coupling is constrained to be $\lambda > 0$ to ensure that the potential is bounded from below and the vacuum is (meta)stable[5]. We have neglected a possible right-handed neutrino or any neutrino mass terms as the form of the neutrino mass terms is as of yet unknown and we will not be concerned with these terms.

We have neglected family indices for the Yukawa terms, and omitted matrix indices (on isospin doublets and colour triplets and octets, and identity operators for singlets) for clarity elsewhere. The gauge fields of $SU(3)_C$ ($G_{a\,\mu}$, $a = 1, ..., 8$), $SU(2)_L$ ($W_{a\,\mu}$, $a = 1, ..., 3$) and $U(1)_Y$ (B_μ) transform under the adjoint representation of their respective groups. The corresponding gauge couplings are g_3, g_2 and g_1 respectively. The running of the SM gauge couplings is known to three loops [11] and for reference these gauge couplings have approximate numerical values of $g_3 \approx 1.22$, $g_2 \approx 0.65$ and $g_1 \approx 0.35$ at the electroweak scale.

We have implicitly used the normalisation $\text{tr}(t^a t^b) = T_R\delta^{ab}$ with Dynkin index $T_R = \frac{1}{2}$ for the $SU(3)_C$ and $SU(2)_L$ groups (and the letter indices label generators of the adjoint representation) to obtain the correct coefficient for the gauge kinetic terms of the non-Abelian groups and we will adhere to this normalisation throughout.

The field strength tensors are defined as follows

$$G^{a\,\mu\nu} = \partial^\mu G^{a\,\nu} - \partial^\nu G^{a\,\mu} - g_3 f^{abc} G^{b\,\mu} G^{c\,\nu}\,, \tag{2.8a}$$

$$W^{a\,\mu\nu} = \partial^\mu W^{a\,\nu} - \partial^\nu W^{a\,\mu} - g_2 \epsilon^{abc} W^{b\,\mu} W^{c\,\nu}\,, \tag{2.8b}$$

$$B^{\mu\nu} = \partial^\mu B^\nu - \partial^\nu B^\mu\,. \tag{2.8c}$$

[4] For the SM Lagrangian written out in full, in physical (mass) basis, see for example [8].

[5] The Higgs potential may have additional structure beyond that considered here, in which case the minimum of the potential as seen here may only be a local minimum and the tunnelling rate to the global minimum must be computed and checked to be greater than the known age of the universe (see e.g. [9]). Given the top quark and Higgs masses and the known radiative corrections to the SM Higgs potential the SM has been found to lie in a narrow metastability strip of parameter space [10].

The covariant derivatives, D_μ, used above are defined in accordance with the charges of the field they act upon, as stated in equation 2.2, such that under gauge transformations they transform in the same way as the matter field upon which they act. This implies that they must be of the form

$$D_\mu = \partial_\mu + ig_3\frac{t^a}{2}G^{a\,\mu} + ig_2\frac{\sigma^a}{2}W^{a\,\mu} + ig_1\frac{Y}{2}B^\mu\,, \tag{2.9}$$

where the Feynman's slash notation is used $\not{D} = \gamma^\mu D_\mu$ (which we will use throughout) and terms proportional to gauge couplings will be absent if that field is a singlet under that gauge group, such that

$$D_\mu\phi = \left(\partial_\mu + ig_2\frac{\sigma^a}{2}W^{a\,\mu} + ig_1\frac{Y}{2}B^\mu\right)\phi\,, \tag{2.10a}$$

$$D_\mu q_L = \left(\partial_\mu + ig_3\frac{t^a}{2}G^{a\,\mu} + ig_2\frac{\sigma^a}{2}W^{a\,\mu} + ig_1\frac{Y}{2}B^\mu\right)q_L\,, \tag{2.10b}$$

$$D_\mu q_R = \left(\partial_\mu + ig_3\frac{t^a}{2}G^{a\,\mu} + ig_1\frac{Y}{2}B^\mu\right)q_R\,, \tag{2.10c}$$

$$D_\mu l_L = \left(\partial_\mu + ig_2\frac{\sigma^a}{2}W^{a\,\mu} + ig_1\frac{Y}{2}B^\mu\right)l_L\,, \tag{2.10d}$$

$$D_\mu l_R = \left(\partial_\mu + ig_1\frac{Y}{2}B^\mu\right)l_R\,, \tag{2.10e}$$

where we have omitted colour and isospin matrix indices (e.g. $\partial_\mu \to \mathbb{1}^{\rm col}_{ij}\mathbb{1}^{\rm iso}_{kl}\partial_\mu$, $t^a \to t^a_{ij}$, $\phi \to \phi_i$, etc.)

The gauge fields $G^{a\,\mu}$, $W^{a\,\mu}$ and B^μ are defined to transform as

$$G^\mu \longrightarrow UG^\mu U^{-1} + i\frac{1}{g}U\partial^\mu U^{-1}\,, \tag{2.11}$$

where we have used the Einstein summation convention $G^\mu = \sum_a G^{a\,\mu}t^a$, as we will from here on, and similarly for W^μ.

The matter fields transform as

$$f \longrightarrow Uf\,, \tag{2.12}$$

where $U = e^{-i\alpha^a(x^\mu)t^a}$ and t^a are the generators of the representation under which the field being acted on transforms, $\alpha^a(x^\mu)$ is the gauge shift parameter, and for $U(1)$ symmetries this reduces to $B^\mu \longrightarrow B^\mu - \frac{1}{q}\partial^\mu\alpha(x)$ with $U = e^{-i\alpha(x)}$ and the fermionic gauge transformation as before. These gauge transformations leave the Lagrangian density invariant under the gauge symmetries imposed above.

For our purposes here and in the rest of this work we shall restrict our attention to bare parameters (masses, gauge couplings, fermionic fields and gauge fields) in the Lagrangian. To make contact with measurable quantities these fields must be renormalised via appropriate wavefunction renormalisation factors and counter

terms of the form

$$m_{\text{bare}} = m_{\text{ren}} + \delta m\,, \tag{2.13a}$$

$$\psi_{\text{bare}} = \sqrt{Z_f}\,\psi_{\text{ren}}\,, \tag{2.13b}$$

$$A^{\mu}_{\text{bare}} = \sqrt{Z_G}\,A^{\mu}_{\text{ren}}\,, \tag{2.13c}$$

$$g_{\text{bare}} = g_{\text{ren}} + \delta g\,, \tag{2.13d}$$

to order-by-order cancel ultraviolet singularities in their radiative corrections. We will however omit the subscript 'bare' for clarity.

Schematically, on physical grounds, we may also write the SM Lagrangian as the sum of the Lagrangian densities of each one of the sectors which constitute it:

$$\mathcal{L} = \mathcal{L}_{\text{QCD}} + \mathcal{L}_{\text{EW}} + \mathcal{L}_{\text{Higgs+Yukawa}} \tag{2.14}$$

2.1.1 The QCD Sector

The first term of the decomposition in equation 2.14 is the one composed of the $SU(3)$ gauge fields and non-singlet fields under this gauge group.

Writing all the possible renormalisable terms under this symmetry (as well as including terms that will allow us to construct Feynman rules from it) we can write this sector as

$$\mathcal{L}_{\text{QCD}} = -\frac{1}{4}G^{a\,\mu\nu}G_{a\,\mu\nu} \;-\; i\,\bar{q}\not{D}q + \;\mathcal{L}_{\text{Gauge-fixing}} \;+\; \mathcal{L}_{\text{Ghost}} \;+\; \mathcal{L}_{\theta-\text{term}} \tag{2.15}$$

where the gauge fixing terms are required to make the gauge kinetic term invertible and allow the definition of its Green function (the gluon propagator). Naïvely this is due to the fact that gauge fields will in principle have 4 degrees of freedom as indicated by their Lorentz index, however massless gauge bosons are known to have only 2 degrees of freedom, and massive ones 3. It is this redundancy in our description which allows for some freedom in fixing some degrees of freedom. Note that gauge fixing is required for all $SU(N)$ gauge theories, and indeed even for Abelian ones such as QED, where the Feynman gauge is a common choice.

For completeness we list the most common choices of gauge-fixing terms (see [12])

$$\mathcal{L}_{\text{Gauge-fixing}} = -\frac{1}{2(1-\zeta)}\left(\partial^{\mu}G^{a}_{\mu}\right)^2 \quad (\text{Linear covariant gauges})\,, \tag{2.16a}$$

$$\mathcal{L}_{\text{Gauge-fixing}} = -\frac{\zeta}{2}\left(n^{\mu}G^{a}_{\mu}\right)^2 \quad (\text{Axial or physical gauges})\,, \tag{2.16b}$$

where the choice $\zeta = 0$ in the linear covariant gauges is known as the Feynman gauge, and in the axial or physical gauge the limit $\zeta \to \infty$ and hence also the $n^{\mu}G^{a}_{\mu} \to 0$ limit must be taken.

While both the options above are Lorentz invariant, gauge invariance is explicitly broken by gauge fixing, and indeed other symmetries may be broken by other choices of gauge. It is worth emphasising that predictions for observable quantities will be unaffected by the choice of gauge, as this is purely a choice made for convenience and allowed for by the redundancy of the gauge theory description of physical states (though in numerical applications some choices may prove advantageous over others).

Furthermore upon gauge fixing (imposing a condition on the gauge field), for some gauge choices we will have spoiled the unitarity of the S-matrix, and will need to restore it by introducing unphysical, propagating degrees of freedom known as Faddeev-Popov ghosts. These fields have odd properties (fermionic anti-commutation despite being scalar fields, one is required for each gauge field, and they only appear in loops, where they introduce an extra factor of -1 as if it were a fermion loop) and are introduced solely with the purpose of restoring unitarity. The details of this procedure are explained in [13].

If required, the ghost term has the form

$$\mathcal{L}_{\text{Ghost}} = \partial_\mu c^a \left(\partial^\mu \delta^{ad} - g_3 f^{abd} A^{b\,\mu}\right) c^d \,, \tag{2.17}$$

where c^a are the scalar Faddeev-Popov ghost fields.

The Feynman gauge has the advantage of giving the simplest form for the propagator, while the physical gauges do not require ghost fields to preserve unitarity and have $\mathcal{L}_{\text{Ghost}} = 0$.

Lastly we should mention that QCD gauge invariance allows for one extra term, which we have labelled the θ-term. This term has the following form

$$\mathcal{L}_{\theta\text{ term}} = g_3^2 \frac{\theta}{64\pi^2} \epsilon_{\mu\nu\rho\lambda} G^{a\,\mu\nu} G^{a\,\rho\lambda} \,. \tag{2.18}$$

Under parity and time reversal this term transforms as $\theta \xrightarrow{\text{PT}} -\theta$ and hence would induce CP violation were it to be non-zero. This would contribute for example to the neutron electric dipole moment. However, since there is no experimental indication of CP violation in the strong sector, and there is a strong upper bound on the the neutron electric dipole moment, the θ term can be deduced to be $|\theta| \lesssim 10^{-10}$ [14], so we will herein assume $|\theta| = 0$ as is conventional.

There also exist an $SU(2)_L$ θ-term (with $G^{a\,\mu\nu} \to W^{a\,\mu\nu}$), as well as $U(1)$ one ($G^{a\,\mu\nu} \to F^{\mu\nu}$). However by shifting the left-handed fields by a phase the $SU(2)_L$ theta term may be rotated away [15], and a $U(1)_Q$ θ-term has indeed been argued to be (at least in principle) observable [16], though it does not give any measurable contribution to any other known and phenomenologically relevant observable, so we omit both of these possible θ-term contributions.

Also note that quarks have masses and acquire them via Yukawa couplings, as will be detailed in a later

section, however for our purposes we will deal only with quarks from the first two generations at the LHC, for which the massless approximation is perfectly appropriate, and hence we have omitted any mass terms for the quarks in the QCD Lagrangian.

Feynman diagram generation within HERWIG++ [17] is done using the HELAS method [18], which employs the unitary gauge for massive propagators, and Feynman-t'Hooft gauge for massless propagators, and this is indeed the gauge choices which we work with. The kinematics of the parton shower stage of event generation are in contrast formulated in the lightlike axial (lightcone) gauge.

Collinear Factorisation

It can be shown (see e.g. [19]) that in the limit of collinear emission ($p_k = (1-z)p_i$, where k is the emitted parton and i is the emitter left with momentum $p_j = z\,p_i$ after the emission) for emission of one extra parton off an n-parton process, both the matrix element squared

$$\sum_{\text{spins}} |\mathcal{M}_{n+1}|^2 \underset{\text{coll}}{=} 2\,\frac{1}{t}\,g_S^2\,P_{ij}(z) \sum_{\text{spins}} |\mathcal{M}_n|^2\,, \tag{2.19}$$

and the phase space

$$d\Phi_{n+1} \underset{\text{coll}}{=} d\Phi_n \frac{1}{4(2\pi)^3} d\phi\,dt\,dz\,, \tag{2.20}$$

factorise.

Here we denote g_3 as g_S (as we will customarily do from here on), and $t = p_i^2 = (p_j + p_k)^2 = 2\,E_j\,E_k(1-\cos\theta) \simeq E_j\,E_k\,\theta^2$ (for small θ) is the virtuality of the emitting parton.

As a result the cross section itself also factorises

$$d\sigma_{n+1} \underset{\text{coll}}{=} d\sigma_n\,\frac{\alpha_S}{2\pi}\,\frac{dt}{t}\,P_{ij}(z)\,dz\,, \tag{2.21}$$

where we have assumed no azimuthal dependence of the amplitude squared on the azimuthal angle to perform the integral $\int d\phi/2\pi = 1$.

This relation holds for both emission off spacelike (initial-state) legs as well as timelike (final-state) ones and will form the basis for the formulation of parton showers, as we will later discuss.

Factorisation Theorem

The factorization theorem broadly posits the factorisation of observable hadronic cross sections and differential distributions into a perturbative partonic component, and non-perturbative distribution functions (whose energy dependence can remarkably nonetheless still be computed by perturbative methods).

This result relies on the collinear factorisation of QCD cross sections shown in the previous section and can more concretely be specified as the ansatz that hadronic observables at energies much larger than the non-perturbative scale of QCD, $Q \gg \Lambda_{\rm QCD}^{\overline{\rm MS}} \sim 200\ {\rm MeV}$ can be described in the following form[6]

$$d\sigma^H = \sum_{i,j} \int dx_1 dx_2\ f_i(x_1,\mu_F)\ f_j(x_2,\mu_F)\ d\sigma_{ij}(x_1 x_2 S, \mu_F, \alpha_S(\mu_R))\ +\ \mathcal{O}\left(\left(\frac{\Lambda_{\rm QCD}}{x_1 x_2 S}\right)^p\right) \tag{2.22}$$

where i,j denote the possible incoming partons, x_1 and x_2 denote the longitudinal momentum fractions of the incoming partons as a fraction of the total hadronic centre of mass energy, S, and μ_F denotes the scale at which we partition the description of the event into perturbatively evolvable (but intrinsically non-perturbative) parton distribution functions (PDFs) $f(x,\mu_F)$, and the purely perturbative description of the hard scattering in the partonic cross section, $d\hat{\sigma}$.

Strictly speaking this formalism is proven only for *sufficiently inclusive* observables (such as total cross sections), where real emission contributions are unrestricted and full cancellation of singularities can take place. This has been shown to fail at three loop order in QCD to $2 \to 2$ processes, or two loop to 2 to three processes [20] and is related to the the existence of so-called superleading logarithms [21].

The second term (where it must be noted that the power p is in principle a process-dependent number) corresponds to power-suppressed higher twist corrections and non-perturbative effects such as hadronization effects, multiparton interactions and contributions of the soft underlying event which arise for example from interactions between the incoming hard partons and the beam. However we will simulate some of these effects elsewhere and we neglect these terms as they are assumed to be subdominant.

The process independence of the collinear factorisation –on which this result relies– confers this property to this equation as well, and herein lies its power and wide-ranging applicability as a method of computing the dominant contributions to hard interaction probabilities.

2.1.2 The Electroweak Sector of the Standard Model

The Electroweak sector of the SM is the subset of terms consisting of the $SU(2)_L$ and $U(1)_Y$ gauge fields as well as all the fermions with non-zero charges under these groups.

Namely these are[7]

$$\mathcal{L}_{\rm EW}\ =\ -\frac{1}{4}W^{a\,\mu\nu}W_{a\,\mu\nu}\ -\ \frac{1}{4}B^{\mu\nu}B_{\mu\nu}\ -\ \sum_{\rm fermions} i\bar{f}_i \not{D} f_i\,. \tag{2.23}$$

However we see here that both the electroweak gauge bosons and the fermions are massless, so a gauge

[6] This relation holds for hadron-hadron collisions, with a single $f(x,\mu_F)$ function it holds for DIS, and with the substitution $f(x,\mu_F) \to \delta(1-x)$ for lepton-lepton collisions.

[7] We neglect gauge fixing and ghost terms from now on.

invariant way of giving them masses (except for the photon), and deducing the their interactions in mass eigenstates must be found[8]. It is also this mechanism of giving masses which we will require later in extensions of the EW sector as well.[9]

Electroweak Symmetry Breaking

At scales $\mathcal{O}(100\ \mathrm{GeV})$ the only known conserved unconfined charge is the electric charge. This means that we must find a way to reduce the symmetry of the SM Lagrangian as follows

$$SU(2)_L \otimes U(1)_Y \longrightarrow U(1)_Q \,. \tag{2.24}$$

The conserved charge resulting from this is the electric charge, and can be computed by the Gell-Mann—Nishijima formula, $Q = t_3 + \frac{Y}{2}$.

This is known as Electroweak Symmetry Breaking (EWSB) and is the mechanism via which the gauge bosons and fermions of the SM acquire mass.

However, since the gauge invariance of the SM Lagrangian must not be compromised and explicit gauge-invariant mass terms cannot be formed, this leaves us with spontaneous symmetry breaking, where a field (which must be electrically neutral to preserve electric charge conservation, colourless to preserve colour conservation and spinless to respect Lorentz invariance) acquires a non-zero vacuum expectation value (vev). It is precisely for this purpose that the scalar Higgs field of equation 2.3 and its Lagrangian in equation 2.6c have been introduced.

When the μ^2 term in this Lagrangian becomes negative, the minimum of the Higgs potential moves away from the origin in the Higgs field space, and the Higgs field has thus acquired an non-zero vev. Minimising the Higgs potential once the Higgs mass coefficient has become negative and the potential has developed a non-zero vacuum expectation value yields the scale which characterises EWSB and which can be obtained by finding the minimum of the potential

$$\left.\frac{dV}{d\phi}\right|_{\phi=\langle\phi\rangle} = 0 \,, \tag{2.25}$$

and solving for $\langle\phi\rangle$ gives the vacuum expectation value

$$\langle\phi\rangle = \frac{v}{\sqrt{2}} = \sqrt{\frac{-\mu^2}{2\lambda}} \,. \tag{2.26}$$

[8]The Higgs mechanism outlined below in the next section is not the only known way to generate masses. The Stückelberg mechanism for example can also be used to generate gauge-invariant mass terms (see [22] for an overview), however this mechanism can only provide Abelian gauge bosons with mass, and is hence implausible for the SM.

[9]We will consider only new massive bosons, the hidden photon case is related but we will not deal with it, see [23] for a review of new massless Abelian bosons.

The exact numerical value for this vev can be deduced by comparison to the four-fermion effective weak interaction and is deduced to be

$$\frac{v^2}{2} = \frac{\left(2^{-1/4} G_F^{-1/2}\right)^2}{2} \approx \frac{(246\ \mathrm{GeV})^2}{2}\,. \tag{2.27}$$

Shifting the Higgs field by this expectation value hence accounts for its now non-zero vev

$$\phi \longrightarrow \phi + \frac{1}{\sqrt{2}} \begin{pmatrix} 0 \\ v \end{pmatrix}\,, \tag{2.28}$$

and it is precisely this new term which will generate the gauge boson and fermion masses when inserted into the Higgs kinetic term and the Yukawa terms, respectively.

Inserting this new term into the Yukawa terms of equation 2.6d immediately yields the fermion mass terms

$$\begin{aligned} \mathcal{L}_{\mathrm{Yukawa}} &= y_i \frac{v}{\sqrt{2}} u_L^\dagger u_R + y_i \frac{v}{\sqrt{2}} d_L^\dagger d_R + y_i \frac{v}{\sqrt{2}} l_L^\dagger l_R + \mathrm{h.c.}\,, \\ m_{f_i} &= y_i \frac{v}{\sqrt{2}}\,. \end{aligned} \tag{2.29}$$

If we now consider the kinetic term of the Higgs from equation 2.6c, with the covariant derivative as defined in equation 2.10a we find that for the $W^\pm$ bosons two of the terms from the covariant derivative involving the $SU(2)_L$ gauge fields can be rewritten as

$$g_2(\sigma_1 W_1^\mu + \sigma_2 W_2^\mu) = g_2 \left(\frac{(\sigma_1 + i\sigma_2)}{\sqrt{2}} \frac{(W_1^\mu - iW_2^\mu)}{\sqrt{2}} + \mathrm{h.c.} \right)\,, \tag{2.30a}$$

$$= g_2 \left(\frac{(\sigma_1 + i\sigma_2)}{\sqrt{2}} \frac{(W_1^\mu - iW_2^\mu)}{\sqrt{2}} + \frac{(\sigma_1 - i\sigma_2)}{\sqrt{2}} \frac{(W_1^\mu + iW_2^\mu)}{\sqrt{2}} \right)\,, \tag{2.30b}$$

$$= g_2 \left(\frac{\sigma^+}{\sqrt{2}} W_\mu^- + \frac{\sigma^-}{\sqrt{2}} W_\mu^+ \right)\,, \tag{2.30c}$$

where we have defined $\sigma^\pm = \sigma_1 \pm i\sigma_2$ and $W_\mu^\pm = (W_1^\mu \pm iW_2^\mu)/\sqrt{2}$

This rearrangement in the covariant derivative (along with rotations of the fermion fields to mass eigenstates) will give $W^\pm$-fermion-anti-fermion vertices of the gauge boson mass eigenstates when inserted into the fermion kinetic term in equation 2.6b, and the $W^\pm$ mass term when inserted into the covariant derivative of the Higgs kinetic term (equation 2.6c)[10].

These two gauge boson mass eigenstates mediate what is known as the *charged current* interactions responsible for flavour-changing interactions in both the quark and lepton sectors and give rise to weak decay processes.

However, by counting helicity degrees of freedom before and after EWSB and requiring that they must be preserved we can deduce the existence of a further massive gauge boson state in addition to the W bosons

[10] Interactions with other gauge bosons arise from the gauge kinetic term, but we will not be concerned with these.

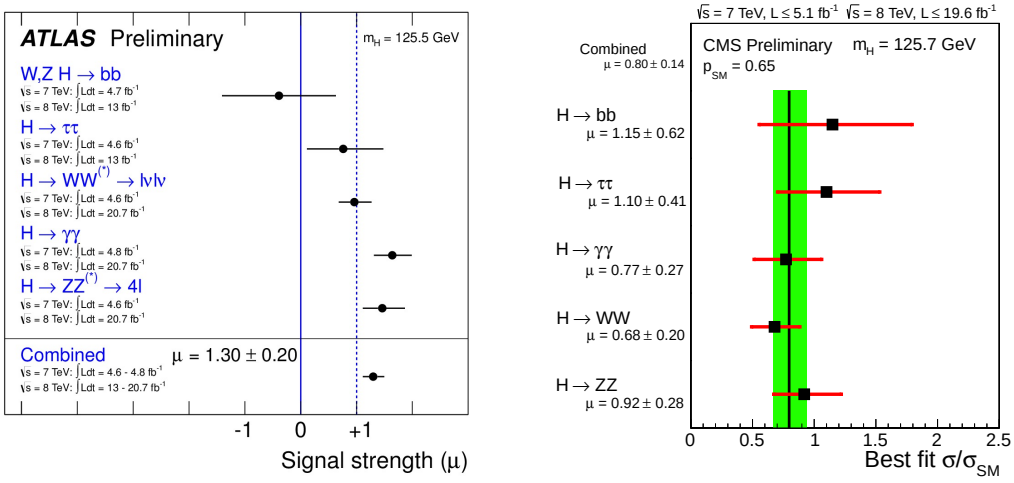

(a) The signal strength fits versus the SM Higgs signal as determined by the ATLAS collaboration for their best fit mass [26].

(b) The signal strength fits versus the SM Higgs signal as determined by the CMS collaboration for their best fit mass [27].

Figure 2.1: Current signal strength fits for the Higgs, as measured by both CMS and ATLAS collaborations.

(and the massless photon as well as the Higgs itself which is not related to any gauge symmetry) [11]

$$\underbrace{2\times 3}_{W^{\mu\,a}} + \underbrace{2}_{B^{\mu}} + \underbrace{4}_{\phi} \xrightarrow{\text{EWSB}} \underbrace{3\times 2}_{W^{\pm}} + \underbrace{3}_{Z^{\mu}} + \underbrace{2}_{A^{\mu}} + \underbrace{1}_{h} \tag{2.31}$$

It is this Z-mediated so-called *neutral current* sector and extensions to it which we will be concerned with in this chapter, and on which we elaborate in section 2.1.3.

The Discovery of the Higgs

On the 4th of July 2012 the discovery of a Higgs-like resonance in multiple decay channels was announced in a joint ATLAS-CMS news conference and published shortly afterwards [24, 25]. The combination of the high mass-resolution $\gamma\gamma$ and $ZZ \to 4\,l$ channels yielded the initial deviation over the $5\,\sigma$ discovery threshold from the null (SM with no Higgs) hypothesis which allowed for the discovery to be claimed.

Since then an integrated luminosity of $5\,\mathrm{fb}^{-1}$ at $\sqrt{s} = 7$ TeV and $20\,\mathrm{fb}^{-1}$ at $\sqrt{s} = 8$ TeV have been accummulated and the couplings of the resonance as measured by both collaborations are so far consistent those of the SM Higgs (see figure 2.1), as previously defined. The best fit mass for the resonance found by each collaboration is shown in table 2.1.

CMS has also produced a plot displaying the signal strength of the resonance in both its bosonic and

[11] Recall that in four spacetime dimensions massless vector fields carry two degrees of freedom/polarisations ($d-2$ in general), massive ones carry three and real scalar fields carry only one. The Higgs as defined in equation 2.3 is a doublet consisting of two complex scalar fields, giving a total of four degrees of freedom before EWSB, and only one after EWSB (three are absorbed as the longitudinal degrees of freedom of the three massive bosons and the remaining one constitutes the physical Higgs field).

Collaboration	Mass (in GeV)
ATLAS	125.5 ± 0.2 (stat.) ± 0.6 (syst.) [28]
CMS	125.7 ± 0.3 (stat.) ± 0.3 (syst.) [27]

Table 2.1: The best fit mass values for the Higgs, as measured by both ATLAS and CMS.

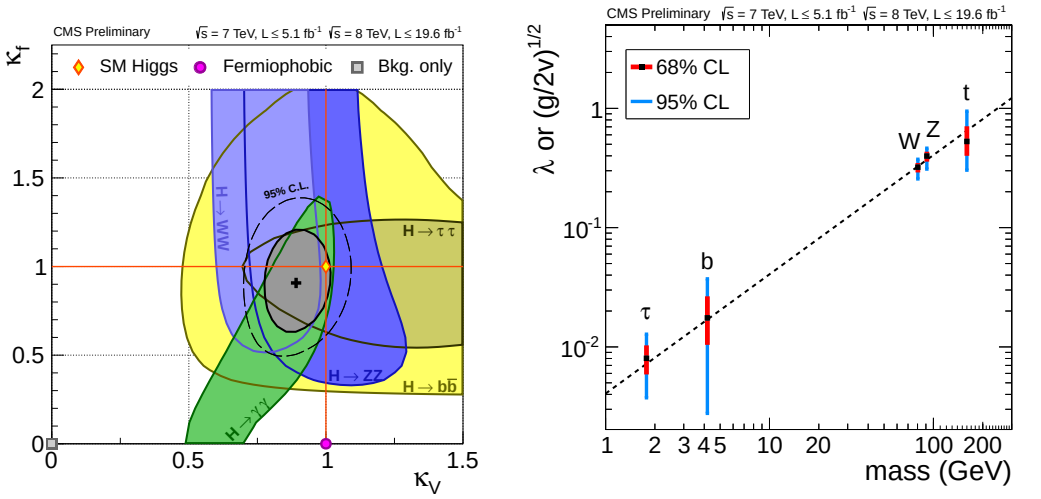

(a) The Higgs couplings to fermions and bosons, channel by channel [27].

(b) The measured Yukawa couplings, λ, to fermions, as well as the couplings to bosons [27]. The scaling of the couplings with mass as expected for the Higgs is seen.

Figure 2.2: The CMS Higgs signal strengths to fermions and bosons, and as a function of mass.

fermionic couplings for all channels measured, and good consistency with the SM expectation is found (see figure 2.2).

The spin and parity of the resonance have been found to be consistent with $J^P = 0^+$ by both collaborations [29, 30], as expected for the SM Higgs, with the spin 2 possibility strongly disfavoured, and the spin 1 option ruled out by the Landau-Yang Theorem [31, 32] as the decay to two photons has been observed.

However despite the resonance having the correct SM quantum numbers, a mass of the correct magnitude to be resposible for EWSB, and coupling to both fermions and bosons as expected for a Higgs candidate, the defining feature of the Higgs is that its coupling must be proportional to the mass of the particle it couples to. As such the definitive proof that the detected resonance is indeed responsible for EWSB and is therefore the/a Higgs, this property must be shown. This has indeed now been measured and has been found to be just as expected for the Higgs boson (see figure 2.2).

We will therefore from hereon (and as suggested from the title of the section) drop the 'Higgs-like' description and refer to the discovered resonance as the Higgs boson.

The SM-like couplings of the Higgs do not rule out the existence of further high mass Higgs resonances

as posited in Two Higgs Doublet Models (2HDM), and in fact in certain limits of such models (such as the *decoupling limit*, $m_{A^0} \gg m_Z$ of the MSSM, see [33, 34]) the lower of the Higgs resonances has couplings indistinguishable from those of the SM Higgs. Note however that special care must be taken in extensions of the Higgs sector as the mass-dependent (mass-proportional) couplings which characterise the Higgs sector can invalidate the assumed decoupling of heavy Higgs states from phenomenology at lower energies [35] which is usually expected from the mass-suppression of propagators and the Appelquist-Carrazone decoupling theorem [36].

The Hierarchy Problem

Such a low mass value for the Higgs –as is needed for the correct mass generation of EW scale fermions and bosons– still poses the question of how the Higgs mass is not susceptible to the $\mathcal{O}(\Lambda^2_{\rm UV})$ (where $\Lambda_{\rm UV}$ is the scale up to which the SM is known or assumed to hold) radiative corrections that as a fundamental scalar field it should receive from the SM fields.

A mechanism to produce this robustness to radiative corrections must therefore be added to the SM[12], either in the form of a cutoff (as in extra dimensional theories), or a symmetry principle generating the cancellation of radiative corrections to all orders (as in Supersymmetry, which will be the topic of the later chapters of this thesis). This is known as the *hierarchy problem*. We will return to this issue in later sections of this thesis and describe a potential solution to it (in the context of Supersymmetry) in section 2.3.1.

2.1.3 The Neutral Current in the Standard Model

We will now focus on the Neutral Current (NC). We will not deal with the charged current, or the Higgs and Yukawa terms.

After EWSB we can further subdivide the electroweak sector into neutral current and charged current (CC) components

$$\mathcal{L}_{\rm EW} = \mathcal{L}_{\rm NC} + \mathcal{L}_{\rm CC} \tag{2.32}$$

In the SM the neutral current Lagrangian arises from the covariant derivatives in the fermionic term in equation 2.6b, and can be rearranged to show that it is the sum of the QED source term and that of the mass eigenstate formed after EWSB by mixing between the B^μ and the $W^{3\,\mu}$ gauge fields via an orthogonal

[12] This is the standard belief of most practitioners. In [37] it is argued that there is no such problem, as in the broken symmetry phase all the fermion and boson masses (the Higgs mass included) are proportional to $v^2(\mu^2)$ (note that the running of the vev is now considered), and hence should be expected to be of the same order. And in the unbroken phase the Higgs mass does indeed grow drastically but this does not pose a problem, and may even be preferrable for cosmological reasons.

transformation

$$\begin{pmatrix} A^\mu \\ Z^\mu \end{pmatrix} = \begin{pmatrix} \cos\theta_W & \sin\theta_W \\ -\sin\theta_W & \cos\theta_W \end{pmatrix} \begin{pmatrix} B^\mu \\ W_3^\mu \end{pmatrix} \tag{2.33}$$

where θ_W is the electroweak mixing angle, otherwise known as the Weinberg angle.

This then gives the neutral current as

$$\mathcal{L}_{\rm NC} = \mathcal{L}_{\rm QED\ source} + \mathcal{L}_{\rm Z\ source}\,, \tag{2.34a}$$

$$= e\, J^\mu_{\rm QED}\, A_\mu \,+\, g_Z J^\mu_{\rm Z}\, Z_\mu\,, \tag{2.34b}$$

where $g_Z = g_2/\cos\theta$ and the QED and Z currents are given by

$$J^\mu_{\rm QED} = \sum_{i=\text{charged fermions}} q_i\, \bar{f}_i\, \gamma^\mu\, f_i\,, \tag{2.35a}$$

$$J^\mu_{\rm Z} = \sum_{i=\text{fermions}} \bar{f}_i\, \gamma^\mu\, \left(g_{i_L}\, P_L \,+\, g_{i_R}\, P_R\right)\, f_i\,, \tag{2.35b}$$

where q_i denotes the electric charge (in units of the positron charge e).

The left- and right-handed couplings are

$$g_{L_i} = t_{3\,i_L} - q_i\, \sin^2\theta_W\,, \tag{2.36a}$$

$$g_{R_i} = t_{3\,i_R} - q_i\, \sin^2\theta_W\,, \tag{2.36b}$$

–but note that $t_{3\,i_R} = 0$ for all right-handed SM fields– and the chiral projection operators are defined as usual:

$$P_L = \frac{1}{2}\left(1 \,-\, \gamma^5\right)\,, \tag{2.37a}$$

$$P_R = \frac{1}{2}\left(1 \,+\, \gamma^5\right)\,, \tag{2.37b}$$

Here we will neglect any potential BSM contributions to the Z coupling, as are considered in [38] and which would introduce corrections of the form $g_{L/R} \to g_{L/R} + \delta g_{L/R}$ to the gauge couplings.

We will not deal with the QED current, that will be included in all results (as well as interferences between it and the other neutral gauge bosons) but we will not go beyond the SM in that sector [13]

2.1.4 Current Status of the SM

As of the time of writing all measurements performed at the LHC are in good agreement with the SM predictions, with no noteworthy discrepancies in any well-understood observables. Figure 2.3 shows the measured

[13] For an overview of extensions of the QED sector with new massless photon-like fields see for example [23].

total fully-inclusive cross sections for benchmark SM processes as measured by the CMS collaboration at the LHC (the ATLAS result is in similarly good agreement), as well as the pull between a global fit of SM parameters as performed by the GFITTER group and their experimentally measured values.

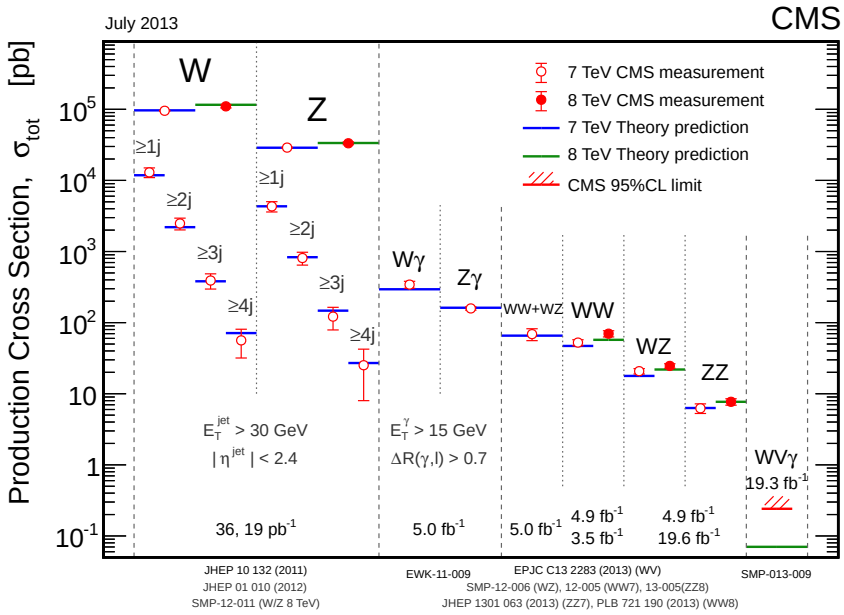

(a) Fully inclusive SM cross sections as measured by the CMS collaboration at the LHC (references in figure).

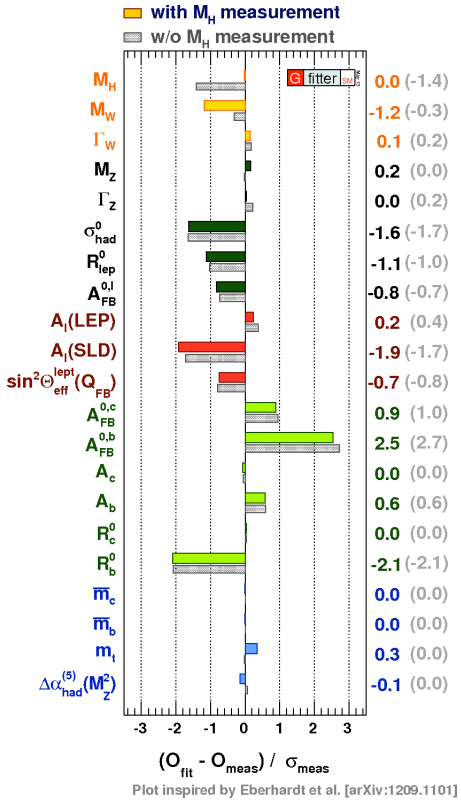

(b) Comparison of global fit of SM parameters to data and direct measurements [39].

Figure 2.3: The status of SM predictions versus measurements. Good agreement and consistency are seen everywhere.

2.2 $U(1)'$ Extensions of the Electroweak Sector

2.2.1 Grand Unified Theories

The Standard Model is now a mature, self-consistent and highly successful model. So successful in fact that no statistically significant deviation from it has been observed so far[14]. However the Standard Model is well known to be incomplete. It lacks a description of gravity (and therefore also dark energy), has no viable dark matter candidate (neutrinos are neutral and colourless but too light to be cold dark matter, as is currently favoured), and is missing a solution for the hierarchy problem described previously.

Additionally, though the Standard Model can be extrapolated up to arbitrarily high energies ($\mathcal{O}(M_{\rm pl})$) without a problem (the Landau pole of QED is above the Planck mass) the prospect of new fields existing in the unexplored 15 orders of magnitude in energy between the highest energies directly probed so far at a collider ($\mathcal{O}(10\ \mathrm{TeV})$) and the Planck scale ($\mathcal{O}(10^{19}\ \mathrm{GeV})$) is not unthinkable and perhaps more plausible than the alternative (the so-called *desert scenario*).

Even within the Standard Model there are at least 19 free parameters which must be measured and whose value cannot be computed from first principles (though their behaviour is well understood)[15]:

- 3 gauge couplings (for example in the gauge kinetic terms $F_{\mu\nu}F^{\mu\nu}$),
- the fermionic kinetic terms $i\overline{f}\not{D}f$ contain no free parameters once the gauge couplings are accounted for,
- 2 couplings from the Higgs sector: the Higgs mass, μ^2, and self-coupling, λ,
- 9 fermion Yukawa couplings (three from each of the up-type quarks, down-type quarks, and down-type leptons, excluding neutrino (up-type lepton) mass terms, whose form is presently unknown),
- 3 Cabibbo-Kobayashi-Maskawa (CKM) mixing angles and 1 phase,
- 1 coupling from the θ-term, namely, θ, the strong CP-violating coupling.

This gives a total of 19 parameters which must be measured. All other SM predictions are calculable from these parameters. It is a perfectly legitimate question to ask if these parameters may arise naturally from

[14] There are discrepancies, such as that observed in the anomalous magnetic moment of the muon, however these are not statistically significant (3.6σ for the muon magnetic moment [40]), and are still subject to theoretical uncertainties (in the case of the magnetic moment of the muon, the hadronic vacuum polarisation contribution, see [41, 42]) which upon clarification may yield full agreement with the SM.

[15] The inclusion of the neutrino sector would yield at least 3+1 more parameters from the corresponding Pontecorvo-Maki-Nakagawa-Sakata (PMNS) mixing matrix and 3 more Yukawa terms (or equivalent mass-related parameters).

a smaller set of parameters of a high energy theory, when its low energy limit is taken[16]. In particular the fermion masses and the hierarchies between them, the SM gauge group structure, the 3 generation structure of the fermions and their charges under the gauge groups, the mechanism via which neutrinos gain mass, the solution to the strong CP problem, the sizes of the mixing angles, etc.

To this end one may consider the viable options which offer an embedding of the SM, provide a consistent extension of it to arbitrarily high energies, yield testable predictions in the near future, and offer explanations for hitherto unexplained features of the Standard Model. These features may be the values for the masses of the quarks and leptons, values of the Yukawa couplings for the fermions, a solution for the strong CP problem, or, perhaps most simply: a unification of the gauge couplings.

This is precisely the aim of Grand Unified Theories (GUTs), which are theories in which the SM product gauge group structure is embedded into a single gauge group, with the gauge couplings unifying into this single gauge coupling at a scale $M_{\rm GUT}$.

We now overview the construction of the simplest GUT model and its embedding into more involved GUTs which form the context of the Z' models we analyse and will work with. For a standard treatment of the most minimal of the GUT models see [43].

The Minimal GUT: The Georgi-Glashow $SU(5)$ Model

The lowest rank group that can accommodate the gauge symmetry structure of the SM is the Georgi-Glashow model [44] where $SU(5)$ is posited as the unified gauge group, which undergoes Spontaneous Symmetry Breaking (SSB) (exactly like that of the Higgs mechanism responsible for EWSB) at a scale $M_{\rm GUT}$ to the SM gauge groups, $G_{\rm SM}$

$$SU(5) \underset{\text{SSB}(M_{\rm GUT})}{\longrightarrow} SU(3)_C \otimes SU(2)_L \otimes U(1)_Y \tag{2.38}$$

This is in fact the most minimal GUT, as $SU(5)$ is the smallest rank group in which the product of the SM gauge groups can be embedded[17]. As most GUTs use the Georgi-Glashow scheme, or in fact are extensions of it (such as the ones we will consider here), we will briefly review this model.

As argued in the original paper by Georgi and Glashow [44], out of the nine possible rank 4 groups, requiring that the SM gauge group structure be a subgroup, as well as demanding complex representations (as required for charge conjugate SM states), and demanding an acceptable value of $\sin^2\theta_W$ leaves $SU(5)$ as the only

[16] One could equally well argue that these parameters are purely environmental and that no explanation is needed, or postulate that they are a subset of possibilities from a multiverse, chosen via anthropic reasoning. We will not consider either of these.

[17] This can be seen from the fact an $SU(N)$ group has rank $N-1$ and the rank of a direct product of groups is the sum of their ranks. Therefore any embedding of the SM gauge groups must be at least of rank 4, which is precisely the rank of $SU(5)$.

viable rank 4 group.

Furthermore, to make $SU(5)$ a realistic possibility for a GUT representations of $SU(5)$ must be found which match the known SM field charges under G_{SM}, as stated in equation 2.2. This can indeed be done, and using the decomposition of the $\overline{\mathbf{5}}$ representation of $SU(5)$ under $SU(3) \otimes SU(2) \otimes U(1)$ (see [45] for details) we see that right-handed down-type quarks and left-handed leptons may be embedded in this representation

$$\overline{\mathbf{5}}: \quad \underbrace{\left(\overline{\mathbf{3}}, \mathbf{1}, \frac{2}{3}\right)}_{d_R^r,\, d_R^g,\, d_R^b} \oplus \underbrace{(\mathbf{1}, \mathbf{2}, -1)}_{e_L^-,\, \nu_e}, \tag{2.39}$$

where the r, g, b indices label the three elements of the fundamental representation of $SU(3)_C$.

This new multiplet structure of fermionic fields implies that the canonical normalisation constraint which states that for each representation the relation

$$\mathrm{Tr}(t^a t^b) = \frac{1}{2}\,\delta^{ab}\,, \tag{2.40}$$

must hold means the hypercharge of the fermionic fields must be adjusted to restore the correct normalisation for this new multiplet.

Redefining the Gell-Mann—Nishijima formula from $Q = t_3 + \frac{Y}{2}$ to $Q = t_3 + Y$ so that the hypercharge absorbs the factor of $1/2$ and changing our charge assignment of the SM right-handed fields to that of the (perfectly equivalent) charge-conjugated left handed fields (so that the colour and isospin representations of the right handed fields are conjugated and their hypercharge is multiplied by -1 relative to the charges for the right handed fields as stated in equation 2.2, as is customary in the formulation of GUTs), the $\overline{\mathbf{5}}$ representation now contains the following SM charges

$$\overline{\mathbf{5}}: \quad \underbrace{\left(\overline{\mathbf{3}}, \mathbf{1}, \frac{1}{3}\right)}_{d_R^r,\, d_R^g,\, d_R^b} \oplus \underbrace{\left(\mathbf{1}, \mathbf{2}, -\frac{1}{2}\right)}_{e_L^-,\, \nu_e}. \tag{2.41}$$

Using these hypercharges and solving for the normalisation correction factor, q, from

$$3\left(\frac{1}{3}\,q\right)^2 \;+\; 2\left(-\frac{1}{2}\,q\right)^2 \;=\; \frac{1}{2}\,, \tag{2.42}$$

gives $q = \sqrt{\frac{3}{5}}$, so that

$$g_1' = g_1\sqrt{\frac{3}{5}}\,, \tag{2.43}$$

and at the unification scale where $g_{i=1,2,3} = g_5$ and therefore $g_1'\sqrt{\frac{5}{3}} = g_5$

$$g_1' = \sqrt{\frac{3}{5}}\,g_5 \quad\Longleftrightarrow\quad g_5 = \sqrt{\frac{5}{3}}\,g_1'\,, \tag{2.44}$$

though from here on and for the rest of this chapter we will omit the prime and consider this variable the $U(1)$ coupling as is done in most of the relevant literature.

It is worth noting that this hypercharge correction factor is crucial to the unification of the couplings, not just in the $SU(5)$ model, but also in GUTs with larger unification gauge groups which contain $SU(5)$ as the final step in the symmetry-breaking pattern.

It is also this hypercharge normalisation which determines the $\sin^2\theta_W$ prediction of the theory. Evaluating the Weinberg–Salam electroweak model relation

$$\sin^2\theta_W = \frac{g_1^2}{g_1^2 + g_2^2}\,, \tag{2.45}$$

at the unification scale where

$$g_1 = g_2 = g_3 = g_5\,, \tag{2.46}$$

gives the well known result

$$\sin^2\theta_W = \frac{\frac{3}{5}\,g_5^2}{\frac{3}{5}\,g_5^2 + g_5^2} = \frac{3}{8} = 0.375\,. \tag{2.47}$$

Both the hypercharge correction factor and $\sin^2\theta_W$ were derived at the GUT scale and will be subject to renormalisation group (RG) running down to the electroweak or TeV scale which is being directly probed. For the weak mixing angle, at the electroweak scale it is found to give $\sin^2\theta_W = 0.204$ [46]. This is plainly incompatible with the measured (best fit) value of $\sin^2\theta_W^{\text{eff}} = 0.23150(10)$ [39]. This alone is enough to rule out the Georgi-Glashow $SU(5)$ model (though its rate of proton decay is also incompatible with the lower bound on the lifetime of the proton).

The $SU(5)$ gauge coupling, g_5, will also undergo RG running, however this effect has generally been found to be negligible even for more involved models [46] and is therefore generally neglected and its unification value of

$$g_5 = \sqrt{\frac{5}{3}}\,g_1\,, \tag{2.48}$$

is used for phenomenology at the electroweak and TeV scales as well.

The $\overline{\mathbf{5}}$ representation however contained only part of the fermionic fields of one generation. The rest of the matter fields can be placed in the $\mathbf{10}$ representation (once again using the $Q = t_3 + Y$ convention and the charge labelling for charge-conjugated left-handed fields instead of that of right-handed ones) as

$$\mathbf{10}: \quad \underbrace{\left(\mathbf{3},\mathbf{2},\frac{1}{6}\right)}_{u_L^r,\,u_L^g,\,u_L^b,\,d_L^r,\,d_L^g,\,d_L^b} \quad\oplus\quad \underbrace{\left(\overline{\mathbf{3}},\mathbf{1},-\frac{2}{3}\right)}_{u_R^r,\,u_R^g,\,u_R^b} \quad\oplus\quad \underbrace{(\mathbf{1},\mathbf{1},1)}_{e_R}\,. \tag{2.49}$$

This $\overline{\mathbf{5}} \oplus \mathbf{10}$ structure now contains a complete generation of the SM, and the same structure is replicated for the other two generations.

Anomaly Cancellation

We now know that $SU(5)$ can accommodate the SM gauge group structure and charges, however a further consistency check is required to ensure the theory is viable: anomaly cancellation. We will deal with this topic more fully in section 2.2.1, but for now we simply state that the most stringent of the conditions this imposes is that the hypercharges cubed of all the chiral fields as specified in equations 2.41 and 2.49 sums to exactly zero. Explicitly we have

$$A(\overline{\mathbf{5}}) = 3\left(\frac{1}{3}\right)^3 + 2\left(-\frac{1}{2}\right)^3 , \tag{2.50a}$$

$$A(\mathbf{10}) = 6\left(\frac{1}{6}\right)^3 + 3\left(-\frac{2}{3}\right)^3 + 1\,(1)^3 , \tag{2.50b}$$

so that the sum over all chiral fields gives

$$A(\mathbf{10}) + A(\overline{\mathbf{5}}) = \frac{5}{36} - \frac{5}{36} = 0\,, \tag{2.51}$$

as expected.

Symmetry Breaking and the Extended Gauge Sector

Note from the multiplet structure for fermions in equations 2.41 and 2.49 that quarks and leptons are included the same multiplet. So combining multiplets to form Lagrangian operators invariant under $SU(5)$ will produce operators which violate baryon and or lepton number[18]. Given that the adjoint representation of an $SU(N)$ group is of dimension $N^2 - 1$ and this determines the total number of gauge bosons present in the theory, for $SU(5)$ there are 24 gauge bosons. 12 of these are the SM gauge bosons (8 gluons, 3 EW bosons and the photon), and the other 12 are entirely new bosons (which we will generically denote by X or Y) which have a mass of the order of the scale M_{GUT} at which they become massive, and which themselves carry electric and colour charge. It is these gauge bosons which are responsible for mediating the baryon- and lepton-violating interactions and therefore also the new proton decay channels[19] (see figure 2.4).

It can be shown that these contributions induce proton decay at a rate which lowers its lifetime below the

[18] Another consequence of this is that given the new structure of the Yukawa terms the down-type quarks and leptons from the five dimensional representation arise from the same Yukawa term and must have the same mass at the GUT scale: $m_d = m_e$, $m_s = m_\mu$, $m_b = m_\tau$. Though these relations hold at the GUT scale, even after RG evolution down to electroweak scales they remain problematic.

[19] There may also be further contributions to proton decay from charged Higgs from the extended Higgs sector, but as these depend on the representation chosen for the Higgs, and such a choice is not unique, we do not include these.

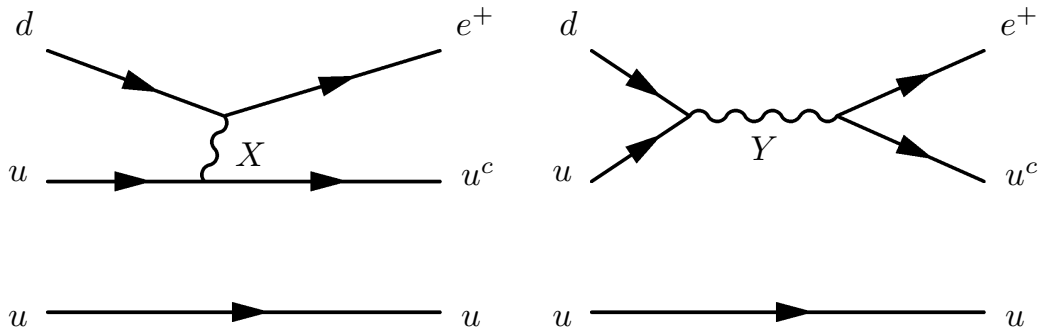

(a) The X-mediated tree level proton decay mode. (b) The Y-mediated tree level proton decay mode.

Figure 2.4: The $SU(5)$ $p \to \pi^0 e^+$ proton decay modes.

measured lower bound on it. It has been calculated that within the Georgi-Glashow model the proton lifetime is given by [46]

$$\tau_p^{SU(5)} \sim 5 \times 10^{32} \text{ yr}\,, \tag{2.52}$$

whereas the current lower bounds on the proton lifetime from Super-Kamiokande are almost all at least of the order of

$$\tau_p > 1 \times 10^{33} \text{ yr}\,. \tag{2.53}$$

This bound (along with the erroneous $\sin\theta_W$ prediction previously mentioned) rules out the minimal $SU(5)$ model as a candidate GUT[20].

As previously mentioned the new gauge boson states must be massive and with a mass of the order of M_{GUT} as this is the scale at which they acquire mass via spontaneous symmetry breaking. This added symmetry breaking step will require a further Higgs, with the representation of $SU(5)$ under which it transforms still to be determined.

In particular, we must construct the Higgs sector such that it can replicate the known EWSB of the Standard Model, and also add an additional Higgs to perform the GUT-scale spontaneous symmetry breaking. Comparing the required SM Higgs charges from equation 2.2 to the SM decomposition of $\overline{\mathbf{5}}$ stated in equation 2.41 (accounting for the change in the Gell-Mann—Nishijima formula to $Q = t_3 + Y$, so that for the SM Higgs $\phi:\ (\mathbf{1},\mathbf{2},1) \to (\mathbf{1},\mathbf{2},1/2)$) we see that the SM Higgs can be embedded into a $\mathbf{5}$, with the multiplet being completed by a triplet of new Higgs states charged as $(\mathbf{3},\mathbf{1},-1/3)$ under the SM (and therefore both coloured and electrically charged, with electric charge $1/3$). These new charged Higgs states must be made very massive

[20]Here, as with most GUT models different symmetry breaking patterns (leading to gauge group structures similar but not exactly like the SM one) and using larger representations for the Higgs can be used to suppress proton decay operators and evade bounds, however we will not consider any of these variants.

to avoid once again inducing proton decay and other deviations from the SM which have not been observed. This requirement of large mass separation between the $SU(2)_L$ Higgs required for EWSB and the $SU(3)_C$ triplet Higgs must be put in by hand or otherwise generated, and this issue is known as the *doublet-triplet splitting problem*.

At the GUT scale a further Higgs multiplet is needed to break the $SU(5)$ group into the SM gauge groups, and to provide a suitable mass for the new vector bosons such an enlarged gauge group entails. This can be accomplished minimally using a Higgs in the $\mathbf{24}$ representation of $SU(5)$. This choice is not unique, though it is the minimal one. Larger representations for this Higgs can be considered and lead to models with considerably different phenomenology and RG evolution. We will not discuss these issues in the present work.

We have finally that the full symmetry breaking pattern required for the minimal $SU(5)$ model as constructed by Georgi and Glashow is therefore of the form

$$SU(5) \quad \xrightarrow[\Psi(\mathbf{24})]{M_{\rm GUT}} \quad SU(3)_C \otimes SU(2)_L \otimes U(1)_Y \quad \xrightarrow[\phi(\mathbf{5})]{M_{\rm EW}} \quad SU(3)_C \otimes U(1)_Q \,, \tag{2.54}$$

where we have made explicit the scale of each symmetry breaking, as well as the Higgs required for it (and its representation under $SU(5)$).

Extended GUTs: $SO(10)$ and E_6

We have seen how the minimal GUT based on $SU(5)$ is ruled out by its prediction of $\sin\theta_W$, its generation of so far unobserved proton decay, and its prediction of mass relations between down-type quarks and charged leptons, which are not observed.

The next possible extension of this model is to consider its supersymmetric extension (we will discuss Supersymmetry in a later chapter). However this minimal SUSY $SU(5)$ is now also ruled out by the lower bound of the lifetime of the proton as measured in the $p \to K^+ \overline{\nu}$ channel by the Super-Kamiokande collaboration [47, 48].

The next option to obtain gauge coupling unification is to consider a larger (rank 5) anomaly-free unification group, such as $SO(10)$. This choice of group has the particularly attractive feature that a whole generation of the SM exactly fills a multiplet, in this case the $\mathbf{16}$ spinor representation of $SO(10)$, which decomposes under $SU(5)$ (to see it in terms of the structure we have already developed) as follows

$$\mathbf{16} \;\longrightarrow\; \mathbf{10} \;\oplus\; \overline{\mathbf{5}} \;\oplus\; \mathbf{1} \,, \tag{2.55}$$

with the singlet state now allowing for the inclusion of right-handed neutrinos, were they to exist[21].

[21] Recall that these right-handed neutrino states would be charged as $(\mathbf{1}, \mathbf{1}, 0)$ under the SM, and would therefore not interact with any of the known fields, apart from their negligible interaction through the Higgs.

In this case it is worth considering whether $SO(10)$ can itself arise from known ultraviolet (UV) completions of the SM, or if the SM gauge group structure can be otherwise obtained from even larger groups posited at energy scales many orders of magnitude larger than the weak scale.

Both scenarios are indeed possible, and the two best known and most studied forms of these models will be outlined below (and can be shown to be equivalent [49]).

The next largest anomaly-free group in which we can embed $SO(10)$ is the exceptional group E_6. This group is the gauge group of ten dimensional string theory which starts with an $E_8 \otimes E_8$ gauge group. One possibility is that one of the E_8 groups is decoupled as it interacts only gravitationally, and the other one can break to $E_6 \otimes SU(3)$ upon compactification. This model was once thought to be unique and hence E_6 as the GUT group was thought to be a unique prediction from these models, and this was the main motivation for their study.

However, this has been found to no longer be a unique option, but is still an important benchmark for phenomenology as for a large class of these models regardless of the exact symmetry breaking pattern (and mechanism: Higgs or Stückelberg), will involve breaking from a rank 6 group (E_6) group to the rank 4 product group of the SM.

The possible UV completions and models from which an extra Abelian group may arise are numerous and are beyond the scope of this study, for a comprehensive review of them see [49]. An additional $U(1)$ local symmetry arising in string-inspired supersymmetric constructions may be used to suppress rapid proton decay from baryon and lepton number violating operators in the superpotential via the gauge invariance it imposes instead of the conventional approach of using R-parity [50]. Such a Z' is distinct from the E_6 variants we will consider, but is a sign of how ubiquitous $U(1)'$ gauge groups can be in ultraviolet completions of the SM.

In terms of E_6 representations we now fill a $\mathbf{27}$ representation of E_6 by decomposing this representation in terms of $SO(10)$ representations, like the one stated in equation 2.55

$$\mathbf{27} \longrightarrow \mathbf{16} \oplus \mathbf{10} \oplus \mathbf{1}\,, \tag{2.56}$$

where the $\mathbf{16}$ contains a generation of SM fermions, while the other multiplets contain entirely new fields (see table 2.2).

Starting from E_6 there are a variety of symmetry breaking patterns possible. For concreteness we will

focus on the following one:

$$E_6 \longrightarrow SO(10) \otimes U(1)_\psi \,, \tag{2.57a}$$

$$\longrightarrow SU(5) \otimes U(1)_\chi \otimes U(1)_\psi \,, \tag{2.57b}$$

$$\longrightarrow G_{\rm SM} \otimes U(1)_\chi \otimes U(1)_\psi \,. \tag{2.57c}$$

We will neglect other possible symmetry breaking patterns such as the left-right symmetric model ($SU(3)_C \otimes SU(2)_L \otimes SU(2)_R \otimes U(1)_L \otimes U(1)_R$) which gives rise to new fields such as W_R. We will not discuss these, and indeed the mass of W_R fields is already constrained to be $M_{W_R} > 1 - 2$ TeV by constraints from the $K_L - K_S$ mass difference [51].

In fact the scenario we have chosen can be further simplified for phenomenological purposes if we consider linear combinations of the two Abelian groups generated by the symmetry breaking, such that we assume one of the two generated gauge bosons is assumed to be much more massive and therefore decoupled. This will indeed be the case if each symmetry breaking (via which the new gauge bosons also acquire a mass of the same order as the breaking scale) happens at different scales, with at least one of them happening at a scale near the GUT scale and therefore being effectively decoupled from phenomenology at the TeV scale, such that we effectively have

$$U(1)_\chi \otimes U(1)_\psi \longrightarrow U(1)_{\theta_{E_6}} \,. \tag{2.58}$$

We have thus obtained a single new gauge boson and reduced the rank of our gauge theory by one unit, from the original rank of 6, to rank 5. These are known as Effective rank-5 Models (ER5M) and are the most wieldy and best studied models for phenomenology, and will be the focus of our study.

Thus in general at the weak scale gauge groups which arise in string constructions can break to give the group structure

$$G_{\rm SM} \times U(1)^n \tag{2.59}$$

where $n \geq 1$ and $G_{\rm SM}$ was defined in equation 2.1.

The models we will consider have $n = 2$, though we will consider linear combinations of the two $U(1)$s, which in two limits (the ψ and χ models) effectively decouple one of the two extra bosons and leave us to consider the $n = 1$ case, with couplings that are a linear combination of those of the two new Abelian groups.

Anomalies

Upon quantisation of any quantum field theory the conserved Nöether currents of the theory which arise from the demand that the action (and therefore the Lagrangian) remain invariant under infinitesimal transformations of the fields (usually from a gauge transformation, e.g. for a $U(1)$, $\phi \to e^{-i\alpha(x^\mu)}$, such that infinitesimally, $\delta\phi = -i\alpha(x^\mu)$) which is defined as

$$j^\mu(x) = \sum_i \frac{\partial \mathcal{L}(x)}{\partial(\partial_\mu \phi_i(x))}\, \delta\phi_i(x)\,. \tag{2.60}$$

These currents receive quantum corrections from triangle diagrams (figure 2.5) which involve a sum over all the possible gauge bosons of the the theory at the vertices, and all the fermionic fields they couple to in the loop[22].

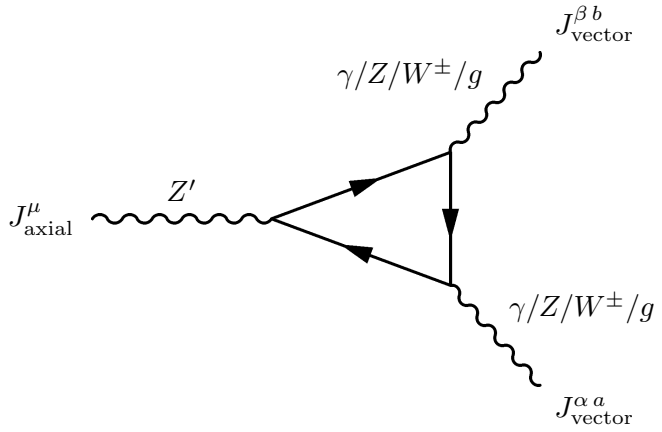

Figure 2.5: A triangle diagram from which the anomaly condition can be calculated. One vertex is the axial current of the Z', $J^\mu_{Z'\ axial} = \sum_{\rm fermions} Q_{Z'\,\rm axial}(f_i)\, \bar{f}_i\, \gamma^\mu\, \gamma^5\, f_i$ and the others can be any of the SM gauge bosons, e.g. $J^\alpha_{\gamma\ \rm vector} = \sum_{\rm charged\,fermions} Q(f_i)\, \bar{f}_i\, \gamma^\alpha\, f_i$.

If these contributions do not vanish, current conservation is spoiled $\partial_\mu j^\mu(x) \neq 0$ and the symmetry and all conservation laws derived from it have been spoiled. This is known as an Adler-Bell-Jackiw anomaly and will typically take the form

$$\partial_\mu j^\mu(x) \;\propto\; g^2\,(\text{group factors})\,\epsilon_{\mu\nu\alpha\beta} F^{\mu\nu} F_{\alpha\beta}\,. \tag{2.61}$$

For global symmetries this is not necessarily a hindrance and can in fact be required (e.g. to allow for the non-zero rate of the decay $\pi^0 \to \gamma\gamma$). However, for local symmetries such as gauge transformations anomalies imply the appearance of negative-norm states and loss of renormalisability which render the theory unviable [53].

[22] It can be shown that higher order corrections do not contribute, this is the Adler-Bardeen theorem [52].

The simplest way for the anomaly in equation 2.61 to vanish identically is for the group factors to be zero. In computing the triangle diagram these group factors arise in the form

$$\sum_{f_L} \mathrm{Tr}\left[t_i^a\{t_i^b, t_i^c\}\right] \; - \sum_{f_R} \mathrm{Tr}\left[t_j^a\{t_j^b, t_j^c\}\right] \,, \tag{2.62}$$

where the indices i and j run over the left- and right-handed fermions, respectively, and the generators are the generators of whichever gauge boson is attached to each of the three vertices (with the one labelled a being the one involving axial couplings, if present).

We see that anomalies may arise for any chiral theory (like the SM) where the left- and right-handed components of given fields transform differently under any of the gauge groups.

In the SM there are thus 10 possible assignments of the three gauge groups to the three vertices. However, most of these (such as the $SU(3)_C^3$ case) will cancel as both chiral components of fermions transform under the same representation under them.

The most constraining anomaly cancellation condition turns out to be the $(U(1)_Y)^3$ case. Here it is remarkable that for the SM for example the quark and lepton hypercharge assignments lead to the desired cancellation

$$\begin{aligned}\sum_{f_L} Y^3 - \sum_{f_R} Y^3 &= \left(3Y(u_L)^3 \; + \; 3Y(d_L)^3 \; + \; Y(l_L)^3 \; + \; Y(\nu_L)^3\right) \\ &\quad - \; \left(3Y(u_R)^3 \; + \; 3Y(d_R)^3 \; + \; Y(l_R)^3\right) \qquad (2.63) \\ &= 0\,. \qquad (2.64)\end{aligned}$$

However, such a requirement will not necessarily be met by any extension of the Standard Model's field or gauge group content and is a strong constraint on such models. We will only deal with models where this cancellation occurs.

Computing the pure $U(1)'^3$ anomaly using the charges laid out in table 2.3 we see that this anomaly indeed vanishes when summing over the SM fields

$$\sum_{f_L} Q_\chi(f_i)^3 \; - \sum_{f_R} Q_\chi(f_j)^3 = \left(\frac{1}{2\sqrt{10}}\right)^3 (48-48) = 0\,, \tag{2.65a}$$

$$\sum_{f_L} Q_\psi(f_i)^3 \; - \sum_{f_R} Q_\psi(f_j)^3 = \left(\frac{1}{2\sqrt{6}}\right)^3 (8-8) = 0\,. \tag{2.65b}$$

Exotics

In E_6 models all fermions are placed in the fundamental $\mathbf{27}$ of E_6, which is then decomposed as follows

$$\begin{aligned} E_6 \quad &\longrightarrow \quad SO(10) \quad \longrightarrow \quad SU(5) \\ \mathbf{27} \quad &\longrightarrow (\mathbf{16}+\mathbf{10}+\mathbf{1}) \longrightarrow (\mathbf{10}+\overline{\mathbf{5}}+\mathbf{1})+(\mathbf{5}+\overline{\mathbf{5}})+\mathbf{1}\,. \end{aligned} \tag{2.66}$$

This structure is imposed on each of the SM generations, such that each generation of SM fermions is embedded into a $\mathbf{16}$ irreducible representation of $SO(10)$, which is further decomposed into a $\mathbf{10}+\overline{\mathbf{5}}+\mathbf{1}$ of $SU(5)$ as follows

E_6	$SO(10)$	$SU(5)$	Fields
$\mathbf{27}$	$\mathbf{16}$	$\mathbf{10}$	q_L, u_R, e_R
		$\overline{\mathbf{5}}$	d_R,ν_L,e_L
		$\mathbf{1}$	ν_R
	$\mathbf{10}$	$\mathbf{5}$	D,L^c
		$\overline{\mathbf{5}}$	D^c,L
	$\mathbf{1}$	$\mathbf{1}$	S

Table 2.2: Embedding of fermions in E_6 models.

Where, for example, the $\overline{\mathbf{5}}$ representation containing SM fields is filled by $d_R^{\rm red}, d_R^{\rm green}, d_R^{\rm blue}, \nu_L, e_L$. Note however that the further $\mathbf{10}_{SO(10)} \to (\mathbf{5}+\overline{\mathbf{5}})_{SU(5)}$ contains new BSM fields, which are referred to collectively as *exotics*, and that all the fields within the same representation of $SU(5)$ have the same charges Q_χ and Q_ψ.

Out of these new fields, ν_L^c and S are singlets under the SM gauge groups (ν_L^c can be taken to be the right handed neutrino), but not under $U(1)'$, D are colour-triplet, isospin-singlet exotic quarks with electric charge $-1/3$, and L are isospin doublets with hypercharge $y(L)=1$, $y(L^c)=-1$, which in supersymmetric incarnations of E_6 models the superfields of these fields can be taken to be the H_u and H_d superfields of the MSSM, and the rest of their component fields are exotic leptons and scalars.

We will assume these fields to be kinematically inaccessible to Z' decays and hence make no contribution to the Z' width (for a table specifying the charges —and hence the couplings— of these exotic fields under the new Abelian group for a variety of different models, see for example [54]). Note, however that allowing any of these fields to have a mass smaller than $m_{Z'}/2$ can reduce the Z' branching fraction to SM leptons, and hence limit the reach of our searches in the dileptonic channel, thereby reducing current exclusion limits and requiring new experimental analyses. Given the unknown masses of these fields (should they exist), we will neglect them to reduce the number of unknown parameters in our model.

Mass Generation for the Z'

The Higgs mechanism is not the only way gauge bosons can become massive, for Abelian gauge bosons the Stückelberg mechanism can also provide a way to dote the gauge boson with mass (see [22] for a review) and such a mechanism indeed arises in string theory constructions[23].

However assuming the Z' sector mimics the Higgs mechanism known to hold within the SM, in supersymmetric forms of E_6 models the scalar components of the SM-singlet ν_L^c and S superfields can be given a vev to break the $U(1)'$ symmetry and make the Z' massive.

The exact symmetry breaking mechanism used to break the $U(1)'$ and yield a massive Z' is a complex topic (see [56] for a review focussing on supersymmetric forms of the models) and we will only assume that the Z' acquires a mass via spontaneous symmetry breaking when a scalar field in an extended Higgs sector acquires a vev, and we otherwise not deal with the exact mass generation mechanism for the Z'.

We will not consider Z' models with Stückelberg mass generation of the form proposed e.g. [57,58]. However these could in principle easily be implemented by adapting the corresponding couplings in equation 2.67.

2.2.2 E_6 and Effective Rank 5 Models

At the weak scale the end result of these models is that the neutral current Lagrangian is modified and acquires one or more source terms from the gauge fields of the extended symmetry group, such that equation 2.34b is extended to

$$\begin{aligned}
\mathcal{L}_{\rm NC} &= g_Z\, J_Z^\mu\, Z_\mu \;+\; g_{Z'}\, J_Z'^\mu\, Z'_\mu\,, \\
&= \frac{g_2}{\cos\theta_W}\, J_Z^\mu\, Z_\mu \;+\; \sqrt{\frac{5}{3}}\, g_1\, J_Z'^\mu\, Z'_\mu\,, \\
&= -i\frac{g_2}{\cos\theta_W} \sum_i \bar{f}_i \gamma^\mu \left[t_{i\,3} - q_i \sin^2\theta_W\right] f_i Z_\mu \\
&\quad - i\sqrt{\frac{5}{3}}\, g_2\, \tan\theta_W \sum_i \bar{f}_i \gamma^\mu \left[Q_\psi \sin\theta_{E_6} + Q_\chi \cos\theta_{E_6}\right] f_i Z'_\mu\,,
\end{aligned} \tag{2.67}$$

where g_Z is the usual prefactor for the Z current coupling,

$$g_Z = \frac{g_2}{\cos\theta_W}\,, \tag{2.68}$$

[23] Note that making the $U(1)'$ gauge massive also inhibits the sort of charge shifts that can occur in fermions charged under two unbroken $U(1)$ groups [55].

and the new coupling introduced for the Z' couplings, $g_{Z'}$, is defined as[24]

$$g_{Z'} = \sqrt{\frac{5}{3}} g_1 \; = \; \sqrt{\frac{5}{3}} \frac{e}{\cos\theta_W} \; = \; \sqrt{\frac{5}{3}}\, g_2 \, \tan\theta_W \tag{2.69}$$

$$\sim 0.46\,, \tag{2.70}$$

and the angle θ_{E_6} is the linear combination of $U(1)$ charges which results from the breaking described in equation 2.58. θ_{E_6} is a free parameter in $[-\pi/2, \pi/2]$ and the cases $\theta_{E_6} = 0, \pi/2$ respectively correspond to the benchmark χ and ψ models, which are models with only one extra $U(1)$ group each, as sketched in equations 2.57b and 2.57c. The Q_ψ and Q_χ charge assignments of the SM fields are as shown in table 2.3[25]. [61–63]

$g_{i,L/R}$	χ	ψ
g_{ν_L}	$\frac{3}{2\sqrt{10}}$	$\frac{1}{2\sqrt{6}}$
g_{ν_R}	$-\frac{5}{2\sqrt{10}}$	$\frac{1}{2\sqrt{6}}$
g_{e_L}	$\frac{3}{2\sqrt{10}}$	$\frac{1}{2\sqrt{6}}$
$g_{e_L^c}$	$-\frac{1}{2\sqrt{10}}$	$\frac{1}{2\sqrt{6}}$
g_{q_L}	$-\frac{1}{2\sqrt{10}}$	$\frac{1}{2\sqrt{6}}$
$g_{u_L^c}$	$-\frac{1}{2\sqrt{10}}$	$\frac{1}{2\sqrt{6}}$
$g_{d_L^c}$	$\frac{3}{2\sqrt{10}}$	$\frac{1}{2\sqrt{6}}$
$\frac{\Gamma_{Z'}}{M_{Z'}}$	0.012	0.006

Table 2.3: E5RM Z' widths and couplings of the Z' to the SM fermions.

We must of course also extend the SM gauge kinetic terms in equation 2.6a (after EWSB and with canonical gauge kinetic terms restored) with the new contribution

$$\mathcal{L}_{\text{Gauge}} = \mathcal{L}^{\text{SM}}_{\text{Gauge}} \; - \; \frac{1}{4} Z'^{\mu\nu} Z'_{\mu\nu}\,, \tag{2.71}$$

so that the most general renormalisable weak scale EW Lagrangian after EWSB (and the Z' has also acquired a mass via a scalar acquiring a vev in an extended Higgs sector) is

$$\mathcal{L}_{\text{EW+Z}'} = \mathcal{L}_{\text{SM}} + \mathcal{L}_{\text{Z}'} + \mathcal{L}_{\text{Mix}} \tag{2.72}$$

[24] As noted previously in section 2.2.1 this definition of the unified gauge coupling holds at the unification scale, however its running down to the TeV scale has been found to be a small effect (though the running of fermion masses in $SO(10)$ models for example is known to not be negligible [59]) and is customarily neglected.

[25] There also exist models where all the SM fermions are uncharged under $U(1)'$, where the Z' couples to the SM only via a higher-dimensional operator involving a BSM mediator [60], which we will not consider here.

where

$$\mathcal{L}_{\rm SM} = -\frac{1}{4}W^{a\,\mu\nu}W_{a\,\mu\nu} - \frac{1}{4}B^{\mu\nu}B_{\mu\nu} + \frac{1}{2}m_Z^2 Z^\mu Z_\mu + \mathcal{L}_{\rm Z\ int}\,, \tag{2.73a}$$

$$\mathcal{L}_{\rm Z'} = -\frac{1}{4}Z'^{\mu\nu}Z'_{\mu\nu} + \frac{1}{2}m_{Z'}^2 Z'^\mu Z'_\mu + \mathcal{L}_{\rm Z'\ int}\,, \tag{2.73b}$$

$$\mathcal{L}_{\rm Mix} = -\frac{\sin\chi}{2}\hat{Z}'^{\mu\nu}\hat{B}_{\mu\nu} + \delta m^2 Z'^\mu Z_\mu\,, \tag{2.73c}$$

and the interaction terms $\mathcal{L}_{\rm Z\ int}$ and $\mathcal{L}_{\rm Z'\ int}$ are as given in equation 2.67.

The operators in $\mathcal{L}_{\rm SM}$ and $\mathcal{L}_{\rm Z'}$ we have previously defined and form the intuitive set of operators to be written down for any Z' extension. However it is the terms in

$$\mathcal{L}_{\rm Mix} = \mathcal{L}_{\rm Kinetic\ mixing} + \mathcal{L}_{\rm Mass\ mixing} \tag{2.74a}$$

$$= -\frac{\sin\chi}{2}\hat{Z}'^{\mu\nu}\hat{B}_{\mu\nu} + \delta m^2 Z'^\mu Z_\mu \tag{2.74b}$$

which require further explanation, and it is these terms on which we shall focus below.

Kinetic Mixing

Kinetic mixing is a feature of any gauge theory containing a group structure of the form

$$U(1)_1 \otimes U(1)_2\,, \tag{2.75}$$

with the possibility of including even more $U(1)$ factors. In our case at the weak scale we have

$$U(1)_Y \otimes U(1)_{\theta_{E_6}}\,, \tag{2.76}$$

where the first group is that of the SM hypercharge, and the second one is the one corresponding to the new gauge boson, as defined in equation 2.58.

Since $U(1)$ field strength tensors are by themselves gauge invariant[26], a term formed by performing a Lorentz contraction between the field strength tensors of the two $U(1)$'s is Lorentz invariant, gauge invariant and a marginal operator, which is admissible and must be considered.

Also note that even if we chose to set the coefficient of this operator to zero at a given scale higher than the weak scale, renormalisation group (RG) running can generate it at lower scales [64]. So this operator must be considered if one is to work in full generality.

The operator of interest here is then

$$\mathcal{L}_{\rm Kinetic\ mixing} = -\frac{\sin\chi}{2}\,\hat{Z}'^{\mu\nu}\hat{B}_{\mu\nu}\,, \tag{2.77}$$

where the form of the coefficient is chosen for later convenience and the field tensors are defined as usual as

[26] Note that this holds only for Abelian gauge groups.

$\hat{Z'}^{\mu\nu} = \partial^\mu Z'^\nu - \partial^\nu Z'^\mu$ and $\hat{B}_{\mu\nu} = \partial_\mu B_\nu - \partial_\nu B_\mu$, but we have added a hat to the variables to distinguish them from the fields we will obtain after rotating to yield canonical gauge kinetic terms.

If we then consider all the gauge kinetic terms of the $U(1)$ fields

$$-\frac{1}{4}\hat{Z'}^{\mu\nu}\hat{Z'}_{\mu\nu} \; - \; \frac{1}{4}\hat{B}^{\mu\nu}\hat{B}_{\mu\nu} \; - \; \frac{\sin\chi}{2}\hat{Z'}^{\mu\nu}\hat{B}_{\mu\nu}\,. \tag{2.78}$$

Following [65] we perform a linear transformation of the form

$$\begin{pmatrix} \hat{B}_\mu \\ \hat{Z'}_\mu \end{pmatrix} = \begin{pmatrix} 1 & -\tan\chi \\ 0 & 1/\cos\chi \end{pmatrix} \begin{pmatrix} B_\mu \\ Z'\mu \end{pmatrix}. \tag{2.79}$$

Each of the terms transforms as

$$-\frac{1}{4}\hat{B}^{\mu\nu}\hat{B}_{\mu\nu} \longrightarrow -\frac{1}{4}(B^{\mu\nu} - \tan\chi\, Z'^{\mu\nu})(B_{\mu\nu} - \tan\chi\, Z'_{\mu\nu})\,, \tag{2.80}$$

$$-\frac{\sin\chi}{2}\hat{Z'}^{\mu\nu}\hat{B}_{\mu\nu} \longrightarrow -\frac{\tan\chi}{2}\, Z'^{\mu\nu}(B_{\mu\nu} - \tan\chi\, Z'_{\mu\nu})\,, \tag{2.81}$$

$$-\frac{1}{4}\hat{Z'}^{\mu\nu}\hat{Z'}_{\mu\nu} \longrightarrow -\frac{1}{4\cos^2\chi}Z'^{\mu\nu}Z'_{\mu\nu}\,, \tag{2.82}$$

Such that collecting terms and recognising a trigonometric identity the canonical form of the gauge kinetic terms is restored,

$$-\frac{1}{4}Z'^{\mu\nu}Z'_{\mu\nu} \; - \; \frac{1}{4}B^{\mu\nu}B_{\mu\nu}\,. \tag{2.83}$$

However this transformation must be performed in the whole Lagrangian, implying that fermions which initially had no coupling to the Z' will now have acquired a coupling to it, as $\hat{B}_\mu \to B_\mu - \tan\chi\, Z'_\mu$, and the initial couplings of the Z' will be rescaled as $\hat{Z'}_\mu \to \frac{1}{\cos\chi}Z_\mu$. Thus in the presence of kinetic mixing, even if the SM fields are uncharged under the new Abelian group, they may still couple to it if kinetic mixing is non-negligible. However, in the supersymmetric E_6 models (E6SSM) even considering the case where mixing between all three U(1)s is allowed, the impact on dileptonic rates at the LHC is negligible [66][27].

After rotating to the mass basis kinetic mixing will also impact on the masses of both the SM Z and the Z'. However for the E_6 models we consider such mixing has been found to be very small [56] and indeed we will deem it negligible (as is also conventionally done).

Mass Mixing

Given that we have inserted a new gauge boson we must consider the possibility that the measured eigenstate of the SM Z, and indeed the mass eigenstate of the Z' no longer coincide with the gauge eigenstates, but

[27] The general treatment of kinetic and mass mixing between three $U(1)$ groups is given in [67]

rather are mixtures of them.

In this case the mass eigenstates $m_{Z_{1,2}}$ are no longer $m_{Z,Z'}$, but are instead given by a matrix with non-zero off-diagonal terms

$$\frac{1}{2}\begin{pmatrix} Z^\mu & Z'^\mu \end{pmatrix}\begin{pmatrix} m_Z^2 & \delta m^2 \\ \delta m^2 & m_{Z'}^2 \end{pmatrix}\begin{pmatrix} Z_\mu \\ Z'_\mu \end{pmatrix}, \tag{2.84}$$

such that rotating by an angle θ the two mass eigenstates are linear combinations of the Z and Z' states. This would lower the mass of the Z and from EW fits (in particular the know mass of the SM Z) it can be deduced that $\sin\theta < 0.01$ [68] for all the models considered. This was later found to be even smaller, and largely sub permille [69].

This rotation would also impact on the couplings of the Z', however since for the models we will consider the rotation is constrained to be negligible by EW precision fits to the Z mass, its impact on the couplings will be minute and we will neglect it. Indeed fits to EW precision data can be used to place model-dependent lower bounds on $m_{Z'}$, as has been done in [69].

Z' Width

The leading order (LO) Z' width to fermions is given by

$$\Gamma(Z(Z'))_\alpha \longrightarrow f_i\overline{f}_i) = \frac{g_{Z(Z')}^2 C_F M_{Z(Z')}}{24\pi}\left[(g_{i,L}^{Z(Z')})^2 + (g_{i,R}^{Z(Z')})^2\right] \tag{2.85}$$

where we have neglected the fermion masses and g_Z and $g_{Z'}$ are as defined in equation 2.67 [28].

For all E5RM Z' models the width is found to be 0.5-1.3% of the resonance mass [61]. The Narrow Width Approximation (NWA) whereby the propagator of the resonance can approximated (as long as $\Gamma \ll m$) by[29]

$$\begin{aligned}\frac{1}{(p^2-m^2)^2+m^2\Gamma^2} &= \left(\int_{-\infty}^{\infty} dp^2\,\frac{1}{(p^2-m^2)^2+m^2\Gamma^2}\right)\delta(p^2-m^2) + \mathcal{O}\left(\frac{\Gamma}{m}\right) \\ &\approx \frac{\pi}{m\Gamma}\,\delta(p^2-m^2)\end{aligned} \tag{2.86}$$

is hence applicable to these models, though we will make no use of it and use the full propagator for the Z' (in the fixed-width scheme, see appendix B.1).

[28] Note that for decays to leptons we must take $C_F \to 1$, whereas this is the Casimir of the fundamental representation of $SU(3)$, $c_F = \frac{N_C^2-1}{2N_C}$, such that $C_F = N_C = 3$ for decays to quark, anti-quark pairs.

[29] For the full form of the expansion in equation 2.86 and a discussion of how when the production or decay processes have a strong p^2 dependence relative to the propagator the neglected contributions are not actually $\mathcal{O}\left(\frac{\Gamma}{m}\right)$ but can be larger, see [70].

γ-Z-Z' Interference

For the dominant dileptonic final states we will be interested in there are six possible bosons which could mediate the interaction: γ, Z, Z', $W^{\pm}$ and h, where h is taken to be the SM Higgs boson with $m_h \approx 125\ \mathrm{GeV}$.

From these we will however neglect the Higgs-mediated contribution as the Higgs coupling to fermions goes as m_f/v, which will hence yield a minuscule contribution when coupling to the dominant u and d type valence quarks of the proton.

The $W^{\pm}$ diagrams will also not be considered and we will not consider dijet final states for the Z' as they are subject to larger –and harder to model, typically requiring side-band analysis techniques[30] in addition to Monte Carlo simulations– SM backgrounds and more involved NLO QCD corrections. We also don't consider the 1 lepton + $\not{p}_T$ final state as FCNC constraints (from $K^0 - \bar{K}^0$ mixing and μ-e conversion in muonic atoms) exclude Z' couplings which are non-diagonal in flavour space up to very high scales, at least for the first two generations [71]. This implies the $W^{\pm}$ channel does not need to be considered. The remaining γ, Z and Z' all contribute to the $e^{\pm}e^{\mp}$, $\mu^{\pm}\mu^{\mp}$ and $\tau^{\pm}\tau^{\mp}$ final states, and must be considered.[31]

We include these contributions adding them coherently, and thus including all the relevant terms, so that the Born contribution is given by

$$|\mathcal{M}_{pp\longrightarrow ll}|^2 = |\mathcal{M}_{pp\to\gamma\to ll} \ + \ \mathcal{M}_{pp\to Z\to ll} \ + \ \mathcal{M}_{pp\to Z'\to ll}|^2 \tag{2.87}$$

The interference terms between diagrams with different mediators must be included and have in fact been found to be important for model discrimination should a discovery be made [54].

Current Z' Limits

Combining the most recent results from ATLAS [72] and CMS [73] on searches for high mass dileptonic resonances, the current 95 % C.L. exclusions on E5RM Z' models are shown in table 2.4.

Model	Mass (TeV)
Z'_{SSM}	2.86 (ATLAS)
Z'_{ψ}	2.38 (ATLAS)
Z'_{χ}	2.54 (ATLAS)

Table 2.4: Combination of most recent LHC lower bounds on Z' mass.

[30] This involves taking assuming Monte Carlo event generation can accurately predict the shape of the differential distribution in question, and fitting the normalisation to a control region where no BSM signal is expected, and then extrapolating the resulting background contribution to the signal region.

[31] We do not consider the $\bar{\nu}\nu$ final state. With the inclusion of a jet this would yield the LO contribution to the monojet + $\not{p}_T$ channel but we have not considered this scenario, though this process is included in our implementation and will be the focus of a future work.

The ATLAS limits are more stringent as they used an integrated luminosity of $20\ \mathrm{fb}^{-1}$ taken at 8 TeV whereas CMS have combined data sets of $5.3\ \mathrm{fb}^{-1}$ and $4.1\ \mathrm{fb}^{-1}$ taken at 7 and 8 TeV, respectively. The expected discovery reach for these models is $4-5\ \mathrm{TeV}$ at a $\sqrt{s}=14\ \mathrm{TeV}$ LHC with $100\ \mathrm{fb}^{-1}$ [74], as the Z' production and dileptonic rate falls off steeply with increasing $m_{Z'}$.

Additionally the effect of a Z' on precision EW fits can also be used to provide a lower bound on the mass of Z' models. Such a fit has been performed [68] and the 95% C.L. lower bounds for the models we consider were

Model	Mass (TeV)
Z'_ψ	1.181
Z'_χ	1.368

Table 2.5: EW fit lower bounds on Z' mass.

For a recent analysis of model-independent limits on Z' couplings from the $8\ \mathrm{TeV}$ LHC run see [75]. For $m_{Z'}=1\ \mathrm{TeV}$ the quark and leptonic couplings of the Z' were expected to be potentially determined to within $10-20\%$ at a $\sqrt{s}=14\ \mathrm{TeV}$ LHC with $100\ \mathrm{fb}^{-1}$, while some model discrimination may be possible (from the forward-backward asymmetry and rapidity ratios) for $m_{Z'}\approx 2\ \mathrm{TeV}$, whilst for $m_{Z'}\approx 3\ \mathrm{TeV}$ little more than discovery is feasible [74].

Z' models where hadronic decays are dominant also exist and have been searched for at the LHC, with a focus on couplings to third generation quarks, and using both conventional and jet substructure techniques [76]. The NLO corrections to these channels are also known [77, 78] but we will not focus on these as they have a larger singularity structure and tend to have smaller signal to background ratios.

For a comprehensive compilation of existing limits on Z' models see the 'Searches for Heavy Bosons Other Than Higgs Boson' section of the latest edition of the Review of Particle Physics by the Particle Data Group [40]. For a Bayesian analysis of limits on Z' models from LEP 2, CDF, and projected limits for LHC data, see [54].

If the Z' is assumed to be massive enough to be outside the kinematic reach of the LHC and integrated out into a dimension 6 operator of the form $\frac{C}{\Lambda^2}(\bar{q_L}\gamma^\mu q)(\bar{l_L}\gamma_\mu l)$ then Electroweak Precision Data (EWPD) can be used to constrain $\frac{C}{\Lambda^2}\in[-0.012, 0.055]$ at the 95% C.L. [79].

Theory Assumptions

From the point of view of the E5RM models the following assumptions are implicitly made in most of the literature of their phenomenology, and we make them here as well, but explicitly state them here for complete-

ness:

- Universal couplings. For Z' masses less than about 100 TeV its couplings must be generation-independent to be consistent with constraints on flavour changing neutral currents (FCNCs).
- No mass mixing. The $Z - Z'$ mass mixing angle is constrained by EW fits and has been constrained to be negligible.
- There are no new particles lighter than the Z' which it could decay into, that is, the Z' is only allowed to decay via SM modes, cascades involving exotic states are neglected.
- No kinetic mixing. This kind of mixing has been calculated and found to be negligible.
- We do not consider potential couplings of the Z' with the other SM bosons.

2.3 Supersymmetry

The Standard Model as presented in chapter 2.1 presents a self-consistent description of all known phenomena at the Teraelectronvolt scale and below. However its parameters as listed in section 2.2.1 remain unexplained, the mechanism which brings about the spontaneous symmetry breaking described in section 2.1.2 is unknown, it fails to account for the dark matter component of the universe (considering the possibility of right-handed sterile neutrinos as BSM for now) and it does not provide a solution for hierarchy problem briefly mentioned in section 2.1.2 which could explain the now known Higgs mass value despite its sensitivity to potentially large radiative corrections.

Supersymmetry is a posited symmetry with novel fermionic generators which, when extending the Standard Model to conform with it, could address all of the previous problems bar the first one. In the following sections we will overview the motivations for –and the well-known construction of– such a model.

2.3.1 Motivation

The motivations underlying the appeal of Supersymmetry as a additional fundamental symmetry are:

1. the bosonic symmetries (of the Poincarè group) are exhausted in the Standard Model, but fermionic symmetry is still yet to be explored;
2. a dark matter candidate is required (assuming dark matter takes the form of a weakly-interacting massive particle (WIMP));
3. the running of the SM gauge couplings is suggestive of an underlying symmetry and unification of the gauge couplings seems desirable[32];
4. a mechanism to explain (dynamically produce) EWSB at the correct scale is desirable;
5. a solution for the hierarchy problem is required.

It is the fact that Supersymmetry can address all these issues at once which is its primary appeal over other BSM alternatives which tend to address a subset of these.

We will now discuss each one of these in turn.

[32] As discussed later, we assume R-parity to hold here, as required to produce unification.

The Super-Poincarè Group

In 1967 Coleman and Mandula proved [80] that if a four-dimensional, local, Lorentz-invariant QFT is to be non-trivial (that is, allow for interaction terms) all of its *bosonic* symmetries (those expressed as generators with no spin themselves, and subject to commutators in their defining algebra) must be a direct product of the Poincarè group (governing spacetime symmetries acting on spacetime coordinates) and their internal symmetry groups (those acting on the fields themselves, such as gauge symmetries), as

$$\text{Poincarè} \otimes \text{internal}\,. \tag{2.88}$$

However, in 1975 Haag, Lopuszanski and Sohnius [81] extended this result to show that an S-matrix could also accommodate *fermionic* symmetries and remain non-trivial, with the extended symmetry of the form

$$\text{super} - \text{Poincarè} \otimes \text{internal}\,, \tag{2.89}$$

where $\otimes$ denotes a direct product. It is this extended fermionic symmetry that Supersymmetry embodies.

We therefore posit the existence of four fermionic generators of this symmetry in the form of two spinors[33]

$$Q_\alpha, \quad \bar{Q}_{\dot{\alpha}} \;\text{ with }\; \alpha \in \{1,2\},\;\; \dot{\alpha} \in \{\dot{1},\dot{2}\}\,. \tag{2.90}$$

Within the group of Lorentz transformations, $SO(3,1)$, these correspond to the $\left(\frac{1}{2},0\right)$ and $\left(0,\frac{1}{2}\right)$ representations of the Lorentz group (otherwise known as the left- and right-handed representations) under the isomorphism

$$SO(3,1) \;\cong\; SU(2) \;\otimes\; SU(2)^*\,. \tag{2.91}$$

This isomorphism can be derived by noting that the Lorentz group is composed of rotations, J_i, and boosts, K_j, with the commutation relations

$$[J_i,\, J_j] = i\,\epsilon_{ijk} J_k, \quad [J_i,\, K_j] = i\,\epsilon_{ijk} K_k, \quad [K_i,\, K_j] = -i\,\epsilon_{ijk} J_k\,, \tag{2.92}$$

which upon defining

$$A_i = \frac{1}{2}(J_i + iK_i), \quad B_i = \frac{1}{2}(J_i - iK_i)\,, \tag{2.93}$$

[33] We only consider one set of fermionic generators corresponding to the minimal $\mathcal{N}=1$ set of $(Q^A_\alpha,\, \bar{Q}^A_{\dot{\alpha}})$ generators, where $A \in \{1,\ldots,\mathcal{N}\}$, as the so-called *extended* Supersymmetries with $\mathcal{N} \geq 2$ contain only *non-chiral* representations. That is, their multiplets necessarily include vector fields transforming in the (by definition) real adjoint representation, and therefore so do the fermions in the same multiplet (gauge generators and SUSY generators commute, so that all fields within the same SUSY multiplet transform under the same representation). This does not allow for fermions to transform under the pseudoreal fundamental representation of $SU(2)$, or its conjugate or singlet representations as required by the chiral nature of SM fermionic electroweak couplings.

decompose into the closed commutators

$$[A_i,\, A_j] = i\,\epsilon_{ijk}A_k, \quad [B_i,\, B_j] = i\,\epsilon_{ijk}B_k, \quad [A_i,\, B_j] = 0\,, \tag{2.94}$$

which are two $SU(2)$ groups as expected. Here ϵ_{ijk} denotes the three-dimensional Levi-Civita symbol which constitutes the *structure constant* of $SU(2)$.

The second factor of $SU(2)$ carries a conjugation as the right-handed representation is the anti-fundamental (conjugate) representation of the left-handed representation, and these are related to each other by a hermitian conjugation on spinors, as

$$(Q_\alpha)^\dagger = \bar{Q}_{\dot{\alpha}}, \quad (\bar{Q}_{\dot{\alpha}})^\dagger = Q_\alpha\,. \tag{2.95}$$

The rotations and boosts of the Lorentz group can be collected as

$$M_{ij} = \epsilon_{ijk}J_k, \quad M_{0j} = -K_j \quad (i,j,k \in \{1,2,3\})\,, \tag{2.96}$$

into a four-dimensional matrix where each entry is itself a generator of rotations or boosts (that is, a four by four complex matrix), giving a compact form of the generators of the Lorentz group[34]

$$(M_{\alpha\beta})^{\mu}_{\ \nu} = i\left(\eta_{\beta\nu}\delta_\alpha^{\ \mu} - \eta_{\alpha\nu}\delta_\beta^{\ \mu}\right), \tag{2.97}$$

where the Minkowski metric is defined with the signature $\eta = \mathrm{diag}(1,-1,-1,-1)$ as always.

Augmenting this by the generator of translations, $P_\mu = -i\partial_\mu$, we obtain the full Poincarè group of transformations acting on spacetime coordinates as

$$x^\mu \xrightarrow{\text{Poincarè}} \Lambda^\mu_{\ \nu}x^\nu + a^\mu\,, \tag{2.98}$$

where $\Lambda^\mu_{\ \nu}$ is a Lorentz transformation and a^μ denotes a finite spacetime translation.

The commutation relations defining the Poincarè group are

$$[P^\mu,\, P^\nu] = 0\,, \tag{2.99a}$$

$$[M^{\mu\nu},\, P^\alpha] = i\,(P^\mu\eta^{\nu\alpha} - P^\nu\eta^{\mu\alpha})\,, \tag{2.99b}$$

$$[M^{\mu\nu},\, M^{\alpha\beta}] = i\left(M^{\mu\beta}\eta^{\nu\alpha} + M^{\nu\alpha}\eta^{\mu\beta} - M^{\mu\alpha}\eta^{\nu\beta} - M^{\nu\beta}\eta^{\mu\alpha}\right). \tag{2.99c}$$

Defining the Lorentz vectors

$$(\sigma^\mu)_{\alpha\dot{\alpha}} = (\mathbb{1}, \vec{\sigma})\,, \tag{2.100a}$$

$$(\bar{\sigma}^\mu)^{\dot{\alpha}\alpha} = (\mathbb{1}, -\vec{\sigma})\,, \tag{2.100b}$$

[34] See section 1.1 of [82] for the derivation and explicit form of these elements.

(where $\vec{\sigma}$ denotes the Pauli matrices) we can also introduce the fermionic generators (and their corresponding anti-commutators) which extend the Poincarè group by a Supersymmetry into the *super-Poincarè* group as[35]

$$\{Q_\alpha, \bar{Q}_{\dot{\beta}}\} = 2\,(\sigma^\mu)_{\alpha\dot{\beta}}\,P_\mu\,, \tag{2.101a}$$

$$\{Q_\alpha, Q_\beta\} = 0\,, \qquad \{\bar{Q}_{\dot{\alpha}}, \bar{Q}_{\dot{\beta}}\} = 0\,. \tag{2.101b}$$

Note that the new fermionic generators commute with both the internal gauge symmetries (precisely by the Coleman-Mandula theorem) and P^2, so that the members of a given SUSY multiplet (representation) must all transform under the same representations of the gauge groups and must also have the same mass.

The use of anti-commutators in the defining relations means SUSY is a so-called *graded* Lie algebra. As the anticommutator of its generators is proportional to the generator of translations (the momentum operator) as seen in equation 2.101a, SUSY is seen to be a spacetime symmetry.

Relative to the generators of the Poincarè group these fermionic generators obey the commutation relations

$$[Q_\alpha,\, P^\mu] = [\bar{Q}^{\dot{\alpha}},\, P^\mu] = 0\,, \tag{2.102a}$$

$$[Q_\alpha, M^{\mu\nu}] = (\sigma^{\mu\nu})_\alpha^{\ \beta} Q_\beta\,, \tag{2.102b}$$

$$[\bar{Q}^{\dot{\alpha}}, M^{\mu\nu}] = (\bar{\sigma}^{\mu\nu})^{\dot{\alpha}}_{\ \dot{\beta}} \bar{Q}^{\dot{\beta}}\,, \tag{2.102c}$$

where we have defined the anti-symmetric tensors

$$(\sigma^{\mu\nu})_\alpha^{\ \beta} = \frac{i}{4}\,(\sigma^\mu\bar{\sigma}^\nu - \sigma^\nu\bar{\sigma}^\mu)_\alpha^{\ \beta}\,, \tag{2.103}$$

$$(\bar{\sigma}^{\mu\nu})^{\dot{\alpha}}_{\ \dot{\beta}} = \frac{i}{4}\,(\bar{\sigma}^\mu\sigma^\nu - \bar{\sigma}^\nu\sigma^\mu)^{\dot{\alpha}}_{\ \dot{\beta}}\,. \tag{2.104}$$

Dark Matter Candidate

Provided a certain discrete symmetry known as *R-parity* is imposed in the Supersymmetric extension of the SM, the Lightest Supersymmetric Particle (LSP) will be stable and can be electrically neutral, weakly interacting, of a mass scale as required for cold dark matter (that is, of the order of the electroweak scale), and may have the correct production and annihilation rates to give the correct relic abundance, providing viable candidates for weakly-interacting massive particle (WIMP) dark matter.

The issue of how likely one is to obtain such candidates from Supersymmetric models, and how (un)likely viable candidate particles are in its parameter space is a complex one. The Supersymmetric form of the Standard Model provides two weakly-interacting, potentially stable (on cosmological timescales) and electrically neutral

[35] See section 2.2.2 of [83] for a derivation of these.

candidates for dark matter: the sneutrino and the neutralino, of which only the latter can have a mass larger than $m_{W^\pm}$ and give the required amounts of relic density [84].

Currently, within the context of CMSSM (and similarly constrained models) which we define in section 2.3.5 dark matter solely composed by the lightest neutralino has become increasingly constrained and difficult to produce in accordance with known experimental constraints, not least due to it generally overestimating the relic abundance [85, 86].

In the more general 19-parameter pMSSM (defined in section 2.3.5) regions in parameter space complying with all known experimental constraints (including the known mass for the lightest Higgs and the bound/requirement from dark matter relic density) are known [87] (or within the context of the 9-parameter p9MSSM [88]), with allowed regions even in the $m_{\widetilde{N}_1} \sim \mathcal{O}(10\ \mathrm{GeV})$ mass range [89, 90]. However the subset of parameter space points consistent with neutralinos as the sole source of dark matter is very reduced, however one wishes to interpret that. In this context the neutralino composition is constrained to be wino-like or Higgsino-like and with a mass $m_{\widetilde{N}_1} \sim 1\ \mathrm{TeV}$ if it is to be the sole component of dark matter (see figure 2 of [91] and figure 1 of [92]).

From naturalness requirements (equation 2.153) if the condition $\mu^2 \sim m_Z^2$ is imposed then the neutralino dark matter candidate is then expected to be Higgsino-like [93] (see equation 2.173), however if this is so, with a mass of order $1\ \mathrm{TeV}$ its cross section will be inaccessibly small for the LHC, but within reach of the next generation dark matter direct detection experiments (namely XENON1T) [94].

For any given point in the Supersymmetry parameter space its relic abundance can be computed using software package such as micrOMEGAs [95] and checked against the current best fit for the relic abundance (provided by PLANCK [96] as of the time of writing).

Gauge Coupling Unification

With the inclusion of threshold corrections from the new SUSY states (assuming R-parity, as will be discussed later) the gauge couplings of the SM now meet to within their theoretical uncertainties, as shown in figure 2.6. See section 4.1 in [97] and [1] for more detailed discussions of this.

Radiative Electroweak Symmetry Breaking

In section 2.1.2 we outlined how electroweak symmetry is broken in the Standard Model. However, within the Standard Model no explanation is available for why the Higgs field spontaneously develops a non-zero expectation value and breaks the electroweak symmetry $SU(2)_L \otimes U(1)_Y$ to $U(1)_Q$, or why this should

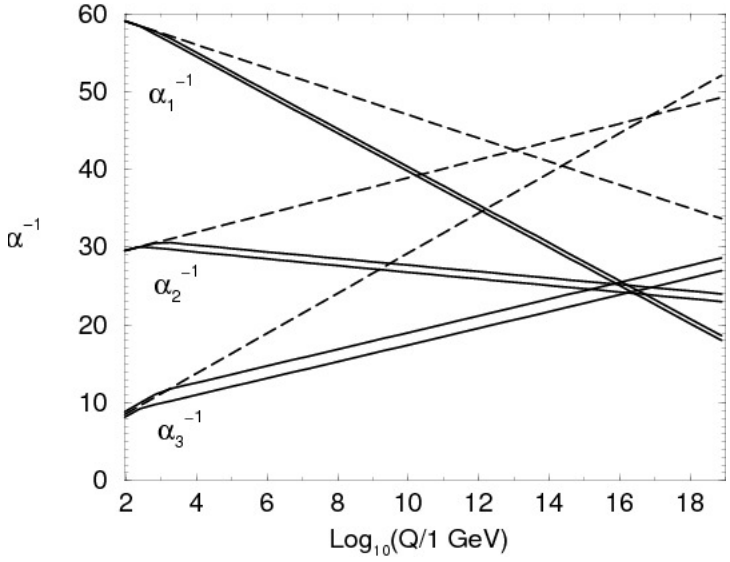

Figure 2.6: The running of the SM gauge couplings within the SM (dashed), and within the MSSM (solid), taken from [1].

happen at the scale at which it does, as is required to correctly generate the SM vector boson masses.

Supersymmetric models can in principle offer a mechanism to dynamically generate this EWSB within their extended Higgs sectors. They do so essentially by considering radiative corrections to the equivalent of the μ parameter in the Higgs potential from equation 2.6c. The renormalisation group evolution generated by these radiative corrections for a minimal supersymmetric spectrum and with the correct high-scale values can drive this parameter from positive to negative precisely at the electroweak ($v \approx 246\ \mathrm{GeV}$) scale, thereby shifting the minimum of the Higgs potential away from zero and generating the electroweak symmetry breaking required (as described in section 2.1.2).

This form of dynamically generating EWSB within SUSY models was put forward in [98] and the requirement that the input high-scale parameters of a SUSY model run down to generate EWSB at the correct scale for EWSB within the SM is one of the constraints commonly placed on scans of the parameter space of such models for regions which remain viable.

Solution to the Hierarchy Problem

As sketched in section 2.1.2, as a fundamental scalar the Higgs is not protected from arbitrarily large radiative self-energy corrections as are the fermions (by chiral symmetry, which is restored in the limit $m_f \to 0$, so that radiative corrections must themselves be proportional to the mass and therefore moderate) and the gauge bosons (by gauge symmetry, which forbids explicit mass terms for the gauge bosons).

It therefore remains an unsolved problem how its mass may remain in the electroweak range when it is sensitive to radiative corrections of the size of the cutoff for the validity of the SM. This problem is not an artefact of using a cutoff as a regularisation method on the loop integrals as one can use dimensional regularisation in which case the corresponding UV pole emerges, and though this pole can be removed by renormalisation with an appropriate counterterm, the hierarchy problem remains in the form of a fine-tuning problem (see for example sections 2.4-2.5 of [99]).

Of the motivations for Supersymmetry previously mentioned fermionic symmetries need not be realised in nature, the dark matter candidate may be non-supersymmetric (though note that if R-parity SUSY exists its lightest supersymmetric particle, the LSP, will necessarily contribute if it is electrically neutral as required by heavy isotope searches) and the unification of gauge couplings is aesthetically pleasing but not required by any known symmetry or principle.

However, the solution of the hierarchy problem given the recent confirmation of the existence of the Higgs at the electroweak scale is a pressing problem which requires an extension of the SM (in the form of either a cutoff –and therefore a threshold where new physics must appear– or a symmetry imposed to regularise the radiative corrections) to be resolved[36]. The most promising solution to this problem (with the added features listed above, which no other SM extension possesses) is the postulation of Supersymmetry as a fundamental symmetry of nature.

Also top-down (theoretical principle $\rightarrow$ model, as opposed to bottom-up data $\rightarrow$ model) arguments for the existence of SUSY as a symmetry of nature (such as those arising from UV completions arising from string theory or string-inspired models) do not necessarily imply that the SUSY spectrum must be found at the electroweak scale. This constraint comes from the requirement that SUSY be of use to provide a solution to the hierarchy problem. In the absence of such a requirement SUSY can be postulated to exist at an arbitrarily high scale, but can be of little relevance for phenomenological purposes[37].

Concretely, a fundamental scalar field such as the SM Higgs field from equation 2.28

$$\phi = \frac{1}{\sqrt{2}} \mathrm{Re}(h(x) \ + \ v) \,, \tag{2.105}$$

is subject to self-energy corrections of which the dominant contribution will be from fermionic loops of the form shown in figure 2.7.

[36] As mentioned previously we will not discuss the proposal in [37], which if correct eliminates the hierarchy problem and as such would strongly diminish the case for electroweak-scale Supersymmetry.

[37] With notable exceptions being radiative corrections to SM processes such as the electric dipole moment of the electron [100] or the magnetic moment of the muon [101], where potential corrections from BSM models at scales considerably higher ($\mathcal{O}(1000 \ \mathrm{TeV})$ [101]) than those which can be probed directly at a collider can still have a measurable impact on observables. Above those scales however the existence or non-existence of SUSY is of no direct relevance to measurable quantities.

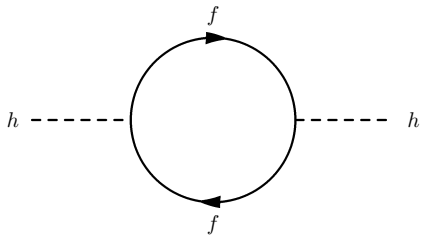

Figure 2.7: Fermionic loop correction to the Higgs self-energy. Given that the Higgs couplings to fermions are proportional to m_f the top quark contribution is strongly dominant.

This diagram (evaluated at zero momentum for the external lines) will give a contribution of the form[38]

$$\begin{aligned}\Pi^f_{hh}(0) &= (-1)\,N(f)\int\frac{d^4k}{(2\pi)^4}\mathrm{tr}\left[\left(i\frac{\lambda_f}{\sqrt{2}}\right)\frac{i}{\not{k}-m_f}\left(i\frac{\lambda_f}{\sqrt{2}}\right)\frac{i}{\not{k}-m_f}\right],\\ &= -2\,N(f)\,\lambda_f^2\int\frac{d^4k}{(2\pi)^4}\frac{k^2+m_f^2}{(k^2-m_f^2)^2},\\ &= -2\,N(f)\,\lambda_f^2\int\frac{d^4k}{(2\pi)^4}\left[\frac{1}{k^2-m_f^2}\;+\;\frac{2\,m_f^2}{(k^2-m_f^2)^2}\right],\end{aligned}\tag{2.106}$$

where the factor of -1 comes from the fermion loop, $N(f)$ is a multiplicity factor ($N(t)=3$ for the three colour eigenstates of the top quark), λ_f is the the Yukawa coupling, and k is the loop four-momentum.

Note that this radiative correction has no dependence on m_h which might make it moderate, and given that $d^4k \propto |\mathbf{k}|^3$ the first term in equation 2.106 is quadratically divergent in the UV limit and herein lies the hierarchy problem.

Postulating the existence of two complex scalar fields $\tilde{f}_L$ and $\tilde{f}_R$ with a Lagrangian of the form[39]

$$\begin{aligned}\mathcal{L}_{\tilde{f}\tilde{f}\phi} &= \lambda_{\tilde{f}}\,|\phi|^2\,(|\tilde{f}_L|^2+|\tilde{f}_R|^2)\;+\;(A_{\tilde{f}}\,\phi\,\tilde{f}_L\,\tilde{f}_R^*\;+\;\mathrm{h.c.})\\ &= \frac{1}{2}\,\lambda_{\tilde{f}}\,h^2\,(|\tilde{f}_L|^2+|\tilde{f}_R|^2)\;+\;v\,\lambda_{\tilde{f}}\,h\,(|\tilde{f}_L|^2+|\tilde{f}_R|^2)\\ &+\;\frac{h}{\sqrt{2}}\,(A_{\tilde{f}}\,\tilde{f}_L\,\tilde{f}_R^*+\mathrm{h.c.})\;+\;\frac{1}{2}\,\lambda_{\tilde{f}}\,v^2\,(|\tilde{f}_L|^2+|\tilde{f}_R|^2)\end{aligned}\tag{2.107}$$

gives further contributions to the Higgs self-energy of the form shown in figure 2.8.

[38] Here we have used $\mathrm{tr}(\gamma^\mu)=0$, $\not{k}^2=k^2$, and we have used partial fractions to obtain the last line.

[39] The mass terms $(A_{\tilde{f}}\,\phi\,\tilde{f}_L\,\tilde{f}_R^*\;+\;\mathrm{h.c.})$ in fact break Supersymmetry as they can give the scalars a different mass than the fermion they are a superpartner of. We include them here as it is this case of unequal masses and broken Supersymmetry in which is experimentally viable and in which the cancellation of the quadratic divergence to the Higgs self-energy must be proven to solve the hierarchy problem. We deal with Supersymmetry breaking in detail in section 2.3.4.

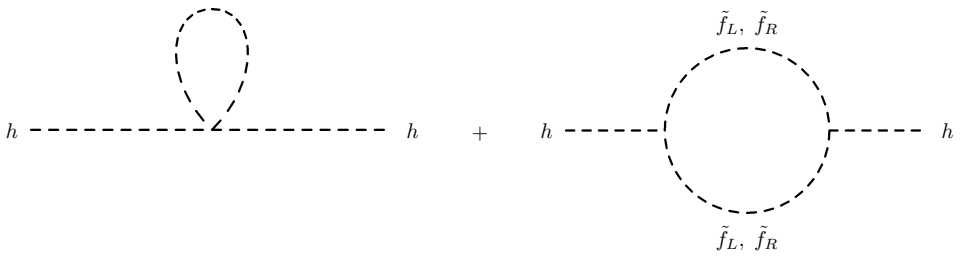

Figure 2.8: Loop corrections from BSM scalar fields to the Higgs self-energy. The fields in the loop are assumed to be new scalar fields.

These contribute to the Higgs self-energy as

$$\begin{aligned}\Pi^{\tilde{f}}_{hh}(0) = \lambda_{\tilde{f}}\, N(\tilde{f}) \int \frac{d^4k}{(2\pi)^4} \left(\frac{1}{k^2 - m^2_{\tilde{f}_L}} \;+\; \frac{1}{k^2 - m^2_{\tilde{f}_R}} \right) \\ +\; \left(\lambda_{\tilde{f}}\, v\right)^2 \, N(\tilde{f}) \int \frac{d^4k}{(2\pi)^4} \left(\frac{1}{(k^2 - m^2_{\tilde{f}_L})^2} \;+\; \frac{1}{(k^2 - m^2_{\tilde{f}_R})^2} \right) \\ +\, |A_{\tilde{f}}|^2\, N(\tilde{f}) \int \frac{d^4k}{(2\pi)^4} \, \frac{1}{k^2 - m^2_{\tilde{f}_L}} \, \frac{1}{k^2 - m^2_{\tilde{f}_R}} \,, \end{aligned} \tag{2.108}$$

where the first term (from the leftmost diagram in figure 2.8) is quadratically divergent and the last two (rightmost diagrams from figure 2.8) are only logarithmically divergent.

Adding the fermionic (equation 2.106) and scalar (equation 2.108) contributions we see that the quadratically divergent contributions from each cancel provided[40]

$$\lambda_{\tilde{f}} = \lambda_f^2 \,, \qquad N(\tilde{f}) \;=\; N(f) \,. \tag{2.109}$$

This solves the hierarchy at the one-loop level and is suggestive that if a symmetry is imposed such that the couplings of fermions and scalars are related and fermionic and bosonic degrees of freedom are constrained to be equal the quadratic sensitivity of the Higgs self-energy would vanish to all orders (logarithmic sensitivity remains but this is not problematic[41]) and the hierarchy/fine-tuning problem has been solved.

These are precisely the symmetries imposed by Supersymmetry. Defining so-called *superfields* which are invariant under Supersymmetry and reformulating the SM in terms of these (to obtain the Supersymmetric Stardard Model (SSM), and ultimately the Minimal Supersymmetric Standard Model (MSSM) as Supersym-

[40] If Supersymmetry were unbroken and held exactly so that $m_{\tilde{f}_{L,R}} = m_f$ and $A_{\tilde{f}} = 0$ the scalar and fermionic contributions cancel exactly so that $\Pi^{\tilde{f}}_{hh}(0) + \Pi^{f}_{hh}(0) = 0$ and the one-loop radiative corrections to the Higgs self-energy vanish.

[41] The total radiative corrections to the Higgs after the cancellation of the quadratic divergences can be shown to be linearly dependent on $m^2_{\tilde{f}} - m^2_f$ and $|A_f|^2$ (see section 2 of [102]), therefore implying that the radiative corrections are moderate as long as these two quantities are as well. This provides one of the strongest constraints on SUSY models, since if the SM-like Higgs is to remain at the EW scale as required, the quantity $m^2_{\tilde{f}} - m^2_f$ must be of the order of the EW scale and the sfermions (at least the ones giving the dominant contributions to the quadratically divergent diagrams, that is: the stops, and via radiative corrections to them also the sbottoms and gluinos) must be found near the EW scale as well.

metry must necessarily be broken to comply with its non-observation so far) gives precisely the relations required to solve the hierarchy problem.

Having discussed all the relevant motivations for considering Supersymmetry as a potential new symmetry of nature we now overview the formal ingredients required for the construction of Supersymmetric extensions of the Standard Model.

2.3.2 Ingredients for the Construction of SUSY-invariant Lagrangians

Superfields

Introducing two constant Grassmann (fermionic) spinors θ^α and $\bar{\theta}_{\dot{\alpha}}$ any function of these spinors may be Taylor-expanded as

$$\begin{aligned} f(x^\mu, \theta^\alpha, \bar{\theta}_{\dot{\alpha}}) = \sum_{m=0}^{2}\sum_{n=0}^{2} a_{mn} f_{mn} = f_{00} + a_{01} f_{01}\theta^\alpha + a_{02} f_{02}(\theta\theta) \\ + a_{10} f_{10}\bar{\theta}_{\dot{\alpha}} + a_{20} f_{20}(\bar{\theta}\bar{\theta}) \\ + a_{11} f_{11}\bar{\theta}_{\dot{\alpha}}\theta^\alpha + a_{22} f_{22}(\theta\theta)(\bar{\theta}\bar{\theta})\,, \end{aligned} \tag{2.110}$$

given that by their anti-commuting property, $(\theta\theta)\theta_\alpha = 0$ and $(\bar{\theta}\bar{\theta})\bar{\theta}^{\dot{\alpha}} = 0$, and all higher powers of these spinors are also zero, hence terminating the series expansion at quadratic terms (and making the Taylor expansion an exact expression for the function).

We therefore define a superfield as

$$\begin{aligned} \mathbf{S}(x^\mu, \theta^\alpha, \bar{\theta}_{\dot{\alpha}}) = \phi(x) \;+\; \theta\psi(x) \;+\; \bar{\theta}\bar{\chi}(x) \\ + (\theta\theta)F(x) \;+\; (\bar{\theta}\bar{\theta})N(x) \\ + \theta\sigma^\mu\bar{\theta}V_\mu(x) \;+\; (\theta\theta)\bar{\theta}\bar{\lambda}(x) \\ + (\bar{\theta}\bar{\theta})\theta\rho(x) \;+\; (\theta\theta)(\bar{\theta}\bar{\theta})D(x) \end{aligned} \tag{2.111}$$

where ϕ is a spin zero field (mass dimension 1, one degree of freedom); N, F and D are *auxiliary* (unphysical, non-propagating) fields of mass dimension 2; ψ, $\bar{\chi}$, $\bar{\lambda}$ and ρ are fermionic fields (Weyl spinors, mass dimension $3/2$, two degrees of freedom each); and V_μ is a vector field (mass dimension 1, four degrees of freedom).

Note that given the mass dimensions of the fields and that $[\theta] = [\bar{\theta}] = -1/2$ the terms in the top two lines of equation 2.111 have mass dimension 1 whilst those from the lower two lines have mass dimension 0. This suggests that this superfield is in fact not an irreducible representation of the SUSY algebra and can in fact be reduced into two smaller (irreducible) representations to accommodate the SM fermions and the SM gauge

fields and their superpartners, respectively. The former are known as (left- or right-handed) *chiral superfields* and the latter as *vector superfields*.

The spacetime-dependent fields on the right hand side of equation 2.111 are known as the *component* fields of the superfield, and this component expansion is required to derive Feynman rules and carry out phenomenology, though Lagrangians expressed in terms of superfields are more convenient from the model-building perspective as the SUSY-invariance is manifest. The degrees of freedom stated are off-shell degrees of freedom, with the total number of fermionic and bosonic degrees of freedom being equal (8), as expected.

Superfields are, by definition, constrained to be invariant under the SUSY transformation, transforming (as a Hilbert vector) as

$$\mathbf{S} \xrightarrow{\text{SUSY}} \exp(i(\zeta Q + \bar{\zeta}\bar{Q}))\,\mathbf{S} \approx \mathbf{S} + i(\zeta Q + \bar{\zeta}\bar{Q})\mathbf{S}\,, \tag{2.112}$$

where we have considered a finite transformation in the first step and the infinitesimal limit in the second, and where ζ^α, $\bar{\zeta}_{\dot{\alpha}}$ are constant spinors (the parameters of the SUSY transformation)[42].

Thus in order for a Lagrangian to be SUSY-invariant it must transform as[43]

$$\delta\mathcal{L} = i(\zeta Q + \bar{\zeta}\bar{Q})\mathcal{L} = \begin{cases} 0 \\ \\ \partial_\mu(\ldots) \end{cases} \tag{2.113}$$

where the bottom case denotes a total derivative, such that upon integration to obtain the action it will result in boundary terms which do not contribute. This latter case is how SUSY Lagrangians are constructed.

Using explicit representations as differential operators of the SUSY algebra elements[44] Q^α and $\bar{Q}_{\dot{\alpha}}$, which can be found in any of the introductions to SUSY cited previously, it can be seen that indeed for the superfield as defined in equation 2.111

$$\delta(\text{boson}) \propto \text{fermion}\,, \tag{2.114a}$$

$$\delta(\text{fermion}) \propto \text{boson}\,, \tag{2.114b}$$

and in particular

$$\delta D = \frac{i}{2}\partial_\mu\left(\zeta\sigma^\mu\bar{\lambda} - \rho\sigma^\mu\bar{\zeta}\right)\,, \tag{2.115}$$

[42] We consider *global* Supersymmetry only. If the parameters of the SUSY transformation are allowed spacetime dependence making SUSY a local symmetry Supergravity (SUGRA) models arise.

[43] Lorentz and translation generators with their respective parameters are neglected here but understood to be present.

[44] We will deliberately misuse notation by using the same notation for the algebra elements and their representations as differential operators, as such a distinction is largely redundant for our purposes.

is a total derivative, such that $\delta D = 0$ and

$$D \xrightarrow{\text{SUSY}} D + \delta D = D\,. \tag{2.116}$$

Terms like these, simply referred to as *D-terms*, can be used to build a SUSY-invariant Lagrangian.

Grassmann Calculus

Here we define integration over Grassmann variables (also known as *Berezin integration*) to act as

$$\int d^2\theta \;\; (\theta\theta) = 1\,, \tag{2.117a}$$

$$\int d^2\bar{\theta} \;\; (\bar{\theta}\bar{\theta}) = 1\,, \tag{2.117b}$$

$$\int d^2\bar{\theta} \int d^2\theta \;\; (\theta\theta)(\bar{\theta}\bar{\theta}) = 1\,, \tag{2.117c}$$

for the cases that will be of interest to us.

Integration can therefore be used as shorthand to denote the extraction of particular terms from a superfield, as

$$\int d^2\theta \;\; \mathbf{S} = [\mathbf{S}]_{\theta\theta} \qquad (\mathrm{F-term})\,, \tag{2.118a}$$

$$\int d^2\bar{\theta} \int d^2\theta \;\; \mathbf{S} = [\mathbf{S}]_{(\theta\theta)(\bar{\theta}\bar{\theta})} \quad (\mathrm{D-term})\,, \tag{2.118b}$$

where the former is known as an *F-term* and also yields a total derivative when subjected to a SUSY transformation.

Derivatives with respect to Grassmann spinors are defined as

$$\partial_\alpha = \frac{\partial}{\partial\theta^\alpha}, \qquad \partial^\alpha = \frac{\partial}{\partial\theta_\alpha}\,, \tag{2.119a}$$

$$\bar{\partial}_{\dot{\alpha}} = \frac{\partial}{\partial\bar{\theta}^{\dot{\alpha}}}, \qquad \bar{\partial}^{\dot{\alpha}} = \frac{\partial}{\partial\bar{\theta}_{\dot{\alpha}}}\,. \tag{2.119b}$$

Derivatives with respect to constant Grassmann spinors evaluate to

$$\partial_\alpha\theta^\beta = \delta_\alpha^\beta \qquad \bar{\partial}^{\dot{\alpha}}\bar{\theta}_{\dot{\beta}} = \delta_{\dot{\beta}}^{\dot{\alpha}}\,, \tag{2.120a}$$

with derivatives over left-handed or right-handed spinors acting only on spinors of the same chirality,

$$\partial_\alpha\bar{\theta}_{\dot{\beta}} = 0, \qquad \bar{\partial}^{\dot{\alpha}}\theta^\beta = 0\,. \tag{2.121}$$

Note that the derivatives with respect to Grassmann spinors are themselves fermionic and therefore anti-

commute with other fermionic spinors, such that, for example

$$\partial_\alpha(\psi\theta) = \frac{\partial}{\partial\theta^\alpha}(\psi^\beta\theta_\beta) = -\psi^\beta\frac{\partial}{\partial\theta^\alpha}\theta_\beta = -\psi^\beta\frac{\partial}{\partial\theta^\alpha}\epsilon_{\beta\lambda}\theta^\lambda = -\epsilon_{\beta\lambda}\psi^\beta\delta^\lambda_\beta = \psi_\beta\,, \tag{2.122}$$

where the Levi-Civita symbol must always be placed to the left of the spinor with which it is to be contracted when contractions are to be made and indices then omitted, and indices to be contracted must be adjacent[45].

In analogy to gauge symmetries we define covariant derivatives such that

$$D_\alpha\mathbf{S} \xrightarrow{\text{SUSY}} D_\alpha\mathbf{S} + \delta(D_\alpha\mathbf{S}) = D_\alpha\mathbf{S}\,, \tag{2.123a}$$

$$\bar{D}_{\dot\alpha}\mathbf{S} \xrightarrow{\text{SUSY}} \bar{D}_{\dot\alpha}\mathbf{S} + \delta(\bar{D}_{\dot\alpha}\mathbf{S}) = \bar{D}_{\dot\alpha}\mathbf{S}\,. \tag{2.123b}$$

Explicit representations of these operators will vary according to the conventions used, but generally have the form (following [83])

$$D_\alpha = \partial_\alpha \;+\; i(\sigma^\mu)_{\alpha\dot\beta}\bar\theta^{\dot\beta}\partial_\mu\,, \tag{2.124a}$$

$$\bar{D}_{\dot\alpha} = -\bar\partial_{\dot\alpha} \;-\; i\theta^\beta(\sigma^\mu)_{\beta\dot\alpha}\partial_\mu\,. \tag{2.124b}$$

Chiral Superfields

Chiral superfields are defined as one of two types: left-handed chiral superfields (LHCSF), $\mathbf{\Phi}$, and right-handed chiral superfields (RHCSF), $\bar{\mathbf{\Phi}} = \mathbf{\Phi}^\dagger$, each of which fulfil the defining property

$$\bar{D}_{\dot\alpha}\mathbf{\Phi} = 0 \qquad\qquad (\text{LHCSF}) \tag{2.125a}$$

$$D_\alpha\bar{\mathbf{\Phi}} = 0 \qquad\qquad (\text{RHCSF})\,, \tag{2.125b}$$

respectively.

In terms of component (Weyl spinor) fields a LHCSF can be written as

$$\begin{aligned}\mathbf{\Phi}(x^\mu,\theta^\alpha,\bar\theta_{\dot\alpha}) = \phi(x) \;+\; \sqrt{2}\theta\psi(x) \;+\; (\theta\theta)F(x) \;+\; i\theta\sigma^\mu\bar\theta\partial_\mu\phi(x) \\ -\frac{i}{\sqrt{2}}(\theta\theta)\partial_\mu\psi(x)\sigma^\mu\bar\theta \;-\; \frac{1}{4}(\theta\theta)(\bar\theta\bar\theta)\partial_\mu\partial^\mu\phi(x)\,.\end{aligned} \tag{2.126}$$

The F field is a non-propagating (unphysical) scalar auxiliary field of mass dimension 2 which can be substituted for when going on mass-shell by solving its Euler-Lagrange field equation

$$\frac{\partial\mathcal{L}}{\partial F} \;-\; \partial_\mu\left(\frac{\partial\mathcal{L}}{\partial(\partial_\mu F)}\right) = 0\,. \tag{2.127}$$

[45] Here the anti-symmetry property of the Levi-Civita symbol has been used to absorb a minus sign and make contracting indices adjacent in the last step).

Note that under a SUSY transformation $i(\zeta Q + \bar{\zeta}\bar{Q})\mathbf{\Phi}$ the F term transforms as

$$F \; + \; \delta F = F \; + \; i\sqrt{2}\bar{\zeta}\bar{\sigma}^{\mu}\partial_{\mu}\psi \, , \tag{2.128}$$

where δF is clearly a total derivative. The F-term of a LHCSF (just like the D-term of a general superfield) can therefore be used to construct a SUSY-invariant Lagrangian.

When embedding the SM field content into its Supersymmetric equivalent a LHCSF would contain the left-handed fermionic fields as well as their scalar partners, and similarly the right-handed fermions and their SUSY partners would be embedded within RHCSFs.

Vector Superfields

Chiral superfields suffice to embed the fermion sector and their SUSY partners but the gauge fields and their Supersymmetric counterparts known as *gauginos* have yet to be included in a SUSY-invariant multiplet. These can be included in separate multiplets in an irreducible representation of the SUSY algebra known as a *vector superfield* (VSF).

A vector superfield is defined as a superfield, $\mathbf{V}$, with the property $\mathbf{V}^{\dagger} = \mathbf{V}$. In component form such a superfield can be written (working in the Wess-Zumino gauge for simplicity, see any of the standard SUSY references cited for further details and the ungauged form) as

$$V(x^{\mu}, \theta^{\alpha}, \bar{\theta}_{\dot{\alpha}}) = (\theta\sigma^{\mu}\bar{\theta})V_{\mu}(x) \; + \; (\theta\theta)(\bar{\theta}\bar{\lambda}(x)) \; + \; (\bar{\theta}\bar{\theta})(\theta\lambda(x)) \; + \; \frac{1}{2}(\theta\theta)(\bar{\theta}\bar{\theta})D(x) \, . \tag{2.129}$$

This superfield carries the vector gauge fields and their spin $1/2$ counterparts, the gauginos. Note that it contains a SUSY-invariant D-term.

Supersymmetric Field Strength

The construction of Lagrangians invariant under both SUSY and gauge symmetries requires special care. In particular, modifications to the gauge transformations and the resulting form of gauge invariant terms must be considered.

Abelian Supersymmetric Field Strength

Defining the generalised gauge transformations

$$\mathbf{\Phi} \longrightarrow \exp(-2iq\mathbf{\Lambda}) \, \mathbf{\Lambda} \, , \tag{2.130a}$$

$$\mathbf{V} \longrightarrow \mathbf{V} + i(\mathbf{V} - \mathbf{V}^{\dagger}) \, , \tag{2.130b}$$

where $\mathbf{\Lambda}$ is a LHCSF and q is the (s)fermion charge under the gauge group, gauge and SUSY-invariant kinetic terms for the fermions and *sfermions* (scalar, SUSY partners to the fermions) can be constructed as

$$\mathbf{\Phi}^\dagger \exp(2q\mathbf{V})\mathbf{\Phi}\,. \tag{2.131}$$

Note that this term (via the expansion of the exponential) will also give the fermion-fermion-gauge boson, sfermion-sfermion-gauge boson and fermion-sfermion-gaugino interaction terms.

The Supersymmetric Abelian field strength used to give the gauge kinetic terms for gauge bosons and gauginos can be constructed as

$$\mathbf{W}_\alpha = -\frac{1}{4}(\bar{D}\bar{D})D_\alpha\mathbf{V}\,, \tag{2.132}$$

where the covariant derivatives are as defined in equation 2.123b and it can be clearly seen that this field strength is itself a LHCSF.

Non-Abelian Supersymmetric Field Strength

In the non-Abelian case both the vector superfield and the LHCSF that acts as the parameter of the generalised gauge transformation must be expanded under the Hermitian generators of the Lie algebra they correspond to as

$$\mathbf{V} = \mathbf{V}^a t^a\,, \tag{2.133a}$$

$$\mathbf{\Lambda} = \mathbf{\Lambda}^a t^a\,, \tag{2.133b}$$

where as usual, a sum over repeated indices is understood.

The chiral and vector superfields are now defined to transform as

$$\mathbf{\Phi} \longrightarrow e^{2ig\mathbf{\Lambda}}\,, \tag{2.134a}$$

$$e^{\mathbf{V}} \longrightarrow e^{i\bar{\mathbf{\Lambda}}}e^{\mathbf{V}}e^{-i\mathbf{\Lambda}}\,, \tag{2.134b}$$

where g is the gauge group coupling.

Given that the gauge transformation superfield and the vector superfield no longer commute the field strength must be redefined as

$$\mathbf{W}_\alpha = -\frac{1}{8g}(\bar{D}\bar{D})(e^{-2g\mathbf{V}}D_\alpha e^{2g\mathbf{V}})\,, \tag{2.135}$$

to remain gauge covariant (and give a gauge invariant term when contracted with W^α and a trace is taken over their product to eliminate exponentials remaining at the ends via cyclic permutations).

The Superpotential

Given that SUSY-covariant derivatives obey the chain rule of differentiation a product of any number of LHCSF is itself a LHCSF. Terms of this form must hence also be included in the Lagrangian. Also, given the relation

$$\int d\theta\, \theta^\alpha = 1\,,$$

and the fact that the mass dimension of the constant Grassmann spinors θ^α and $\bar{\theta}_{\dot{\alpha}}$ is $-1/2$, this implies that the measure over a Grassmann spinor in fact has dimension $1/2$.

Grouping the terms polynomial in the LHCSFs into the *superpotential* function and taking its F term hence gives SUSY-invariant contributions to the Lagrangian, as

$$\int d^2\theta\ \ \mathbf{W}(\mathbf{\Phi})\,. \tag{2.136}$$

Since the Grassmann measure here has mass dimension 1, the superpotential must be at most cubic in $\mathbf{\Phi}$ to include only relevant and marginal operators so that the Lagrangian remains renormalisable.

The superpotential is also required to be *holomorphic*, involving only functions of $\mathbf{\Phi}$ and none of its hermitian conjugate (though the hermitian conjugate of the superpotential, which itself can only be a function of $\bar{\mathbf{\Phi}} = \mathbf{\Phi}^\dagger$ must also be included in the full Lagrangian).

The renormalisable superpotential will therefore be of the form

$$\mathbf{W}(\Phi) = a_i\, \mathbf{\Phi}_i \ + \ \frac{1}{2!}\, m_{ij}\, \mathbf{\Phi}_i \mathbf{\Phi}_j \ + \ \frac{1}{3!}\, A_{ijk}\, \mathbf{\Phi}_i \mathbf{\Phi}_j \mathbf{\Phi}_k\,, \tag{2.137}$$

where the prefactors account for the possible permutations of the fields.

It is a remarkable feature of the superpotential that by virtue of its holomorphicity it is not subject to any radiative corrections (or rather, they vanish to all orders) and therefore does not require any form of renormalisation. The proof of this statement is the so-called *non-renormalisation theorem* (see for example [103, 104] for proof and detailed discussions of this theorem).

Gauge invariance restricts the linear term to be a gauge singlet (and therefore possibly absent, depending on the model), the quadratic (mass) term requires the superfields to either transform under the adjoint representation such that

$$\mathbf{\Phi} \longrightarrow e^{i\mathbf{\Lambda}} \mathbf{\Phi} e^{-i\mathbf{\Lambda}}\,, \tag{2.138}$$

or under the fundamental, $\mathbf{\Phi}$ and conjugate-fundamental $\tilde{\mathbf{\Phi}}$ representations

$$\mathbf{\Phi} \longrightarrow e^{i\mathbf{\Lambda}} \mathbf{\Phi}\,, \tag{2.139a}$$

$$\tilde{\mathbf{\Phi}} \longrightarrow \tilde{\mathbf{\Phi}} e^{-i\mathbf{\Lambda}}\,, \tag{2.139b}$$

giving a mass term of the form $\tilde{\mathbf{\Phi}}\mathbf{\Phi}$, in order to preserve gauge invariance.

2.3.3 The Supersymmetric Standard Model (SSM)

There are a wealth of excellent introductory treatments of Supersymmetry (see [83, 97, 99, 102–117] and references therein) so we will only briefly overview its principles and the construction of the Minimal Supersymmetric Standard Model (MSSM) upon which we base our studies on.

Given the tools outlined in section 2.3.2 we may now construct a Supersymmetric gauge theory, and the the Supersymetric Standard Model (SSM)[46] in particular. Schematically the Lagrangian is constructed as[47],

$$\mathcal{L} = \mathbf{K}\Big|_D \; + \; \left(\mathrm{tr}\left(\mathbf{W}^\alpha \mathbf{W}_\alpha\right)\Big|_F + \mathrm{h.c.}\right) \; + \; \left(\mathbf{W}\Big|_F + \mathrm{h.c.}\right) . \tag{2.140}$$

More concretely the Lagrangian for a SUSY-invariant gauge theory must be of the form

$$\begin{aligned} \mathcal{L} \;\; &= \; \int d^2\theta \int d^2\bar{\theta} \;\; \mathbf{K}\left(\bar{\mathbf{\Phi}}, e^{2g\mathbf{V}}, \mathbf{\Phi}\right) \\ &+ \tau \int d^2\theta \;\; \mathrm{tr}(\mathbf{W}^\alpha \mathbf{W}_\alpha) \; + \; \tau^* \int d^2\bar{\theta} \;\; \mathrm{tr}(\bar{\mathbf{W}}_{\dot{\alpha}} \bar{\mathbf{W}}^{\dot{\alpha}}) \\ &+ \int d^2\theta \;\; \mathbf{W}(\mathbf{\Phi}) \; + \; \int d^2\bar{\theta} \;\; \bar{\mathbf{W}}(\bar{\mathbf{\Phi}}) , \end{aligned} \tag{2.141}$$

where the function $\mathbf{K}$ is known as the *Kähler potential* and τ is a complex constant which may be adjusted to provide the desired normalisation for the gauge kinetic terms.

Physically, the terms in the last three lines give, in order:

1. $\mathbf{K}\left(\bar{\mathbf{\Phi}}, e^{2g\mathbf{V}}, \mathbf{\Phi}\right)\Big|_D = \bar{\mathbf{\Phi}} e^{2g\mathbf{V}} \mathbf{\Phi}\Big|_D$, upon expanding the exponential as $e^{\pm\mathbf{V}} = 1 \pm \mathbf{V} + \frac{1}{2}\mathbf{V}^2$ (in the Wess-Zumino gauge which gives the minimal field content, for simplicity) this gives the fermion and sfermion kinetic terms, as well as their interactions with the gauge bosons and gauginos (fermion-fermion-gauge boson, sfermion-sfermion-gauge boson, and fermion-sfermion-gaugino)[48];
2. $\left(\mathrm{tr}\left(\mathbf{W}^\alpha \mathbf{W}_\alpha\right)\Big|_F + \mathrm{h.c.}\right)$, kinetic terms for gauge bosons and gauginos, as well as gauge boson and gaugino self-interactions for non-Abelian groups;
3. $\left(\mathbf{W}\Big|_F + \mathrm{h.c.}\right)$, Yukawa-type (scalar-fermion-fermion) interactions and mass contributions.

We exemplify the construction of SUSY-invariant gauge theory Lagrangians by showing the overall structure of an Abelian case, that of Supersymmetric Quantum Electrodynamics (SQED), and a non-Abelian, that of

[46] Not to be confused with the acronym for Sequential Standard Model used in chapter 2.2 and which we will no longer use with that meaning.

[47] We neglect the presence of a Fayet-Iliopoulos term (the D-term of a vector superfield) which can be present only for $U(1)$ theories as the vector boson fields do not carry any $U(1)$ charge themselves and are therefore singlets and gauge invariant.

[48] See [103] for derivation for Supersymmetric QED for example.

Supersymmetric Quantum Chromodynamics (SQCD) in the next two subsections. These together encapsulate the SSM (after EWSB).

The Supersymmetric Quantum Electrodynamics Lagrangian

The Lagrangian of SQED at the level of superfields is

$$\begin{aligned}\mathcal{L} = &\int d^2\bar{\theta} \int d^2\theta \ \left(\bar{\mathbf{\Phi}}_i e^{2g\mathbf{V}} \mathbf{\Phi}_i \ + \ \tilde{\mathbf{\Phi}}_i e^{-2g\mathbf{V}} \bar{\tilde{\mathbf{\Phi}}}_i\right) \\ &- \frac{1}{4g^2} \int d^2\theta \ \mathbf{W}^\alpha \mathbf{W}_\alpha \ - \ \frac{1}{4g^2} \int d^2\bar{\theta} \ \bar{\mathbf{W}}_{\dot{\alpha}} \bar{\mathbf{W}}^{\dot{\alpha}} \\ &+ \int d^2\theta \ m \, \tilde{\mathbf{\Phi}}_i \mathbf{\Phi}_i \ + \ \int d^2\bar{\theta} \ m^* \, \bar{\mathbf{\Phi}}_i \bar{\tilde{\mathbf{\Phi}}}_i \,,\end{aligned} \tag{2.142}$$

where the field strengths are as defined in equation 2.132 and the index i runs through the flavours of all electrically charged chiral superfields.

The Supersymmetric Quantum Chromodynamics Lagrangian

Defining the LHCSFs $\mathbf{Q}_i$ and $\tilde{\mathbf{Q}}_i$(with $i = 1, \ldots, n_f$, where $n_f = 6$ is the number of quark flavours) transforming under the fundamental and conjugate-fundamental representations of $SU(3)$, respectively, the SQCD Lagrangian is

$$\begin{aligned}\mathcal{L} = &\int d^2\bar{\theta} \int d^2\theta \ \left(\sum_i \bar{\mathbf{Q}}_i e^{2g\mathbf{V}} \mathbf{Q}_i \ + \ \sum_i \tilde{\mathbf{Q}}_i e^{-2g\mathbf{V}} \bar{\tilde{\mathbf{Q}}}\right) \\ &- \frac{\tau}{8} \int d^2\theta \ \mathbf{W}^\alpha \mathbf{W}_\alpha \ - \ \frac{\tau^*}{8} \int d^2\bar{\theta} \ \bar{\mathbf{W}}_{\dot{\alpha}} \bar{\mathbf{W}}^{\dot{\alpha}} \\ &+ \int d^2\theta \ m_i \, \tilde{\mathbf{Q}}_i \mathbf{Q}_i \ + \ \int d^2\bar{\theta} \ m_i^* \, \bar{\mathbf{Q}}_i \bar{\tilde{\mathbf{Q}}}_i \,,\end{aligned} \tag{2.143}$$

where the field strengths are as defined in equation 2.135.

The Supersymmetric Standard Model Field Content

Embedding the SM fields into chiral or vector superfields as dictated by their spin, with each SUSY multiplet transforming under the representation dictated by the SM field within it, and imposing the SM gauge groups and charges under them and inserting the corresponding Kähler, superpotential and field strengths, one can in this way obtain the Supersymetric Standard Model.

The field content of the SSM is exactly that of the SM fields with a SUSY partner added for each field, both fermionic and bosonic, as shown in tables 2.6 and 2.7.

The only additional fields that must be added are two Higgs chiral superfields, $\mathbf{H}_u$ and $\mathbf{H}_d$, instead of just

Name	LHCSF	spin 0	spin $\frac{1}{2}$	$(SU(3)_C, SU(2)_L, U(1)_Y)$
squarks and quarks	$\mathbf{Q}$	$(\tilde{u}_L, \tilde{d}_L)$	(u_L, d_L)	$(\mathbf{3}, \mathbf{2}, \frac{1}{6})$
	$\mathbf{U}$	$\tilde{u}_R^\dagger$	$u_R^\dagger$	$(\bar{\mathbf{3}}, \mathbf{1}, -\frac{2}{3})$
	$\mathbf{D}$	$\tilde{d}_R^\dagger$	$d_R^\dagger$	$(\bar{\mathbf{3}}, \mathbf{1}, \frac{1}{3})$
sleptons and leptons	$\mathbf{L}$	$(\tilde{\nu}, \tilde{e}_L)$	(ν, e_L)	$(\mathbf{1}, \mathbf{2}, -\frac{1}{2})$
	$\mathbf{E}$	$\tilde{e}_R^*$	$e_R^\dagger$	$(\mathbf{1}, \mathbf{1}, 1)$
Higgs and Higgsinos	$\mathbf{H}_u$	(h_u^+, h_u^0)	$(\tilde{h}_u^+, \tilde{h}_u^0)$	$(\mathbf{1}, \mathbf{2}, \frac{1}{2})$
	$\mathbf{H}_d$	(h_d^0, h_d^-)	$(\tilde{h}_d^0, \tilde{h}_d^-)$	$(\mathbf{1}, \mathbf{2}, -\frac{1}{2})$

Table 2.6: The chiral superfield content of the SSM. This field content is replicated for each of the three families/generations. Note that the representations and $U(1)_Y$ charges stated are exactly as for the SM in table 2.2, except we now use the $Q = t_3 + Y$ form of the Gell-Mann–Nishijima relation (instead of $Q = t_3 + Y/2$), as we have done since chapter 2.2. Fields paired up within braces denote $SU(2)$ doublets.

Name	VSF	spin $\frac{1}{2}$	spin1	$(SU(3)_C, SU(2)_L, U(1)_Y)$
gluinos and gluons	$\mathbf{G}$	$\tilde{g}$	g	$(\mathbf{8}, \mathbf{1}, 0)$
winos and W fields	$\mathbf{W}$	$\widetilde{W}_{1,2}$, $\widetilde{W}_3$	$W_{1,2}$, W_3	$(\mathbf{1}, \mathbf{3}, 0)$
bino and B field	$\mathbf{B}$	$\widetilde{B}$	B	$(\mathbf{1}, \mathbf{1}, 0)$

Table 2.7: The vector superfield content of the SSM.

one. The reason for this is twofold: contrary to the SM where the same Higgs field can be used to provide masses for both up- and down-type fields of $SU(2)$ doublets by using its conjugate (as defined in equation 2.3 and used to give masses to up-type quarks in equation2.6d), the holomorphicity of the superpotential where this term must be placed does not allow for this. A separate Higgs must therefore be introduced to give mass to up-type quarks.

Secondly, the introduction of a single Higgs chiral superfield includes the introduction of a fermionic partner of the Higgs (the *Higgsino*) which carries non-zero hypercharge (the Higgs is an isospin doublet but has no electric charge so hypercharge must counter the third component of isospin to give zero electric charge after EWSB). This fermion would spoil the accidental anomaly cancellation inherited from the SM (equation 2.63), and therefore a second Higgs chiral superfield with its fermionic component carrying the opposite $Y = \pm 1/2$ hypercharge is required to restore anomaly cancellation.

These two requirements lead to the introduction of the $\mathbf{H}_u$ and $\mathbf{H}_d$ chiral superfields, in addition to the gauge boson and gaugino fields, as shown in table 2.6. The scalar component of these superfields give the Higgs isospin doublets required to give mass to up- and down-type fermions, respectively.

The Supersymmetric Standard Model Superpotential

Writing the set of all gauge-invariant mass dimension 3 operators involving only LHCSFs the superpotential of the SSM is obtained as

$$\mathbf{W} \;=\; \mathbf{W}_R \;+\; \mathbf{W}_{\not R}\,, \tag{2.144}$$

where the distinction between these two terms (and the reason why we shall not include the latter in the SSM) will be treated in the next subsection.

For now we state only the contents the first term, which are

$$\mathbf{W}_R = (y_u)_{ij}\,\mathbf{Q}_i\cdot\mathbf{H}_u\,\mathbf{U}_j \;+\; (y_d)_{ij}\,\mathbf{Q}_i\cdot\mathbf{H}_d\,\mathbf{D}_j \;+\; (y_e)_{ij}\,\mathbf{L}_i\cdot\mathbf{H}_d\,\mathbf{E}_j \;+\; \mu\,\mathbf{H}_u\cdot\mathbf{H}_d\,, \tag{2.145}$$

where the i,j indices run over the three generations and $\cdot$ denotes a contraction of $SU(2)$ doublet indices via a Levi-Civita symbol.

The first three terms of $\mathbf{W}_R$ can be seen to give the fermion Yukawa terms which give masses to the up- and down-type quarks and the down-type leptons, whilst the last term gives the mass terms for the Higgs and Higgsinos.

R-Parity

The second part of the superpotential as stated in equation 2.144 contains the terms

$$\mathbf{W}_{\not R} \;=\; \frac{1}{2}\,\lambda_{ijk}\,\mathbf{L}_i\cdot\mathbf{L}_j\,\mathbf{E}_k \;+\; \lambda'_{ijk}\,\mathbf{L}_i\cdot\mathbf{Q}_j\,\mathbf{D}_k \;+\; \frac{1}{2}\,\lambda''_{ijk}\,\mathbf{U}_i\,\mathbf{D}_j\,\mathbf{D}_k \;+\; \kappa_i\,\mathbf{L}_i\cdot\mathbf{H}_u\,, \tag{2.146}$$

where the term $\frac{1}{2}\,\lambda'''_k\,\mathbf{H}_d\mathbf{H}_d\mathbf{E}_k = \frac{1}{2}\,\lambda'''_k\,\epsilon^{ab}\,(\mathbf{H}_d)_a(\mathbf{H}_d)_b\mathbf{E}_k$ is gauge invariant and should be included but is identically equal to zero due to the asymmetry of the Levi-Civita symbol used to contract the two isospin doublets into a singlet, and the symmetric pair of fields it is contracted with. Said contraction of isospin doublets with a Levi-Civita symbol is understood everywhere they appear, and a further contraction $\epsilon^{ijk}\,\mathbf{U}_i\,\mathbf{D}_j\,\mathbf{D}_k$ is understood in the corresponding term to obtain an (anti-symmetric) gauge invariant combination of the three colour triplets.

Considering the lepton and baryon number assignments of the chiral superfields as indicated in table 2.8 (recall that the conjugates of the component fields go into the $\mathbf{U}$, $\mathbf{D}$ and $\mathbf{E}$ superfields as shown in table 2.6, such that these carry negative lepton and baryon numbers) and that these combine additively we see that the first, second and last terms of $\mathbf{W}_{\not R}$ violate lepton number conservation whilst the third one violates baryon number conservation.

As such the terms in $\mathbf{W}_{\not R}$ are customarily disallowed by imposing an *ad hoc* discrete symmetry known as

LHCSF	$\mathbf{Q}$	$\mathbf{U}$	$\mathbf{D}$	$\mathbf{L}$	$\mathbf{E}$	$\mathbf{H}_u$	$\mathbf{H}_d$
B	$+1$	-1	-1	0	0	0	0
L	0	0	0	$+1$	-1	0	0

Table 2.8: The baryon and lepton number assignments of the SSM chiral superfields.

R parity where each component field is assigned a charge according to

$$(-1)^{3B+L+2S}, \tag{2.147}$$

where B and L are the baryon and lepton numbers, respectively, and S is the spin.

In this way the SM fields have R-parity $+1$ and their superpartners have R-parity -1. If R-parity is defined to combine multiplicatively and its conservation is enforced at every vertex all the terms in $\mathbf{W}_{\not R}$ can be seen to now be forbidden.

This is more obvious if one considers (the completely equivalent) *matter parity* defined as

$$(-1)^{3B+L} \tag{2.148}$$

which applies to a whole chiral superfield. The lepton and quark LHCSFs then have matter parity -1 and the Higgs and VSFs have matter parity $+1$. The terms in $\mathbf{W}_R$ can then be seen to have matter parity $+1$ whilst the ones in $\mathbf{W}_{\not R}$ have matter parity -1 and can be forbidden by this criteria.

The presence of some operators from $\mathbf{W}_{\not R}$ can in fact be considered in so-called R-parity violating (RPV) SUSY models, in which they generate novel 3-body decays. However these models must allow only lepton number violation or only baryon number violation at a time, since if both baryon- and lepton-number violating operators are simultaneously included this would produce unacceptable rates of unobserved processes (such as proton decay, which also strongly constrains GUT theories as discussed in section 2.2.1). We will not consider such models and we will assume R parity conservation at all times.

2.3.4 Soft SUSY-breaking

Thus far the extension of the SM into the SSM has involved essentially no new free parameters. All the masses and couplings are set as in the SM for each respective superfield. However, it can be seen for example from the mass terms in the superpotential in the last lines of equations 2.142 and 2.143 that both the fermions and sfermions within a given chiral superfield are restricted to have exactly the same mass. This constraint imposed by SUSY must somehow be relaxed given that no such degenerate states to the SM fields have been directly detected.

This requires that SUSY be broken, but only in a way which will not spoil the relations crucial to the

cancellation of quadratic divergences in the Higgs self-energy and the resulting solution of the hierarchy problem (that is, equation 2.109). SUSY is then said to be *softly broken*.

The first approach to induce SUSY breaking would be to spontaneously break it by allowing a scalar component-field to acquire a non-zero expectation value. These approaches are known as *F-term breaking* or *D-term breaking* but are unviable as they lead to super-trace relations which predict for example that for each SM Weyl fermion its two corresponding scalars will have a mass symmetric mass gap relative to it, with one scalar being heavier than it and one lighter (see any of the standard sources cited at the beginning of section 2.3.3). This is unacceptable from a phenomenological point of view as no SUSY partners lighter than the SM fields have been detected. A more ad hoc procedure of manually inserting all the possible mass terms which break SUSY and give mass contributions only to the SUSY partners is therefore required.

This snag is a source of significant complication as failing to break SUSY softly (and spontaneously) using its own field content implies that SUSY-breaking must occur at a higher scale in a so-called *hidden sector* with a separate field content which couples to the visible sector only via non-renormalisable operators, and in doing so transmits the effects of SUSY-breaking to the visible sector. This also implies the existence of *messenger fields* which mediate this breaking between the two sectors.

These models therefore have at least three relevant scales: the SUSY-breaking scale in the hidden sector, the scale of the messenger field(s), and the scale at which SUSY is broken in the visible sector (these last two are not necessarily the same as loop factors may intervene, depending on how the messenger fields couple to the visible sector).

This must be done with the constraint that operators which can affect the couplings in equation 2.109 in such a way as to break their equality via radiative corrections must not be allowed in order to break SUSY softly. Most of these operators have been found to be of mass dimension two [118], that is, mass contributions, but which act only on the component fields for the SUSY partners (e.g. the sleptons but not the leptons), exactly as desired.

The most general soft SUSY-breaking Lagrangian is given in terms of component fields by

$$\begin{aligned}
\mathcal{L}_{\cancel{\text{SUSY}}} = &-\frac{1}{2}\left(M_1\tilde{B}\tilde{B} \;+\; M_2\sum_{a=1}^{3}\tilde{W}^a\tilde{W}_a \;+\; M_3\sum_{a=1}^{8}\tilde{g}^a\tilde{g}_a\right) \;+\; \text{h.c.} \\
&-\; m_{H_u}h_u^\dagger h_u \;-\; m_{H_d}h_d^\dagger h_d \;-\; (B\,\mu\,h_u\,h_d \;+\; \text{h.c.}) \\
&-\sum_{i,j\in\text{fam}}\Big((A_u)_{ij}(y_u)_{ij}\tilde{u}_{R,i}\tilde{Q}_j h_u \;+\; (A_d)_{ij}(y_d)_{ij}\tilde{d}_{R,i}\tilde{Q}_j h_d \;+\; (A_e)_{ij}(y_e)_{ij}\tilde{e}_{R,i}\tilde{L}_j h_u\Big) \;+\; \text{h.c.} \\
&-\sum_{i,j\in\text{fam}}\Big(\,m^2_{\tilde{Q},i}\tilde{Q}_i^\dagger\tilde{Q}_i \;+\; m^2_{\tilde{L},i}\tilde{L}_i^\dagger\tilde{L}_i \;+\; m^2_{\tilde{u},i}\tilde{u}^\dagger_{R,i}\tilde{u}_{R,i} \;+\; m^2_{\tilde{d},i}\tilde{d}^\dagger_{R,i}\tilde{d}_{R,i} \;+\; m^2_{\tilde{e},i}\tilde{e}^\dagger_{R,i}\tilde{e}_{R,i}\Big)\,,
\end{aligned} \tag{2.149}$$

where the first line corresponds to the bino, wino and gluino mass terms, the second to bilinear and mass terms for the Higgs fields, the third to the trilinear couplings between the scalar fermions and the Higgs bosons, and the bottom line to scalar fermion mass terms.

It is these terms which introduce 105 new free parameters into the model. However a number of these can be eliminated by rotations and by exploiting its symmetries. We refer the reader to [119] for a comprehensive review of this issue and of the soft SUSY-breaking Lagrangian in general.

These terms can (and must, strictly speaking) be viewed as the effective field theory operators of an unknown UV completion in which they arise as non-renormalisable operators with degrees of freedom that have decoupled and been integrated out at the low scales at which we may probe them.

The possible sources of such terms are many and are the source of the most intensive model-building efforts in SUSY. Schematically most of them can be classified in one of three classes (or combinations thereof):

- gauge-mediated SUSY-breaking models;
- gravity-mediated SUSY-breaking models;
- anomaly-mediated SUSY-breaking models.

We will not discuss these as there are vast amounts of literature available which discuss dozens of variants of them: see [99, 110] for example for introductory material, and [119] for a comprehensive overview.

Instead, we will not concern ourselves with the mechanism via which SUSY-breaking may be transmitted and will only make the assumption that this has somehow happened. From the point of view of phenomenology this allows for broader searches as no restrictions or correlations between parameters are assumed. The implementation of NLO SUSY processes in this thesis follows this general approach and works for any given set of electroweak-scale masses of the SUSY partners, provided they can be specified within the SLHA framework [120]. As such any masses can be considered, and if the tools to generate electroweak-scale mass spectra for any particular UV-scale model exist, they can then be input into the present implementation.

2.3.5 The MSSM

The Lagrangians such as those stated in equations 2.142 and 2.143 with the superpotential in equation 2.145 (which implements R-parity conservation as defined in equation 2.147), and the field contents in tables 2.6 and 2.7 as well as the soft SUSY-breaking Lagrangian of equation 2.149 together comprise the Minimal Supersymmetric Standard Model (MSSM) which is the most minimal $\mathcal{N} = 1$ Supersymmetric form of the Standard Model that can be obtained without committing to any particular UV completion.

This is the standard workhorse for experimental searches and model-building alike and is the model upon which the present implementation of NLO SQCD production of sleptons and gauginos is built upon. In particular we build on the MSSM implementation in HERWIG++ as described in [17] and the latest release version of which is described in [121].

The full set of Feynman rules for the MSSM if needed can be found for example in [122–125].

Minimal models: The CMSSM

The constrained MSSM (CMSSM) is (used to be) the most commonly studied form of the MSSM. It consists of taking high-scale unification constraints from minimal Supergravity (mSUGRA)[49] to reduce the number of free parameters of the MSSM down to a more manageable 5 parameters set at a high scale ($m_{\mathrm{GUT}} \sim 2\times10^{16}\ \mathrm{GeV}$) by setting groups of soft SUSY-breaking parameters equal to a single free parameter at this scale, as follows:

$$m_{1/2} := M_1(m_{\mathrm{GUT}}) = M_2(m_{\mathrm{GUT}}) = M_3(m_{\mathrm{GUT}}), \tag{2.150a}$$

$$A_0 := A_u(m_{\mathrm{GUT}}) = A_d(m_{\mathrm{GUT}}) = A_e(m_{\mathrm{GUT}}), \tag{2.150b}$$

$$\begin{aligned} m_0 &:= m_{H_u}(m_{\mathrm{GUT}}) = m_{H_d}(m_{\mathrm{GUT}}) = m_{\tilde{Q}}(m_{\mathrm{GUT}}) = m_{\tilde{u}}(m_{\mathrm{GUT}}) \\ &= m_{\tilde{d}}(m_{\mathrm{GUT}}) = m_{\tilde{L}}(m_{\mathrm{GUT}}) = m_{\tilde{e}}(m_{\mathrm{GUT}}), \end{aligned} \tag{2.150c}$$

with all parameters defined as in equation 2.149.

Additionally, considerations arising from EWSB imply there is one further parameter which must be specified

$$\tan\beta := \frac{\langle h_u^0 \rangle}{\langle h_d^0 \rangle}, \tag{2.151}$$

as well as one sign

$$\mathrm{sgn}(\mu), \tag{2.152}$$

where $\langle h_u^0 \rangle$ and $\langle h_d^0 \rangle$ denote the vacuum expectation values of the Higgs and μ is as defined in the MSSM superpotential (equation 2.145). Denoting the vacuum expectation values of the up-type and down-type Higgs as $v_u = \langle h_u^0 \rangle$ and $v_d = \langle h_d^0 \rangle$ as is conventionally done, their ratio is constrained to lie on the tangent of an angle from the constraint that $v_u^2 + v_d^2 = v^2$ (with v as defined in equation 2.27 to correctly produce the SM vector boson masses after EWSB) which can be trivially satisfied by defining $v_u = v\sin\beta$ and $v_d = v\cos\beta$.

[49] mSUGRA imposes the additional relations involving the gravitino mass $m_{3/2} = m_0$ and the bilinear B parameter at the GUT scale, $B_0 = A_0 - m_0$ (see for example [126]). These are relaxed in the CMSSM.

The modulus of the μ parameter is fixed by the condition[50]

$$\frac{1}{2}\, m_Z^2 \;=\; \frac{(m_{H_d} + \Delta_d) - (m_{H_u} + \Delta_u)\, \tan^2\beta}{\tan^2\beta - 1} \;-\; \mu^2\,, \tag{2.153}$$

which must be fulfilled by the general MSSM (and any variant of it) to correctly generate EWSB (that is, it comes from a minimisation of the Higgs potential in the general Higgs sector of the full MSSM), though its sign is unconstrained. All parameters in this expression are taken at the electroweak scale and the $\Delta_{u,d}$ variables denote radiative corrections.

However, μ is a parameter of the MSSM superpotential and has no *a priori* relation to the electroweak scale (or SUSY breaking) and could instead be expected to be of the order of a UV completion at a scale where SUSY lies unbroken. The large degree of fine-tuning therefore required on the right-hand side to cancel SUSY-breaking terms with the μ parameter to correctly give the mass of the Z boson is known as the *little hierarchy problem* and can be addressed within models such as the Next-to-Minimal Supersymmetric Standard Model (NMSSM) or the Giudice-Masiero mechanism [127], in which the electroweak value of μ in the superpotential is generated dynamically when a SM-singlet chiral superfield or a messenger field from a gravity-mediated UV completion acquires a vev, respectively. This fine-tuning issue however remains an open problem whilst there is no evidence of superpartners or which model they may have arisen from.

The CMSSM is therefore fully defined by a set of 4 free parameters set at the GUT scale, and one sign:

$$m_{1/2};\; m_0;\; A_0;\; \tan\beta;\; \mathrm{sgn}(\mu)\,. \tag{2.154}$$

From their high-scale values the renormalisation group evolution of each sparticle mass down to the electroweak scale (see for example figure 2.9) can be computed using software packages such as SOFTSUSY [128] or SPHENO [129] to yield the corresponding mass spectrum relevant for phenomenology.

Current Experimental Constraints on the CMSSM

Since the dominant (gaugino) loop contributions from the MSSM to the anomalous magnetic moment of the muon are proportional to μ if this anomaly is taken to be significant this gives a preference for $\mu > 0$ and therefore $\mathrm{sgn}(\mu) = +$ [130]. The measured value of the Higgs mass is also towards the maximum values for it that CMSSM-type models can generate and generically constrains[51] $\tan\beta \gtrsim 10$ [131].

Exclusions on the other CMSSM parameters are currently on a strong upwards trend as more LHC data

[50] The superpotential parameter μ may be complex and carry a phase, but we neglect this and take it to be real by definition of the MSSM, to neglect the CP-violating effects and contributions to electric dipole moments of the leptons such a phase could have.

[51] The observable with the strongest discriminating power for large $\tan\beta$ is the process $B_s \to \mu^+\mu^-$, as $\mathrm{Br}(B_s \to \mu^+\mu^-)_{MSSM} \propto \tan^6\beta$.

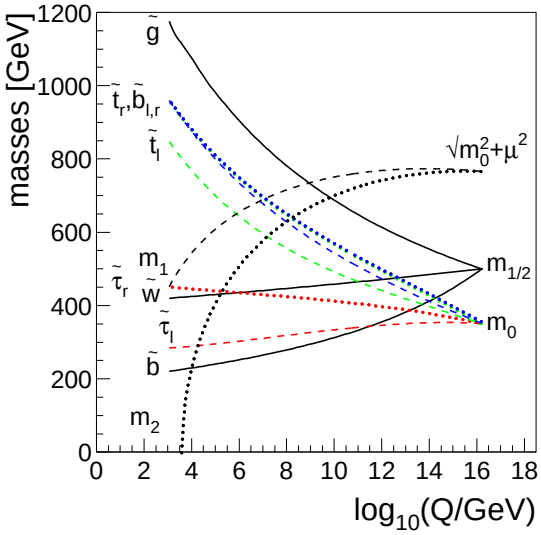

Figure 2.9: Running of the parameters of the CMSSM taken from [1]. Note that $m_2 = m_{H_u}$ runs to negative values at roughly the electroweak scale, as required for radiative EWSB.

is taken and analysed but at the time of writing the state-of-affairs of the other CMSSM parameters can summarised by the latest ATLAS exclusion plot shown in figure 2.10.

The pMSSM

If instead of considering such a highly-constrained top-down scenario such as the CMSSM where one sets unified parameters at a high scale one decides to impose the minimal set of constraints at the measurable electroweak scale which are compatible with the two strongest constraints on the full set of of parameters of the MSSM (that is, the constraint of no FCNCs or CP-violation beyond that of the SM), one obtains the phenomenological MSSM (pMSSM) as defined for example in [132, 133].

Imposing the requirement of no CP violation sets the phases of all the matrices in the soft SUSY-breaking terms to zero, and the requirement of no FCNCs makes the sfermion mass matrices and trilinear couplings ($(A_u)_{ij}$, $(A_d)_{ij}$, $(A_e)_{ij}$) diagonal (and hence each described by a single parameter, for example $(A_u)_{ij} \to A_u\,\delta_{ij}$).

Constraints from kaon mixing further imply that the first two generations of squarks must be mass degenerate to a good approximation, and since the trilinear couplings must be proportional to the fermion masses (given their proportionality to the Yukawa couplings $y_{u,d,e}$), the trilinear couplings of the first two generations can be safely set to zero.

Incorporating the parameters describing EWSB and their respective constraints the result is the presence

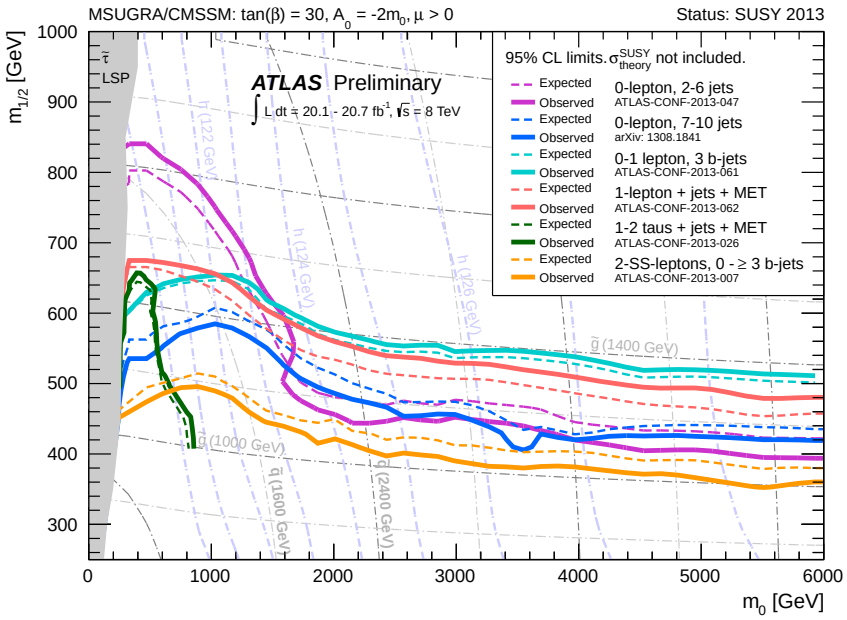

Figure 2.10: Current ATLAS exclusion of CMSSM parameters in the $(m_0, m_{1/2})$ parameter plane, with the other parameters fixed as indicated in the top margin of the plot. This exclusion is fairly independent of the values of the fixed parameters, within currently viable and reasonable ranges. The current CMS result is virtually identical. Taken from the ATLAS Supersymmetry Public Results webpage.

of only 19 free parameters (aside from those of the SM):

$$\begin{gathered} M_1;\, M_2;\; M_3; \\ m_{\tilde{Q}};\; m_{\tilde{u}_R};\, m_{\tilde{d}_R};\; m_{\tilde{L}};\; m_{\tilde{e}_R}; \\ m_{\tilde{Q};3};\; m_{\tilde{t}_R};\, m_{\tilde{b}_R};\; m_{\tilde{L}_3};\; m_{\tilde{\tau}_R}; \\ A_t;\, A_b;\; A_\tau; \\ \mu;\, m_A;\; \tan\beta\,, \end{gathered} \tag{2.155}$$

where the numeric subindex indicates generation/family number and m_A is the mass of the pseudoscalar Higgs[52].

The CMSSM(pMSSM) are only the most constrained(general -without considering the full MSSM-) forms of the MSSM. For an overview of some of the many variants in between these two see for example [132].

Model variants with correlations or lack thereof between specific MSSM parameters can be built largely to taste, depending on preference for particular types of UV completions, experimental constraints to be addressed (for example, gravity-mediated scenarios avoid FCNC constraints since gravity is flavour-blind), or whichever theoretical or experimental criteria is favoured.

Simplified Models

To avoid the theoretical assumptions of the CMSSM or the large parameter space of the pMSSM one can instead choose to restrict the MSSM by setting only a few of the superpartner masses to be kinematically accessible and taking simple limits of their mixings (for the sleptons and gauginos where mixing is relevant).

This strongly restricts the possible SUSY partners that can be produced and greatly simplifies the cascades via which their decays can proceed. These models are therefore regarded as a (semi)model-independent way to deduce constraints or target searches for only one specific superpartner and its decay modes, and are indeed the models often chosen for ATLAS and CMS searches.

However, when considering experimental results which used simplified models for their exclusions, their caveats (neglected decay modes, other mixing admixtures which reduce the coupling and nullify the exclusion, etc.) must be considered and these should not be regarded as unambiguous SUSY exclusions.

The theoretical feasibility of the simplified model must sometimes be examined as well. It is not unheard-of for non-sensical simplified models to be used for experimental searches. For example in the latest ATLAS trilepton search [134] where second mass-eigenstate neutralinos are assumed to be mostly wino, yet in one of

[52] This is one of the 5 Higgs mass eigenstates of the MSSM: two heavy charged Higgs ,$H^{\pm}$, a heavy CP-even Higgs, H^0, a CP-odd (pseudoscalar) Higgs, A^0, and the SM-like (in the *decoupling limit* in which $m_{A^0} \gg m_Z$ limit of the MSSM) Higgs, h^0.

the scenarios considered their decay is assumed to proceed exclusively via Z bosons, even though neutralinos couple to Z bosons only via their higgsino component which has been set to be negligible by assumption. This scenario is a perfectly valid search analysis, but not of SUSY, and this must be recognised and stated as such.

2.3.6 Sleptons: Mixing and Mass Eigenstates

When the SM leptons are embedded within a left(right)-handed chiral superfields as described in section 2.3.3 each of the two chiralities of the fermion are each embedded in a corresponding left(right)-handed chiral superfield and are hence now each accompanied by a complex scalar field, a *slepton*, of the same flavour[53].

The left- and right-handed sleptons of the same flavour[54] however transform under the same representations of the EW-scale unbroken gauge groups (colour and electric charge) and have the same quantum numbers (spin and R-parity) so possible mixing between them must be accounted for and the propagating mass eigenstates (those of the Klein-Gordon equation here) will generally not be identical to the interaction basis fields, but these two will be related by a similarity transformation.

Sfermion mass contributions in the MSSM come from three distinct sources:

- the superpotential (equation 2.145),

$$\begin{aligned}
\mathbf{W}_R \supset\ (y_e)_{ij}\,\mathbf{L}_i\cdot\mathbf{H}_d\,\mathbf{E}_j\Big|_{\text{scalar}} \ &=\ (y_e)_{ij}\,\tilde{e}^*_{j\,R}\,\left(\tilde{\nu}_{i\,L}\,h_d^-\ -\ \tilde{e}_{i\,L}\,h_d^0\right)\\
\Rightarrow\ -\sum_i\left|\frac{\partial\mathbf{W}_R}{\partial\phi_i}\right|^2\ &\supset\ -y_e\,\left(\left|h_d^0\right|^2\,\left|\tilde{e}_R\right|^2\ +\ \left|\tilde{\nu}_L\right|^2\,\left|h_d^-\right|^2\ +\ \left|\tilde{e}_L\right|^2\,\left|\tilde{e}_R\right|^2\ +\ \left|\tilde{\nu}_L\right|^2\,\left|\tilde{e}_R\right|^2\right)\\
&\underset{h_d^0\to v_d}{\overset{\text{EWSB}}{\supset}}\ -y_e^2\,v_d^2\,\left|\tilde{e}_R\right|^2\ ,
\end{aligned}$$

  where we have set the Yukawa matrix over families diagonal (therefore neglecting flavour mixing) and considered only the first family contribution, analogous terms follow for the other generations.

  Similarly, the superpotential term above together with the μ-term

$$\mathbf{W}_R \supset\ (y_e)_{ij}\,\mathbf{L}_i\cdot\mathbf{H}_d\,\mathbf{E}_j\Big|_{\text{scalar}}\ +\ \mu\,\mathbf{H}_u\cdot\mathbf{H}_d\Big|_{\text{scalar}}\ =\ (y_e)_{ij}\,\tilde{e}^*_{j\,R}\,\left(\tilde{\nu}_{i\,L}\,h_d^-\ -\ \tilde{e}_{i\,L}\,h_d^0\right)\ +\ \mu\,(h_u^+\,h_d^-\ -\ h_u^0\,h_d^0)\,,$$

[53] As the sleptons are scalars they clearly have no chirality but the left(right)-handed labelling is preserved to distinguish the two distinct scalars according to the superfield they are embedded in.

[54] In principle mixing between different slepton flavours is possible, however such lepton flavour violation (LFV) would introduce measurable rates of decays such as $\mu\ \to\ e\,\gamma$ which so far remain unobserved and are tightly constrained ($\text{Br}(\mu^+\ \to\ e^+\,\gamma) < 5.7\ \times\ 10^{-13}$ [135]). The dominant SM contribution to this process is via a W-ν loop where the neutrino oscillates from muon to electron flavour and the W boson emits a photon. This decay has an unmeasurably small branching ratio. The dominant SUSY contributions are from slepton-neutralino and sneutrino-chargino loops and these can produce measurable rates (see for example [136,137]). Limits on the electric dipole moment of the SM leptons further constrain flavour mixing in the slepton sector (see [138] for detailed treatment of these issues). As such flavour mixing in the slepton sector is tightly constrained and we neglect it as is customarily done.

give off-diagonal left-right mixed mass terms proportional to the μ parameter of the form

$$\sum_i \left|\frac{\partial \mathbf{W}_R}{\partial \phi_i}\right|^2 \supset \left|\frac{\partial \mathbf{W}_R}{\partial h_d^0}\right|^2 = \mu^2 |h_u^0|^2 + |y_e\, \tilde{e}^*_{j\,R}\, \tilde{e}_{i\,L}|^2 + 2\,\mu\, y_e\, h_u^0\, \tilde{e}^*_{j\,R}\, \tilde{e}_{i\,L}$$
$$\overset{\text{EWSB}}{\underset{h_u^0 \to v_u}{\supset}} 2\,\mu\, y_e\, v_u\, \tilde{e}^*_{j\,R}\, \tilde{e}_{i\,L}\,.$$

- Explicit mass terms in the soft SUSY-breaking Lagrangian, (equation 2.149)

$$m^2_{\tilde{L},i} \tilde{L}_i^\dagger \tilde{L}_i\,, \qquad m^2_{\tilde{e},i} \tilde{e}^\dagger_{R,i} \tilde{e}_{R,i}\,;$$

- trilinear terms in the soft SUSY-breaking Lagrangian,

$$(A_e)_{ij}(y_e)_{ij} \tilde{e}_{R,i} \tilde{L}_j h_u^0 + \text{h.c.}$$

These contributions can be put together in matrix form, defining for each slepton flavour mass terms of the form

$$\tilde{\mathbf{f}}^\dagger\, \mathcal{M}\, \tilde{\mathbf{f}} = \begin{pmatrix} \tilde{l}^*_L & \tilde{l}^*_R \end{pmatrix} \mathcal{M}_{2\times 2} \begin{pmatrix} \tilde{l}_L \\ \tilde{l}_R \end{pmatrix} \tag{2.156}$$

where[55]

$$\begin{aligned} \mathcal{M}_{\tilde{\nu}} &= \begin{pmatrix} m^2_{\tilde{f}_L} + m_f^2 + \Delta(f) & A_f \frac{y_f}{\sqrt{2}} v_u - \mu\, y_f\, v_d \\ A_f \frac{y_f}{\sqrt{2}} v_u - \mu\, y_f\, v_d & m^2_{\tilde{f}_R} + m_f^2 + \Delta(f) \end{pmatrix} \\ &= \begin{pmatrix} m^2_{\tilde{f}_L} + m_f^2 + \Delta(f) & m_\nu\,(A_f - \mu\, \cot\beta) \\ m_\nu\,(A_f - \mu\, \cot\beta) & m^2_{\tilde{f}_R} + m_f^2 + \Delta(f) \end{pmatrix} \end{aligned} \tag{2.157}$$

for up-type sleptons, and

$$\begin{aligned} \mathcal{M}_{\tilde{e}} &= \begin{pmatrix} m^2_{\tilde{f}_L} + m_f^2 + \Delta(f) & A_f \frac{y_f}{\sqrt{2}} v_d - \mu\, y_f\, v_u \\ A_f \frac{y_f}{\sqrt{2}} v_d - \mu\, y_f\, v_u & m^2_{\tilde{f}_R} + m_f^2 + \Delta(f) \end{pmatrix} \\ &= \begin{pmatrix} m^2_{\tilde{f}_L} + m_f^2 + \Delta(f) & m_l\,(A_f - \mu\, \tan\beta) \\ m_l\,(A_f - \mu\, \tan\beta) & m^2_{\tilde{f}_R} + m_f^2 + \Delta(f) \end{pmatrix} \end{aligned} \tag{2.158}$$

for down-type sleptons[56].

Here we have defined

$$\Delta(f) = (t_{3,\,i} - q_i \sin\theta_W)\, m_Z^2 \cos 2\beta\,,$$

and the slepton mass parameters and trilinear couplings in these mass matrices are those from the soft SUSY-breaking Lagrangian (equation 2.149).

[55] The squark mass matrices are exactly of the same form.

[56] These are equivalent under the replacements $v_u \leftrightarrow v_d$ or $\cot\beta \leftrightarrow \tan\beta$. We have used equation 2.29 to recognise the fermion masses in the off-diagonal terms.

These 2×2 mass matrices are real, symmetric and diagonalisable. However given that the off-diagonal terms are proportional to the mass of the SM leptonic partner of the same flavour, the mixing terms are negligible for most sleptons (and indeed sfermions), except the stau (sbottom and stop). The left- and right-handed interaction eigenstates of the selectron, smuon and all the flavours of sneutrinos can be taken to be mass eigenstates to a very good approximation, with their masses given by the diagonal terms of the matrices in equations 2.158 and 2.157, respectively.

This treatment of the sfermion masses is clearly accurate only at tree level and all parameters in the mixing matrix (except μ) are defined at the scale of measurement (or at the electroweak scale, m_Z, which is commonly used as a proxy). These masses (except the μ parameter which is protected by a non-renormalisation theorem, see section 2.3.2) are of course subject to radiative corrections, which are generally known to 1 loop and can be numerically computed using one of several different software packages available (see [139] for a dated but insightful review and comparison of these tools).

2.3.7 Gauginos: Gaugino-Higgsino Mixing and the Chargino(Neutralino) Mass Eigenstates

In a similar fashion as we overviewed the construction of the mixing of left- and right-handed slepton gauge eigenstates into physical (propagating) mass eigenstates in equation 2.158, the bino, wino and Higgsino fields will mix (according to electric charge) and this mixing must be accounted for to derive the corresponding physical (propagating) mass eigenstates.

The details of such mixing are more intricate here than for the slepton case, and the derivation of it can be found in several sources (for example see section 8.3.5 of [140]). Ultimately it is found that the mixing matrix describing the relation of gauge and mass eigenstates —at tree level— takes the forms given in the following subsections. In the following the sub-index i labels the mass eigenstates by increasing mass.

Chargino Masses

Defining the charged wino (2-component, Weyl spinor) component fields as $\widetilde{W}^{\pm} = (\widetilde{W}_1 \mp i\,\widetilde{W}_2)/\sqrt{2}$ from the superfields $\mathbf{W}_a$ (see table 2.7) and noting that they have the same quantum numbers [57] as the charged Higgsino component fields from the superfields $\mathbf{H}_u$ and $\mathbf{H}_d$ (see table 2.6) and we can construct the vectors $\tilde{\psi}^+ = (-i\,\widetilde{W}^+,\ \tilde{h}_u^+)^T$ and $\tilde{\psi}^- = (-i\,\widetilde{W}^-,\ \tilde{h}_d^-)^T$ and from them construct the *chargino* (mass eigenstate)

[57] Under the $SU(3)_C \otimes U(1)_Q$ symmetry group left unbroken after EWSB, as well as spin and R-parity.

Dirac mass terms in terms of Weyl spinors as

$$\mathcal{L}_{\tilde{C}^+}^{\text{mass}} = \tilde{\psi}^{-T}\, M_{\tilde{\psi}^+}\, \tilde{\psi}^+ \;+\; \text{h.c.}\,, \tag{2.159}$$

where the matrix describing the mass contributions to gauge eigenstates is given by

$$M_{\tilde{\psi}^+} = \begin{pmatrix} M_2 & \sqrt{2}\, m_W\, \sin\beta \\ \sqrt{2}\, m_W\, \cos\beta & \mu \end{pmatrix}. \tag{2.160}$$

This mass matrix can be diagonalised by two unitary matrices $U_{2\times 2}$ and $V_{2\times 2}$ (which neglecting CP violation are real and therefore orthogonal matrices) which rotate $\tilde{\psi}^{\pm}$ into chargino mass eigenstates

$$U\, \tilde{\psi^-} = \widetilde{\chi}^-\,, \tag{2.161a}$$

$$V\, \tilde{\psi^+} = \widetilde{\chi}^+\,, \tag{2.161b}$$

such that the mass terms become of the form

$$\tilde{\psi}^{-T}\, \mathcal{M}_{\tilde{\psi}^+}\, \tilde{\psi}^+ \;=\; \underbrace{\tilde{\psi}^{-T}\, U^T}_{\tilde{\chi}^{-T}}\; \underbrace{U^*\, \mathcal{M}_{\tilde{\psi}^+}\, V^\dagger}_{\text{diag}(m_{\tilde{\chi}_1}, m_{\tilde{\chi}_2})}\; \underbrace{V\, \tilde{\psi}^+}_{\tilde{\chi}^+} \;=\; \tilde{\chi}_i^{-T}\, m_{\tilde{\chi}_i}\, \delta_{ij}\, \tilde{\chi}_j^+\,, \tag{2.162}$$

where $\tilde{\chi}^{\pm}$ denote 2-component Weyl spinors.

These Weyl spinors will form the Dirac spinors as

$$\widetilde{C}_i = \begin{pmatrix} \tilde{\chi}_i^+ \\ \tilde{\chi}_i^{-\,*} \end{pmatrix} \tag{2.163}$$

as expected, so that the mass term 2.159 reads, in terms of Dirac spinors[58]

$$m_{\widetilde{C}_i}\, \overline{\widetilde{C}}_i\, \tilde{C}_i = m_{\widetilde{C}_i}\, \overline{\widetilde{C}}_i\, P_L\, \tilde{C}_i \;+\; m_{\widetilde{C}_i}\, \overline{\widetilde{C}}_i\, P_R\, \tilde{C}_i = m_{\widetilde{C}_i}\, \overline{\tilde{C}_{i\,R}}\, \tilde{C}_{i\,L} \;+\; m_{\widetilde{C}_i}\, \overline{\tilde{C}_{i\,L}}\, \tilde{C}_{i\,R}\,, \tag{2.164}$$

as expected for Dirac fermions.

Analytic solutions for these mass eigenstates exist and can be found by computing the eigenvalues of $M_{\tilde{\psi}^+}^\dagger M_{\tilde{\psi}^+}$, and the result can be found in the literature (see for example [141]) but we will not state them here.

[58] Equation 2.163 can be substituted into this expression to rewrite it in terms of Weyl spinors and equation 2.162 is reproduced, as expected.

Neutralino Masses

Similarly, defining the basis $\tilde{\psi}^0 = (-i\widetilde{B},\ -i\widetilde{W}_3,\ \tilde{h}_d^0,\ \tilde{h}_u^0)^T$ made of 2-component spinors, the neutralino mass terms are given by

$$\mathcal{L}_{\widetilde{N}}^{\text{mass}} = \frac{1}{2}\,\tilde{\psi}^{0\,T}\,M_{\tilde{\psi}^0}\,\tilde{\psi}^0 \;+\; \text{h.c.}\,, \tag{2.165}$$

where the tree-level neutralino mixing matrix is given by the real, symmetric matrix[59]

$$M_{\tilde{\psi}^0} = \begin{pmatrix} M_1 & 0 & -m_W\,\tan\theta_W\,\cos\beta & m_W\,\tan\theta_W\,\sin\beta \\ 0 & M_2 & m_W\,\cos\beta & -m_W\,\sin\beta \\ -m_W\,\tan\theta_W\,\cos\beta & m_W\,\cos\beta & 0 & -\mu \\ m_W\,\tan\theta_W\,\sin\beta & -m_W\sin\beta & -\mu & 0 \end{pmatrix} \tag{2.166}$$

Diagonalisation of this matrix to find the mass eigenstates (which requires only a single unitary matrix since it is symmetric) is performed by Takagi diagonalisation using a single unitary matrix, $N_{4\times4}$,[60]

$$N^*\,M_{\tilde{\psi}^0}\,N^\dagger = \text{diag}(m_{\widetilde{\chi}_1^0},\ m_{\widetilde{\chi}_2^0},\ m_{\widetilde{\chi}_3^0},\ m_{\widetilde{\chi}_4^0})\,, \tag{2.168}$$

and a corresponding rotation to the 2-component spinors of neutralino mass eigenstates, $\widetilde{\chi_i^0}$,

$$\widetilde{\chi}_i^0 \;=\; N_{ij}\,\tilde{\psi}_j^0\,, \tag{2.169}$$

such that the Weyl spinor neutralino mass terms are of the form

$$\tilde{\psi}^{0\,T}\,M_{\tilde{\psi}^0}\,\tilde{\psi}^0 \;=\; \underbrace{\tilde{\psi}^{0\,T}\,N^T}_{\widetilde{\chi}^{0\,T}}\;\underbrace{N^*\,M_{\tilde{\psi}^0}\,N^\dagger}_{\text{diag}(m_{\widetilde{\chi}_1^0},\,m_{\widetilde{\chi}_2^0},\,m_{\widetilde{\chi}_3^0},\,m_{\widetilde{\chi}_4^0})}\;\underbrace{N\,\tilde{\psi}^0}_{\widetilde{\chi}^0}\,. \tag{2.170}$$

Neutralinos are Majorana fermions and as such their Dirac spinors are constructed from the Weyl spinors we have just constructed as

$$\widetilde{N}_i \;=\; \begin{pmatrix} \widetilde{\chi}_i^0 \\ \widetilde{\chi}_i^{0\,*} \end{pmatrix}\,, \tag{2.171}$$

[59] This matrix is sometimes written in terms of gauge couplings and vevs using the relations $v_d = v\,\sin\beta$, $v_u = v\,\cos\beta$, $m_W = v\,g_2/2$ and $g_1 = g_2\,\tan\theta_W$.

[60] Takagi diagonalisation is not an eigenvalue decomposition but instead a special case of a singular value decomposition of an arbitrary rectangular (and possibly singular) matrix, $A \in \mathbb{C}^{m\times n}$ as

$$V^*\,A\,W^\dagger = \text{diag}(\sigma_1,\ \ldots\ ,\sigma_{\bar{n}}) \tag{2.167}$$

where V and W are unitary matrices, σ_i are the *singular values* of A, $\bar{n} = \min(m,\,n)$ and Takagi diagonalisation corresponds to the special case $V = W$. Unlike eigenvalue decomposition the matrix A may be singular ($\det(A) = 0$), so that this decomposition is possible even for degenerate or nearly-degenerate mass solutions, where the matrix becomes singular and eigenvalue decomposition becomes impossible. The matrices V and W are constructed from the orthonormal eigenvectors of AA^T and A^TA, respectively. For a full treatment of Takagi diagonalisation see appendix A in [142].

with the Majorana mass terms correspondingly being of the form

$$-\frac{1}{2}\, m_{\widetilde{N}_i}\, \overline{\widetilde{N}_i}\, \widetilde{N}_i\,. \tag{2.172}$$

Within this context if the spinor components giving the mass eigenstate are heavily dominated by a given gauge eigenstate the neutralino is referred to as

$$\begin{aligned} \widetilde{\chi}_i^0 \;\approx\; \tilde{\psi}_1^0 \quad &\Rightarrow \quad \widetilde{N}_i \;\; \mathrm{bino-like\,(photino)}\,, \\ \widetilde{\chi}_i^0 \;\approx\; \tilde{\psi}_2^0 \quad &\Rightarrow \quad \widetilde{N}_i \;\; \mathrm{wino-like\,(zino)}\,, \\ \widetilde{\chi}_i^0 \;\approx\; \tilde{\psi}_{3,\,4}^0 \quad &\Rightarrow \quad \widetilde{N}_i \;\; \mathrm{Higgsino-like}\,. \end{aligned} \tag{2.173}$$

More generally if $M_1,\ M_2 \ \gg\ \mu$ the corresponding neutralinos will be referred to as 'gaugino-like', and conversely if $\mu \ \gg\ M_1,\ M_2$ they are referred to as 'Higgsino-like'[61].

It is worth noting that the Higgsino component of neutralinos couples only to the Z boson (the coupling can be seen to be proportional to $N_{i,\,3}$ and $N_{i,\,4}$ only). Higgsino-like neutralinos are therefore typically the most constrained near the Z pole, with other compositions significantly less constrained.

The diagonalisation of the mass matrix can yield negative mass solutions and there are two different but equivalent conventions in dealing with these: either the diagonalising matrix N is allowed to be complex in which case it can be guaranteed that the mass solutions will be positive, or N can be restricted to be real, in which case negative mass solutions can occur[62]. In the latter case these can be dealt with by taking the absolute value as the physical mass and multiplying the corresponding field by a phase (effectively a factor of i in its Feynman rules), as $\widetilde{\chi}_j^0 \to e^{i\pi/2}\, \widetilde{\chi}_j^0$.

Typically the diagonalisation of the mass matrices is performed numerically by software packages such as SPHENO [129] and SOFTSUSY [128], which also perform the RG evolution of the SUSY GUT-scale parameters down to the weak scale. The known one-loop radiative corrections [143] to these masses are also implemented and automatically included by these software packages. We therefore use them to produce mass spectra as input for our event generation.

2.3.8 Naturalness

Though the MSSM solves the hierarchy problem, it is not without fine-tunings of its own, as mentioned previously in the context of the little hierarchy problem in section 2.3.5. As such various quantitative measure of such fine-tuning can be adopted and the so-called *naturalness* of variants of the MSSM can be computed

[61] Any set of neutralinos or charginos (regardless of their composition) may be referred to collectively as 'gauginos' or 'electroweakinos', and we will hereon follow this convention.

[62] The latter is the chosen for the SUSY Les Houches Accord (SLHA) conventions [120], which we adhere to.

and compared, generally based on the Giudice-Barbieri measure [144] of how much fine-tuning the model requires to satisfy equation 2.153.

Furthermore, one can define the naturalness of a parameter being small judging by whether the theory acquires any new symmetries in the limit that such a parameter vanishes (*technical naturalness* as credited to t' Hooft, 1980) or *absolute naturalness* as is considered for MSSM models (see [145] for a general discussion).

Moreover, even measures of absolute naturalness are ambiguous [146–149]. One could even consider defining naturalness as how likely a given model (say, the MSSM) is likely to appear from certain types of UV completions. In this context, $\mathcal{N} = 1$ SUSY was for example found to be unlikely/unnatural for the SM gauge groups from the perspective of a flat scan over 10^7 four-dimensional heterotic string theory models [150].

We therefore will not discuss naturalness (and possible measures of it) here and we refer the reader to general discussions such as those in [147, 151, 152].

2.3.9 Status of Current SUSY Searches

Present SUSY exclusions are constantly being updated and becoming out-dated, and are each a function of the SUSY model variant (CMSSM, pMSSM, a particular simplified model, etc.) within which they were deduced. Given this model-dependence and that the exclusions can expected to continue to grow (or yield a discovery) as data taken is progressively analysed and the data taking resumes in 2015 for the $13\ \mathrm{TeV}$ run of the LHC, experimental limits are continuously being updated and the reader is referred to the Public Results pages of the ATLAS and CMS collaborations for up-to-date information on SUSY searches:
ATLAS Supersymmetry Public Results:
`https://twiki.cern.ch/twiki/bin/view/AtlasPublic/SupersymmetryPublicResults`
CMS Supersymmetry Physics Results:
`https://twiki.cern.ch/twiki/bin/view/CMSPublic/PhysicsResultsSUS`

For a comprehensive (but only annually updated) review of SUSY limits see the 'Supersymmetry, Part II (Experimental)' section of the Particle Data Group annual review [40]. For overviews of the implications of current experimental constraints for SUSY model-building see [147, 153].

Despite the model-dependence of individual SUSY searches, the combination of relatively inclusive searches can yield arguably universal mass limits [154], with the universal exclusions and blind spots of such combinations of multiple searches also currently being studied [155]. Computationally-intensive scans over the parameter space of the pMSSM to identify excluded and allowed regions have also been performed [156] and yield relatively model-independent results.

For an overview of all experimental constraints on the CMSSM accurate at the time of writing see [157]. As a rough indication of the range of current mass exclusions in SUSY searches from ATLAS and CMS see figure 2.11, and within the context of the CMSSM see figure 2.10. The only overall conclusion of all SUSY searches so far is that there is so far no statistically significant deviation from the SM which could signal an unambiguous detection of a superpartner to a SM particle.

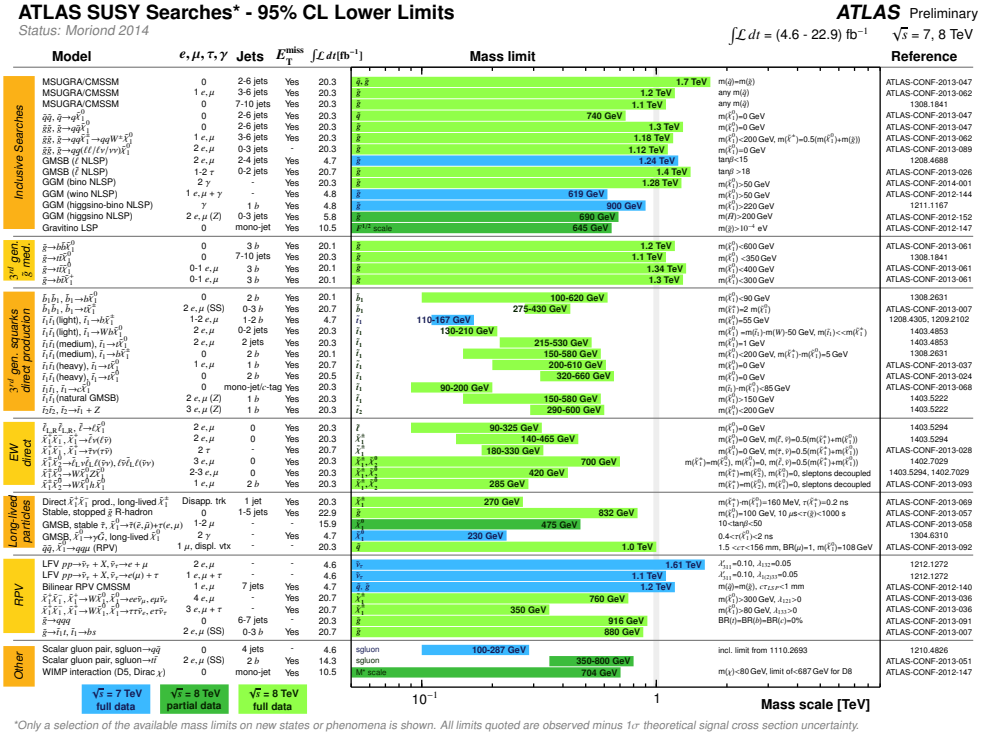

(a)

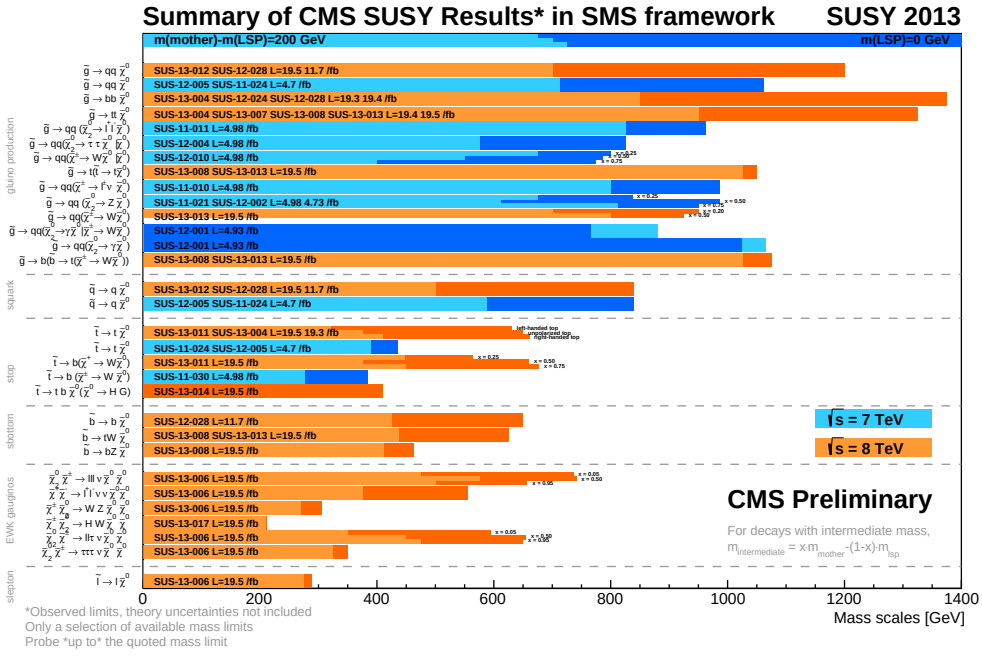

(b)

Figure 2.11: The current ATLAS (a) and CMS (b) mass exclusion limits for R-parity conserving models. For the CMS limits the dark bars indicate limits obtained with $m_{\widetilde{N}_0} = 0$ GeV and lighter bars assume $m_{\text{mother}} - m_{\widetilde{N}_0} = 200$ GeV. CMS mass limits are shown from 0 GeV for simplicity but the lower end of the mass exclusion will be determined by thresholds and kinematic limits of each particular channel and the corresponding resolutions and backgrounds of each search and analysis.
Mass limits from both ATLAS and CMS shown here are to be taken as upper bounds on the excluded masses for the assumed production channel and decay modes. The corresponding exclusion for models with more possible decay modes, production channels and admixtures will be more modest.

Chapter 3

The Anatomy of Next-to-Leading Order Calculations

Our current understanding of fundamental processes as probed at colliders relies on one fundamental relation which underlies the computability of large invariant-mass ($s \gg \Lambda_{\mathrm{QCD}}$) interactions in the Standard Model. This is the perturbative expansion in powers of a coupling, allowing for differential partonic scattering cross sections to be computed as[1]

$$d\sigma = \sum_n \alpha^n d\sigma^{(n)}\,, \tag{3.1}$$

where the sum starts from the power in the coupling of the leading order process, α, (which is defined as $\alpha = \frac{g^2}{4\pi}$ relative to the gauge coupling, g) and $d\sigma^{(0)}$ are partonic cross sections computable by Feynman diagrams or other methods.

Leading order calculations of a physical process (i.e. those containing only the first term in the perturbative expansion in equation 3.1) only provide a first approximation to the shape of differential distributions, and an order of magnitude estimate of the cross section. In fact for observables where the Born process is the leading order contribution (that is, it provides a meaningful physical result) the first true prediction of the observable's normalisation first arises only at NLO. Consequently, when searching for BSM processes an accurate prediction of both the signal normalisation and effect on the shape of distributions is crucial.

The processes we deal with produce colour-singlet final states at the Born level, and hence are not subject

[1]For the most part in this chapter we will work at the level of partonic cross sections. To obtain observable hadronic cross sections the convolution with parton distribution functions and sum over initial states indicated in equation 2.22 must be carried out.

to as large NLO QCD corrections at a hadron collider as they would be if the final state had colour charge, however corrections are still typically $\mathcal{O}(10\%)$, and are hence not negligible given that current experimental uncertainties can already be of that order or smaller.

Signals from BSM scenarios are typically small, with the dominant radiative corrections yielding a *K factor*[2] usually larger than 1 in most regions of phase space. Such an increase in the signal cross section is therefore desirable to reliably predict potential signal sizes in data samples (whether for reach determination, exclusion, or model discrimination).

Moreover, even if the NLO corrections were to induce very little change in the normalisation or shape of the observable, they strongly reduce the scale variation (of both the renormalisation scale, μ_R and the factorisation scale μ_F when they are set equal to each other) of both the total and the differential cross sections, thereby reducing the theory uncertainty of the signal prediction[3].

3.1 Drell-Yan Production

The first hadron-hadron process to be calculated in the framework of the (then new) parton model as proposed by Feynman was the 1970 calculation by Drell and Yan of the differential cross section $d\sigma/dQ^2$ for the collision of two hadrons whereby the inelastic scattering of two 'non-"wee" ' (sic) i.e. hard partons produces a massive lepton pair [159].

$$p\,p' \longrightarrow \gamma \longrightarrow l\,\bar{l}\,, \tag{3.2}$$

where p, p' are used here to designate any hadron.

Drell and Yan originally considered only the photon-mediated process, but Drell-Yan is now used to refer to the EW gauge boson-mediated processes too, and it is in this general sense that we refer to it here (see figure 3.1).

This was also the first process for which NLO QCD radiative corrections were calculated, both using dimensional regularisation [160] and massive parton regularisation [161]. Additionally this process is one of the very few for which the factorisation theorem from equation 2.22 has been rigorously proven, for the $\frac{d\sigma}{dQ^2 dy}$

[2]Defined globally as $K = \frac{\sigma_{\mathrm{NLO}}}{\sigma_{\mathrm{LO}}}$ or locally as $K(\mathbf{\Phi}) = \frac{d\sigma_{\mathrm{NLO}}(\mathbf{\Phi})/dO(\mathbf{\Phi})}{d\sigma_{\mathrm{LO}}(\mathbf{\Phi})/dO(\mathbf{\Phi})}$ where $\mathbf{\Phi}$ denotes the relevant phase space, O denotes the observable under consideration and σ_{LO} and σ_{NLO} are the total fully-inclusive cross sections, respectively.

[3]This holds if scale variation can indeed be taken as a proxy for approximate theoretical uncertainty. Such uncertainty is by no means Gaussian and the variation under $\frac{1}{2}\mu_{R(F)} \to \mu_{R(F)} \to 2\mu_{R(F)}$ does not in any way correspond to any number of standard deviations. For our purposes we will consider scale variation as a lower bound on theoretical uncertainty. However even this approach can fail as simultaneous variation of both μ_F and μ_R could in principle result in opposite and partly cancelling contributions from the parton distribution functions and the partonic cross sections at certain scales, producing an underestimation of the theory uncertainty. A statistical analysis of how well scale variation can be said to be a measure of theoretical uncertainty is performed in [158].

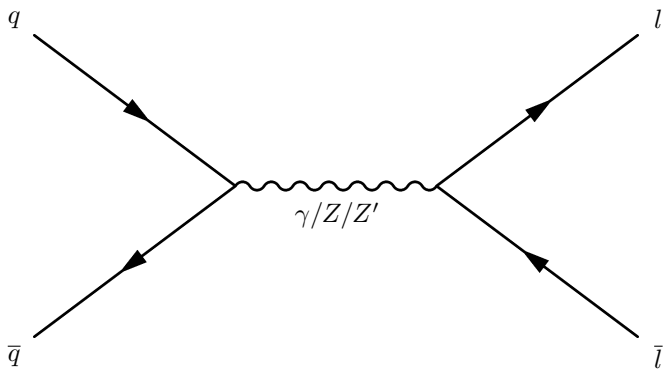

Figure 3.1: The leading order Drell-Yan process.

differential distribution at LO [162], and later also at NLO [163].

As of the time of writing the NNLO radiative corrections in QCD for the fully inclusive cross section [164] and also the rapidity distribution [165] are both known. The NLO QCD, photonic and EW radiative corrections within both the SM and the MSSM (Minimal Supersymmetric Standard Model) have also been calculated [166].

The effects of next-to-next-to-leading logarithm (NNLL) resummation (matched to NLO QCD corrections) are also known, both for soft gluon resummation [167] and p_T resummation [168]. The effects of resummation of higher-order large logarithms in a high-energy limit have also been calculated [169].

Tools to compute Drell-Yan observables at NNLO in QCD exist in the form of the software packages FEWZ [170] and DYNNLO [171]. The effects of soft gluon resummation for Drell-Yan observables can also be computed using the software package ResBos [172]. Therefore Drell-Yan is possibly the best understood hadron-hadron process in particle physics [4] and forms the basis for the first part of the work in this thesis. In the following sections of this chapter we thus focus on this process and the NLO QCD radiative corrections to it.

We now overview the structure and relevant features and the Feynman-diagrammatic calculation techniques of next-to-leading order corrections.

[4] Followed by the other known colour-singlet production process: Higgs production.

3.2 The Born Contribution

The parton-level Born contribution for photon-mediated[5] Drell-Yan production of lepton pairs[6] is given by the diagrams shown in figure 3.1 where each possible mediator constitutes a separate diagram and their interference must be computed.

Firstly we shall compute the total leading order contribution, in $d = 4 - 2\epsilon$ dimensions. Note that to make a UV divergent integral well defined we would require $d < 4$, and likewise infrared (IR) divergent integrals require $d > 4$ to converge. Here we will focus on IR divergences so we will define $\epsilon < 0$, though for our purposes the sign of ϵ will not be directly relevant. The differential partonic cross section is given by the product of the spin and colour averaging factors, the two particle flux factor, the spin and colour summed amplitude squared and the relevant phase space, in this case

$$d\sigma_B = \frac{1}{2}\frac{1}{2}\frac{1}{3}\frac{1}{3}3\frac{1}{2s}\left|\overline{\mathcal{M}_B}\right|^2 d\phi_2\,, \tag{3.3}$$

where s denotes the partonic centre-of-mass energy (obtained from the hadronic one, S, via $s = x_1x_2S$) and the bar over the amplitude denotes a sum over spin and colour[7].

Using p_i to denote incoming four momenta and k_j to label outgoing final state momenta the n-body Lorentz invariant phase space is defined to be

$$d\phi_n = \prod_j^n \left(\frac{1}{(2\pi)^{(d-1)n}}\frac{d^{d-1}k_j}{2\omega_j}\right)\delta^d\left(\sum_i p_i - \sum_j k_j\right)\,. \tag{3.4}$$

In the Born contribution the relevant phase space in $d = 4 - 2\epsilon$ is then

$$d\phi_2 = \frac{1}{(2\pi)^{d-2}}\frac{d^{d-1}k_1}{2\omega_1}\frac{d^{d-1}k_2}{2\omega_2}\,\delta^d(p_1 + p_2 - k_1 - k_2)\,. \tag{3.5}$$

The fully integrated phase space (where we have implicitly assumed that the amplitude squared has no angular dependence, as is indeed the case for Drell-Yan at leading order) can then be shown to be

$$\int d\phi_2 = \frac{1}{8\pi}\left(\frac{4\pi}{Q^2}\right)^{\epsilon}\frac{\Gamma(1-\epsilon)}{\Gamma(2-2\epsilon)}\,. \tag{3.6}$$

For future reference the two-body phase space unintegrated in angular variables (for processes which have angular dependence) for a massless particle and a massive one (with mass m, so that $Q^2 \to m^2$ in the equation

[5] The $W^{\pm}/Z$ contribution is readily by including the diagrams with the relevant couplings modified before squaring and computing traces.

[6] We neglect the $q\bar{q}$ final state as it is is susceptible to much higher (for example, dijet) background rates and involves a considerably more complicated infrared singularity structure at NLO.

[7] Elsewhere in the main body of this thesis this barred notation denotes both the sum over spin and colour as well as the averaging over them for the initial state.

below, or an off-shell massless one with virtuality Q^2) is, using $y = (1+\cos\theta)/2$ as the angular variable,

$$\int d\phi_2 = \frac{1}{8\pi}\,\frac{(4\pi)^\epsilon}{\Gamma(1-\epsilon)}\,\frac{(s-Q^2)^{1-2\epsilon}}{s^{1-\epsilon}}\,\int_0^1 dy\,[y(1-y)]^{-\epsilon}\,. \tag{3.7}$$

We now proceed to the calculation of the amplitude squared, where the only contributing diagram is that shown in figure 3.1. For simplicity we will consider the photon mediated diagrams rather than the Z mediated ones, however these can readily be obtained by replacing the couplings and propagator in the amplitude as $Q_i e_f \to \frac{g_2}{\cos\theta_W}(t_{3i} - Q_i \sin^2\theta_W)$ and $\frac{1}{q^2} \to \frac{1}{(q^2-m_Z^2)+im\Gamma}$ before squaring.

The amplitude from this Feynman diagram (using Feynman gauge for the propagator) is given by

$$\mathcal{M}_B = \overline{v}(p_2)(ieQ_f\gamma^\mu)u(p_1)\frac{-ig_{\mu\nu}}{q^2}\overline{u}(k_1)(ie\gamma^\nu)v(k_2)\,, \tag{3.8}$$

which upon squaring yields

$$|\mathcal{M}|^2 = \mathcal{M}_B^\dagger\mathcal{M}_B \;=\; e^4\,Q_f^2\,\frac{1}{(q^2)^2}\,\mathrm{Tr}[\not{p}_1\gamma_\nu\not{p}_2\gamma_\beta]\,\mathrm{Tr}[\not{k}_2\gamma^\nu\not{k}_1\gamma^\beta] \;=\; e^4\,Q_f^2\,\frac{1}{(q^2)^2}\,H_{\nu\beta}\,L^{\nu\beta}\,. \tag{3.9}$$

Current conservation implies that for both fermionic currents contraction with the photon momentum must yield zero $q_\nu L^{\nu\beta} = 0$, $q^\nu H_{\nu\beta} = 0$. In particular given that the only Lorentz structures available are q^ν and $g^{\nu\beta}$ this implies that the leptonic tensor for example must have the form $L^{\nu\beta} = (q^2 g_{\nu\beta} - q_\nu q_\beta)\,L(q^2)$. Taking the trace over the Lorentz indices we see that $g_{\nu\beta}L^{\nu\beta} = L^\nu_\nu = 3q^2\,L(q^2)$. Computing $g_{\nu\beta}L^{\nu\beta}$ directly from equation 3.9 gives

$$g_{\nu\beta}L^{\nu\beta} = -4(1-\epsilon)s\,, \tag{3.10}$$

from which it can be deduced that

$$L(q^2) = -\frac{4(1-\epsilon)}{3}\,. \tag{3.11}$$

The Lorentz trace over the hadronic tensor proceeds analogously and yields

$$g^{\nu\beta}H_{\nu\beta} = -4(1-\epsilon)s\,. \tag{3.12}$$

Using these ingredients we can then compute the contraction of the leptonic and hadronic tensors required, via $H_{\nu\beta}L^{\nu\beta} = q^2 g^{\nu\beta}H_{\nu\beta}\,L(q^2)$ giving the amplitude squared as

$$|\mathcal{M}|^2 = e^4\,Q_f^2\,\frac{1}{(q^2)^2}\,H_{\nu\beta}\,L^{\nu\beta} \;=\; \frac{16}{3}\,(1-\epsilon)\,e^4\,Q_f^2\,. \tag{3.13a}$$

Inserting this amplitude squared and the phase space defined in equation 3.6 into the equation for the partonic cross section (equation 3.3) and defining $\alpha = \frac{e^2}{4\pi}$ one finds the total LO partonic Drell-Yan cross

section to be

$$\sigma_B = \frac{4}{9}\frac{1}{s}\,\pi\,\alpha^2\,Q_f^2\,(1-\epsilon)\,\left(\frac{4\pi}{s}\right)^{\epsilon}\,\frac{\Gamma(1-\epsilon)}{\Gamma(2-2\epsilon)}\,. \tag{3.14}$$

Which upon taking the $d = 4$ ($\epsilon \to 0$) limit yields the well known total leading-order partonic Drell-Yan cross section

$$\sigma_B = \frac{4\pi\alpha^2}{9\,s}\,Q_f^2\,. \tag{3.15}$$

It is worth noting that this result was infrared finite at all times, so computing within dimensional regularisation was unnecessary but done for consistency with the NLO contributions which will be computed next.

3.3 Next-to-leading Order Contributions

We will now overview the $\mathcal{O}(\alpha_S)$ contributions to Drell-Yan. This consists of the diagrams shown in figure 3.2.

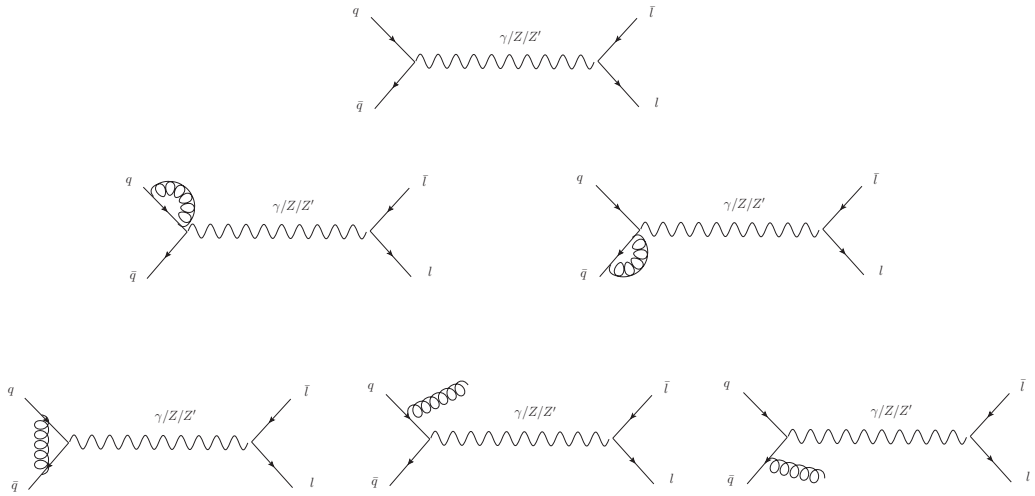

Figure 3.2: The next-to-leading order corrections to Drell-Yan lepton pair production. The leading order (Born) contribution is shown in the first row, the virtual self-energy corrections to the incoming partons are shown in the second row, and the vertex correction and real emission contributions are shown in the last row.

The first calculation of these next-to-leading order corrections was performed in [160]. We follow [173–175] but equivalent treatments can be found in [176]. For a treatment including dipole subtraction see section 6.1 of [177].

3.3.1 Real Emission

In this section we will compute the $q\overline{q} \to g\bar{l}l$ contribution. There are two diagrams associated with gluon emission (as well as an interference term between them, with the corresponding factor of two), these are shown in figure 3.3 (there are also three terms corresponding to $qg \to qll$ and $\bar{q}g \to \bar{q}ll$ which we omit).

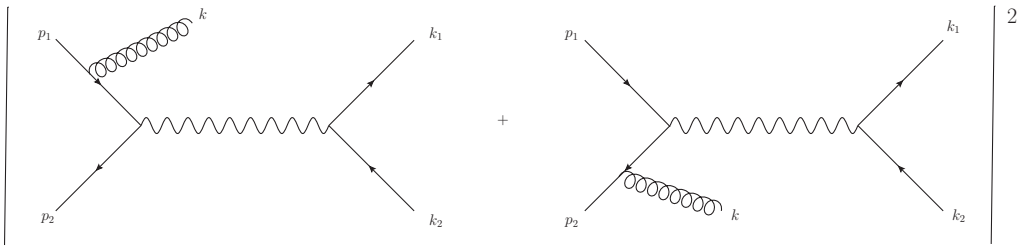

Figure 3.3: The real emission contributions to Drell-Yan at NLO.

The real contribution to the partonic cross section is given by

$$d\sigma_R = \frac{1}{2}\frac{1}{2}\frac{1}{3}\frac{1}{3}4\frac{1}{2s}\left|\overline{\mathcal{M}_R}\right|^2 d\phi_3\,, \tag{3.16}$$

where the factors of $1/2$ come from spin averaging over the two initial state fermions, the factors of $1/3$ from their colour averaging and the factor of 4 from the trace over the colour generators (in the adjoint representation) from the gluon vertex squared (where using the relation $\mathrm{Tr}\, t^a t^b = \frac{1}{2}\delta^{ab}$ we see that the relevant trace $\mathrm{Tr}\, t^a t^a = \frac{1}{2}\,\delta^{aa} = \frac{1}{2}8 = 4$).

The 3-body phase space is given by

$$d\phi_3 = \frac{d^{d-1}k_1}{(2\pi)^{d-1}2E_1}\,\frac{d^{d-1}k_2}{(2\pi)^{d-1}2E_2}\,\frac{d^{d-1}k_3}{(2\pi)^{d-1}2E_3}\,(2\pi)^d\,\delta^d(p_1+p_2-k_1-k_2-k_3)\,. \tag{3.17}$$

We begin by factorising the three-body phase space into the product of two 2-body phase spaces by inserting the identity

$$1 = \int \frac{dQ^2}{2\pi}\int \frac{d^{d-1}q}{(2\pi)^{d-1}2E_q}(2\pi)^d\delta^d(q-k_1-k_2)\,, \tag{3.18}$$

(where the virtual boson momenta is given by $q = k_1 + k_2$) and rearranging the terms so that the phase space is split into a 2-body phase space for k_3 and q, and another one for k_1 and k_2, with a delta distribution

matching the momenta between the two

$$\begin{aligned} d\phi_3 &= \frac{dQ^2}{2\pi}\left[\frac{d^{d-1}k_3}{(2\pi)^{d-1}2E_3}\,\frac{d^{d-1}q}{(2\pi)^{d-1}2E_q}\,(2\pi)^d\,\delta^d(p_1+p_2-q-k_3)\right] \\ &\times\left[\frac{d^{d-1}k_1}{(2\pi)^{d-1}2E_1}\,\frac{d^{d-1}k_2}{(2\pi)^{d-1}2E_2}\,(2\pi)^d\,\delta^d(q-k_1-k_2)\right], \\ &= \frac{dQ^2}{2\pi}d\phi_2^{q,k_3}\,d\phi_2^{k_1,k_2}\,. \end{aligned} \tag{3.19}$$

We now note that $d\phi_2^{k_1,k_2}$ is precisely of the form of the Born-level phase space, and can be fully integrated to give equation 3.6, while $d\phi_2^{q,k_3}$ is given by the general 2-body phase space expression, equation 3.7, where the angular integration has not yet been performed as the matrix element will depend on it.

After this phase space factorisation the real emission contribution is now given by

$$d\sigma_R = \frac{1}{2}\frac{1}{2}\frac{1}{3}\frac{1}{3}4\frac{1}{2s}\,\overline{|\mathcal{M}_R|^2}\frac{dQ^2}{2\pi}d\phi_2^{q,k_3}\,d\phi_2^{k_1,k_2}\,. \tag{3.20}$$

There are two diagrams associated with gluon emission (as well as an interference term between them, with the corresponding factor of two), these are shown in figure 3.3.[8]

Since the leptonic tensor is identical to the Born case we will focus on the hadronic contribution which is where the NLO corrections and hence the singularity structure resides.

Considering gluon emission with momentum k off the quark with momentum p_1 will yield an amplitude of the form (neglecting the photon propagator, the vertex to the leptons and the leptonic tensor from here on)

$$\mathcal{M}_R^{p_1} = i\,e\,Q_f\,g_S\,t^a\,\mu^\epsilon\,\left(\frac{1}{t}\,\overline{v}(p_2)\,\gamma^\alpha\,(\not{p}_1-\not{k})\,\gamma^\mu\,u(p_1)\right)\,\epsilon^*_{\alpha\,\lambda}(k) \tag{3.21}$$

where $\epsilon^*_{\alpha\,\lambda}(k)$ denotes the polarisation four-vector for the emitted gluon of helicity λ and is not be confused with the dimensional regularisation parameter.

Upon squaring and performing the colour sum and the sum over gluon polarisations using $\sum_{\lambda,\lambda'}\epsilon^*_{\alpha\,\lambda}(k)\epsilon_{\beta\,\lambda'}(k) = -g_{\alpha\beta}$, the relevant amplitude squared is[9]

$$|\mathcal{M}_R^{p_1}|^2 = -e^2\,Q_f^2\,g_S^2\,C_F\,\mu^{2\epsilon}\,\frac{1}{t^2}\,\mathrm{Tr}\left[\not{p}_1\,\gamma_\mu\,(\not{p}_1-\not{k})\,\gamma_\alpha\,\not{p}_2\,\gamma^\alpha\,(\not{p}_1-\not{k})\,\gamma^\mu\right]\,, \tag{3.22}$$

where we have defined $t=(p_1-k)^2$ (and analogously $u=(p_2-k)^2$).

Performing the trace yields

$$\frac{1}{t^2}\,\mathrm{Tr}\left[\not{p}_1\,\gamma_\mu\,(\not{p}_1-\not{k})\,\gamma_\alpha\,\not{p}_2\,\gamma^\alpha\,(\not{p}_1-\not{k})\,\gamma^\mu\right] = 8\,\frac{u}{t}\,(1-\epsilon)^2\,. \tag{3.23}$$

[8] Note that there are also three terms corresponding to $qg\to qll$ and $\bar{q}g\to\bar{q}ll$ which we omit.

[9] We work in the conventional dimensional regularisation scheme where all momenta and polarisation vectors are taken in d dimensions, as well as the the numerator algebra ($\gamma^\nu\gamma_\nu = d$, $\{\gamma^\mu,\gamma^\nu\} = 2g^{\mu\nu}$, $\{\gamma^\mu,\gamma^5\} = 0$, $(\gamma^5)^2 = 1$, $(\gamma^0)^2 = 1$, $(\gamma^\mu)^\dagger = \gamma^0\gamma^\mu\gamma^0$, etc.) are assumed to hold, and for spin-averaging purposes quarks still have 2 degrees of freedom but gluons have $d-2 = 2-2\epsilon$ degrees of freedom, as that is how many transverse directions there are in d dimensions.

So that the amplitude squared is

$$|\mathcal{M}_R^{p_1}|^2 = -8\, e^2\, Q_f^2\, g_S^2\, C_F\, \mu^{2\epsilon}\, \frac{u}{t}\, (1-\epsilon)^2\,. \tag{3.24}$$

Emission off the anti-quark will yield an identical expression with the exchange $t \leftrightarrow u$ (or $p_1 \leftrightarrow p_2$ at the amplitude level)

$$|\mathcal{M}_R^{p_2}(s,t,u)|^2 = |\mathcal{M}_R^{p_1}(s,t\leftrightarrow u)|^2 \;=\; -8\, e^2\, Q_f^2\, g_S^2\, C_F\, \mu^{2\epsilon}\, \frac{t}{u}\, (1-\epsilon)^2\,. \tag{3.25}$$

The interference term (emission off one quark leg times the complex conjugate of emission off the other incoming leg) has the form

$$|\mathcal{M}_R^{p_1,p_2}|^2 = -e^2\, Q_f^2\, g_S^2\, C_F\, \mu^{2\epsilon}\, \frac{1}{t\,u}\, \mathrm{Tr}\left[\not{p}_2\, \gamma^\alpha\, (\not{p}_2 - \not{k})\, \gamma_\mu\, \not{p}_1\, \gamma_\alpha\, (\not{p}_1 - \not{k})\, \gamma^\mu\right]\,, \tag{3.26}$$

where the corresponding Dirac trace gives

$$\frac{1}{t\,u}\, \mathrm{Tr}\left[\not{p}_2\, \gamma^\alpha\, (\not{p}_2 - \not{k})\, \gamma_\mu\, \not{p}_1\, \gamma_\alpha\, (\not{p}_1 - \not{k})\, \gamma^\mu\right] \;= -8\, \frac{s\,Q^2}{t\,u}\, (1-\epsilon) + 8\epsilon(1-\epsilon)\,. \tag{3.27}$$

Here we already see the singularity structure of amplitude squared, as $t \to 0$ and $u \to 0$ correspond to singular collinear limits and $t, u \to 0$ corresponds to a soft singularity.

Adding the amplitudes squared for emission off each leg, and the interference term of the two (with its corresponding factor of 2) gives the total $q\bar{q} \to g\bar{l}l$ real emission contribution we seek

$$|\mathcal{M}_R|^2 = |\mathcal{M}_R^{p_1}|^2 + |\mathcal{M}_R^{p_2}|^2 + 2\,|\mathcal{M}_R^{p_1,p_2}|^2\,, \tag{3.28a}$$

$$= -e^2\, Q_f^2\, g_S^2\, C_F\, \mu^{2\epsilon}\, (1-\epsilon)\left[16\, \frac{s\,Q^2}{t\,u} + 8(1-\epsilon)\left(\frac{u}{t} + \frac{t}{u}\right) - 16\epsilon\right]\,. \tag{3.28b}$$

Reinserting the photon propagator and the leptonic vertex and tensor, as well as defining $\alpha = e^2/4\pi$ and $\alpha_s = g_s^2/4\pi$ and recognising the Born cross section, σ_B, and inserting the amplitude squared in the equation for the partonic cross section gives

$$\frac{d\sigma_R^{q\bar{q}}}{dQ^2} = \frac{1}{2}\frac{1}{2}\frac{1}{3}\frac{1}{3} 4 \frac{1}{2Q^2}\, |\overline{\mathcal{M}_R}|^2\, L_\nu^\nu\, \frac{1}{s\,Q^2}\, e^2\, \frac{1}{2\pi} d\phi_2^{q,k_3}\, d\phi_2^{k_1,k_2} \tag{3.29}$$

$$= \frac{1}{36\pi}\frac{1}{Q^2}\left(-e^2\, Q_f^2\, g_S^2\, C_F\, \mu^{2\epsilon}\right)(1-\epsilon)$$

$$\times \int d\phi_2^{k_1,k_2} L_\nu^\nu \int d\phi_2^{q,k_3}\; \left[16\, \frac{s\,Q^2}{t\,u} + 8(1-\epsilon)\left(\frac{u}{t} + \frac{t}{u}\right) - 16\epsilon\right] \tag{3.30}$$

The integral over the 2-body phase space over the leptons can be fully integrated over to give equation 3.6, but we not substitute this in here and we will focus on the integration over the photon and gluon phase space as this is where the singular structure and the NLO corrections lie. Inserting the unintegrated phase space over a two body phase space (where one particle is massless and the other has an invariant mass Q^2) given

by equation 3.7 gives

$$\begin{aligned}\frac{d\sigma_R^{q\bar{q}}}{dQ^2} &= \frac{1}{36\pi}\frac{1}{s}\left(-e^2\,Q_f^2\,g_S^2\,C_F\,\mu^{2\epsilon}\right)(1-\epsilon)\\ &\times\left(\int d\phi_2^{k_1,k_2}\right)(-4\,s)\,\frac{1}{s\,Q^2}\,e^2\\ &\times\frac{1}{8\pi}\,\frac{(4\pi)^\epsilon}{\Gamma(1-\epsilon)}\,\frac{(s-Q^2)^{1-2\epsilon}}{s^{1-\epsilon}}\int_0^1 dy\,[y(1-y)]^{-\epsilon}\,\left[16\,\frac{s\,Q^2}{t\,u}+8(1-\epsilon)\left(\frac{u}{t}+\frac{t}{u}\right)-16\epsilon\right], \qquad (3.31)\end{aligned}$$

where the angular variable

$$y = 1/2(1+\cos\theta)\,, \qquad (3.32)$$

has been introduced.

Condensing the prefactors, using $e^2 = 4\pi\,\alpha$ and factoring the Born cross section (equation 3.15) we have

$$\begin{aligned}\frac{d\sigma_R^{q\bar{q}}}{dQ^2} &= \frac{1}{\pi}\,\sigma_B\,\alpha_s\,C_F\,\left(\int d\phi_2^{k_1,k_2}\right)(1-\epsilon)\,\frac{(4\pi\mu^2)^\epsilon}{\Gamma(1-\epsilon)}\,\frac{(s-Q^2)^{1-2\epsilon}}{s^{1-\epsilon}}\\ &\times\int_0^1 dy\,[y(1-y)]^{-\epsilon}\,\left[2\,\frac{s\,Q^2}{t\,u}+(1-\epsilon)\left(\frac{u}{t}+\frac{t}{u}\right)-2\epsilon\right]. \qquad (3.33)\end{aligned}$$

For convenience we now also introduce the dimensionless variable

$$z = Q^2/s\,, \qquad (3.34)$$

so that the amplitude squared is now a function of the centre-of-mass (CM) energy, a variable that describes the energy of the emission, and an angular variable which describes the angle of emission of the gluon off in the emission's CM frame.

In terms of these new variables the Mandelstam invariant s becomes

$$s = (p_1+p_2)^2 = \frac{Q^2}{z}\,, \qquad (3.35)$$

whilst the t variable becomes

$$\begin{aligned}t &= (p_1-k)^2 = -2\,p_1\cdot k\\ &= -2\,\frac{\sqrt{s}}{2}\,|\underline{k}|\,(1-\cos\theta)\\ &= -\frac{Q^2}{z}(1-z)(1-y) \qquad (3.36)\end{aligned}$$

where we have used the relations $|\underline{p_1}| = \sqrt{s}/2$ and $|\underline{k}| = (1-z)|\underline{p_1}|$. Similarly using the relation $s+t+u = Q^2$ the u variable becomes

$$\begin{aligned}u &= (p_2-k)^2\\ &= -\frac{Q^2}{z}\,(1-z)\,y \qquad (3.37)\end{aligned}$$

In these new variables $\frac{(s-Q^2)^{1-2\epsilon}}{s^{1-\epsilon}} \to Q^{-2\epsilon}\, z^\epsilon\, (1-z)^{1-2\epsilon}$, and inserting the expressions for the Mandelstam variables gives

$$\frac{d\sigma_R^{q\bar{q}}}{dQ^2} = \frac{1}{\pi}\,\sigma_B\,\alpha_s\,C_F\,\left(\int d\phi_2^{k_1,k_2}\right)\,(1-\epsilon)\,\left(\frac{4\pi\mu^2}{Q^2}\right)^\epsilon\,\frac{z^\epsilon\,(1-z)^{1-2\epsilon}}{\Gamma(1-\epsilon)} \times \int_0^1 dy\,[y(1-y)]^{-\epsilon}\,\left[\frac{2\,z}{(1-z)^2\,y\,(1-y)} + (1-\epsilon)\,\left(\frac{1-y}{y}+\frac{y}{1-y}\right) - 2\,\epsilon\right]. \tag{3.38}$$

The collinear singularities in the limits $\theta = 0, \pi$ (that is, the limits $y \to 0, 1$) are now clear to see in the integral over the angular variable.

To evaluate the integrals required we will make use of the β function

$$\beta(a,b) = \int_0^1 dy\, y^{a-1}\,(1-y)^{b-1} = \frac{\Gamma(a)\,\Gamma(b)}{\Gamma(a+b)}\,. \tag{3.39}$$

The first integral evaluates to

$$\int_0^1 \frac{[y(1-y)]^{-\epsilon}}{y\,(1-y)} = \frac{\Gamma^2(-\epsilon)}{\Gamma(-2\epsilon)} = -\frac{2}{\epsilon}\,\frac{\Gamma^2(1-\epsilon)}{\Gamma(1-2\epsilon)}\,, \tag{3.40}$$

where in the second equality we have used the relation

$$\Gamma(1-z) = -z\,\Gamma(-z)\,. \tag{3.41}$$

The following two integrals can be seen to give the same result by the symmetry property of the β function $\beta(a,b) = \beta(b,a)$, so that each gives a contribution of

$$\int_0^1 [y(1-y)]^{-\epsilon}\,\frac{1-y}{y} \;=\; \int_0^1 [y(1-y)]^{-\epsilon}\,\frac{y}{1-y} \;=\; -\frac{1}{\epsilon}\,\frac{1-\epsilon}{1-2\epsilon}\,\frac{\Gamma^2(1-\epsilon)}{\Gamma(1-2\,\epsilon)}\,, \tag{3.42}$$

where in the third equality we have made repeated use of equation 3.41.

The same technique can be applied to the last remaining integral to give

$$\int_0^1 [y(1-y)]^{-\epsilon} \;=\; \frac{\Gamma^2(1-\epsilon)}{\Gamma(2-2\epsilon)} \;=\; \frac{1}{1-2\epsilon}\,\frac{\Gamma^2(1-\epsilon)}{\Gamma(1-2\epsilon)}\,. \tag{3.43}$$

Using these results on equation 3.38 we get

$$\frac{d\sigma_R^{q\bar{q}}}{dQ^2} = \frac{1}{\pi}\,\sigma_B\,\alpha_s\,C_F\,\left(\int d\phi_2^{k_1,k_2}\right)\,(1-\epsilon)\,\left(\frac{4\pi\mu^2}{Q^2}\right)^\epsilon\,\frac{z^\epsilon\,(1-z)^{1-2\epsilon}}{\Gamma(1-\epsilon)} \times \left[-\frac{2\,z}{(1-z)^2}\,\frac{2}{\epsilon}\,\frac{\Gamma^2(1-\epsilon)}{\Gamma(1-2\epsilon)} - 2(1-\epsilon)\,\left(\frac{1}{\epsilon}\,\frac{1-\epsilon}{1-2\epsilon}\,\frac{\Gamma^2(1-\epsilon)}{\Gamma(1-2\,\epsilon)}\right) - 2\,\epsilon\,\frac{1}{1-2\epsilon}\,\frac{\Gamma^2(1-\epsilon)}{\Gamma(1-2\epsilon)}\right]. \tag{3.44}$$

Grouping all the terms that tend to unity in the limit $\epsilon \to 0$ into the function

$$D(\epsilon) := \left(\frac{4\pi\mu^2}{Q^2}\right)^\epsilon\,\frac{\Gamma(1-\epsilon)}{\Gamma(1-2\,\epsilon)} \tag{3.45}$$

gives

$$\begin{aligned}\frac{d\sigma_R^{q\bar{q}}}{dQ^2} &= -\frac{1}{\pi}\,\sigma_B\,\alpha_s\,C_F\,\left(\int d\phi_2^{k_1,k_2}\right)\,(1-\epsilon)\,D(\epsilon)\,z^\epsilon\,(1-z)^{1-2\epsilon}\\ &\times 2\left[\frac{2\,z}{(1-z)^2}\,\frac{1}{\epsilon}\;+\;\frac{1}{\epsilon}\,\frac{(1-\epsilon)^2}{1-2\epsilon}+\,\epsilon\,\frac{1}{1-2\epsilon}\right]\\ &= -\frac{1}{\pi}\,\sigma_B\,\alpha_s\,C_F\,\left(\int d\phi_2^{k_1,k_2}\right)\,(1-\epsilon)\,D(\epsilon)\,z^\epsilon\,(1-z)^{1-2\epsilon}\\ &\times\frac{2}{\epsilon}\left[\frac{2\,z}{(1-z)^2}\;+\;\frac{(1-\epsilon)^2+\epsilon^2}{1-2\epsilon}\right]\\ &= -\frac{1}{\pi}\,\sigma_B\,\alpha_s\,C_F\,\left(\int d\phi_2^{k_1,k_2}\right)\,(1-\epsilon)\,D(\epsilon)\,z^\epsilon\,(1-z)^{1-2\epsilon}\\ &\times\frac{2}{\epsilon}\left[\frac{2\,z}{(1-z)^2}\;+\;1+\;\frac{2\,\epsilon^2}{1-2\epsilon}\right]\end{aligned}\tag{3.46}$$

Using l'Hôpital's rule the last term in the square brackets can be seen to vanish in the $d=4$ limit $\left(\lim_{\epsilon\to 0}\left(\frac{2}{\epsilon}\,\frac{2\,\epsilon^2}{1-2\epsilon}\right)=0\right)$ and we will therefore neglect it from here on.

The $q\bar{q}$ real emission contribution now has the simple form

$$\begin{aligned}\frac{d\sigma_R^{q\bar{q}}}{dQ^2} &= -\frac{1}{\pi}\,\sigma_B\,\alpha_s\,C_F\,\left(\int d\phi_2^{k_1,k_2}\right)\,(1-\epsilon)\,D(\epsilon)\\ &\times\frac{2}{\epsilon}\,z^\epsilon\,\left[2\,z\,(1-z)^{-1-2\epsilon}\;+\;(1-z)^{1-2\epsilon}\right]\,.\end{aligned}\tag{3.47}$$

The pole in ϵ we have here arose from the integrals over the angular variable and hence corresponds to a collinear singularity.

So far this result is exact and no expansions about a small parameter have been made. However to reveal full the pole structure in ϵ we must expand about $\epsilon=0$. Using the relation

$$a^\epsilon = e^{\epsilon\,\log a}\simeq 1+\epsilon\;\log a\,,\tag{3.48}$$

and

$$\frac{\Gamma(1-\epsilon)}{\Gamma(1-2\,\epsilon)}\simeq 1-\gamma_E\epsilon+\left(\frac{\gamma_E^2}{2}-\frac{\pi^2}{4}\right)\epsilon^2\,,\tag{3.49}$$

we have that to order ϵ^1

$$D(\epsilon)\simeq 1+\epsilon\,\left(\log 4\pi-\gamma_E+\log\frac{\mu^2}{Q^2}\right)\,.\tag{3.50}$$

If inserted back into equation 3.47 this will contribute constant finite terms as well as producing a logarithmic scale dependence. Some of the constant finite terms may be omitted depending on the renormalisation scheme used. We have shown the expanded form of this factor to illustrate its contribution to the differential cross section but we will not use the expanded form in the following.

Our differential expression for gluon emission in equation 3.47 still contains a further divergence in the

limit $z \to 1$ when $\epsilon = 0$ which we will now deal with. To do this we will define a *plus distribution* as

$$\int dx\, f(x)\, [g(x)]_+ = \int dx\, (f(x) - f(x_0))\, g(x)\,, \tag{3.51}$$

where the function $f(x)$ is finite everywhere in the region of integration and the function $g(x)$ is singular at x_0. This allows us to rewrite an integral with a divergent integrand as

$$\int dx\, f(x)\, g(x) = \int dx\, [f(x) - f(x_0) + f(x_0)]\, g(x) = \int dx\, f(x)\, [g(x)]_+ + \int dx\, f(x_0)\, g(x)\,. \tag{3.52}$$

What we gain by doing this is that the first term is now finite in the $z \to 1$ (i.e. the soft gluon) limit, and if the second term is simple enough to be integrated analytically in d dimensions (which it may be as $f(x_0)$ is now a constant) it will contain the singularity as poles in ϵ, thus isolating the singular part of the integral.

In the case at hand our cross section is differential in Q^2 and thus the corresponding integration over Q^2 (from 0 to s, or in our choice of variables, over z, from 0 to 1) is divergent for the term proportional to $2\,z\,(1-z)^{-1-2\epsilon}$.

Applying the plus prescription to an integral of this form yields

$$\begin{aligned}\int_0^1 dz\, \frac{f(z)}{(1-z)^{1+2\epsilon}} &= \int_0^1 dz\, \frac{f(z) - f(1) + f(1)}{(1-z)^{1+2\epsilon}} \\ &= \int_0^1 dz\, \frac{f(z)}{[(1-z)^{1+2\epsilon}]_+} + \int_0^1 dz\, \frac{f(1)}{(1-z)^{1+2\epsilon}}\,.\end{aligned} \tag{3.53}$$

The integral in the second term can be evaluated analytically in d dimensions using equation 3.39 to give

$$\begin{aligned}f(1) \int_0^1 dz\, \frac{1}{(1-z)^{1+2\epsilon}} &= f(1)\, \frac{\Gamma(1)\,\Gamma(-2\epsilon)}{\Gamma(1-2\epsilon)} \\ &= f(1)\, \left(-\frac{1}{2\,\epsilon}\right)\,,\end{aligned} \tag{3.54}$$

where in the second equality we have used $\Gamma(1) = 1$ and equation 3.41.

Using this result and the expansion

$$\begin{aligned}(1-z)^{-1-2\epsilon} &= \frac{1}{1-z}\, e^{-2\epsilon\, \log(1-z)} \\ &\simeq \frac{1}{1-z}\, (1 - 2\epsilon\, \log(1-z) + \mathcal{O}(\epsilon^2))\end{aligned} \tag{3.55}$$

we can rewrite equation 3.53 as

$$\begin{aligned}\int_0^1 dz\, \frac{f(z)}{(1-z)^{1+2\epsilon}} &= \int_0^1 \frac{f(z)}{[1-z]_+} (1 - 2\epsilon\, [\log(1-z)]_+)\, dz - f(1) \frac{1}{2\epsilon} \\ &= \int_0^1 dz\, \frac{f(z)}{[1-z]_+} - 2\epsilon \int_0^1 dz\, f(z)\, \left[\frac{\log(1-z)}{1-z}\right]_+ - \frac{1}{2\epsilon} \int_0^1 dz\, f(z)\, \delta(1-z)\,.\end{aligned} \tag{3.56}$$

Working at the integrand level and neglecting the test function $f(z)$ we can write

$$\frac{1}{(1-z)^{1+2\epsilon}} = \frac{1}{[1-z]_+} - 2\epsilon \left[\frac{\log(1-z)}{1-z}\right]_+ - \frac{1}{2\epsilon}\,\delta(1-z) + \mathcal{O}(\epsilon^2)\,, \tag{3.57}$$

where it is understood that a convolution with a test function will take place later.

We now also expand the factor of z^ϵ and the second term in equation 3.47 about $\epsilon = 0$ using equation 3.48 (to get $z^\epsilon \simeq 1 + \epsilon \log z$ and $(1-z)^{1-2\epsilon} \simeq (1-z)(1-2\epsilon\log(1-z))$) and use the expansion

$$z^\epsilon (1-z)^{-1-2\epsilon} = \frac{1}{[1-z]_+} - 2\epsilon \left[\frac{\log(1-z)}{1-z}\right]_+ - \frac{1}{2\epsilon}\,\delta(1-z) + \epsilon\,\frac{\log z}{1-z} + \mathcal{O}(\epsilon^2)\,. \tag{3.58}$$

Using these expansions, as well as equation 3.57 into our differential cross section (equation 3.47) we obtain the well known result

$$\frac{d\sigma_R^{q\bar{q}}}{dQ^2} = \frac{\alpha_S}{\pi}\,\sigma_B\,C_F\,D(\epsilon)\left[\frac{2}{\epsilon^2}\delta(1-z) - \frac{2}{\epsilon}\frac{1+z^2}{(1-z)_+} + 4\,(1+z^2)\left[\frac{\log(1-z)}{1-z}\right]_+ - 2\left(\frac{1+z^2}{1-z}\right)\log z\right]. \tag{3.59}$$

Note that the last term is in fact finite in the limit $z \to 1$ so it does not require any regularisation ($\lim_{z\to 1}(\log z/(1-z)) = -1$).

The contribution from $gq \to ll\bar{q}$ (or equivalently $g\bar{q} \to llq$ by charge conjugation) can be obtained from equation 3.33 by crossing symmetry, i.e. $s \to u$, $t \to s$, $u \to t$ and multiplication by an overall minus sign [175]

$$\frac{d\sigma_R^{qq}}{dQ^2} = \frac{1}{4}\,\frac{\alpha_S}{\pi}\,\sigma_B\,C_F\left[[z^2+(1-z)^2]\left(-\frac{1}{\epsilon}\frac{\Gamma(1-\epsilon)}{\Gamma(1-2\epsilon)} + \log\left(\frac{Q^2}{4\pi}\frac{(1-z)^2}{z}\right)\right) - \frac{3}{2}z^2 + z + \frac{3}{2}\right] \tag{3.60}$$

Note that as expected, whereas the gluon emission has both soft and collinear ($1/\epsilon^2$) and collinear ($1/\epsilon$) singularities, the quark emission diagram only has a collinear singularity as the soft singularity is suppressed by the fact that the (anti)quark spinor vanishes in the soft limit (e.g. $\bar{u}(p_3) \xrightarrow{p_3 \to 0} 0$).

Also as expected the collinear singularities in the cross sections are proportional to standard splitting kernels

$$\frac{d\sigma_R^{q\bar{q}}}{dQ^2} \supset P_{qq}(z) = C_F \frac{1+z^2}{(1-z)_+}\,, \tag{3.61}$$

$$\frac{d\sigma_R^{qq}}{dQ^2} \supset P_{gq}(z) = T_F[z^2+(1-z)^2]\,, \tag{3.62}$$

where $P_{ij}(z)$ are the regularised four-dimensional Altarelli-Parisi splitting splitting kernels as defined in figure 4.1.

3.3.2 Virtual Contribution

The QCD virtual radiative corrections to Drell-Yan are given by the self-energy corrections to the incoming quark(anti-quark) legs (with the corresponding wavefunction/field renormalisation), and the correction to the

vertex. For a full derivation of the virtual contribution see [178].

Quark Self-energy Corrections

We will now compute the self-energy corrections to the incoming (anti)quark legs as shown in figure 3.4.

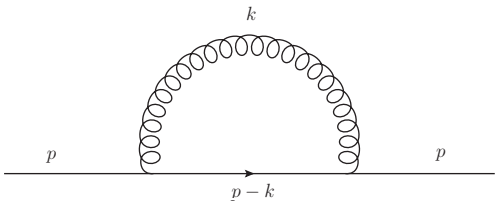

Figure 3.4: QCD self-energy corrections to the incoming (anti)quark propagator.

We begin by explicitly beginning to compute the loop integral involved. The quark self-energy contributions have the form

$$\delta m_q = \int \frac{d^d k}{(2\pi)^d} \frac{\gamma_\mu \left(\not{p} - \not{k}\right) \gamma^\mu}{\left(k^2 + i\,\epsilon\right)\left((p-k)^2 + i\,\epsilon\right)}\,, \tag{3.63}$$

where p is the external momentum and k is the loop momentum.

Using the relation $\gamma_\mu \not{a} \gamma^\mu = -2(1-\epsilon)\not{a}$ and the Feynman parametrisation

$$\frac{1}{AB} = \int_0^1 dx\, \frac{1}{[Ax + B(1-x)]^2}\,, \tag{3.64}$$

with $A = k^2$ and $B = (p-k)^2 = -2p\cdot k + k^2$ this can be rewritten as

$$\delta m_q = -2(1-\epsilon) \int \frac{d^d k}{(2\pi)^d} \int_0^1 dx\, \frac{\not{p} - \not{k}}{[k^2 - 2k\cdot xp]^2}\,, \tag{3.65}$$

which using the translational invariance of the integral[10] to perform the substitution $l = k - xp$ and eliminate the gluon momentum gives

$$\delta m_q = -2(1-\epsilon) \int \frac{d^d l}{(2\pi)^d} \int_0^1 dx\, \frac{(1-x)\not{p} - \not{l}}{[l^2 + i\,\epsilon]^2} \tag{3.66}$$

$$= -2(1-\epsilon) \int \frac{d^d l}{(2\pi)^d} \frac{1}{[l^2 + i\,\epsilon]^2} \left(\frac{1}{2}\not{p} - \not{l}\right) \tag{3.67}$$

where we have assumed massless quarks ($p^2 = 0$).

The self-energy loop integral is therefore of the form

$$\delta m_q = \int \frac{d^d l}{(2\pi)^d} \frac{1}{(l^2)^2}\,. \tag{3.68}$$

[10] For a review of the properties and techniques used to evaluate Feynman integrals see e.g. [179].

This integral can be argued to vanish since the integrand is a Lorentz scalar so the result must be proportional to something with the same Lorentz structure but the only scale available is $p^2 = 0$, and indeed this is a valid statement if the quark self-energy is considered with no regard to the rest of the NLO corrections and their renormalisation. Within this interpretation the quark self-energy can be argued to vanish and, though we omitted to include it, the UV pole existing in the vertex correction can be assumed to be renormalised separately.

However a more consistent view of the singularity cancellation and renormalisation can be taken if the quark self-energy singularity structure is pulled apart, and the full pole structure (including the UV pole) of the vertex correction[11] are considered.

In this case the vertex correction from equation 3.75 contains a UV pole $1/\epsilon_{\mathrm{UV}}$, and the singularity structure of the self-energy loop integral can be teased apart as follows.

Using a Wick rotation such that $d^d l \to i d^d l$ and integrating over the spherical component, $d\Omega_d$, of the measure $d^d l = l^{d-1}\, d\Omega_d\, dl$ gives

$$\delta m_q = \int \frac{d^d l}{(2\pi)^d}\,\frac{1}{(l^2)^2} = i \int \frac{1}{(2\pi)^d}\, d\Omega_d \int_0^\infty \frac{l^{d-1}}{l^4}\, dl \tag{3.69}$$

$$= \left(\frac{i}{(2\pi)^d}\frac{2\pi^{\frac{d}{2}}}{\Gamma(d/2)}\right)\int_0^\infty l^{d-5}\, dl\,. \tag{3.70}$$

Integrating the angular part in $d = 4$ gives a constant factor of $\frac{i}{8\pi^2}$ which we shall ignore, whilst the radial part evaluated in d dimensions gives

$$\int_0^\infty l^{d-5}\, dl = \frac{1}{d-4}\Big[l^{d-4}\Big]_0^\infty\,, \tag{3.71}$$

where the upper limit can only be evaluated if $d < 0$, and the lower one if $d > 0$. We therefore split the integral as

$$\int_0^\infty l^{d-5}\, dl \;=\; \underbrace{\int_0^\Lambda l^{d-5}\, dl}_{d=4-2\epsilon_{\mathrm{IR}},\ \epsilon_{\mathrm{IR}}<0} \;+\; \underbrace{\int_\Lambda^\infty l^{d-5}\, dl}_{d=4-2\epsilon_{\mathrm{UV}},\ \epsilon_{\mathrm{UV}}>0}\,, \tag{3.72}$$

with the sign of ϵ and therefore d set accordingly for each term.

These integrals give

$$\int_0^\Lambda l^{d-5}\, dl = -\frac{1}{2\epsilon_{\mathrm{IR}}}\,\Lambda^{-2\epsilon_{\mathrm{IR}}} \;=\; -\frac{1}{2\epsilon_{\mathrm{IR}}} e^{-2\epsilon_{\mathrm{IR}}\log\Lambda} \;\approx\; -\frac{1}{2\epsilon_{\mathrm{IR}}} + \log\Lambda\,, \tag{3.73a}$$

$$\int_\Lambda^\infty l^{d-5}\, dl = \frac{1}{2\epsilon_{\mathrm{UV}}}\,\Lambda^{-2\epsilon_{\mathrm{UV}}} \;=\; \frac{1}{2\epsilon_{\mathrm{UV}}} e^{-2\epsilon_{\mathrm{UV}}\log\Lambda} \;\approx\; \frac{1}{2\epsilon_{\mathrm{UV}}} - \log\Lambda\,, \tag{3.73b}$$

[11] a standard but incomplete form of which is presented in equation 3.75.

such that

$$\int_0^\infty l^{d-5}\, dl \;=\; \frac{1}{2\epsilon_{\mathrm{UV}}} \;-\; \frac{1}{2\epsilon_{\mathrm{IR}}}\,. \tag{3.74}$$

It is here where one may choose how to proceed, with all choices being equivalent as long as they are carried out consistently. The poles in the above expression can be straight away argued to cancel against each other, in which case the self-energy of the massless quark vanishes as expected from dimensional arguments, and the vertex correction can undergo renormalisation to remove its UV pole. Or instead one may define the self-energy renormalisation counterterm (which is also equal to the vertex correction counterterm) to cancel exactly the two poles in equation 3.74, in which case when used as the vertex correction counterterm it will also cancel the UV pole there (as well as give a contribution to its IR single pole).

Care must therefore be taken to ensure consistency, and both the loop corrections and their corresponding counterterms should be defined ensuring to fully account for the singularity structure of the entire virtual contribution. Indeed the vertex correction stated in equation 3.75 omits the UV pole and already contains the single IR pole contribution which would be obtained from the counterterm built from equation 3.74, as this result is commonly quoted.

Vertex Correction

The vertex correction is both IR and UV divergent. However the UV divergences cancel by a Ward identity guaranteeing that EW couplings are not renormalised by QCD corrections at one loop, therefore all the divergences are of IR origin.

The vertex correction to Drell-Yan can be shown to be

$$\frac{d\sigma_V}{dQ^2} = \frac{\alpha_S}{\pi}\,\sigma_B\, C_F\, D(\epsilon)\,\delta(1-z)\,\left[-\frac{2}{\epsilon^2} - \frac{3}{\epsilon} - 8 + \frac{2\pi^2}{3} + \mathcal{O}(\epsilon)\right], \tag{3.75}$$

where the double pole corresponds to a soft and collinear singularity whilst the single pole is a purely collinear singularity.

3.3.3 Mass Factorisation

So far we have worked at the partonic level and have neglected the convolution required with with parton distribution functions (as shown in equation 2.22) to properly account for the resummation of collinear logarithms and the probability of each possible initial state being obtained from a hadron at a given energy, which are both required to produce a well defined observable.

The sum of the NLO contributions to the partonic cross section leads to the cancellation of soft and

collinear singularities, but for processes with initial-state partons collinear singularities will remain. Given that observables must be finite and the hadronic cross section is computed via equation 2.22 this implies the parton distribution functions at NLO must also be singular, and must contain exactly the same collinear singularities as those remaining after the sum of real and virtual contributions to the partonic cross section.

We now derive the form of the singularity structure of the parton distribution functions at NLO required to cancel the collinear poles remaining in the partonic amplitude and show that the source of these singularities is in fact the corresponding NLO corrections to deep inelastic scattering (DIS) from which the parton distribution functions are inferred.

Let us assume that the parton distribution functions, $f_i(z)$ (where we momentarily neglect the dependence on Q^2 they acquire at NLO) can be renormalised by a convolution with a singular *transition function*, $\Gamma_{ij}(z)$ as

$$f_i^{\rm ren}(\eta) = \int_0^1 dz \int_0^1 dx\, f_j(x)\, \Gamma_{ji}(z)\, \delta(\eta - xz) \tag{3.76}$$

$$= \int_\eta^1 \frac{dz}{z}\, f_j(\eta/z)\, \Gamma_{ji}(z)\,, \tag{3.77}$$

where i, j label the partons involved, and where we have defined the momentum fraction of the emitting parton as $\eta = x\, z$, where x is the LO momentum fraction of the parton with respect to the hadron momenta and z is the momentum fraction left to the emitting parton after the emission.

A transition function $\Gamma_{fi}(z)$, $fi \in \{qq, gg, qg, gq\}$ is a probability density (in z, i.e. the probability in $[z, z+dz]$) that a parton $i = q, \bar{q}, g$ with momentum p after an emission will become a parton f.

These same transition functions must yield the collinear singularity structure left over in the partonic cross section, so that a convolution with these same transition functions must give the singular partonic cross section

$$d\sigma_{ik}(s) = \int\int dz_1 dz_2\, \Gamma_{ij}\, d\sigma_{jl}^{\rm ren}(z_1 z_2 s)\, \Gamma_{lk} \tag{3.78}$$

where for example $\eta_1 = x_1 z_1$.

We can then write an equation for the hadronic cross section equivalent to equation 2.22 but where all the ingredients are renormalised, finite, and numerically computable

$$d\sigma^H = \sum_{i,j} \int d\eta_1 d\eta_2\; f_i^{\rm ren}(\eta_1, \mu_F)\; f_j^{\rm ren}(\eta_2, \mu_F)\; d\sigma_{ij}^{\rm ren}(\eta_1 \eta_2 S, \mu_F, \alpha_S(\mu_R))\,. \tag{3.79}$$

Note that inserting the definition for the renormalised parton distribution functions (equation 3.76) into this equation and performing the integrations over η using the corresponding delta distributions (so that these integrals reduce to a factor of 1) and identifying equation 3.78 in the result returns the original relation for the hadronic cross section in terms of unrenormalised quantities (equation 2.22), proving that these two relations

are equivalent.

In order to derive the form of the hadronic cross section order by order in perturbation theory we now assume that both the transition functions and the singular and renormalised partonic cross sections have a well defined perturbative expansion of the form of equation 3.1

$$d\sigma = \sum_{n=0}^{\infty} \alpha_S^n \, d\sigma^{(n)} \,, \tag{3.80a}$$

$$d\sigma_{\rm ren} = \sum_{n=0}^{\infty} \alpha_S^n \, d\sigma_{\rm ren}^{(n)} \,, \tag{3.80b}$$

$$\Gamma_{ij}(z) = \delta_{ij}\delta(1-z) + \sum_{n=1}^{\infty} \alpha_S^n \, \Gamma_{ij}^{(n)}(z) \,, \tag{3.80c}$$

where the first term in the transition function accounts for the possibility of no parton emission (i.e. the infinitely soft emission limit, $z = 1$).

To first order in α_S the transition functions have the form

$$\Gamma_{ij}^{(0)}(z) + \alpha_S \Gamma_{ij}^{(1)}(z) = \delta_{ij}\delta(1-z) - \frac{\alpha_S}{\pi}\frac{2}{\epsilon}\left(\frac{4\pi\mu^2}{Q^2}\right)^{\epsilon} P_{ij}(z) \,, \tag{3.81}$$

where $P_{ij}(z)$ is a regularised splitting function in four dimensions (see figure 4.1). Note that analogously to equation 3.45, the factor $(\mu^2/Q^2)^{\epsilon}$ will, upon expansion about $\epsilon = 0$, give a logarithmic contribution.

Performing these expansions to order α_S and inserting them into equation 3.78 for the partonic cross section gives

$$\begin{aligned} d\sigma_{il}^{(0)} + \alpha_S \, d\sigma_{il}^{(1)} = \int\int dz_1 dz_2 \Big[&\Big(\delta_{ij}\delta(1-z_1) + \alpha_S \, \Gamma_{ij}^{(1)}(z_1)\Big) \\ &\times \Big(d\sigma_{jk}^{\rm ren\,(0)} + \alpha_S \, d\sigma_{jk}^{\rm ren\,(1)}\Big) \times \Big(\delta_{kl}\delta(1-z_2) + \alpha_S \, \Gamma_{kl}^{(1)}(z_2)\Big)\Big] \,, \end{aligned} \tag{3.82}$$

where for example $\Gamma_{kl=qg}^{(1)}(z)$ is the NLO ($\mathcal{O}(\alpha_S)$) correction to the quark parton distribution function from initial state gluons (i.e. the $gl \to q\bar{q}l$ contribution to the NLO corrections to deep inelastic scattering).

To $\mathcal{O}(\alpha_S)$ this gives

$$\begin{aligned} d\sigma_{il}^{(0)} + \alpha_S \, d\sigma_{il}^{(1)} = \int\int dz_1 dz_2 \Big[&\delta_{ij} \, \delta(1-z_1) \, d\sigma_{jk}^{\rm ren\,(0)} \, \delta_{kl} \, \delta(1-z_2) \\ &+\alpha_S \, \delta_{ij} \, \delta(1-z_1) \, d\sigma_{jk}^{\rm ren\,(1)} \, \delta_{kl} \, \delta(1-z_2) \\ &+\alpha_S \, \Gamma_{ij}^{(1)}(z_1) \, d\sigma_{jk}^{\rm ren\,(0)} \, \delta_{kl} \, \delta(1-z_2) \\ &+\alpha_S \, \delta_{ij} \, \delta(1-z_1) \, d\sigma_{jk}^{\rm ren\,(0)} \, \Gamma_{kl}^{(1)}(z_2)\Big] \,. \end{aligned} \tag{3.83}$$

Performing the integrations over delta distributions, keeping only the NLO ($\mathcal{O}(\alpha_S)$) terms and rearranging

to find the renormalised, finite partonic cross section gives

$$d\sigma_{il}^{\mathrm{ren}\,(1)} = d\sigma_{il}^{(1)} - \int dz_1\, \Gamma_{ij}^{(1)}(z_1)\, d\sigma_{jl}^{\mathrm{ren}\,(0)} \; - \int dz_2\, d\sigma_{ik}^{\mathrm{ren}\,(0)} \Gamma_{kl}^{(1)}(z_2)\,. \tag{3.84}$$

The collinear singularities remaining after the sum of real and virtual contributions will therefore be cancelled by terms consisting of a convolution of a singular transition function with the LO partonic cross section, one for each incoming parton.

Since parton distribution functions are obtained from DIS, these collinearly divergent transition functions are in fact the NLO corrections to DIS. The convolution of each of these NLO parton distribution functions (one for each incoming parton) with the LO partonic cross section (for any given perturbatively calculable observable, not just Drell-Yan) hence provides the required cancellation of remaining singularities yielding a consistently renormalised observable (provided everything is computed consistently in the same renormalisation scheme, and to the same fixed order in the coupling).

Note that the factorisation of collinear singularities from both DIS and the process in question is what allows parton distribution functions from DIS to be used to compute any process, and which allows for the exact cancellation of singularities.

The cancellation between the collinear singularities left over after the combination of real emission and virtual contributions of the NLO corrections to DIS and Drell-Yan can be seen explicitly. The sum of the real and virtual contributions for the initial-state gluon contribution to DIS generates a NLO quark parton distribution function of the form [175]

$$\begin{aligned} q(x,\mu_F^2) = \; & q_0(x) \\ & + \frac{\alpha_S}{4\pi}\, C_F\, \frac{1}{1-\epsilon} \int_x^1 \frac{dy}{y} g(y) \\ & \left[[z^2 + (1-z)^2] \left(-\frac{1}{\epsilon} \frac{\Gamma(1-\epsilon)}{\Gamma(1-2\epsilon)} + \log\left(\frac{\mu_F^2}{4\pi} \frac{1-z}{z} \right) \right) + 6\, z\, (1-z) \right], \end{aligned} \tag{3.85}$$

where we have introduced the *factorisation scale*, μ_F as the virtuality at which the NLO correction to DIS is calculated, and which will later be seen to be a scale up to which the NLO parton distribution functions sum collinear logarithms.

If we compute the Born level hadronic cross section inserting equation 3.14 into equation 2.22 (but with only LO parton distribution functions)

$$\sigma_B = \frac{4\pi\, \alpha^2\, Q_f}{9\, s}\, (1-\epsilon)\, D(\epsilon) \int_0^1 dx_1 dx_2\, \left[q(x_1)\, \bar{q}(x_2) \; + \; q(x_2)\, \bar{q}(x_1) \right], \tag{3.86}$$

we see that taking only the $\mathcal{O}(\alpha_S)$ term from each of the products of the parton distribution functions this equation is exactly of the form of equation 3.84 that is required to renormalise the partonic cross section.

Replacing for example $\bar{q}(x_2)$ with the NLO parton distribution function from equation 3.85 and taking only the $\mathcal{O}(\alpha_S)$ term gives

$$-\int dz\,\Gamma^{(1)}(z)\,d\sigma^{\mathrm{ren}\,(0)} \subset -\frac{\alpha_S}{4\pi}\,C_F\,\sigma_B\int dx_1\int dx_2\,q(x_1)\,g(x_2) \times\left[[z^2+(1-z)^2]\,\left(-\frac{1}{\epsilon}\frac{\Gamma(1-\epsilon)}{\Gamma(1-2\epsilon)}+\log\left(\frac{\mu_F^2}{4\pi}\frac{1-z}{z}\right)\right)+6\,z\,(1-z)\right]. \quad (3.87)$$

If we now consider one of the two terms in the convolution of LO parton distribution functions with the NLO gq contribution to Drell-Yan from equation 3.60 to give the hadronic Drell-Yan cross section this gives

$$\frac{d\sigma_R^{gq\,H}}{dQ^2}=\frac{\alpha_S}{4\pi}C_F\,\sigma_B\int dx_1\int dx_2\,q(x_1)\,g(x_2) \left[[z^2+(1-z)^2]\left(-\frac{1}{\epsilon}\frac{\Gamma(1-\epsilon)}{\Gamma(1-2\epsilon)}+\log\left(\frac{Q^2}{4\pi}\frac{(1-z)^2}{z}\right)\right)-\frac{3}{2}z^2+z+\frac{3}{2}\right]. \quad (3.88)$$

As expected from equation 3.84, we see that the remaining collinear pole cancels in the sum between these two contributions, and we are left with a finite total hadronic cross section as desired.

3.3.4 The Full NLO Cross Section

Schematically, the singularity structure from the previous sections was of the form

$$\begin{aligned}
\delta m_{q,\bar{q}} &= 0 \qquad (\text{for massless quarks})\,,\\
d\sigma_R^{q\bar{q}} &\supset -\frac{1}{\epsilon_{\mathrm{IR}}},\ \frac{1}{\epsilon_{\mathrm{IR}}^2}\,,\\
d\sigma_R^{gq,g\bar{q}} &\supset -\frac{1}{\epsilon_{\mathrm{IR}}}\,,\\
d\sigma_V^{\mathrm{vertex}} &\supset -\frac{1}{\epsilon_{\mathrm{IR}}^2} \quad (\text{UV finite by a Ward identity})\,,\\
\sigma_B\,\times\,q^{(1)}(x,\mu_F^2) &\supset \frac{1}{\epsilon_{\mathrm{IR}}}\,,\\
\sigma_B\,\times\,\bar{q}^{(1)}(x,\mu_F^2) &\supset \frac{1}{\epsilon_{\mathrm{IR}}}\,,
\end{aligned} \quad (3.89)$$

where $f^{(1)}(x,\mu_F^2)$ are the NLO corrections to the parton distribution functions (computed from the corresponding NLO correction to DIS). The mutual cancellation of all the divergences between the contributions to the hadronic cross section is hence apparent.

This cancellation can in fact be shown to hold generally, order by order. This was first proven in the context of soft final state singularites in Abelian gauge theories (namely QED) by Bloch and Nordsieck in 1937 [180]. This theorem proves that soft infrared singularities (no purely collinear singularities exist as they dealt with the case of massive fermions) from photon radiation off final state massive fermions cancel when a sum over all the soft unobserved photons is performed.

A generalisation of this theorem to both soft and collinear singularities (i.e. for emission off massless particles), for non-Abelian theories, and both for emission off initial and final state singularities was proven by Kinoshita, Lee and Nauenberg [181, 182], we will from here on refer to this result as the KLN (Kinoshita-Lee-Nauenberg) theorem. This theorem broadly states that soft and collinear divergences cancel in the sum over degenerate (experimentally indistinguishable) initial and final states.

This cancellation is in fact only guaranteed to happen for *infrared safe* observables, which are constructed to be insensitive to soft and collinear emissions (which are hence integrated over and provide the cancellation with the virtual contribution) and whose technical definition we defer to section 3.4 (equation 3.96).

3.3.5 The Running Strong Coupling

Though we have so far not discussed it, to obtain a consistent NLO result the strong coupling, α_S, used in the calculation must be formally at least of the same order as the rest of the calculation, i.e. we must use the one-loop ($\mathcal{O}(\alpha_S^2)$, but this is the LO result for the running coupling) running coupling evaluated in the $\overline{\text{MS}}$ scheme (the one-loop running coupling is in fact renormalisation scheme-independent at this order, though at higher orders –three loops onwards– it will not be)

$$\alpha_S(Q^2) = \frac{1}{\beta_0 \, \log\left(\frac{Q^2}{\Lambda_{\text{QCD}}}\right)}\,, \tag{3.90}$$

where $\beta_0 = (11\,C_A - 2\,N_f)/12\pi$ and $\Lambda_{\text{QCD}} \approx 200\ \text{MeV}$ corresponds to the Landau pole of QCD, the exact value depending on the number of quark flavours, N_f considered[12].

For Drell-Yan the NLO partonic cross section, parton distribution functions and coupling constant are all the ingredients needed for a fully NLO prediction[13].

However if the final state being computed included particles which are themselves charged under the group whose coupling we're expanding with respect to, this would require further calculations of emission (and virtual) corrections off the final state legs (or NLO corrections to their decay rates if they are unstable) and possibly also the usage of fragmentation functions (the equivalent of parton distribution functions, but for final states).

For the full hadronic NLO cross section for Drell-Yan see for example equations 9.5 and 12.3 in [175].

[12] To two-loop accuracy (though the exact form of the result depends on how the perturbative series is truncated) the strong coupling is given by $\alpha_S(Q^2) = \frac{1}{\beta_0 \, \log\left(\frac{Q^2}{\Lambda_{\text{QCD}}}\right)} - \frac{\beta_1}{\beta_0^3} \frac{\log\log\left(\frac{Q^2}{\Lambda_{\text{QCD}}}\right)}{\log^2\left(\frac{Q^2}{\Lambda_{\text{QCD}}}\right)}$ where $\beta_1 = (17\,C_A^2 - 5\,C_A\,N_f - 3\,C_F\,N_f)/24\pi^2$. The running of the strong coupling is currently known to 4 loops.

[13] Here and henceforth when we mention NLO accuracy it is understood that this is for processes sufficiently inclusive for this to be the case, i.e. in the case of Drell-Yan for processes exclusive in one or two leptons, but inclusive in everything else. The computation carried out in the previous sections which we referred to as NLO will in fact only be LO if for example the observable under consideration requires two leptons and a jet.

3.4 Notation

For the discussions in the remaining sections of this work we will work with the following notation to allow the clearest possible discussion of the NLO corrections and how their inclusion within a parton shower, which we perform in this work, is carried out.

The '0' subscript will be used to denote matrix elements squared which contain divergences, with their finite versions lacking the subscript.

The matrix elements squared themselves will be denoted using calligraphic font and will always be averaged(summed) over incoming(outgoing) spin and colour, unless otherwise stated. The flux factor $1/(2\,s)$ where $s = (p_a + p_b)^2$ for the amplitudes with Born kinematics, or $1/(2\,p^2)$ for $p^2 = (p_1 + p_2)^2$ for amplitudes involving real emission (where p_a, p_b denote the incoming partonic momenta and p_1, p_2 denote momenta of the outgoing colour-singlet states) will also always be assumed. For example

$$\mathcal{B} = \frac{1}{S_a}\frac{1}{S_b}\frac{1}{C_a}\frac{1}{C_b}\frac{1}{N_{\text{symm}}}\frac{1}{2s}\sum_{\text{spin}}\sum_{\text{colour}}|\mathcal{M}_B|^2_{ij}\,, \tag{3.91}$$

corresponds to the Born amplitude, where $S_{a,b}$ and $C_{a,b}$ are the number of spin and colour degrees of freedom of the incoming partons, $1/N_{\text{symm}}$ is the symmetry factor for final states with identical particles and we have omitted the i, j labels for the flavours of the incoming partons on the left hand side.

The product of parton distribution functions will be absorbed into the function

$$\mathcal{L}(x_a, x_b, \mu_F) = f_i^{\text{LO(NLO)}}(x_a, \mu_F)\, f_j^{\text{LO(NLO)}}(x_b, \mu_F)\,, \tag{3.92}$$

where we suppress the partonic flavour labels on the left-hand side and use LO or NLO PDF sets as appropriate[14]. The arguments of the $\mathcal{L}$ function may be suppressed where they are clear from context, and notation on the partonic momentum fractions in the argument may be implied if used on the $\mathcal{L}$. When convoluted with a matrix element squared the sum over all the relevant partonic flavours will also be understood.

Where the arguments of the $\mathcal{L}$ function are clear from context it may be subsumed into the matrix element squared, which is then no longer written in calligraphic font, for example

$$V = \mathcal{L}(x_a, x_b, \mu_F)\,\mathcal{V}\,. \tag{3.93}$$

The measure over the Born phase space, $\mathbf{\Phi}_n$, will be denoted as

$$d\mathbf{\Phi}_n = dx_a\, dx_b\, d\phi_n(p_1, \ldots, p_n)\,, \tag{3.94}$$

where $d\phi_n$ is the general phase space as defined in equation 3.4. The real emission phase space will be denoted

[14] The strong coupling, α_S, used in the calculation of the matrix elements must also be chosen appropriately to the fixed-order accuracy desired, with the one-loop result being the minimum required for NLO cross sections.

$d\mathbf{\Phi}_{n+1}$ and will be given by the equivalent expression with the replacement $n \to n+1$.

In this notation the Born hadronic cross section for example can be written as

$$d\sigma_B = f_i^{\mathrm{LO(NLO)}}(x_a, \mu_F)\, f_j^{\mathrm{LO(NLO)}}(x_b, \mu_F)\, \frac{1}{S_a}\frac{1}{S_b}\frac{1}{C_a}\frac{1}{C_b}\frac{1}{N_{\mathrm{symm}}}\frac{1}{2s}\sum_{\mathrm{spin}}\sum_{\mathrm{colour}} |\mathcal{M}_B|^2_{ij}\, d\mathbf{\Phi}_n\,, \tag{3.95a}$$

$$= \mathcal{L}(x_a, x_b, \mu_F)\, \mathcal{B}\, d\mathbf{\Phi}_n\,, \tag{3.95b}$$

$$= B\, d\mathbf{\Phi}_n\,. \tag{3.95c}$$

All observables, O, considered will also be assumed to be infrared safe as defined in equation 3.96 such that the observable as applicable to events with $n+1$ kinematics reduces to its equivalent for n kinematics in the soft and collinear limits of any two colour-connected partons. In the notation defined here[15]

$$\begin{aligned} O(\mathbf{\Phi}_{n+1}) = O(p_1, p_2, \ldots, p_i, \lambda\, p_j, \ldots, p_{n+1}) &\underset{\lambda\to 0}{\longrightarrow} O(\mathbf{\Phi}_n) = O(p_1, \ldots, p_i, \ldots, p_n)\,, \\ O(\mathbf{\Phi}_{n+1}) = O(p_1, p_2, \ldots, p_i, p_j, \ldots, p_{n+1}) &\underset{\mathbf{p}_i \| \mathbf{p}_j}{\longrightarrow} O(\mathbf{\Phi}_n) = O(p_1, \ldots, p_i + p_j, \ldots, p_n)\,. \end{aligned} \tag{3.96}$$

The expectation value for any given observable satisfying this requirement is then given by its convolution (with its kinematic-dependent n or $n+1$ form being chosen appropriately to match the phase space) with each matrix element contributing to the differential cross section, for example at the Born level the expectation value of an observable is given by

$$\langle O \rangle = \int B\, O(\mathbf{\Phi}_n)\, d\mathbf{\Phi}_n\,. \tag{3.97}$$

3.5 Numerical Calculation of NLO Amplitudes

Schematically, using the notation defined in section 3.4 a NLO calculation has the form

$$d\sigma^{NLO} \;=\; B\, d\mathbf{\Phi}_n \;+\; V_0\, d\mathbf{\Phi}_n \;+\; R_0\, d\mathbf{\Phi}_{n+1} \;+\; \underbrace{G_{a\,0}\, d\mathbf{\Phi}_n \;+\; G_{b\,0}\, d\mathbf{\Phi}_n}_{\text{For ISR only}}\,, \tag{3.98}$$

where the individual contributions are the Born, virtual, real emission, and the collinear remnant contributions generated by initial-state radiation (ISR) from each of the incoming partons, a and b. As discussed in section 3.3.3 on mass factorisation, these left-over singularities are generated from initial-state radiation only, not from final-state radiation, and ultimately cancel with corresponding singularities in the NLO PDFs leaving only a finite remainder with Born kinematics, as described in detail in section 3.3.3.

[15] Observables will further be assumed to vanish in the limit of in which two singular regions may overlap. This may happen for example when the Born-level process itself contains singular limits (as is the case for example when the Born process considered is Z + jet) so that an IR singular limit from an additional emission will reduce to a splitting function times the Born process, which itself may be in a singular region. This will not be an issue for us as all processes we consider are finite throughout the phase space at the Born level.

When computing the total, fully-inclusive NLO cross section the integrals may be amenable to analytic integration as exemplified in chapter 3. However, when required to compute observables by convolving each contribution with them, and in the presence of integration bounds set by elaborate experimental cuts (which are subsumed into the observable if imposed at the analysis level, or into the integration bounds if imposed at the event generation level) as

$$\begin{aligned}\langle O\rangle = &\int B\, O(\mathbf{\Phi}_n)\, d\mathbf{\Phi}_n \;+\; \int V\, O(\mathbf{\Phi}_n)\, d\mathbf{\Phi}_n \;+\; \int R\, O(\mathbf{\Phi}_{n+1})\, d\mathbf{\Phi}_{n+1} \\ &+\; \int G_a\, O(\mathbf{\Phi}_n)\, d\mathbf{\Phi}_n \;+\; \int G_b\, O(\mathbf{\Phi}_n)\, d\mathbf{\Phi}_n\,, \end{aligned} \tag{3.99}$$

these integrals are no longer analytically tractable and must be performed numerically.

However, not only are several contributions to the cross section individually divergent, but this comes with the additional complication that the separately divergent contributions from the real emission and virtual parts are integrated over different phase spaces ($n+1$- and n-body phase space, respectively). So that in order to ensure their divergences cancel either the possibility to perform analytic integration over the singular soft and collinear regions must be restored, or a way must be found to embed both of these contributions into the same integrand so the cancellation can happen numerically, or some combination of these two techniques must be used.

We also note that as discussed in chapter 3 the singularities in NLO calculations can be of both ultraviolet and infrared origin, with those of ultraviolet origin necessarily residing in the unrestricted loop momentum integrals in the virtual contribution. We outline how the cancellation of these UV-divergent loop contributions occurs in section 3.3.2.

To numerically compute NLO amplitudes containing IR divergences there exist three well known techniques: phase space slicing, judicious use of plus prescriptions, and subtraction methods. In the following sections we discuss the two latter ones as we make use of these in the present work.

3.5.1 Plus-Prescription Subtraction

In chapter 3 (and more in detail in section 3.3.1) we have already reviewed how the plus distribution as defined in equation 3.51 can be used to isolate the pole structure of a divergent integral by separating it into a finite part and an analytically solvable singular integral which gives the pole structure. This method is generally applied to extract the pole structure from the real emission contribution, which can then be cancelled against that from the virtual correction leaving only a finite correction.

3.5.2 Subtraction Methods

The most commonly used methods to numerically integrate NLO amplitudes currently in use are the subtraction methods. They have an advantage over the phase space slicing method in that they make no use of soft or collinear approximations to the amplitudes, and they introduce no unphysical cut-off scales of any kind. There are two formulations of this method, one proposed by Catani and Seymour [183] (and concisely reviewed in [184]), which we will from here on refer to as *dipole subtraction*, and another formulated by Frixione, Kunszt and Signer [185, 186]. We will focus on the former as this is the method chosen for our implementation.

Subtraction methods rely on the factorisation of QCD amplitudes in the soft and collinear limits (as we have discussed in sections 2.1.1 and 4.4). This implies that the infrared singularity structure of these amplitudes at the NLO level is universal, and that in the soft and collinear limits they can always be factored into a Born-level amplitude (that is, the real emission amplitude minus an emission) and a universal (process independent) factor which contains the soft and collinear limits.

Absorbing for now any possible observable under consideration (or equivalently an identity operator to obtain the total cross section) into the relevant amplitude, for example $\mathcal{B}\,O(\mathbf{\Phi}_n) \longrightarrow \mathcal{B}$ (with the amplitude as defined in equation 3.91) we can schematically write the singularity structure of the real emission amplitude as

$$\mathcal{C}^{(d)} = \sum_i \mathcal{B}^{(4)} \otimes \mathbf{V}_i^{(d)}\,, \tag{3.100}$$

where $\mathbf{V}_i$ schematically denotes what is known as a *dipole splitting function/operator*[16] and the '$\otimes$' symbol here denotes a convolution with the dipole's phase space and the inclusion of the dipole in the sum over spin and colour.

These operators can be shown to reduce to the appropriate forms in the soft and collinear limits (equations 4.22 and 2.19, respectively; see sections 4.2 and 4.3 and the discussion between equations 5.11 and 5.15 of the arXiV version of the original paper [183]) as expected, and hence can be used to subtract the IR singularities as desired[17].

The combination

$$\mathcal{D}_{ij,\,k} = \mathcal{B}^{(4)} \otimes \mathbf{V}_{ij,\,k}^{(d)}\,, \tag{3.101}$$

[16] Explicit forms for the splitting functions we will require will be given in due course. More generally these are operators in helicity space, $\mathbf{V}_{ij,\,k}$, with dependence on the helicity of the partons ij and k, however once projected (sandwiched) onto a given helicity configurations they are nothing but function of a single Lorentz scalar variable.

[17] Note however that unlike the splitting kernels $J^2(k)$ and $P^{ab}(z)$ defined in the exact soft and collinear limits, the splitting operators $\mathbf{V}^{ab,i}$ have a dependence on the kinematic mapping required for the phase space factorisation of the dipole phase space and hence have a different form for initial-initial, final-final, or initial-final dipoles.

defines what is known as a *dipole*. The sum over the possible dipoles for a given Born configuration encapsulates the full IR-singular behaviour of the QCD amplitude[18], such that

$$\mathcal{C} = \sum_{j} \sum_{k \neq j} \mathcal{D}_{ij,\,k}\,. \tag{3.102}$$

By the KLN theorem this is also the singularity structure of the virtual contribution, with which it will cancel upon summing (after analytically integrating the dipole over the soft/collinear emission of the dipole, see equation 3.103[19]).

A dipole consists of three partons labelled as the *emitter*, the *emitted*, and the *spectator*[20]. The first two are intuitively clear to identify, and the spectator is the parton to which the emitted parton is colour-connected. Each dipole corresponds to a different (soft or collinear) kinematic configuration of the $n+1$-body amplitude, and is therefore effectively an n-body kinematics amplitude times an eikonal or collinear splitting function with its corresponding 2-body phase space. Hence a sum over all dipoles is required to retain the full singularity structure of the amplitude.

Kinematic mappings (which must preserve momentum conservation and the on-shell condition for external partons) are therefore required to map the $n+1$-body real-emission phase space into an n-body Born configuration to which it is degenerate in a particular singular limit, and the phase space which the dipole must be integrated over, producing the *dipole factorisation* shown in equation 3.100.

We will further write the (analytically performed) integral of the dipole over the emission as[21]

$$\mathbf{I}(\epsilon) = \sum_{i} \int_{1} \mathbf{V}_{i}^{(d)}\,, \tag{3.103}$$

such that

$$\begin{aligned} \int_{n+1} \mathcal{C}^{(d)} &= \sum_{i} \int_{n} \mathcal{B}^{(4)} \otimes \int_{1} \mathbf{V}_{i}^{(d)} \\ &= \int_{n} \left[\mathcal{B}^{(4)} \otimes \mathbf{I}(\epsilon)\right]. \end{aligned} \tag{3.104}$$

where ϵ denotes the standard dimensional regularisation parameter. This is known as the *insertion operator*[22].

The factorisation of the counterterms in equation 3.104 into the Born and the dipole contribution is possible thanks to both soft and collinear factorisation of the amplitudes as well as a factorisation of the phase space into that of the Born process and that of the singe emission which is made possible by a kinematic mapping. Each type of dipole therefore requires its own type of kinematic mapping of the momenta it is evaluated with

[18] Assuming it is everywhere finite at the Born level, as is the case for all cases we consider.
[19] See equations 5.28, 5.32-34 of the arXiV version of the original paper [183] for proof.
[20] In equation 3.102 the parton j denotes the emitter, i the emitted parton, and k the spectator parton.
[21] We will from here on denote the dimensionality of the phase space being integrated over by a subscript under the corresponding integral, for example $\int d\mathbf{\Phi}_1 \longrightarrow \int_1$.
[22] It is in principle an operator in colour space as it includes colour generators.

to guarantee this factorisation and such a mapping must be specified and applied correspondingly with each dipole for the method to work.

To construct the full set of required dipoles for a given process one therefore requires the correct type of dipoles, as grouped by whether it is initial- or final-state partons which are colour-connected to the emission, as shown in table 3.1, where we have used superscript a, b to denote partons in the initial state, subscript i, j to denote partons in the final state, i is always the emitted parton, and we have used a comma to separate the emitter and the emitted parton from the spectator if they are all superscript or subscript.

	Initial state spectator	Final state spectator
Initial state emitter	$\mathcal{D}^{ai,b}$	$\mathcal{D}^{ai}_{j}$
Final state emitter	$\mathcal{D}^{a}_{ij}$	$\mathcal{D}_{ij,k}$

Table 3.1: Classification of dipoles.

As mentioned, each possible type of dipole will also require its own set of $n+1 \to n$ kinematic mappings as defined in [183], and the sum over all possible spectator partons must be taken for emission from all possible external partons.

The universality of the dipoles (and therefore also of their integrated form) implies they need to be calculated only once and once their form is known they can be applied generally to any NLO QCD amplitude. The form of such dipoles and insertion operators is given in the original paper [183].

With these definitions we can now write the relation for an observable at NLO accuracy where each contribution is separately finite and therefore numerically computable as

$$\sigma_{NLO} = \int_n \mathcal{B} \; + \; \int_n \mathcal{V}_0 \; + \; \int_{n+1} \mathcal{C}^{(d)} \; + \; \int_{n+1} \left(\mathcal{R}_0^{(d)} - \mathcal{C}^{(d)} \right) . \tag{3.105}$$

Since the counterterm and the real emission terms act on the same phase space and possess the same singularity structure (by definition of the counterterms), the last integrand is therefore finite and can be directly evaluated numerically in $d = 4$. The compensating counterterm in the third term is by contrast kept in $d = 4 - 2\epsilon$ dimensions and combined with the virtual contribution using equation 3.104, giving

$$\sigma_{NLO} = \int_n \left[\left(\mathcal{B} \; + \; \underbrace{\mathcal{V}_0 \; + \; [\mathcal{B}^{(4)} \otimes \mathbf{I}(\epsilon)]}_{\text{finite}} \right) \Bigg|_{\epsilon=0} \right] \; + \; \int_{n+1} \left(\underbrace{\mathcal{R}_0^{(4)} - \mathcal{C}^{(4)}}_{\text{finite}} \right) , \tag{3.106}$$

where all integrals are now finite and numerically computable, and we have specified $\epsilon = 0$ where any IR poles should have already cancelled but any remaining terms of order ϵ, ϵ^2 or higher are dropped to recover the $d = 4$ limit.

For processes involving initial-state radiation the form of the dipoles changes, the kinematic mappings

required change, the PDFs must now be taken into consideration (as they are required for mass factorisation), and the NLO cross section acquires extra terms corresponding to the collinear remnants as

$$\sigma_{NLO} = \int_n \left[\left(\mathcal{B} \; + \; \underbrace{\mathcal{V}_0 \; + \; [\mathcal{B}^{(4)} \otimes \mathbf{I}(\epsilon)] \; + \; \int_0^1 dz\, \mathcal{G}_{a\,0}(z) \; + \; \int_0^1 dz\, \mathcal{G}_{b\,0}(z)}_{\text{finite}} \right) \Bigg|_{\epsilon=0} \right] + \int_{n+1} \underbrace{\left(\mathcal{R}_0^{(4)} - \mathcal{C}^{(4)} \right)}_{\text{finite}}, \tag{3.107}$$

but the essence of the dipole subtraction procedure is unaltered.

The precise form of all dipoles and their corresponding kinematic mappings and integrals can be found in table C.1 of the original paper [183].

3.5.3 The Implementation of Dipole Subtraction

Having defined the general framework of dipole subtraction we now describe its implementation as relevant to the processes computed in this work.

The components required for the dipole-subtracted numerical NLO computation are:

- the initial emitter-initial spectator dipoles, $\mathcal{D}_i$ (equation 3.100), for the numerical subtraction of the real emission IR singularities, with their corresponding kinematic mappings of –in this case, all– final state momenta;
- the analytic form of the $d = 4 - 2\epsilon$ subtraction term integrated over the phase space of the single emission (that is, the insertion operator $\mathbf{I}(\epsilon)$ from equation 3.103);
- the finite collinear remnants with Born kinematics, computed consistently in the same renormalisation scheme as the rest of the amplitude (the $\overline{\text{MS}}$ scheme here).

All these must be computed for a generic process with two initial-state partons and no other external legs with colour charge (in the cases relevant to us, with channels $q\bar{q}$, gq and $g\bar{q}$).

The Dipoles

For radiation involving an initial-state emitter as well as an initial-state spectator[23] where no other partons exist, as discussed in section 3.5.2 the Catani-Seymour dipole subtraction method specifies dipoles of the form

$$\left|\mathcal{M}^{(n+1)}_{ab;\,i}(p_a,\,p_b;\,\{p_f\})\right|^2 \underset{\text{soft(collinear)}}{\longrightarrow} \left(\sum_a \sum_{b\neq a} V^{ai,\,b}(x_{i,\,ab})\right) \left|\mathcal{M}^{(n)}_{ab}(\tilde{p}_{ai},\,p_b;\,\{\tilde{p}_f\})\right|^2 , \tag{3.108}$$

where a and b denote the emitter and spectator initial state partons respectively, i labels the emitted parton, and the tilde denotes momenta after the required kinematic mapping for the dipoles required. Note that the momentum of the spectator parton is unchanged by the kinematic mapping.

More generally, the right hand side of equation 3.108 is the sum over the all the relevant dipoles which are given in general at the operator level ($\mathbf{T}_a$ are operators over the colour space and the dipole splitting operators $\mathbf{V}^{ai,\,b}$ are operators over helicity space) by

$$\begin{aligned}\mathcal{D}^{ai,\,b}(p_a,\,p_b;\,p_1,\,\ldots\,,p_{n+1}) = &-\frac{1}{2\,p_a\cdot p_i}\,\frac{1}{x_{i,\,ab}} \\ &\times {}_{n,\,ab}\Big\langle \widetilde{ai},\,b;\,\tilde{1},\,\ldots\,,\widetilde{n+1}\Big|\,\frac{\mathbf{T}_b\cdot\mathbf{T}_{ai}}{\mathbf{T}^2_{ai}}\,\mathbf{V}^{ai,\,b}\,\Big|\widetilde{ai},\,b;\,\tilde{1},\,\ldots\,,\widetilde{n+1}\Big\rangle_{n,\,ab}\,,\end{aligned} \tag{3.109}$$

where the bras and kets denote states of definite momentum, colour charge and helicity. The subscript $n,\,ab$ denotes the Born configuration with initial partons a, b, where the would-be emitter parton a is replaced by ai, with the rescaled momentum

$$\tilde{p}^{\mu}_{ai} = x_{i,\,ab}\,p^{\mu}_a\,, \tag{3.110}$$

where the variable

$$x_{i,\,ab} = 1\;-\;\frac{p_i\cdot p_a\;+\;p_i\cdot p_b}{p_a\cdot p_b}\,, \tag{3.111}$$

has been defined.

Defining the four-momenta

$$K^{\mu} = p^{\mu}_a\;+\;p^{\mu}_b\;-\;p^{\mu}_i\,, \tag{3.112a}$$

$$\widetilde{K}^{\mu} = \tilde{p}^{\mu}_{ai}\;+\;p^{\mu}_b\,, \tag{3.112b}$$

all the final-state momenta (colour-charged or otherwise) are mapped as

$$\tilde{k}_j\;=\;k^{\mu}_j\;-\;\frac{2\,k_j\cdot(K\;+\;\widetilde{K})}{(K\;+\;\widetilde{K})^2}\,(K\;+\;\widetilde{K})^{\mu}\;+\;\frac{2\,k_j\cdot K}{K^2}\,\widetilde{K}^{\mu}\,, \tag{3.113}$$

[23] Which is the case relevant in the processes we consider, and which we denote as an *initial-initial* configuration for brevity.

where this transformation can be shown to correspond to a Lorentz transformation.

The action of the dipole splitting operator on the helicity states for the $q(\bar{q}) \to q(\bar{q})g$ and $g \to \bar{q}q$ initial-state splittings of interest to us give[24]

$$\begin{aligned}
\langle s| \, \mathbf{V}^{q_a g_i,\, b}(x_{i,\,ab}) \, |s'\rangle &= 8\pi\mu^{2\epsilon}\alpha_S C_F \left[\frac{2}{1 \,-\, x_{i,\,ab}} \,-\, (1 \,+\, x_{i,\,ab}) \,-\, \epsilon\,(1 \,-\, x_{i,\,ab})\right] \delta_{s\,s'}\,, \\
\langle s| \, \mathbf{V}^{g_a \bar{q}_i,\, b}(x_{i,\,ab}) \, |s'\rangle &= 8\pi\mu^{2\epsilon}\alpha_S T_R \left[1 \,-\, \epsilon \,-\, 2\,x_{i,\,ab}\,(1 \,-\, x_{i,\,ab})\right] \delta_{s\,s'}\,,
\end{aligned} \tag{3.114}$$

where the s, s' denote the spins of the fermions and the $d = 4$, $\epsilon \to 0$ limit is taken for the computation of the dipoles.

Given that we deal with configurations with $n_{\text{partons}} \leq 3$ the projection of the colour operators gives a scalar in colour space (a function of Casimir invariants) which can be factorised out of the sandwich in equation 3.109 as a simple prefactor multiplying the Born amplitude.

The expectation value of a colour charge operator for the emission of a gluon with colour (adjoint) index c off a parton a is given by

$$\langle c_1,\, \ldots\,, c_a,\, \ldots\,, c_n| \; \mathbf{T}_a \; |c'_1,\, \ldots\,, c'_a,\, \ldots\,, c'_n\rangle = \delta_{c_1\,c'_1} \; \ldots \; t^c_{c_a\,c'_a} \; \ldots \; \delta_{c_n\,c'_n} \tag{3.115}$$

where $t^c_{\alpha\beta}$ is the Gell-Mann matrix representation of $SU(3)$ for an outgoing quark[25] or incoming anti-quark, $-(t^c)^T = -(t^c)^*$ (Gell-Mann matrices are Hermitian) are the colour matrices used for an incoming quark or outgoing anti-quark, and $-if^{abc}$ for incoming or outgoing gluons[26].

Using this formalism we have that,

$$\mathbf{T}_i^2 \; |c_1,\, \ldots\,, c_i,\, \ldots\,, c_n\rangle = C_{R(i)} \; |c_1,\, \ldots\,, c_i,\, \ldots\,, c_n\rangle \;. \tag{3.116}$$

For two coloured states,

$$\begin{aligned}
&\left(\sum_a \mathbf{T}_a\right)^2 |a,\, b\rangle = (\mathbf{T}_a \,+\, \mathbf{T}_b)^2 \, |a,\, b\rangle = 0 \qquad\qquad (3.117) \\
&\qquad\qquad \Rightarrow \mathbf{T}_a \cdot \mathbf{T}_b \, |a,\, b\rangle = -\mathbf{T}_a^2 \, |a,\, b\rangle = -\mathbf{T}_b^2 \, |a,\, b\rangle = -C_{R(a)} \, |a,\, b\rangle = -C_{R(b)} \, |a,\, b\rangle
\end{aligned}$$

where $C_{R(a)}$ is the Casimir invariant of the parton a transforming under the representation R of $SU(3)$[27] and

[24] We will in fact always deal with the unpolarised (spin-averaged) dipole splitting functions,

$$\left\langle \mathbf{V}^{ai,\,b} \right\rangle_{\text{spin}} \;=\; \frac{1}{n_s} \sum_{s,\,s'} \mathbf{V}^{ai,\,b} \;\propto\; \frac{1}{n_s} \sum_{s,\,s'} \delta_{s\,s'} \;=\; 1\,,$$

as we work only with hadron-hadron processes with unpolarised beams. We can therefore make the replacement $\delta_{s\,s'} \to 1$ in equation 3.114 and no spin dependence remains.

[25] For radiation from quarks α labels the external leg quark and β labels the quark attached to the hard interaction. We will now continue to omit the colour matrix indices as we have consistently done so far.

[26] a denotes the external leg gluon and b the gluon in the hard interaction.

[27] Recall $C_F = \frac{N_C^2 - 1}{2N_C}$ and $C_A = N_C$ (where $N_C = 3$ is the number of colours) for emission off partons transforming under

we have used the colour-conservation relation $\sum_i \mathbf{T}_i \, |a, \, b\rangle = 0$, as all colour states we use are colour singlets by definition.

Applying equations 3.114, 3.116 and 3.117 to the initial-initial dipole definition (equation 3.109) gives us the dipoles we require as

$$\mathcal{D}^{qg,\,\bar{q}} = \frac{8\pi}{2\,\tilde{p}_{qg}\cdot p_g}\,\alpha_S\,C_F\left[\frac{2}{1\,-\,x_{g,\,q\bar{q}}}\,-\,(1\,+\,x_{g,\,q\bar{q}})\right]\mathcal{B}(\tilde{p}_{qg},\,p_{\bar{q}};\,\tilde{k}_1,\,\ldots\,,\,\tilde{k}_n)\,, \tag{3.118a}$$

$$\mathcal{D}^{gq,\,q} = \frac{8\pi}{2\,\tilde{p}_{gq}\cdot p_q}\,\alpha_S\,T_R\,[1\,-\,2\,x_{q,\,g\bar{q}}\,(1\,-\,x_{q,\,g\bar{q}})]\,\mathcal{B}(\tilde{p}_{gq},\,p_{\bar{q}};\,\tilde{k}_1,\,\ldots\,,\,\tilde{k}_n)\,, \tag{3.118b}$$

where in agreement with the notation set out in section 3.4 (and equation 3.91 in particular), $\mathcal{B}$ denotes the Born amplitude with symmetry and averaging factors included. The tilded momenta are subject to the kinematic mappings of equations 3.110 and 3.113.

The dipoles corresponding to gluon emission off the incoming anti-quark, and the dipole corresponding to the anti-quark (originating from a gluon splitting) going into the hard process are identical to those above and must also be included

$$\mathcal{D}^{\bar{q}g,\,q} = \mathcal{D}^{qg,\,\bar{q}}\,, \tag{3.119a}$$

$$\mathcal{D}^{g\bar{q},\,\bar{q}} = \mathcal{D}^{gq,\,q}\,. \tag{3.119b}$$

These dipoles encapsulate the full IR singularity structure of the process we will deal with and are used to perform the singularity subtraction of the $d = 4$ real emission contribution, with a counterterm as constructed in equation 3.102 and used to eliminate the singular component of the total cross section or observable as set out in equation 3.107.

The Insertion Operator

The subtraction of the corresponding singularity structure from the virtual component of the NLO amplitude involves the construction of an operator over colour space, $\mathbf{I}(\epsilon;\,\{p\},\,\alpha_S(\mu_R))$, with Born kinematics which is a function only of the Mandelstam invariant s (the partonic invariant mass of the hard interaction), the factorisation scale, μ_F, the renormalisation scale (through the strong coupling constant), μ_R, and the dimensional regularisation parameter, ϵ.

As schematically defined in equation 3.103 this operator is obtained from the analytic integration over the

the fundamental and adjoint (quarks and gluons, respectively) representations. These relations hold for a general $SU(N_C)$.

emission phase space of the relevant dipole splitting functions and is given explicitly by

$$\mathbf{I}\left(\epsilon;\,\{p\},\,\alpha_S(\mu_R)\right) = -\frac{\alpha_S}{2\pi}\,\frac{1}{\Gamma(1-\epsilon)}\,\sum_I\left\{\frac{1}{\mathbf{T}_I^2}\,V_I(\epsilon)\,\sum_{J\neq I}\left[\mathbf{T}_I\cdot\mathbf{T}_J\,\left(\frac{4\pi\mu^2}{2p_I\cdot p_J}\right)^{\epsilon}\right]\right\}, \tag{3.120}$$

where I, J label any initial- or final-state parton and $\{p\}$ denotes the set of the momenta of all the partons present. The functions $V_I(\epsilon)$ are obtained directly from the analytic integration over the dipole splitting functions and for (anti)quarks are given by

$$V_q(\epsilon) = C_F\,\left[\frac{1}{\epsilon^2}\,+\,\frac{3}{2\epsilon}\,+\,5\,-\,\frac{\pi^2}{2}\,+\,\mathcal{O}(\epsilon)\right], \tag{3.121}$$

with $V_{\bar{q}}(\epsilon) = V_q(\epsilon)$.

For the Born configuration $q\bar{q}\to(\text{colour singlet})$ this gives

$$\begin{aligned}\mathbf{I}\left(\epsilon;\,\{p\},\,\alpha_S(\mu_R)\right) = -\frac{\alpha_S}{2\pi}\,\frac{1}{\Gamma(1-\epsilon)}\,\Bigg[&\frac{1}{\mathbf{T}_q^2}\,V_q(\epsilon)\,\mathbf{T}_q\cdot\mathbf{T}_{\bar{q}}\,\left(\frac{4\pi\mu^2}{2p_q\cdot p_{\bar{q}}}\right)^{\epsilon}\\ &+\,\frac{1}{\mathbf{T}_{\bar{q}}^2}\,V_{\bar{q}}(\epsilon)\,\mathbf{T}_{\bar{q}}\cdot\mathbf{T}_q\,\left(\frac{4\pi\mu^2}{2p_{\bar{q}}\cdot p_q}\right)^{\epsilon}\Bigg].\end{aligned} \tag{3.122}$$

Computing the expectation value of this operator using equations 3.116 and 3.117 we see that the expectation value of the colour operators is given by

$$\langle q,\,\bar{q}|\;\mathbf{T}_q\cdot\mathbf{T}_{\bar{q}}\;|q',\,\bar{q}'\rangle\;=\;\langle q,\,\bar{q}|\;\mathbf{T}_{\bar{q}}\cdot\mathbf{T}_q\;|q',\,\bar{q}'\rangle\;=\;-C_F\;\langle q,\,\bar{q}\,|\,q',\,\bar{q}'\rangle\;=\;-C_F\,\mathcal{B}, \tag{3.123}$$

such that the insertion function relevant to us is given by

$$\begin{aligned}I\left(\epsilon;\,\{p\},\,\alpha_S(\mu_R)\right) &= \frac{\alpha_S}{2\pi}\,\frac{1}{\Gamma(1-\epsilon)}\,2\,V_q(\epsilon)\,\left(\frac{4\pi\mu^2}{s}\right)^{\epsilon}\,\mathcal{B}\\ &= \frac{\alpha_S}{2\pi}\,\frac{C_F}{\Gamma(1-\epsilon)}\,\left(\frac{4\pi\mu^2}{s}\right)^{\epsilon}\,\left[\frac{2}{\epsilon^2}\,+\,\frac{3}{\epsilon}\,+\,10\,-\,\pi^2\,+\,\mathcal{O}(\epsilon)\right]\mathcal{B}.\end{aligned} \tag{3.124}$$

Note that as expected this matches and cancels the IR singularity structure of the virtual contribution of the SM NLO Drell-Yan calculation in equation 3.75, and as we will later see, the singular part of the virtual contribution to slepton pair production in equation 6.27 must also be identical to the singularity structure of this insertion operator[28].

The Collinear Remnants

The collinear remnants which we derived in section 3.3.3 from the cancellation of collinear singularities from initial-state emission between the fixed-order amplitude and the parton distribution functions leave a corresponding finite remainder which may be included partly in the amplitude and partly in the PDFs, according to

[28] However since we take the finite virtual contribution from PROSPINO2 we must assume the finite contribution of this insertion operator has already been consistently included in their result.

the factorisation scheme chosen, but which must be consistently accounted for to obtain the full NLO result.

Within the Catani-Seymour dipole subtraction scheme these terms are split into the (finite) $\mathbf{K}^{a,\,a'}$ and $\mathbf{P}^{a,\,a'}$ insertion operators (over colour space), which are defined (for the case where only initial-state partons exist) as

$$\mathbf{P}^{a,\,a'}(\{p\};\,z;\,\mu_F) = \frac{\alpha_S}{2\pi}\,P^{aa'}(z)\,\frac{1}{\mathbf{T}^2_{a'}}\sum_{I\neq a'}\mathbf{T}_I\cdot\mathbf{T}_{a'}\,\ln\frac{\mu_F^2}{2zp_a\cdot p_I}\,, \tag{3.125}$$

$$\begin{aligned}\mathbf{K}^{a,\,a'}(z) = {}& \frac{\alpha_S}{2\pi}\left\{\bar{K}^{aa'}(z)\;-\;K^{aa'}_{\mathrm{F.S.}}(z)\;+\;\delta^{aa'}\sum_i\mathbf{T}_i\cdot\mathbf{T}_a\frac{\gamma_i}{\mathbf{T}_i^2}\left[\left(\frac{1}{1-z}\right)_+\;+\;\delta(1-z)\right]\right\}\\ &-\;\frac{\alpha_S}{2\pi}\frac{\mathbf{T}_b\cdot\mathbf{T}_{a'}}{\mathbf{T}^2_{a'}}\,\widetilde{K}^{a,\,a'}(z)\,,\end{aligned} \tag{3.126}$$

where I denotes any parton, a and a' denote the initial-state parton before and after the branching, b denotes the spectator parton, and i denotes any final-state parton.

The factorisation-scheme dependent term $K^{aa'}_{\mathrm{F.S.}}(z)$ vanishes in the $\overline{\mathrm{MS}}$ scheme which we work in, and the constants

$$\gamma_q = \gamma_{\bar{q}} = \frac{3}{2}C_F, \qquad \gamma_g = \frac{11}{6}C_A - \frac{2}{3}T_R n_f\,, \tag{3.127}$$

and the functions

$$\overline{K}^{gq}(z) = \overline{K}^{g\bar{q}}(z) = P^{gq}(z)\,\ln\frac{1-z}{z}\;+\;T_R\,2z(1-z)\,, \tag{3.128a}$$

$$\begin{aligned}\overline{K}^{qq}(z) = \overline{K}^{\bar{q}\bar{q}}(z) = {}& C_F\left[\left(\frac{2}{1-z}\ln\frac{1-z}{z}\right)_+\;-\;(1\,+\,z)\ln\frac{1-z}{z}\;+\;(1\,-\,z)\right]\\ &-\;\delta(1-z)\,(5-\pi^2)\,C_F\,,\end{aligned} \tag{3.128b}$$

$$\widetilde{K}^{qq}(z) = \widetilde{K}^{\bar{q}\bar{q}} = C_F\left[\left(\frac{2}{1-z}\ln(1-z)\right)_+\;-\;\frac{\pi^2}{3}\delta(1-z)\;-\;(1+z)\ln(1-z)\right], \tag{3.128c}$$

$$\widetilde{K}^{gq}(z) = \widetilde{K}^{g\bar{q}} = P^{gq}(z)\,\ln(1-z)\,, \tag{3.128d}$$

fully specify the insertion operators. The Altarelli-Parisi functions used here, $P^{ab}(z) = P_{ab}(z)$, are the regularised $d = 4$ forms of the splitting functions as defined in figure 4.1.

The insertion operators $\mathbf{K}^{a,\,a'}$ and $\mathbf{P}^{a,\,a'}$ correspond precisely to the type of mass factorisation terms derived in section 3.3.3, specifically to the finite terms arising from the sum of equations 3.87 and 3.88 (where the singular components cancel in the sum, as expected).

These operators (once projected onto the colour states to obtain the expectation value of the operators) give the finite collinear remnant terms $\mathcal{G}_{a\,0}$ and $\mathcal{G}_{b\,0}$ from equation 3.107.

Explicitly, for the processes relevant to us $\mathbf{P}^{a,\,a'}$ evaluates to

$$P^{q,\,q}(\{p\};\ z;\ \mu_F) = -\frac{\alpha_S}{2\pi}\,C_F\,\left(\frac{1+z^2}{1-z}\right)_+ \ln\frac{\mu_F^2}{2z\tilde{p}_{qg}\cdot p_{\bar{q}}}\,, \tag{3.129}$$

$$P^{g,\,q}(\{p\};\ z;\ \mu_F) = -\frac{\alpha_S}{2\pi}\,T_F\,\left[z^2+(1-z)^2\right]\,\ln\frac{\mu_F^2}{2z\tilde{p}_{gq}\cdot p_{\bar{q}}}\,, \tag{3.130}$$

where we may recognise $s = 2z\tilde{p}_{qg}\cdot p_{\bar{q}} = 2z\tilde{p}_{gq}\cdot p_{\bar{q}}$ as the hard interaction invariant mass of real emission configurations.

The $\mathbf{K}^{a,\,a'}$ operators are likewise given by

$$\begin{aligned} K^{q,\,q}(z) = \frac{\alpha_S}{2\pi}\,C_F\,\Bigg\{ &\left[\frac{2}{1-z}\ln\frac{1-z}{z}\right]_+ - (1+z)\,\ln\frac{1-z}{z} + (1-z) - \delta(1-z)\,\left(5-\frac{2\pi^2}{3}\right) \\ &+ \left[\frac{2}{1-z}\ln(1-z)\right]_+ - (1+z)\,\ln(1-z)\Bigg\}, \end{aligned} \tag{3.131}$$

and

$$K^{g,\,q}(z) = \frac{\alpha_S}{2\pi}\,T_R\,\left\{\left[z^2+(1-z)^2\right]\,[2\,\ln(1-z)-\ln z] + 2\,z\,(1-z)\right\}\,, \tag{3.132}$$

where we have omitted the Born contribution which all the $P^{a,\,a'}(\{p\};\ z;\ \mu_F)$ and $K^{a,\,a'}(z)$ functions are proportional to and which results from the computation of the expectation value of their corresponding operators.

Together these functions form the full collinear remnant contribution, with equivalent contributions from each incoming parton a and b, as[29]

$$\mathcal{G}_a^{q\bar{q},\,g}(z) = \{P^{q,\,q}(\{p\};\ z;\ \mu_F) + K^{q,\,q}(z)\}\,\mathcal{B}(z\,x_a,\,x_b;\ k_1,\,k_2)\,, \tag{3.133a}$$

$$\begin{aligned} &= \frac{\alpha_S}{2\pi}\,C_F\,\Bigg\{ -\left(\frac{1+z^2}{1-z}\right)_+ \ln\frac{\mu_F^2}{2z\tilde{p}_{qg}\cdot p_{\bar{q}}} + \left[\frac{2}{1-z}\ln\frac{1-z}{z}\right]_+ - (1+z)\,\ln\frac{1-z}{z} \\ &+ (1-z) - \delta(1-z)\,\left(5-\frac{2\pi^2}{3}\right) + \left[\frac{2}{1-z}\ln(1-z)\right]_+ - (1+z)\,\ln(1-z)\Bigg\}\,\mathcal{B}(\overline{\mathbf{\Phi}}_n)\,, \end{aligned}$$

$$\mathcal{G}_a^{gq,\,\bar{q}}(z) = \{P^{g,\,q}(\{p\};\ z;\ \mu_F) + K^{g,\,q}(z)\}\,\mathcal{B}(z\,x_a,\,x_b;\ k_1,\,k_2)\,, \tag{3.133b}$$

$$= \frac{\alpha_S}{2\pi}\,T_R\,\left\{\left[z^2+(1-z)^2\right]\,\left[2\,\ln(1-z) - \ln z - \ln\frac{\mu_F^2}{2z\tilde{p}_{gq}\cdot p_{\bar{q}}}\right] + 2\,z\,(1-z)\right\}\,\mathcal{B}(\overline{\mathbf{\Phi}}_n)\,,$$

constitutes the contribution from parton a, with an equivalent contribution with the replacements $a \to b$ and $q \leftrightarrow \bar{q}$ from parton b. Note that the Born factor is evaluated using underlying n-body configuration kinematics. The resulting expressions for these collinear remnants have been compared for example to those of [187] (equations 4.30,31) and are identical.

[29] Note that the subscript '0' is no longer present as these are the finite part of the mass factorisation term after cancellation of the singularities with the parton distribution functions has occurred.

So far we have omitted the convolution with the parton distribution functions and the presence of any possible observable. However for these collinear remnants there are two subtleties which must be accounted for when integrating over them:

- they imply an extra integration over the collinear momentum fraction variable, z, of which all the collinear remnant functions above are a function of, as well as a Jacobian factor of $1/z$, such that the integration phase space for the collinear remnants is as defined in equation 5.48b, giving terms such as the last two terms of equation 5.51;
- for emission off initial-state partons the z variable is introduced via a Dirac delta distribution (see equations 2.33-35 in [188]), such that the momentum fraction of the incoming parton considered in the collinear remnant must be rescaled to x/z, implying that for the collinear remnant terms the luminosity function are redefined from equation 3.92 to

$$\tilde{\mathcal{L}}_a = f_i\left(x_a/z,\, \mu_F\right)\, f_j(x_b,\, \mu_F)\,, \tag{3.134}$$

  for emission from the parton a, and similarly for parton b.

Explicitly, the collinear remnant terms are therefore given by

$$\left(\int_{x_a}^1 \frac{dz}{z}\, \tilde{\mathcal{L}}_a \left[\mathcal{G}_a^{q\bar{q},\, g}(z) \;+\; \mathcal{G}_a^{gq,\, \bar{q}}(z)\right]\, O(z\, x_a,\, x_b;\, k_1,\, k_2)\right) \quad + \quad (a \leftrightarrow b)\,, \tag{3.135}$$

for consistent combinations of parton pairs ($ab \in \{q\bar{q},\, qg,\, \bar{q}g\}$). Note that the observable is evaluated using the underlying Born kinematics, $\overline{\mathbf{\Phi}}_n^a = \{z\, x_a,\, x_b;\; k_1,\, k_2\}$[30], as well.

It remains to apply the corresponding kernel and integration to the plus-prescription terms in $P^{q,\,q}(\{p\};\; z;\; \mu_F)$ and $K^{q,\,q}(z)$ to yield expressions amenable to numerical evaluation. As just discussed the integration required will be of the form

$$\int_x^1 \frac{dz}{z} \left(\quad \Big(\quad \cdots \quad \Big)_+ \; + \quad \cdots \quad \right) f\left(\frac{x}{z},\, \mu_F\right)\,, \tag{3.136}$$

where we have omitted prefactors and the other parton distribution which has no z-dependence and is unaffected by the integration.

The terms including a plus distribution in $K^{q,\,q}(z)$ can be rewritten as

$$\int_x^1 \frac{dz}{z} \left(\frac{2}{1-z} \ln \frac{(1-z)^2}{z}\right)_+ f\left(\frac{x}{z},\, \mu_F\right)\,, \tag{3.137}$$

[30] Likewise, the factor of z multiplies x_b for $\overline{\mathbf{\Phi}}_n^b$. We omit the $a(b)$ index and use of the appropriate one is understood.

whilst that from $P^{q,\,q}(\{p\};\,z;\,\mu_F)$ can also be trivially rewritten as

$$\int_x^1 \frac{dz}{z}\,\left(\frac{2}{1\,-\,z}\;-\;(1\,+\,z)\right)_+ f\left(\frac{x}{z},\,\mu_F\right)\,. \tag{3.138}$$

Here the relation[31]

$$\begin{aligned}\int_x^1 f(z)_+\,g(z)\,dz &= \int_0^1 dz\;f(z)_+\,g(z)\;-\;\int_0^x dz\;f(z)\,g(z)\\ &= \int_x^1 dz\;\left[g(z)\;-\;g(1)\right]\,f(z)\quad-\quad g(1)\int_0^x f(z)\,dz\,,\end{aligned} \tag{3.139}$$

can be used, such that with the the replacement $g(z)\,=\,\frac{1}{z}f\left(\frac{x}{z},\,\mu_F\right)$ these plus-distribution terms can be shown to give

$$\begin{aligned}K^{q,\,q}(z)\;\supset\;\frac{\alpha_S}{2\pi}\,C_F\,\Bigg\{&\left(2\,\ln^2(1-x)\;-\;\frac{\pi^2}{3}\right)\,f(x)\;+\;\int_x^1\frac{dz}{z}\,\left(\frac{4}{1-z}\,\ln(1-z)\right)\,\left[f\left(\frac{x}{z}\right)\;-\;z\,f(x)\right]\\ &-\;\int_x^1\frac{dz}{z}\,\frac{2}{1-z}\,\ln(z)\,f\left(\frac{x}{z}\right)\Bigg\},\end{aligned} \tag{3.140}$$

and

$$\begin{aligned}P^{q,\,q}(\{p\};\,z;\,\mu_F)\;\supset\;\frac{\alpha_S}{2\pi}\,C_F\,\ln\left(\frac{s}{\mu_F}\right)\,\Bigg\{&\frac{3}{2}f(x)\;-\;\int_x^1\frac{dz}{z}(1+z)\,f\left(\frac{x}{z}\right)\;+\;2\,\ln(1-x)\,f(x)\\ &+\;2\int_x^1\frac{dz}{z}\,\frac{1}{1-z}\,\left[f\left(\frac{x}{z}\right)\;-\;z\,f(x)\right]\Bigg\},\end{aligned} \tag{3.141}$$

where we have suppressed the scale and parton dependence of the PDFs everywhere, $f(\,\cdot\,)=f_q(\,\cdot\,,\,\mu_F)$, and the relation

$$\begin{aligned}\int_0^x\frac{dz}{1-z}\,\ln(z) &=\;\int_0^1\frac{dz}{1-z}\,\ln(z)\;-\;\int_x^1\frac{dz}{1-z}\,\ln(z)\\ &=\;-\mathrm{Li}_2(1)\;-\;\int_x^1\frac{dz}{1-z}\,\ln(z)\;=\;-\frac{\pi^2}{6}\;-\;\int_x^1\frac{dz}{1-z}\,\ln(z)\,,\end{aligned} \tag{3.142}$$

has been used to obtain equation 3.140.

Including the the rest of the terms which do not involve plus distributions the total z-integrated collinear

[31] Note that the plus prescription is missing on the second term of the first line on the right hand side. This seemingly inconsistent absence is because the singularity at $z=1$ is outside the range of integration of this term and therefore must not be subtracted.

counterterms from a $q(\bar{q}) \to gq(\bar{q})$ splitting are given by

$$\int_x^1 \frac{dz}{z}\, \mathcal{G}_a^{q\bar{q},\,g}(z) f_q\left(\frac{x}{z},\,\mu_F\right) = \frac{\alpha_S}{2\pi}\, C_F \tag{3.143}$$
$$\times \Bigg\{ f_q(x,\,\mu_F^2)\, \left[2\,\ln^2(1-x) \,-\, 5 \,+\, \frac{\pi^2}{3} \,+\, \ln\left(\frac{s}{\mu_F^2}\right)\left(\frac{3}{2} \,+\, 2\,\ln(1-x)\right)\right]$$
$$+ \int_x^1 \frac{dz}{z}\, \left[f_q\left(\frac{x}{z},\,\mu_F\right) \,-\, z\, f_q\left(x,\,\mu_F\right)\right] \left[\frac{4}{1-z}\,\ln(1-z) \,+\, \frac{2}{1-z}\ln\left(\frac{s}{\mu_F^2}\right)\right]$$
$$+ \int_x^1 \frac{dz}{z} f_q\left(\frac{x}{z},\,\mu_F\right) \left[(1-z) \,-\, (1+z)\,\ln\left(\frac{(1-z)^2}{z}\right) \,-\, \frac{2}{1-z}\ln(z) \,-\, (1+z)\ln\left(\frac{s}{\mu_F^2}\right)\right] \Bigg\}.$$

The $g \to q\bar{q}$ contributions to the collinear remnants contain no plus distributions and can be integrated as is,

$$\int_x^1 \frac{dz}{z}\, \mathcal{G}_a^{gq,\,\bar{q}}(z)\, f_g\left(\frac{x}{z},\,\mu_F\right) = \int_x^1 \frac{dz}{z}\, \frac{\alpha_S}{2\pi}\, T_R \Bigg\{ \left[z^2 + (1-z)^2\right]\, \ln\left(\frac{(1-z)^2}{z}\frac{s}{\mu_F^2}\right)$$
$$+\, 2\,z\,(1-z) \Bigg\}\, f_g\left(\frac{x}{z},\,\mu_F\right). \tag{3.144}$$

Note that the Born contribution which multiplies the P and K collinear remnant functions is evaluated at the underlying Born configuration such that the z momentum fraction has been absorbed into the emitting partonic fraction as $z\,x$ and the Born contribution therefore contains no explicit z dependence to consider or integrate over.

Chapter 4

Parton Showers and Resummation

The generation of hadron-hadron collisions in a Monte Carlo event generator is performed by several consecutive (but sometimes necessarily interleaved) stages: the generation of the hard partonic interaction (i.e. generation of the relevant amplitude squared and sampling over the corresponding phase space, convolved with the relevant parton distribution functions), the decay of extremely short-lived unstable particles (namely the top quark and $Z/W^{\pm}$ bosons, and the longer-lived tau lepton), the generation of QCD, QED (and for some select processes EW) emission off initial and final state legs, hadronisation of all final-state partons when the scale of perturbative emissions becomes non-perturbative ($\sim 2\ \mathrm{GeV}$), and finally the decay of all unstable hadrons produced (for example, the ubiquitous $\pi^0 \to \gamma\gamma$).

For a fully realistic attempt at event simulation the generation of the *underlying event* (UE)[1] which includes the single and double (elastic and inelastic) diffractive scattering components (collectively known as *minimum bias*) of the total proton-proton cross section, must also be included. However all these components are difficult and computationally expensive to generate accurately and we will assume they can be largely neglected for our purposes as for BSM searches we will be interested in high-p_T ($p_T \gtrsim 20\ \mathrm{GeV}$), central (pseudorapidity $\eta \lesssim |2.5|$) events.

However perhaps the most distinctive property of Monte Carlo event generators –as opposed to software packages which generate a single one (e.g. matrix element generation from MadGraph, UE from Jimmy, tau decay via TAUOLA, etc.) of the stages above– is the generation of highly multiplicity, fully-exclusive events. This task is performed in the generation of QCD and QED emission from initial- and final-state legs by the parton shower.

[1] For our purposes we will refer to all activity unrelated to the hardest interaction and its emissions and decays as the underlying event. This will include multi-parton interactions (MPI) from softer interactions between other partons within the colliding hadrons.

The parton shower algorithm has in fact two purposes, both related by unitarity (the probability of emission and no emission must add to one), and both amenable to simulation via a hit-or-miss Markovian[2] process:

a) The generation of emissions (in the collinear approximation stated in equation 2.21) from the probability of emission.

b) The resummation of inifinite towers of large logarithms (of the form $\alpha_S^n L^m$, where L is the logarithm of the ratio of the relevant scales) related to the integration over unobserved collinear and soft emissions (which generates the Sudakov suppression which dominates observables in the $p_T \ll Q$ region, where Q is the invariant mass exchanged), from the probability of no emission.

We will deal with the latter more formal property first, and relate it by unitarity to the algorithm for doing the former.

4.1 Logarithms from Fixed Order Calculations

Next-to-leading order calculations such as the one we carried out in the previous chapter contain logarithms which arise from the small ϵ expansion of the $D(\epsilon) \supset \left(\frac{\mu^2}{Q^2}\right)^\epsilon$ in the phase space and get multiplied by a collinear pole i.e. in equation 3.47. Namely, when equations 3.86 and 3.87 were added a logarithmic term associated with a collinear singularity arises with the form

$$\alpha_S \log\left(\frac{Q^2}{4\pi}\frac{(1-z)^2}{z}\right) - \alpha_S \log\left(\frac{\mu_F^2}{4\pi}\frac{1-z}{z}\right) = \alpha_S \log\left(\frac{Q^2}{\mu_F^2}\right) + \alpha_S \log(1-z)\,. \tag{4.1}$$

Since μ_F comes from a NLO correction to the DIS used to determine PDFs at $\mu_F^2 \sim (1\text{–}10\ \mathrm{GeV})^2$ and for Drell-Yan we will consider $Q^2 \sim (100\ \mathrm{GeV})^2$, this term can be easily be of order unity, $\alpha_S \log\left(\frac{Q^2}{\mu_F^2}\right) \sim 1$, implying that our NLO correction has become of the same order as the Born contribution and our perturbative result is no longer reliable.

To ameliorate this problem this contribution can be absorbed into the PDFs, where it can later be resummed. Taking our NLO PDF as shown in equation 3.85 and differentiating with respect to $\log \mu_F^2$ gives

$$\frac{d}{d\log\mu_F^2}\, q(x,\mu_F^2) = \frac{\alpha_S}{2\pi}\int_x^1 \frac{dy}{y} g(y) P_{qg}(x/y)\,, \tag{4.2}$$

where $z = x/y$ and $P_{qg}(z) = \frac{1}{2}[z^2 + (1-z)^2]$.

Integrating this from $\log \mu_F^2$ to $\log Q^2$ in order to evolve the PDF up to the invariant mass at which we

[2] This implies that the forward evolution of the process depends only on the current state of the system, and not on any of the previous evolution that drove it there.

shall be working gives

$$q(x,Q^2) = q(x,\mu_F^2) + \frac{\alpha_S}{2\pi}\,\log\left(\frac{Q^2}{\mu_F^2}\right)\int_x^1 \frac{dy}{y} g(y) P_{qg}(x/y)\,. \tag{4.3}$$

If we now use this PDF instead of $q(x,\mu_F^2)$ when computing equation 3.87 the logarithmic dependence in the partonic cross section will cancel, and we have thus fully absorbed it into the PDF. It is this acquired logarithmic dependence of the PDFs that gives the observed violation of Björken scaling (which states that the structure functions of DIS must have no Q^2 dependence at high Q^2, as expected for a pointlike target), whereas the logarithmic dependence expected from QCD is observed and is a confirmation of the parton model and QCD.

However this contribution remains large and is in fact only the first term (first emission) in an infinite tower of similarly large logarithmic terms of the form $\alpha_S \log Q^2$. In order to obtain physically meaningful observables the possibility of infinitely many unobserved collinear emissions must be accounted for, meaning we must *resum* it to all orders to guarantee that our perturbative results remain valid. This can be acheived by substituting the LO PDF, $g(y)$, by its NLO counterpart, $g(y,Q^2)$ in equation 4.2 giving

$$\frac{d}{d\log Q^2}\, q(x,Q^2) = \frac{\alpha_S(Q^2)}{2\pi}\int_x^1 \frac{dy}{y} g(y,Q^2) P_{qg}\left(\frac{x}{y}\right)\,, \tag{4.4}$$

where $P_{ij}(z)$ are the regularised splitting functions.

For quark PDFs we must add the contributions from $P_{qq}(z)$ and $P_{qg}(z)$, for gluon PDFs the contributions come from $P_{gg}(z)$ and $P_{qg}(z)$. The full set of regularised Altarelli-Parisi splitting functions in four dimensions is shown in figure 4.1, so that a sum over possible splittings must be included, giving the Dokshitzer-Gribov-Lipatov-Altarelli-Parisi (DGLAP) equation

$$\frac{d}{d\log Q^2}\, f_i(x,Q^2) = \sum_j \frac{\alpha_S(Q^2)}{2\pi}\int_x^1 \frac{dy}{y} f_j(y,Q^2) P_{ij}\left(\frac{x}{y}\right)\,. \tag{4.5}$$

That this equation does indeed sum an infinite tower of logarithms which we claim it does is shown in section 4.1.1.

4.1.1 Proof of DGLAP Resummation

To show that the DGLAP equation does indeed sum these collinear logs to all orders we may rewrite equation 4.4 using a delta distribution

$$\frac{d}{d\log Q^2}\, q(x,Q^2) = \frac{\alpha_S(Q^2)}{2\pi}\int_0^1 dy\, g(y,Q^2)\int_0^1 dz\, P_{qg}(z)\,\delta(x - y\,z)\,. \tag{4.6}$$

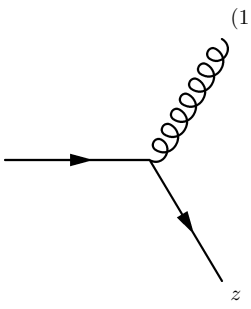

$$P_{qq}(z) = C_F \left(\frac{1+z^2}{1-z}\right)_+ = C_F \left[\frac{1+z^2}{(1-z)_+} + \frac{3}{2}\,\delta(1-z)\right]$$
$$\hat{P}_{qq}(z,\epsilon) = C_F \left[\frac{1+z^2}{1-z} - \epsilon\,(1-z)\right]$$
$$\hat{P}^{\text{excl}}_{q,qg}(z) = \hat{P}_{qq}(z,0)$$

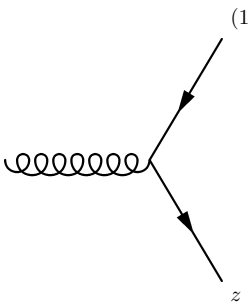

$$P_{gq}(z) = T_R \left[z^2 + (1-z)^2\right]$$
$$\hat{P}_{gq}(z,\epsilon) = T_R \left[1 - \frac{2\,z\,(1-z)}{1-\epsilon}\right]$$
$$\hat{P}^{\text{excl}}_{g,q\bar{q}}(z) = \hat{P}_{qg}(z,0)$$

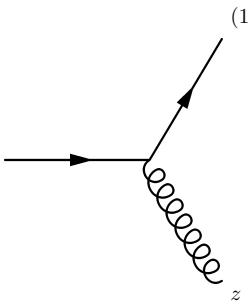

$$P_{qg}(z) = C_F \frac{1+(1-z)^2}{z}$$
$$\hat{P}_{qg}(z,\epsilon) = C_F \left[\frac{1+(1-z)^2}{z} - \epsilon\,z\right]$$
$$\hat{P}^{\text{excl}}_{q,gq}(z) = \frac{\hat{P}_{qg}(z,0)}{1-z}$$

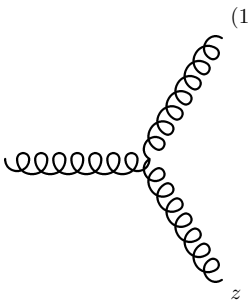

$$P_{gg}(z) = 2\,C_A \left[\frac{z}{(1-z)_+} + \frac{1-z}{z} + z\,(1-z)\right] + \frac{1}{6}\,(11\,C_A - 4\,n_f\,T_R)\,\delta(1-z)$$
$$\hat{P}_{gg}(z,\epsilon) = 2\,C_A \left[\frac{z}{1-z} + \frac{1-z}{z} + z\,(1-z)\right]$$
$$\hat{P}^{\text{excl}}_{g,gg}(z) = \frac{\hat{P}_{gg}(z,0)}{2}$$

Figure 4.1: The one-loop regularised Altarelli-Parisi splitting functions. We use the standard $T_R = 1/2$ Dynkin index normalisation for the Lie algebra, and for $SU(3)_C$ as in QCD, the Casimir operators of the fundamental and adjoint representations are $C_F = 4/3$ and $C_A = 3$, respectively. n_f denotes the number of quark flavours used (typically 4 or 5). We assign the momentum fraction z to the hard parton, and $1 - z$ to the potentially soft one. For a derivation of these splitting functions see [189].

We now perform a Mellin transform to see that this factorises as

$$\int_0^1 \frac{dx}{x}\, x^n\, \frac{d}{d\log Q^2}\, q(x,Q^2) = \frac{\alpha_S(Q^2)}{2\pi} \int_0^1 dy\, g(y,Q^2) \int_0^1 dz\, P_{qg}\,(z) \int_0^1 \frac{dx}{x}\, x^n\, \delta(x - y\,z)$$

$$\underbrace{\int_0^1 \frac{dx}{x}\, x^n\, \frac{d}{d\log Q^2}\, q(x,Q^2)}_{\frac{dM_n(Q^2)}{d\log Q^2}} = \frac{\alpha_S(Q^2)}{2\pi}\ \underbrace{\int_0^1 \frac{dz}{z}\, z^n\, P_{qg}(z)}_{A_n}\ \underbrace{\int_0^1 \frac{dy}{y}\, y^n\, g(y,Q^2)}_{M_n(Q^2)}\,. \tag{4.7}$$

Neglecting the Q^2 dependence of α_S and solving for $M_n(Q^2)$ gives the relation

$$\begin{aligned} M_n(Q^2) &= c_n\, \exp\left(\frac{\alpha_S}{2\pi}\, A_n\, \log Q^2\right) \\ &= c_n \sum_{m=0}^{\infty} \frac{1}{m!} \left(\frac{\alpha_S}{2\pi}\, A_n\right)^m \log^m Q^2\,. \end{aligned} \tag{4.8}$$

from which the all orders sum of logarithms is apparent.

4.2 Origin, Argument and Size of Logarithmic Contributions

The appearance of large logarithmic contributions can be simply observed in the case of $e^+e^- \to q\bar{q}$ where a resonance of invariant mass Q^2 decays into two partons each of momentum p, and we consider an extra emission (with momentum k) off one of these two partons (i.e. the NLO QCD contribution) in the soft and collinear approximation, as given by

$$\sigma_{\rm NLO} \sim \sigma_{\rm LO} \left(1 + \frac{\alpha_S}{\pi}\, C_F \int_0^{E_p} \frac{d\omega}{\omega} \int_0^1 \frac{d\theta^2}{\theta^2}\, \left[\Theta(m_J^2 - E_p\,\omega\,\theta^2) - 1\right]\right), \tag{4.9}$$

where the invariant mass of the jet generated is given by $m_J^2 = 2\,p\cdot k = 2\,E_p\,\omega\,(1-\cos\theta) \simeq E_p\,\omega\,\theta^2$, so that the step function gives the real emission contribution, and the -1 accounts for the virtual contribution which must exactly cancel the real contribution in the soft and collinear limit by the KLN theorem.

The term in square brackets can be rewritten as $-\Theta(E_p\,\omega\,\theta^2 - m_J^2)$ which gives a lower bound of $\theta^2 > \frac{m_J^2}{\omega\,E_p}$ on the angular integration, and imposing the collinear condition $\theta^2 < 1$ gives a lower limit on the gluon energy of $\omega > \frac{m_J^2}{E_p}$

$$\begin{aligned} \sigma_{\rm NLO} &\sim \sigma_{\rm LO} \left(1 - \frac{\alpha_S}{\pi}\, C_F \int_{\frac{m_J^2}{E_p}}^{E_p} \frac{d\omega}{\omega} \int_{\frac{m_J^2}{\omega\,E_p}}^1 \frac{d\theta^2}{\theta^2}\right), \\ &= \sigma_{\rm LO} \left(1 - \frac{\alpha_S}{\pi}\, C_F\, \frac{1}{2} \log^2 \frac{E_p^2}{m_J^2}\right), \\ &= \sigma_{\rm LO} \left(1 - \frac{\alpha_S}{2\pi}\, C_F\, \log^2 \frac{Q^2}{4\,m_J^2}\right), \end{aligned} \tag{4.10}$$

where we have used $E_p = Q/2$.

We therefore see that if we require the jet invariant mass to be small relative to Q, this logarithm becomes

large and if we set the renormalisation scale to the scale of this process, $\mu_R^2 = Q^2$ we see from the one-loop expression for α_S (equation 3.90)

$$\alpha_S(Q^2)\,\log^2\left(\frac{Q^2}{4\,m_J^2}\right) \sim \frac{\log^2(Q^2/4\,m_J^2)}{\beta_0\,\log\left(Q^2/\Lambda_{\rm QCD}\right)}\,, \tag{4.11}$$

which can be seen to become $\mathcal{O}(1)$ at $Q \gtrsim 70$ GeV for a jet mass $m_J \approx 10$ GeV ($\beta_0 \approx 0.61$, $\Lambda_{\rm QCD} \approx 200\,{\rm MeV}$). These logarithms can therefore become sizeable to the point where they jeopardise the perturbative series under consideration.

Terms of this form thus invalidate our perturbative expansion for the observable, and when considering higher order (or indeed all-order) expressions they will arise with each further emission generated (and therefore generate an infinite tower double-logarithmic and less-logarithmic terms).

4.3 The Logarithms of Perturbative QCD

Note that since the logarithms resummed by the DGLAP equation are of purely collinear origin the logarthmic structure is of the form $\alpha_S^n\,\log^n$. In fact the logarithmic structure generated by multiple emissions is more generally of the form

$$\alpha_S^n \log^m \tag{4.12}$$

where $m \leq 2n$.

The general soft and/or collinear logarithmic structure of fixed order calculations is, order by order:

Order in α_S	IR Logarithmic structure
$\mathcal{O}(\alpha_S^0)$	no IR QCD logs
$\mathcal{O}(\alpha_S)$	$\alpha_S\,\log^2$ $\alpha_S\,\log$
$\mathcal{O}(\alpha_S^2)$	$\alpha_S^2\,\log^4$ $\alpha_S^2\,\log^3$ $\alpha_S^2\,\log^2$ $\alpha_S^2\,\log$
$\vdots$	$\vdots$
$\mathcal{O}(\alpha_S^n)$	$\alpha_S^n\,\log^{2n}$ $\ldots$ $\alpha_S^n\,\log^n$ $\ldots$ $\alpha_S^n\log$

Table 4.1: The logarithmic structure of fixed-order calculations of radiative QCD corrections.

This logarithmic structure arises from the fact that for each emission (each power of α_S), for gluon emission off a quark (which may generate both collinear and soft and collinear singularities) there may be (up to) both soft and collinear logarithms (see equations 2.21 and 4.34), schematically giving two powers of the logarithm for each power of the coupling

$$\alpha_S\,\log_{\rm collinear}\log_{\rm soft} \sim \alpha_S\,\log^2\,. \tag{4.13}$$

This double-logarithmic term gives the dominant logarithmic contribution, followed by contributions which are, for example only collinear, and give subdominant ($\alpha_S \log$) terms.

The size of these soft and collinear, or purely soft, or collinear logarithms is governed by the limits of integration over the phase space of the soft and/or collinearly divergent contributions of the cross section. These are themselves defined by the intrinsic scales of the process (e.g. masses of particles involved and transverse momenta of external massless legs) as well as the experimental cuts placed on the phase space, or the kinematically available limits of the phase space and the respective limits on the angular and energy integrals these imply.

In regions with widely separated scales, where kinematic configurations of a scale far from the experimental cuts or intrinsic mass scales of the process are considered these logarithmic contributions become large such that they nullify the relative smallness of the gauge coupling which accompanies them, $\alpha_S^n \log^{2n}(\text{scale1}/\text{scale2}) \sim 1$, and the perturbative series under consideration becomes ill-defined. An explicit example of the origin, arguments and potential size of logarithmic contributions is constructed in section 4.2.

For future reference note that the transverse momentum variable defined as[3]

$$p_T^2 = \frac{t\,u}{s}\,, \tag{4.14}$$

captures both the soft and collinear limits in a single variable such that in the double leading-logarithmic approximation (see section 4.5 for definitions of logarithmic accuracy) the cross section has the form

$$\frac{1}{\sigma}\,\frac{d\sigma}{dp_T^2} \propto \alpha_S\,C_F\,\frac{\log\frac{Q^2}{p_T^2}}{p_T^2}\,. \tag{4.15}$$

4.4 Single Emission

Consider a single emission of a (potentially soft) gluon off a quark in the collinear approximation from equation 2.21, as shown in figure 4.2.

The dimensionful aspect of this splitting can be parametrised in terms of at least three possible variables with the required behaviour in the collinear limit, $t \to 0$. These are the virtuality of the parent parton at the splitting, Q^2, the relative transverse momentum of the daughter partons with respect to the parent, p_T, or the angular separation, θ, of the daughter partons.

Using the configuration shown in figure 4.2 the functional form of the possible ordering variables can be derived. From $\sin\theta_1 = \frac{p_T}{z\,E}$ and $\sin\theta_2 = \frac{p_T}{(1-z)\,E}$ and using the small-angle approximation $\sin\theta \approx \theta$ we can

[3] This is the transverse momentum generated by the $2 \to 2$ Born level hard scattering, the final state will also include transverse momentum contributions from the multiple emissions generated by the parton shower, for which the transverse momentum is computed for the $1 \to 2$ splittings in the small angle limit, as defined in equation 4.16.

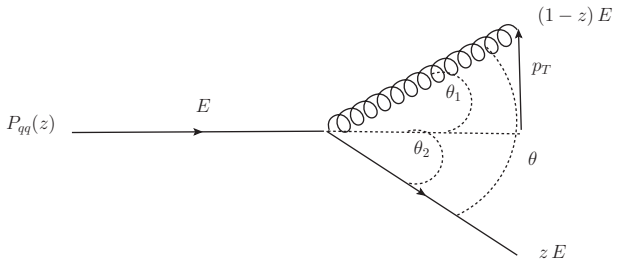

Figure 4.2: Collinear splitting of a gluon off a hard quark.

write $\theta_1 \approx \frac{p_T}{z\,E}$ and $\theta_2 \approx \frac{p_T}{(1-z)\,E}$. Combining these using $\theta = \theta_1 + \theta_2$, rearranging for p_T and squaring we find

$$t = p_T^2 \approx z^2\,(1-z)^2\,E^2\,\theta^2\,. \tag{4.16}$$

This is one possible choice of dimensionful variable to describe the energy dependence of the splitting.

Considering the virtuality of the splitting we have

$$\begin{aligned} t = Q^2 &= 2\,k_1 \cdot k_2 = 2\,z\,(1-z)\,E^2\,(1-\cos\theta) \\ &\approx E^2\,\theta^2\,z\,(1-z)\,, \end{aligned} \tag{4.17}$$

which constitutes another possible choice of dimensionful variable.

Lastly we can directly use the properly energy-scaled angle of the splitting as the variable of choice

$$t = E^2\,\theta^2\,. \tag{4.18}$$

4.5 Coherence and Angular Ordering

A priori all three of these variables seem equally well suited as an ordering variable with which to generate emissions. As we now explain it is in fact this last choice of angular variable which is physically preferable to correctly describe coherence in soft, wide-angle radiation.

Consider the emission of a soft gluon with momentum k off an external leg consisting of a hard (anti)quark with momentum p

$$\mathcal{M}_{n+1} = g_S\,t^a\,\epsilon^*_\mu(k)\,\bar{u}(p)\gamma^\mu\,\frac{\not{p}+\not{k}+m}{(p+k)^2-m^2}\mathcal{M}_n \underset{k\to 0}{\approx} g_S\,t^a\,\epsilon^*_\mu(k)\,\frac{p^\mu}{p\cdot k}\,\bar{u}(p)\,\mathcal{M}_n\,, \tag{4.19}$$

where we have used the relations $\{\gamma^\mu,\gamma^\nu\} = 2\,g^{\mu\nu}$ and $\bar{u}(p)(\not{p}-m) = 0$, and taking the $k \to 0$ approximation in the numerator is known as the *eikonal approximation*.

Summing over all the external coloured legs which could radiate gives the *eikonal current* as

$$J^{\mu\,a}(k) = \sum_j t_j^a \frac{p_j^\mu}{p_j \cdot k}\,, \tag{4.20}$$

(where we have omitted the matrix indices on the colour operator t_j^a acting on parton j) so that at the amplitude squared level in the soft limit the factorisation takes the form[4]

$$\begin{aligned} |\mathcal{M}_{n+1}|^2 &\underset{k\to 0}{\approx} -g_S^2\, J^{\mu\,a}(k)\, g_{\mu\nu}\, J^{\nu\,a}(k)\, |\mathcal{M}_n|^2 \\ &= -g_S^2\, J^2(k)\, |\mathcal{M}_n|^2\,, \end{aligned} \tag{4.21}$$

where we have performed the sum over the gluon polarisations, $\sum_{\lambda,\lambda'} \epsilon^{*\mu}_{\lambda'}\, \epsilon^\nu_\lambda \to -g^{\mu\nu}$, and we have defined

$$J^2(k) = \sum_{i,j} \frac{p_i \cdot p_j}{(p_i \cdot k)(p_j \cdot k)}\, t_i^a t_j^a\,. \tag{4.22}$$

Writing the contracted momenta as

$$p_i \cdot p_j = E_i\, E_j\, (1 - \cos\theta_{ij})\,, \tag{4.23a}$$

$$p_i \cdot k = E_i\, \omega\, (1 - \cos\theta_{ik})\,, \tag{4.23b}$$

$$p_j \cdot k = E_j\, \omega\, (1 - \cos\theta_{jk})\,, \tag{4.23c}$$

(in the splitting parton's rest frame) and using the fact that the sum over all colour generators must equal zero as the matrix element is a colour singlet overall, $\sum_i t_i^a = 0$, to rewrite the sum over all generators instead as a sum over half the generators times two, we can rewrite the eikonal factor squared as

$$J^2(k) = -\frac{2}{\omega^2} \sum_{i<j} t_i^a\, t_j^a\, \frac{(1 - \cos\theta_{ij})}{(1 - \cos\theta_{ik})(1 - \cos\theta_{jk})}\,, \tag{4.24}$$

where we can see from the crossterm between the angles of emission for ik and jk that interference between the emissions is accounted for. Note that this expression also displays the correct collinear singularity structure when partons i, k or j, k become collinear.

This eikonal squared (neglecting for now the sum over colour generators) can be rewritten in terms of two *antenna functions* as

$$\begin{aligned} J_{ij}^2(k) &= -\frac{1}{2\omega^2} \left(\left[\frac{(1 - \cos\theta_{ij})}{(1 - \cos\theta_{ik})(1 - \cos\theta_{jk})} + \frac{1}{1 - \cos\theta_{ik}} - \frac{1}{1 - \cos\theta_{jk}} \right] + (i \leftrightarrow j) \right) \\ &= -\frac{1}{\omega^2} \left(W_{ij}^{[i]} + W_{ij}^{[j]} \right) \end{aligned} \tag{4.25}$$

Each one of these antenna functions can integrated over the azimuthal angle between the gluon and each

[4] We are working with the case of soft gluon emission off a quark, but exactly the same result can be shown for soft gluon emission from a gluon, and the 4 gluon vertex can be shown to be finite in the soft limit and hence subdominant [190].

corresponding antenna function to give (see [189] for proof)

$$\int_0^{2\pi} d\phi_{ik}\, W_{ij}^{[i]} = \begin{cases} \frac{\pi}{1-\cos\theta_{ik}} & \text{if} \quad \theta_{ik} < \theta_{ij} \\ 0 & \text{otherwise} \end{cases}, \tag{4.26}$$

and similarly for $W_{ij}^{[j]}$ with the replacement $i \leftrightarrow j$.

The significance of this result is that soft emission from a hard parton (in the eikonal approximation) is limited to lie within a cone whose half-angle reaches the nearest colour-connected parton. Physically this is a consequence of coherence, whereby interference in soft, wide-angle emissions is destructive and such radiation is therefore suppressed.

This suggests that a natural ordering variable when generating emissions is the angular separation between partons, with wide angle resolvable emissions being generated before smaller ones. This *angular ordering* should hence correctly describe the effect of colour coherence and the suppression of soft, wide-angle emissions known as the *Chudakov effect* (which has been experimentally observed in lepton-lepton collisions at PETRA and LEP, and most recently at the LHC [191]).

Returning to equation 4.24 we can consider emission from only one parton (say i) and further take the collinear limit of this expression to reveal the soft and collinear singularity structure produced by emission of a single gluon off a quark at the amplitude squared level

$$\begin{aligned} J_i^2(k) &\underset{\theta_{ik}\to 0}{=} -\frac{1}{\omega^2}\left[\underbrace{\frac{2\,t_i^a}{1-\cos\theta_{ik}}}_{\approx \frac{4\,t_i^a}{\theta_{ik}^2}} \underbrace{\sum_{j\neq i} t_j^a}_{=-t_i^a} \underbrace{\frac{1-\cos\theta_{ij}}{1-\cos\theta_{jk}}}_{\approx 1} + (\text{terms finite for } \theta_{ik}\to 0)\right], \\ &\approx \frac{1}{\omega^2}\,\frac{4\,C_R^{(i)}}{\theta_{ik}^2}\,, \end{aligned} \tag{4.27}$$

where we have used the relations

$$1-\cos\theta \equiv 2\,\sin^2\frac{\theta}{2} \approx \frac{\theta^2}{2}\,, \tag{4.28}$$

$$\sum_{j\neq i} t_j^a = -t_i^a \;\; (\text{from} \sum t_j^a = 0)\,, \tag{4.29}$$

$$(t_i^a)^2 = C_R^{(i)} = \begin{cases} C_F = \frac{4}{3} & \text{for } i = q, \bar{q}\,, \\ C_A = 3 & \text{for } i = g\,, \end{cases} \tag{4.30}$$

$$\theta_{ik} \approx 0 \Leftrightarrow \theta_{ij} \approx \theta_{jk}\,. \tag{4.31}$$

Note that in this soft and collinear limit all signs of cross terms (interference) have vanished and we have

independent emission with no coherence. The significance of this is that the effect of coherence in soft, wide-angle emission can be correctly approximated by incoherent emissions, provided these are angular ordered.

To obtain the eikonal cross section we must take the soft limit of the emission phase space as well. This can be written as

$$\begin{aligned}\frac{d^3\vec{k}}{(2\pi)^3\,2\omega} &= \frac{|\vec{k}|^2\,dk\,d\Omega}{(2\pi)^3\,2\omega} \\ &= \frac{\omega^2\,d\omega\,\sin\theta\,d\theta\,d\phi}{(2\pi)^3\,2\omega}\,.\end{aligned} \tag{4.32}$$

Integrating over the azimuthal variable which does not affect neither the soft nor collinear behaviour and taking the small angle approximation in the polar angle to focus on the collinear region, $\sin\theta\,d\theta = d\,\cos\theta \approx d\theta^2/2$ (by equation 4.28) we obtain the emission phase space in the soft and collinear approximation

$$\frac{d^3\vec{k}}{(2\pi)^3\,2\omega} = \frac{\omega\,d\omega\,d\theta^2}{4\,(2\pi)^2}\,. \tag{4.33}$$

Inserting equation 4.27 into equation 4.21 and multiplying by the soft and collinear phase space derived above in equation 4.32 we obtain the cross-section factor for a single emission in the soft and collinear approximation as

$$d\sigma_1 \approx \frac{\alpha_S}{\pi}\,C_R^{(i)}\,\frac{d\omega}{\omega}\,\frac{d\theta^2}{\theta^2}\,\Theta(\theta_{\max}-\theta) \tag{4.34}$$

where we have imposed angular ordering by hand by inserting the Heaviside step function.

Comparing this to collinear factorisation in equation 2.21, the singularity structure coincides provided we use $t \propto \theta^2\,E^2$ (with the factor of energy there for dimensional consistency), and the soft limit is contained in the splitting functions, with the only structural difference being the newly introduced angular ordering.

In fact the collinear factorisation formula corresponds to the the substitution $\frac{\alpha_S}{\pi}\,\frac{d\omega}{\omega} \to \frac{\alpha_S}{\pi}\,\hat{P}_{ij}(z)\,dz$ in equation 4.34, with $\hat{P}_{ij}(z)$ being the unregularised, one loop splitting version of the splitting functions shown in figure 4.1[5].

However, given that the collinear factorisation in equation 2.21 contains the exact form of the soft singularities for each possible type of splitting and not just for soft gluon emission from a quark, it is this form of the factorisation we will use and which indeed forms the basis of the parton shower.

4.5.1 Choice of Ordering Variable and Type of Logarithm Resummed

Now including the splitting functions and therefore the soft singularity structure, if we choose virtuality as our ordering parameter, $t = E^2\,\theta^2\,z\,(1-z)$, we can set $\theta^2 = 1$ (as we expect $\theta^2 < 1$), solve this for z, and expand

[5]This structure encapsulates the Leading Logarithmic (LL) contribution.

about $t = 0$ to $\mathcal{O}(\sqrt{t})$ to find the thresholds which define the limits of the integration over z to get, for a single splitting $q \to qg$ proportional to $P_{qq}(z)$

$$\begin{aligned}\text{virtuality}: \ \alpha_S \int \frac{dt}{t} \int_{t/E^2}^{1-t/E^2} \frac{dz}{1-z} &= \int \frac{dt}{t} \left[-\log(1-z)\right]_{t/E^2}^{1-t/E^2} \,, \\ &= \int \frac{dt}{t} \left[-\log(t/E^2) + \log(1-t/E^2)\right] \,, \\ &= -\frac{1}{2}\log^2 \frac{t}{E^2} - \mathrm{Li}_2 \frac{t}{E^2} \,, \end{aligned} \tag{4.35}$$

where $\mathrm{Li}_2(x) := -\int_0^x \frac{\log(1-t)}{t}$ is the order 2 polylogarithm (also known as the dilogarithm function).

The analogous procedure for p_T as the ordering variable, $t = E^2\,\theta^2\,z^2\,(1-z)^2$, gives

$$\begin{aligned} p_T: \ \ \alpha_S \int \frac{dt}{t} \int_{\sqrt{t}/E}^{1-\sqrt{t}/E} \frac{dz}{1-z} &= \int \frac{dt}{t} \left[-\log(\sqrt{t}/E) - \log(1-\sqrt{t}/E)\right] \,, \\ &= -\log^2 \frac{\sqrt{t}}{E} + 2\,\mathrm{Li}_2 \frac{\sqrt{t}}{E} \,. \end{aligned} \tag{4.36}$$

Numerically we find that for both choices above, for values of the argument t/E^2, $\sqrt{t}/E \lesssim 0.4$ (respectively) the log squared dominates over the dilogarithm, and is hence the dominant logarithmic contribution.

Lastly, considering the purely angular ordering variable, $t = E^2\,\theta^2$, the integral over z is unconstrained and must be regulated with an IR cutoff, λ, giving

$$\text{angular}: \ \alpha_S \int \frac{dt}{t} \int_0^{1-\lambda/E} \frac{dz}{1-z} = -\log\frac{\lambda}{E}\,\log\frac{t_{\max}}{t_{\min}} \,. \tag{4.37}$$

The exact form of the logarithms produced from emission in the collinear approximation therefore depends on the choice of ordering variable, though at the leading logarithmic level, they all produce the correct soft and collinear $\alpha_S\,\log^2$ structure and are therefore equivalent (see section 2 of [192] for an overview of the above discussion on choice of ordering variable).

However, as we have seen, in order to correctly generate the suppression of soft, wide-angle emissions due to coherence the choice of ordering variable should be the angular one. It is this choice that is implemented in HERWIG++ and which we use here[6].

The evolution variable used for final-state radiation in HERWIG++ is [17]

$$t_{\mathrm{FS}} = \frac{q_{\widetilde{ij}}^2 - m_{\widetilde{ij}}^2}{z\,(1-z)} \,. \tag{4.38}$$

[6]Other Monte Carlo event generators (such as PYTHIA and SHERPA) use virtuality or p_T ordered showers, with a veto on soft emissions at angles larger than previous emissions. This treatment is equivalent to angular ordering.

Neglecting the parent parton's rest mass, $m_{\widetilde{ij}}$, and taking the collinear limit we see that

$$t_{\mathrm{FS}} \approx \frac{q^2_{\widetilde{ij}}}{z\,(1-z)} \;=\; \frac{2\,p_i\cdot p_j}{z\,(1-z)} \;=\; 2\,\frac{E_i\,E_j}{z\,(1-z)}\,(1-\cos\theta_{\widetilde{ij}}) \;=\; 2\,\frac{z\,E_{\widetilde{ij}}\,(1-z)\,E_{\widetilde{ij}}}{z\,(1-z)}\,\sin^2\frac{\theta_{\widetilde{ij}}}{2}$$
$$\underset{\theta_{\widetilde{ij}}\to 0}{\longrightarrow} E^2_{\widetilde{ij}}\,\theta^2_{\widetilde{ij}}\,, \tag{4.39}$$

so that the evolution variable has the angular dependence expected for the angular ordering as required. The variable $m_{\widetilde{ij}}$ is the rest mass of the parent parton and is introduced to account for the so-called *dead cone* in the radiation pattern caused by the non-zero mass of the emitting parton.

Similarly the evolution variable for radiation from initial state (spacelike) partons is

$$t_{\mathrm{IS}} = \frac{m_i^2 - q_i^2}{1-z}\,. \tag{4.40}$$

Here the i index labels the spacelike parton which evolves towards the hard scattering.

4.6 Multiple Emissions

Fixed order calculations in perturbative QCD (pQCD) such as the one presented in the previous chapter are reliable only when all the scales in the process are of the same order. The introduction of new scales (masses, or hard emissions each with their own characteristic p_T) or vetoes (and the corresponding threshold for the veto) will result in the suppression of phase space for real emission.

However, since the virtual contribution cannot be in any way suppressed –although the exact cancellation between real and virtual contributions to the event in the exact soft limit still holds– in regions of the phase space the real and virtual contributions will be highly unbalanced thereby also generating its tell-tale logarithms of ratios of the scales involved, as the integrals over singular (collinear and/or soft) contributions from the real emission contribution acquire widely separated limits and become sizeable.

These logarithms are hence an issue in observables exclusive in hadrons, i.e. with tagged (identified) hadrons, where the integrals over these detected states is bound to be restricted by experimental requirements.

If we consider multiple collinear emissions of the form of equation 2.21 and shown in figure 4.3 the integration over the emissions will be a set of nested integrals of the form (considering only the collinear contribution and not the soft singularity structure from the splitting functions, and neglecting the functional dependence of the coupling for now)

$$\alpha_S^n \int \frac{dt_n}{t_n} \int \frac{dt_{n-1}}{t_{n-1}} \;\cdots \int \frac{dt_1}{t_1} \tag{4.41}$$

It now remains to fix the integration limits for each emission. For this we should impose the requirement

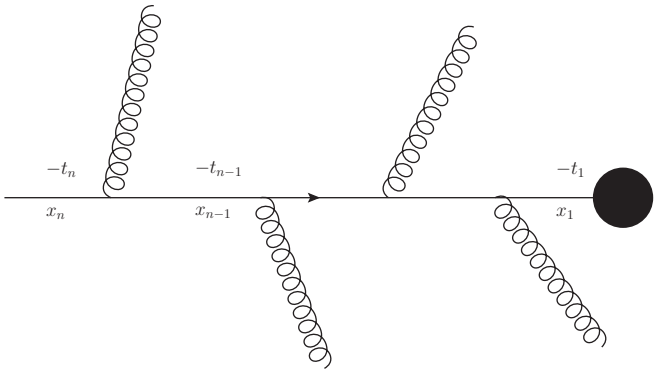

Figure 4.3: Parton shower evolution as a function of the ordering variable and momentum fractions.

that the phase space in the angular (collinear) variable, t, of each emission is bounded from above by the scale of the next emission, for two distinct reasons:

- This gives the dominant logarithmic contribution. In terms of the logarithms involved, this will produce double-logarithmic terms of the form $\alpha_S \log^2$ which are the leading contribution.
- Physically, limiting each emission by the scale of the next one allows us to neglect the emitter's virtuality at each step of the shower for simplicity.

Concretely, considering the case of only two emissions we have

$$t_1 > t_2 : \ \alpha_S^2 \int_\lambda^{Q^2} \frac{dt_1}{t_1} \int_\lambda^{t_1} \frac{dt_2}{t_2} = \alpha_S^2 \frac{1}{2} \log^2 \frac{Q^2}{\lambda} , \tag{4.42}$$

$$t_1 < t_2 : \ \alpha_S^2 \int_\lambda^{q} \frac{dt_1}{t_1} \int_\lambda^{Q^2} \frac{dt_2}{t_2} = \alpha_S^2 \log \frac{Q^2}{\lambda} \log \frac{q}{\lambda} , \tag{4.43}$$

where λ has been introduced as an IR cutoff and q is some scale lower than the hard interaction scale, $|q| < |Q^2|$.

The latter ordering can be seen to be subdominant to the former unless $q \sim Q^2$, in which case it matches it. Hence to obtain the dominant contributions we will choose the ordering $t_1 > t_2$, or more generally for multiple emissions, $Q^2 > t_1 > t_2 > \ \ldots \ > t_n > \lambda$. This requirement is known as *strong ordering* and is chosen to encapsulate the dominant contributions in the collinear limit[7].

It must be emphasized that strong ordering is chosen to give the dominant logarithmic contributions, and that some form of ordering is necessary as the phase space available for emission is bounded by the total invariant mass of the original hard emitter, and is further reduced by each emission.

[7] This is consistent with our choice of angular ordering from wide angles to smaller ones, as $t \propto \theta^2$, so that $\theta_1 > \theta_2 \iff t_1 > t_2$.

It is worth noting that the precise form of the logarithms involved (namely their argument) will depend on the functional form of the variable, t, which itself is the ordering variable of the emissions. Therefore the choice of ordering variable defines the precise form of the logarithms generated by the emissions (and resummed by the shower). The leading logarithmic contribution from all of them is however equivalent. We discuss these issues in section 4.5.1.

In order to obtain a fully exclusive observable we must allow for arbitrarily many emissions to occur, and they must be properly accounted for (resummed) to provide a finite, well-defined observable with unresolved emissions being integrated over. An overview of how these all-order real emission and virtual contributions and the towers of logarithms they entail are dealt with is given in section 5.1.

The resummation of soft and collinear gluons as described in section 5.1 clearly has a particularly strong impact on transverse momentum distributions, particularly in the $p_T^2 \ll Q^2$ region. It can generally affect the shape of many observables (even far from the partonic $p_T^2 \ll s$ limit, through the convolution with the PDFs) and will provide a greatly reduced scale dependence for most observables.

Also note that the terms in brackets in equation 5.2 that are due to multiple emissions must integrate to unity when the integral over the full phase space is performed to guarantee that the total cross section is still given by the fixed order result as expected. Physically this is a consequence of the separation of scales between the fixed order process, which occurs at a scale of order Q^2 and describes the probability of the hard scattering, and the soft and collinear emissions which are constrained to occur at smaller scales and should not affect the total normalisation of the observable (provided it is appropriately constructed to be infrared safe, see equation 3.96). In the context of parton showers which we will develop later this is known as *shower unitarity*.

The previously mentioned exponentiation of radiative corrections in the soft and collinear limit can be obtained by exponentiating the first order correction in the same limit (equation 2.21), producing the so-called *Sudakov form factor*[8]

$$\Delta_i(t, t_0) = \exp\left(-\sum_j \int_{t_0}^{t} \frac{dt'}{t'} \int \frac{\alpha_S(p_T^2)}{2\pi} \hat{P}_{ij}(z)\, dz\right), \tag{4.44}$$

where $\hat{P}_{ij}(z)$ are the *unregularised* splitting functions (the splitting functions from figure 4.1 without the plus prescription) and from now on we will omit the subindex j on the left-hand side which denotes the parton type ($j = q, \bar{q}, g$) to which the form factor applies. The functional form of the Sudakov form factor can be motivated in several ways, which we discuss in section 4.7.

[8] See [193] for a recent review and derivation of this *Sudakov resummation*.

4.7 Motivation and Properties of the Sudakov Form Factor

If we consider the generation of emissions as a Markovian process consisting of independent emissions the expected probability distribution of emissions is that of a Poisson distribution. If the probability of observing p events (emissions) when n is the expected rate of events (the probability density for emission contained in the argument of the Sudakov) is given by $\frac{n^p}{p!}\mathrm{e}^{-n}$, then if we consider the probability of observing no emissions at all ($p = 0$), we recover the Sudakov form factor as expected. The exponential functional form of the Sudakov can also be divined from equation 4.8.

Note that this function obeys the relations

$$\Delta(t,t) = 1\,, \tag{4.45a}$$

$$\Delta(t_1,t_2) = \frac{\Delta(t_1,t_0)}{\Delta(t_2,t_0)}\,, \tag{4.45b}$$

$$\Delta(t_1,t_2) \leq 1\,. \tag{4.45c}$$

This form factor can be shown (using a generating functional method, see [190]) to be the probability of no resolvable emission being produced by a parton evolving from a scale t_0 to a scale t. As such it contains the unresolved real emission contribution (as well as the virtual contributions, if the regularised form of the splitting function is considered[9]), suitably resummed to all orders.

Note that the Sudakov is always less than or equal to unity, thus the interpretation of the Sudakov as a no-emission probability allows for two features: simulation of emission (or lack thereof) becomes amenable to simulation via generation of (pseudo)random numbers via a hit-or-miss algorithm, and by unitarity emissions can therefore be simulated with the probability $1 - \Delta(t,t')$.

These features are together used to generate fully exclusive events with multiple parton emission beyond that which can be currently obtained via direct computation of fixed order amplitudes[10]. The Sudakov form factor defined in equation 4.44 constitutes the building block of the resummation of soft and collinear logarithms as performed by the parton shower[11].

[9] The unregularised splitting functions with a cutoff for resolvable emission are used in the Sudakov form factors for parton showers.

[10] Such emissions are generated from the soft and collinear kernel in equation 2.21, so they are generated in the collinear approximation, though in general they need not be collinear. This is an approximate method of generating emissions beyond those which we can compute from fixed order matrix elements.

[11] Other forms of logarithms appear in radiative corrections to coloured processes (small-x logarithms, non-global logarithms, etc). These require different treatments to be resummed (BFKL resummation, dipole shower accurate in the hard non-collinear limit, etc) which are not dealt with in the standard parton shower formalism which we use here.

4.8 The Parton Shower

Starting from the DGLAP equation (equation 4.5 for a single parton type, for simplicity) and rewriting it in terms of the unregularised splitting functions by writing out the action of the plus distribution explicitly and using the substitution $y = \frac{x}{z}$ we get

$$\begin{aligned} t\,\frac{\partial f_i(x,t)}{\partial t} &= \int_x^1 \frac{dz}{z}\frac{\alpha_S}{2\pi}\,P_{ij}(z)\,f_j\left(\frac{x}{z},t\right)\,, \\ t\,\frac{\partial f_i(x,t)}{\partial t} &= \int_0^1 dz\,\frac{\alpha_S}{2\pi}\,\hat{P}_{ij}(z)\left[\frac{1}{z}\,f_j\left(\frac{x}{z},t\right) - f_j(x,t)\right]\,. \end{aligned} \tag{4.46}$$

Rewriting the second term on the right hand side in terms of the Sudakov from equation 4.44 using $\frac{\partial\Delta(t,t_0)}{\partial t} = -\left(\frac{\alpha_S}{2\pi}\frac{1}{t}\int dz\hat{P}_{ij}(z)\right)\Delta(t,t_0)$ we get

$$t\,\frac{\partial f_i(x,t)}{\partial t} = \int_0^1 \frac{dz}{z}\,\frac{\alpha_S}{2\pi}\,\hat{P}_{ij}(z)\,f_j\left(\frac{x}{z},t\right) + t\,\frac{1}{\Delta}\,\frac{\partial\Delta}{\partial t}\,f_j(x,t)\,. \tag{4.47}$$

Moving the second term to the left hand side and using $\frac{\partial}{\partial t}\left(\frac{f}{\Delta}\right) = \frac{1}{\Delta}\frac{\partial f}{\partial t} - f\,\frac{1}{\Delta^2}\frac{\partial\Delta}{\partial t}$ gives

$$\begin{aligned} t\,\frac{\partial f_i(x,t)}{\partial t} - t\,\frac{1}{\Delta}\,\frac{\partial\Delta}{\partial t}\,f_j(x,t) &= \int_0^1 \frac{dz}{z}\,\frac{\alpha_S}{2\pi}\,\hat{P}_{ij}(z)\,f_j\left(\frac{x}{z},t\right) \\ t'\,\Delta(t')\,\frac{\partial}{\partial t}\left(\frac{f}{\Delta}\right) &= \int_0^1 \frac{dz}{z}\,\frac{\alpha_S}{2\pi}\,\hat{P}_{ij}(z)\,f_j\left(\frac{x}{z},t\right) \end{aligned} \tag{4.48}$$

where we have used the shorthand notation $\Delta(t') := \Delta(t',t_0)$.

Integrating this with the boundary condition $f_i(x,t)|_{\min} = f_i(x,t_0)$ gives

$$\begin{aligned} \frac{f_i(x,t)}{\Delta(t)} &= \int \frac{dt'}{t'}\,\frac{1}{\Delta(t')}\int_0^1 \frac{dz}{z}\,\frac{\alpha_S}{2\pi}\,\hat{P}_{ij}(z)\,f_j\left(\frac{x}{z},t'\right) + c \\ &= \int \frac{dt'}{t'}\,\frac{1}{\Delta(t')}\int_0^1 \frac{dz}{z}\,\frac{\alpha_S}{2\pi}\,\hat{P}_{ij}(z)\,f_j\left(\frac{x}{z},t'\right) + f_i(x,t_0)\,, \end{aligned} \tag{4.49}$$

which finally gives

$$f_i(x,t) = \int \frac{dt'}{t'}\,\frac{\Delta(t)}{\Delta(t')}\int_0^1 \frac{dz}{z}\,\frac{\alpha_S}{2\pi}\,\hat{P}_{ij}(z)\,f_j\left(\frac{x}{z},t'\right) + \Delta(t)\,f_i(x,t_0)\,. \tag{4.50}$$

This equation is known as a *shower equation* and it illustrates how the Sudakov form factor may be used in a way which replicates DGLAP (i.e. collinear) evolution, and has a simple interpretation in terms of branching probabilities: the second term is the probability of no emissions between scales t_0 and t, whereas the first term is the probability of no emission between the scales t and t' (the factor $\frac{\Delta(t)}{\Delta(t')}$), and then a single emission at the scale t'.

Equation 4.50 is therefore the formal underpinning (i.e. the proof that shower algorithms simulate collinear evolution according to the DGLAP equation) of shower algorithms, and also their basic building block.

Additionally, comparisons between analytic resummation, resummation as performed by parton showers (as

implemented in PYTHIA and HERWIG) and data (for the case of Drell-Yan, Higgs production and diphoton production) have been performed and have found all three to be in good agreement, validating their equivalence at the leading-logarithmic level [194, 195].

The previously mentioned Sudakov suppression at low p_T (equation 5.8) is also experimentally observed. In this region the Sudakov form factor smoothly smears and combines the otherwise divergent (and opposite) real and virtual contributions to yield physically meaningful and well-defined differential distributions in the low p_T region.

4.9 The Logarithmic Accuracy of the Parton Shower

The kernel of the Sudakov form factor, whether it is the Altarelli-Parisi splitting functions, or a real emission matrix element (which must reduce to the Altarelli-Parisi splitting functions in the collinear limit by virtue of the collinear factorisation theorem described in section 2.1.1), contains both the soft and collinear singularities of an emission. As such its exponentiation in the Sudakov form factor is guaranteed to resum the (soft and collinear) double logarithms which (as detailed in section 5.1) constitute the full LL contribution. These kernels in fact also contain parts of the NLL contribution, for example in

$$\hat{P}^{\text{excl}}_{q,qg}(z) = C_F \frac{1+z^2}{1-z} = \frac{2C_F}{1-z} - C_F(1+z)\,, \tag{4.51}$$

the second term lacks a soft ($z \to 1$) singularity and is therefore only singly (collinear) logarithmic and of the form $\alpha_S\, L$ (where L indicates a logarithm, as in section 5.1).

However these contributions contain only part of the NLL corrections and this is not sufficient to claim NLL accuracy. Using the notation of equation 5.6 the resummation factor is schematically of the form

$$\exp\left(A\,L^2 \;+\; B\,L \;+\; \mathcal{O}\left(\frac{p_T^2}{Q^2}\right)\right)\,, \tag{4.52}$$

where the coefficients A and B have perturbative expansions, $A = \sum_i \alpha_{S,\,i} A_i$ and $B = \sum_i \alpha_{S,\,i} B_i$.

LL accuracy requires only the coefficient A_1 (i.e. terms $\mathcal{O}(\alpha_S\, L^2)$) to be known and included. NLL accuracy additionally requires both A_2 (which is $\mathcal{O}(\alpha_S^2\, L^2)$) and B_1 (of $\mathcal{O}(\alpha_S\, L)$) to be known and used. As just discussed, the $\mathcal{O}(\alpha_S\, L)$ purely collinear logarithmic terms are included in the parton shower kernels, but since terms $\mathcal{O}(\alpha_S^2\, L^2)$ are not present only LL accuracy can be claimed.

Additionally, the exponentiation of the finite part of the real emission contribution in the POWHEG Sudakov introduces extra spurious logarithmic cross terms. Explicitly writing the power of the coupling and expanding

the difference between the POWHEG Sudakov and the NLL resummation exponential schematically gives

$$\Big(\exp\left[A\,\alpha_S\,L^2\,+\,B\,\alpha_S\,L\,+\,c\,\alpha_S\right]\,-\,\exp\left[A\,\alpha_S\,L^2\,+\,B\,\alpha_S\,L\right]\Big)\Big|_{\mathcal{O}(\alpha_S^2)}\,= \tag{4.53}$$
$$c\,\alpha_S\,+\,\frac{1}{2}\,c^2\,\alpha_S^2\,+\,c\,B\,\alpha_S^2\,L\,+\,c\,A\,\alpha_S^2\,L^2\,,$$

where the $\alpha_S^2\,L^2$ cross term is of NLL and would hence destroy the NLL accuracy, had it been obtained.

Lastly, it must be pointed out that this resummation is observable-dependent. In analytic approaches the resummation is performed for a given variable (observable) in which there are regions of phase space where it is known that resummation is required (e.g. the $T \to 1$ of the thrust in e^+e^-, or the $p_T \to 0$ for the transverse momentum of the lepton pair in Drell-Yan). The resummation is therefore explicitly observable-dependent.

The resummation performed by the parton shower is roughly analogous to the soft-gluon resummation in analytic calculations and the large logarithmic contributions it resums arise only in the regions of certain observables which are sensitive to these soft and/or collinear emissions. The parton shower resummation therefore is, like its analytic counterpart, observable-dependent.

Chapter 5

Matching Next-to-Leading Order Calculations with Parton Showers

In chapter 3 we have reviewed the structure of QCD NLO radiative corrections, and the accurate predictions they can provide for scales $p_T \gg \Lambda_{\rm QCD}$ thanks to the factorisation theorem. And in chapter 4 we have sketched how the enhanced soft and collinear emission regions can be accounted for and treated to all orders.

In summary, the strengths of fixed order calculations such as the one performed in chapter 3 are:

- appropriate description of high p_T regions of observables (up to higher-order radiative corrections, which can be significant);
- a correct description of widely separated jets and jet multiplicities (where the Born contribution contains final-state partons);
- first prediction for the normalisation of observables for which the Born level prediction is already physically meaningful;
- full inclusion of interference effects in the hard scattering;
- inclusion of finite N_C contributions (where N_C is the number of colours).

Fixed-order predictions are however

- unphysical in low p_T regions;

- give generally low multiplicity events given the complexity of computing high-multiplicity matrix elements (particularly at NLO or beyond), this is in contrast with the high jet multiplicity observed in typical hadron-hadron collider events;
- are useful for highly inclusive observables (such as the total cross section), but inadequate for observables requiring fully exclusive, high multiplicity events;
- are susceptible to large logarithmic corrections in low transverse momentum regions.

Likewise the Sudakov resummation outlined in chapter 4 provides

- physically meaningful predictions for low p_T regions of observables;
- accurate predictions for jet substructure;
- proper all-orders description of the dominant perturbative soft, collinear and soft and collinear enhanced emission contributions to the low p_T regions;
- fully exclusive, high multiplicity events;
- scale evolution of partons from the hard interaction scale down to the hadronisation scale.

The Sudakov resummation formalism has the disadvantage of (strictly speaking) only describing the soft and/or collinear limits, failing to correctly describe hard non-collinear emission and generating *dead cones* where it cannot correctly describe emission.

It is therefore desirable to consistently *match* the NLO fixed order description with the all-orders resummation as sketched in the previous chapter to obtain the best possible description, using both of the complementary approaches to provide theoretically sound predictions over the full scale and multiplicity range of a hadron-hadron collider.

This is the focus of the present work, the matching of NLO fixed order amplitudes for BSM processes to a parton shower algorithm to produce predictions for differential distributions accurately at up to NLO and LL level, for sufficiently inclusive observables.

5.1 Generalities of Resummation and Matching

To all orders the logarithmic structure of QCD (and incidentally also QED as the argument is kinematical and follows through exactly in the same way substituting colour generators with electric charges) is therefore

an extension of figure 4.1 from the leading log contribution down to non-logarithmic contributions, for each power of α_S, for all powers of α_S, as in equation 5.1 for the partonic cross section

$$\begin{aligned}\sigma_{\text{res}} &= \sigma_{\text{LO}} \left[1 + \sum_{n=1}^{\infty} \sum_{m=0}^{2n} c_{nm}\, \alpha_S^n\, L^m\right] + D\,, \\ &= \sigma_{\text{LO}} \left[1 + \alpha_S \left(c_{12}\, L^2 + c_{11}\, L + c_{10}\right) + \right. \\ &+ \left. \alpha_S^2 \left(c_{24}\, L^4 + c_{23} L^3 + c_{22} L^2 + c_{21} L + c_{20}\right) + \ldots\right] + D\,, \end{aligned} \tag{5.1}$$

where L denotes a soft or collinear logarithm (and L^2 denotes both) and D is a finite function in the soft and collinear limit, so we will not be concerned with it here and drop it from hereon.

More generally, the fixed-order partonic cross section (at leading order denoted σ_{LO} in the above equation) is itself a perturbative expansion (but in α_S instead of $\alpha_S\, L$) by equation 3.1, so the full expansion is of the form

$$\begin{aligned}\sigma_{\text{res}} &= \sum_n \alpha_S^n\, \sigma^{(n)} \left[1 + \sum_{n=1}^{\infty} \sum_{m=0}^{2n} c_{nm}\, \alpha_S^n\, L^m\right], \\ &= \left(\sigma_{\text{LO}} + \sigma_{\text{NLO}} + \ldots\right) \times \left[1 + \alpha_S \left(c_{12}\, L^2 + c_{11}\, L + c_{10}\right) + \right. \\ &+ \left. \alpha_S^2 \left(c_{24}\, L^4 + c_{23} L^3 + c_{22} L^2 + c_{21} L + c_{20}\right) + \ldots\right]. \end{aligned} \tag{5.2}$$

Starting from equation 5.2 we may schematically rearrange the logarithmic terms such that the leading logarithmic structure can be seen to be correctly reproduced from a Maclaurin expansion of an exponential

$$\exp(\alpha_S\, c_{12}\, L^2) \underset{\alpha_S \approx 0}{\approx} 1 + \alpha_S\, c_{12}\, L^2 + \frac{1}{2}\alpha_S^2\, c_{12}^2\, L^4 + \frac{1}{6}\alpha_S^3\, c_{12}^3\, L^6 + \ldots \tag{5.3}$$

Similarly the next-to-leading logarithmic structure can be written as

$$\exp(\alpha_S\, c_{11}\, L) \underset{\alpha_S \approx 0}{\approx} 1 + \alpha_S\, c_{11}\, L + \frac{1}{2}\alpha_S^2\, c_{11}^2\, L^2 + \frac{1}{6}\alpha_S^3\, c_{11}^3\, L^3 + \ldots \tag{5.4}$$

So that the NLL-accurate expression is given by

$$\begin{aligned}\exp(\alpha_S\, c_{12}\, L^2 + \alpha_S\, c_{11}\, L) \underset{\alpha_S \approx 0}{\approx} & 1 + \alpha_S \left(c_{12} L^2 + c_{11} L\right) + \alpha_S^2 \left(\frac{1}{2} c_{12}^2 L^4 + c_{11} c_{12} L^3 + \frac{1}{2} c_{11}^2 L^2\right) \\ & + \alpha_S^3 \left(\frac{1}{6} c_{12}^3 L^6 + \frac{1}{2} c_{11} c_{12}^2 L^5 + \frac{1}{2} c_{11}^2 c_{12} L^4 + \frac{1}{6} c_{11}^3 L^3\right) + \ldots \end{aligned} \tag{5.5}$$

Using this on equation 5.2 we find that the combination of a fixed order and an NLL resummed result has the form

$$\begin{aligned}\sigma_{\text{FO+NLL}} &= \sigma_{\text{FO}} \times \exp(\alpha_S\, c_{12}\, L^2 + \alpha_S\, c_{11}\, L)\,, \\ &= \sigma_{\text{FO}} \times \exp(L\, g_1(\alpha_S L) + g_2(\alpha_S L))\,, \end{aligned} \tag{5.6}$$

where g_1 and g_2 are functions that have a well defined perturbative expansion, and which contain the LL and NLL contributions, respectively[1].

Equation 5.6 holds schematically (see [193] for a more accurate and detailed description), but if the fixed-order partonic cross section already contains one or more QCD emissions the above relation will contain a double counting of some emissions and their corresponding logarithms (cf. table 4.1) which will be present in both the fixed order and the all-orders expressions, and an adequate *matching* procedure is called for.

In analytic treatments this is accomplished by expanding the resummed result to the same order as the fixed order one and removing it from the full resummed result before combining it with the fixed order result

$$\sigma_{\mathrm{FO+res}} = \sigma_{\mathrm{FO}}^{(n)} + \sigma_{\mathrm{res}} - \sigma_{\mathrm{res}}^{(n)} \,. \tag{5.7}$$

In the context of parton showers this separation is performed by carefully restricting the hardest emission(s) to be produced using the fixed order result, and allowing all others to be generated by the shower algorithm (with a veto to avoid the overlap), as we discuss in chapter 5.

In the above all orders expansion the infinite tower of terms of the form $\alpha_S^n \, L^{2n}$ are known as the Leading Logarithms (LL), those of the form $\alpha_S^n \, L^{2n-1}$ are the Next-to-Leading Logarithms (NLL) and so on. If only the single term with the highest logarithmic power at a given order of α_S is considered this is known as the Double Leading Logarithmic (DLL) approximation.

In fact the dominant terms of the above logarithmic structure (LL, NLL, and even NNLL for some processes) can be summed up to all orders provided they are amenable to *exponentiation*. This is a property that has been proven for DIS and Drell-Yan [197–199] and for Drell-Yan the resummation of leading logarithms was shown to give

$$\begin{aligned} \frac{d\sigma}{dp_T^2} &= \sigma \, \frac{d}{dp_T^2} \exp\left\{ -\frac{\alpha_S}{2\pi} \, C_F \, \log^2 \frac{Q^2}{p_T^2} + \mathcal{O}\left(\alpha_S \, \log \frac{Q^2}{p_T^2} \right) \right\} \\ &\underset{\mathrm{LL}}{=} \frac{\alpha_S}{\pi} \, \sigma \, C_F \, \frac{\log \frac{Q^2}{p_T^2}}{p_T^2} \, \exp\left\{ -\frac{\alpha_S}{2\pi} \, C_F \, \log^2 \frac{Q^2}{p_T^2} \right\} , \end{aligned} \tag{5.8}$$

where we see that compared to the single emission (i.e. DLL accurate) logarithmic structure from equation 4.15, the all-orders emissions have exponentiated (or equivalently, the LL all-orders result is given by exponentiating the first order correction). This is the basis for the construction of the Sudakov form factor (and the Sudakov resummation it corresponds to) discussed in sections 4.6 and 4.7.

Note that in contrast to the singularity structure of the fixed-order NLO calculation which yields equal and

[1] We have presented a very naïve and schematic treatment of the counting of logarithms here, see [196] for a more complete treatment.

opposite divergences in the $p_T = 0$ ($\delta(1-z)$ kinematics) limit, here

$$\lim_{p_T \to 0} \frac{d\sigma}{dp_T^2} = 0\,, \tag{5.9}$$

which is finite.

However this *Sudakov suppression* is in fact too strong and the relevant measured distributions do not go to zero at small transverse momentum. This is due to a lack of full momentum conservation in the resummation performed: the only way for a $p_T = 0$ configuration to arise is for no emission to take place whatsoever, and the probability of this for any finite evolution in energy is vanishingly small given the exponential form of the probability for no emission which we discuss in sections 4.6 and 4.7. The possibility of generating this configuration by balancing recoil from multiple emissions is not taken into account. This can be remedied but we will not discuss the effect of these non-logarithmic momentum-reshuffling contributions.

The same exponentiation is known to hold for Drell-Yan at the NLL level for both the total cross section, and the double differential cross section $\frac{d\sigma}{dx_1\,dx_2}$ in the semi-inclusive $x_1,\, x_2 \to 0$ limit [200][2], and is largely assumed to hold for any differential distribution for Drell-Yan and for all other commonly studied perturbatively calculable collider processes.

5.2 Leading Order + Leading Logarithmic Matching

Monte Carlo event generators have long consistently included both fixed-order and all-orders parton shower resummation. This matching consisted of generating a strictly leading-order matrix element, generating events weighted according to it, and evolving any partons via the parton shower algorithm to perform the Sudakov resummation and generate fully exclusive, high-multiplicity events.

Such an algorithm starts from the following relation for a fully differential cross section for the hardest emission

$$d\sigma = B\,\left[\Delta(t_I, t_0)\;+\;\Delta(t, t_0)\,\mathcal{K}(t, z)\,dt\,dz\right]\,d\mathbf{\Phi}_n\,, \tag{5.10}$$

where t_I is the initial scale of the shower, the splitting kernel is given by

$$\mathcal{K}(t, z) = \frac{\alpha_S}{2\pi}\,\frac{1}{t}\,\sum_j \hat{P}_{jk}^{\mathrm{excl}}(z)\,, \tag{5.11}$$

[2]This resummation by exponentiation has also been shown to hold for e^+e^- observables of the form of equation 4.10 in [201].

and the Sudakov form factor is that from equation 4.44 which we repeat here for convenience

$$\Delta_j(t, t_0) = \exp\left(-\sum_j \int_{t_0}^{t} \frac{dt'}{t'} \int \frac{\alpha_S(p_T^2)}{2\pi} \hat{P}_{ij}^{\text{excl}}(z)\, \theta\left(p_T(\mathbf{\Phi}_{n+1}) - p_T^{\min}\right)\, dz\right). \tag{5.12}$$

An assumption here is made that the dominant contribution to the cross section comes from the hardest emission (see [202] for discussion). This approximation will hold when one emission is much harder than all others in the event, and is an approximation made in both the standard parton shower formulation, and the motivation in improvements to the shower such as the ones for BSM processes we will study here.

The splitting function used in the Sudakov and everywhere from here on is now the exclusive, unregularised splitting functions $\hat{P}_{i,jk}^{\text{excl}}$ as defined in figure 4.1, though we will omit the 'excl' label for clarity. Note that formally this splitting kernel is not uniquely defined but must have the correct soft and collinear limits as it determines which logarithms get resummed. As it is singular a lower bound must be introduced using a Heaviside step function to define the threshold for *resolvable* emission and allow for numerical simulation.

In full, the functional dependence of the Sudakov is

$$\Delta_i(t,\, t_0;\, p_T^{\min};\, \alpha_S(p_T^2)) = \exp\left(-\sum_j \int_{t_0}^{t} \frac{dt'}{t'} \int \frac{\alpha_S(p_T^2)}{2\pi} \hat{P}_{ij}^{\text{excl}}(z)\, \theta\left(p_T(\mathbf{\Phi}_{n+1}) - p_T^{\min}\right)\, dz\right) \tag{5.13}$$

though we will omit the parent parton flavour label, i, the strong coupling will be evaluated at the transverse momentum of the splitting since this is known to contain some of the NLL contributions (see section 6.7.2 of [17]), $t = (E_{\text{CM}}/2)^2$ is the maximum scale for parton shower emissions, $t_0 \approx 2^2\,\text{GeV}^2$ is the parton shower IR cut-off where hadronisation and non-perturbative evolution is deemed to take over, and the threshold for resolvable emission we use is $p_T^{\min} = 1\,\text{GeV}$.

The interpretation of equation 5.10 is as follows: A hard interaction event is generated with weight according to B. The parton shower algorithm is then applied to all external partons. The first term in the square brackets corresponds to the probability of no resolvable emission occurring at all when evolving from a scale t to a scale t_0 ($t > t_0$). The second term corresponds to the product of the probability of a resolvable emission in the infinitesimal range $[z + dz]$, $[t + dt]$ around the scale t, given by $\mathcal{K}(t, z)\, dt\, dz$, times the probability that emission has not already happened, given by $\Delta(t, t_0)$, and as such correctly generates the conditional probability for (the hardest) emission to occur at the scale t. These probabilities can be solved numerically for the scale, t, at which the emission occurs, and also for its momentum fraction $(1 - z)$, as well as azimuthal variable (which is spread evenly from 0 to 2π). How this is done is explained in section A.6.

For final-state (timelike) partons this procedure can be recursively applied to populate the soft and collinear phase space down to a scale t_0 at which the strong coupling growth no longer allows a perturbative treatment

and hadronisation takes place. For initial-state (spacelike) partons, for reasons involving computational efficiency and consistency with the DGLAP equation, the parton shower must undergo *backwards evolution* from the hard interaction scale.

This implies a modification of the Sudakov form factor for initial-state showers as follows

$$\Delta_j(t,t_0) = \exp\left(-\sum_j \int_{t_0}^{t} \frac{dt'}{t'} \int \frac{\alpha_S(p_T^2)}{2\pi} \hat{P}_{ij}^{\mathrm{excl}}(z)\, \frac{f_{\widetilde{ij}}(x/z),t)}{z\, f_{\widetilde{ij}}(x),t)}\, \theta\left(p_T(\mathbf{\Phi}_{n+1}) - p_T^{\min}\right)\, dz\right)\,, \tag{5.14}$$

but the splitting kernels and formulation of the shower are otherwise unaltered.

For a more detailed treatment of the shower kinematics in HERWIG++ see [203, 204].

5.2.1 Shower Unitarity

We note two properties of equation 5.10 which are crucial and must be preserved in any extensions or improvements of the shower. The first is *shower unitarity*, which is the requirement that the sum of terms in square brackets (as used to produce the hardest emission) give unity when the second term within it is integrated over the phase space of the emission (as it would be when computing the expectation value of an observable). This preserves the normalisation of the fixed-order calculation (in this case the Born normalisation given by B in equation 5.10) and allows for a probabilistic interpretation of the terms in square brackets, which is crucial to the numerical generation of the parton shower.

We rewrite equation 5.10 in a more general form as

$$d\sigma = B\, \left[\Delta(p_T^{\min})\, +\, \Delta(p_T)\, \mathcal{K}(\mathbf{\Phi}_1)\, d\mathbf{\Phi}_1\right]\, d\mathbf{\Phi}_n\,, \tag{5.15}$$

where we momentarily consider the Sudakov as a function only of the threshold for resolvable emission, p_T:

$$\Delta(p_T) = \exp\left(-\int \mathcal{K}(\mathbf{\Phi}_1)\, \theta(k_T - p_T)\, d\mathbf{\Phi}_1\right)\,. \tag{5.16}$$

When using 5.15 to compute the expectation value of an observable, the convolution of this expression with the observable will be taken, with the integral over the full phase space being evaluated. Considering the terms in the square brackets from equation 5.15 with the integral over the radiative phase space of the hardest emission gives

$$\Delta(p_T^{\min})\, +\, \int \Delta(p_T)\, \mathcal{K}(\mathbf{\Phi}_1)\, d\mathbf{\Phi}_1\,. \tag{5.17}$$

Multiplying the second term by

$$1 = \int_{p_T^{\min}}^{\infty} dp_T\, \delta(k_T - p_T) \tag{5.18}$$

equation 5.17 becomes

$$\Delta(p_T^{\min}) \;+\; \int_{p_T^{\min}}^{\infty} dp_T \; \underbrace{\Delta(p_T) \int \mathcal{K}(\mathbf{\Phi}_1)\,\delta(k_T - p_T)\,d\mathbf{\Phi}_1}_{=\frac{d}{dp_T}\Delta(p_T)} = \Delta(p_T^{\min}) \;+\; (\Delta(\infty) \;-\; \Delta(p_T^{\min})) \tag{5.19}$$

where we have used the relation $\delta(k_T - p_T) = -\frac{d}{dp_T}\,\theta(k_T - p_T)$ to identify the derivative of the Sudakov and we have used the relation $\Delta(\infty) = 1$.

Therefore equation 5.10 satisfies the shower unitarity relation

$$\Delta(p_T^{\min}) \;+\; \int \Delta(p_T)\,\mathcal{K}(\mathbf{\Phi}_1)\,d\mathbf{\Phi}_1 = 1\,, \tag{5.20}$$

as expected.

The probabilistic interpretation of equation 5.10 as the probability of generating the hardest emission at a given scale allows for the numerical simulation of said process. The problem to be solved is the solution of the second term of equation 5.10 for the scale, t, of the emission and its momentum fraction, z. This corresponds to generating values of t and z according to the distribution

$$\mathcal{P}(t, z) = \mathcal{K}(t, z)\,\Delta(t, t_0)\,. \tag{5.21}$$

The technique used to tackle the problem of generating values according to equation 5.21 is known as the *veto algorithm* and is defined in appendix A.6 and explicitly implemented for the cases of interest to us in sections 6.1.2 and 6.2.2.

5.3 Next-to-Leading-Order + Leading Logarithmic Matching

Extending the LO+LL matching to NLO+LL will require modifications to equation 5.10 to include the NLO fixed-order calculation without double-counting contributions, as there will be regions of phase space into which both the fixed-order amplitude and the parton shower could radiate.

The double-counting problem between the NLO amplitude and the parton shower lies essentially in the $\mathcal{O}(\alpha_S)$ corrections that are already included in the Sudakov, and therefore the first emission from the shower as well. Hence one must choose whether to keep the contribution from the shower, or the NLO amplitude, but one of the two must be removed to avoid double-counting this contribution.

In accordance with the observation that the dominant contributions to the cross section will originate from the hardest emission of the event (it is this contribution which we seek to improve in keeping with the formulation of equation 5.10) and given that such emission will be accurately described by the fixed order prediction, it is its $\mathcal{O}(\alpha_S)$ contribution which we must keep, and the corresponding contribution in the shower

should be discarded. This is exactly the same issue as discussed around equation 5.7 for matching in analytic calculations, and the solutions here are analogous as well.

The challenge is thus to consistently insert the hardest parton emission as generated from the fixed-order amplitude whilst ensuring that the parton shower does not generate any emissions as hard or harder than it, and respecting both shower unitarity and the functional form of equation 5.21 required for the veto algorithm to work as formulated there.

In order to achieve this matching we are formally free to insert terms of NNLO or higher if required to permit or improve the numerical implementation, however such terms can be numerically important in high-p_T regions of phase space and are an unavoidable vulnerability of the presently known matching techniques.

In terms of formal accuracy we are also free to include (that is, to exponentiate by including within the Sudakov form factor) finite terms aside from the contributions containing the LL soft and collinear contributions. Though once again this inherent ambiguity can be numerically important, particularly in high-p_T regions, but indeed throughout the phase space as both low- and high-p_T regions are coupled by the requirement of shower unitarity (namely, an excess or deficiency in one region necessarily translates into the opposite contribution in the other for the overall fixed-order normalisation to be preserved).

In essence, by using one of the methods described in section 3.5 we are now able to generate hard-scattering events according to a NLO amplitude and use them to compute any IR-safe observable desired. In section 5.2 we have sketched a method to match LO amplitudes to a parton shower which can perform LL Sudakov resummation using the veto method. The next step is to extend this procedure to obtain a NLO+LL matching and obtain the benefits of both the NLO inclusive accuracy and the LL resummation and fully exclusive event generation of the parton shower.

The simplest way to achieve this is by finding a way to adapt equation 5.10 to include equation 3.107 without double-counting overlapping contributions from the NLO amplitude and the shower. Two methods have so far been proposed to accomplish this, we first briefly overview the alternative method in section 5.3.1 for completeness and for comparison, and then focus on the one used in the present implementation.

5.3.1 The MC@NLO Method

The first NLO+parton shower matching method to be proposed was the MC@NLO matching method introduced in [205].

Considering the second term in equation 5.10 which describes the probability to generate the hardest

emission from the shower, we can define

$$\mathcal{R}^{\mathrm{MC}} \;=\; \mathcal{B}\,\mathcal{K}(t,z)\,\Delta(t,t_0)\,. \tag{5.22}$$

where $\mathcal{B}$ and $\mathcal{K}(t,z)$ are defined in equations 3.91 and 5.11. The exact functional form of $\mathcal{R}^{\mathrm{MC}}$ will vary from amongst different implementations of the parton shower algorithm as there will be differences in the ordering variable, the corresponding integration limits in the Sudakov, or the exact form of the splitting kernels, for example[3]. $\mathcal{R}^{\mathrm{MC}}$ and its components will therefore schematically stand for any of these possible implementations in this section.

Note that use of this term in the implementation will therefore make it specific to a particular shower implementation though the general method would remain the same for other choices of $\mathcal{R}^{\mathrm{MC}}$. The $\mathcal{R}^{\mathrm{MC}}$ expression must be transformed from parton shower variables to the variables of the fixed order matrix element and this operation is an event-generator dependent calculation.

Using equation 5.22 equation 5.10 can be more generally written as

$$d\sigma = \mathcal{B}\,\left[\Delta(t_I,t_0)\;+\;\frac{\mathcal{R}^{\mathrm{MC}}}{\mathcal{B}}\,d\mathbf{\Phi}_1\right]\,, \tag{5.23}$$

where we have rewritten the Sudakov form factor as

$$\Delta(t,t_0) = \exp\left(-\sum_j \int_{t_0}^{t} \frac{\mathcal{R}^{\mathrm{MC}}}{\mathcal{B}}\,\theta(p_T(\mathbf{\Phi}_{n+1}) - p_T^{\min})\,d\mathbf{\Phi}_1\right)\,. \tag{5.24}$$

Expanding equation 5.22 to $\mathcal{O}(\alpha_S)$ yields

$$\begin{aligned}\mathcal{R}^{\mathrm{MC}} &= \mathcal{B}\,\mathcal{K}(t,z)\,\left(1-\int_{t_0}^{t}\mathcal{K}(t,z)\,d\mathbf{\Phi}_1\;+\;\ldots\right)\\ \mathcal{R}^{\mathrm{MC}}\Big|_{\mathcal{O}(\alpha_S)} &= \mathcal{B}\,\mathcal{K}(t,z)\,,\end{aligned} \tag{5.25}$$

which gives the NLO shower contribution which must be removed to avoid double-counting when the fixed-order NLO contribution is inserted.

We can therefore modify equation 5.10 to generate the hardest emission weight according to the NLO amplitude, with the counterterms used by the subtraction method to render the NLO amplitude numerically integrable modified to include these $\mathcal{O}(\alpha_S)$ shower contributions, and thereby avoiding any double-counting.

This is how MC@NLO performs the NLO+LL matching, which we can summarise by stating that the hard

[3] See Appendix A.5 in the original paper [205] for the construction of $\mathcal{R}^{\mathrm{MC}}$ for FORTRAN HERWIG.

interaction events should now be generated (schematically) according to

$$d\sigma_{NLO}^{\text{MC@NLO}} = \underbrace{\left[\mathcal{B} \,+\, \mathcal{V}_0 \,-\, \sum_i \int \mathcal{C}_i \, d\mathbf{\Phi}_1 \,+\, \int \mathcal{R}^{\text{MC}}\Big|_{\mathcal{O}(\alpha_S)} d\mathbf{\Phi}_1 \,+\, \mathcal{G}_{a\,0} \,+\, \mathcal{G}_{b\,0}\right] d\mathbf{\Phi}_n}_{\mathbb{S}}$$
$$+ \underbrace{\left[\mathcal{R}_0 \,-\, \mathcal{R}^{\text{MC}}\Big|_{\mathcal{O}(\alpha_S)}\right] d\mathbf{\Phi}_{n+1}}_{\mathbb{H}}, \tag{5.26}$$

where $\mathcal{C}_i$ are the subtraction terms necessary to regularise the virtual contribution and $\mathcal{R}^{\text{MC}}\Big|_{\mathcal{O}(\alpha_S)}$ are the $\mathcal{O}(\alpha_S)$ terms from the parton shower, which must be subtracted. Note that both $\mathbb{S}$ events containing only shower emissions and $\mathbb{H}$ events containing an NLO real emission are separately finite (lower integration bounds on integrals over $\mathcal{R}^{\text{MC}}\Big|_{\mathcal{O}(\alpha_S)}$ are removed here so it acts as a local subtraction term).

The parton shower should then be run on each $\mathbb{S}$- or $\mathbb{H}$-type generated event, with no need for a veto on hard shower emissions as the $\mathbb{H}$ events are non-singular in the soft and collinear limits such that overlap with parton shower emissions should be suppressed.

Note however that both $\mathbb{S}$ and $\mathbb{H}$ events are not guaranteed to have positive weights as the modified subtraction terms $\tilde{\mathcal{R}}$ may in some regions of phase space exceed their relevant amplitudes. The MC@NLO method therefore will generally produce a non-negligible fraction of events with negative weights. It is this issue which is highly inconvenient for detector-level simulations, and which motivates us to use the other available method, which we now present and which is the method this work is based on.

5.3.2 The POWHEG Method

The Positive Weight Hardest Emission Generator (POWHEG) method as formulated in [188,206,207] generates the hardest emission of an event according to the NLO amplitude and then inserts it into a parton shower with a corresponding veto on emissions harder than that generated from the fixed-order amplitude to avoid double-counting.

If the parton shower algorithm is ordered in transverse momentum the hardest emission from POWHEG can be inserted as the first one and then the shower can be evolved as usual, but with the presence of a veto (this is known as the *vetoed shower*). If (as is the case in this work, and in general for HERWIG++) the shower is angular-ordered, then the hardest emission is no longer guaranteed to be the first one and softer wide-angle emissions should precede it. These form what is know as the *truncated shower* (or *vetoed truncated shower* indicating the presence of a veto on emissions harder than the POWHEG one here as well) and must be consistently inserted to restore the soft coherence of the shower, as we will now discuss.

Shower Reorganisation

Using the formalism established in [206] we represent the full shower evolution of a parton i from the scale t to the scale t_0 with a veto on emission harder than $p_{T,h}$ by a generating functional

$$\mathcal{S}_i(t,\, t_0;\, p_{T,h})\,, \tag{5.27}$$

with the lower scale and veto scale assumed to be t_0 and zero, respectively, if absent[4].

The hardest emission (which will now be generated from the NLO amplitude) is denoted using the subscript 'h'. The sum over all possible splittings $\widetilde{ij} \to i\ j$ in the splitting kernel will be explicitly written (in contrast to equation 5.11 where it was absorbed into the kernel).

In the standard LO+LL formulation of the shower every emission (including the hardest) can be rewritten in this formalism from equation 5.10 to

$$\begin{aligned}\mathcal{S}_{\widetilde{ij}}(t_I) &= \Delta_{\widetilde{ij}}(t_I, t_0)\ \mathcal{S}_{\widetilde{ij}}(t_0) \\ &+ \int_{t_0}^{t_I} dt\ \Delta_{\widetilde{ij}}(t_I, t)\ \sum_{ij} \left(\mathcal{K}_{\widetilde{ij}\to ij}(t,z)\right)\ \mathcal{S}_i(z\,t)\ \mathcal{S}_j((1-z)\,t)\,.\end{aligned} \tag{5.28}$$

This shower is applied recursively by iteratively substituting this expression back into the shower generating functionals on the right-hand side to generate the full parton shower, stopping when

$$\prod_{\mathrm{i}}^{\text{iterations}} z_i\, t_I \le t_0\,, \tag{5.29}$$

and then proceeding to the hadronisation stage of the Monte Carlo event generation.

We now seek to modify this by inserting a truncated shower before the hardest emission (with a veto on emissions with[5] $p_T > p_{T,h}$), followed by the hardest emission described by $(t_h,\, z_h,\, \phi_h)$, and then a vetoed shower (with the same transverse momentum constraint). This must be done with the constraint that the functional form of equation 5.28 is preserved. The reason for this is twofold: by unitarity, the no-branching probability density in the integrand in the Sudakov must match the branching probability used to generate emissions, and also the functional form in the second term should match that of equation 5.21 for the veto algorithm to be applicable.

In the following we illustrate the required modifications to the parton shower using the final-state (timelike) shower.

Imposing the required transverse momentum veto condition on equation 5.28 and inserting the truncated shower as required yields a shower equation for the parton shower line producing the hardest emission of the

[4] Note that $\mathbb{S}(t_0,\, t_0) = \mathbb{1}$, meaning the shower generates no resolvable emission.

[5] Transverse momentum is defined as in section 4.4, with respect to the parent parton for FSR, and with respect to the beam for ISR.

form[6]

$$\mathcal{S}_{\widetilde{ij}}(t_I) = \Delta_{\widetilde{ij}}(t_I, t_0)\, \mathcal{S}_{\widetilde{ij}}(t_0) + \int_{t_0}^{t_I} dt\, \mathcal{S}^T_{\widetilde{ij}}(t_I, t_h;\, p_{T,\,h})\, \sum_{ij} \left(\mathcal{K}_{\widetilde{ij}\to ij}(t_h, z_h) \right)\, \mathcal{S}^V_i(z_h\, t_h;\, p_{T,\,h})\, \mathcal{S}^V_j((1-z_h)\, t_h;\, p_{T,\,h})\,. \tag{5.30}$$

The truncated shower here is given by the recursive equation

$$\begin{aligned}\mathcal{S}^T_{\widetilde{ij}}(t_I, t_h;\, p_{T,\,h}) = \Delta_{\widetilde{ij}}(t_I, t_h) &\\ + \int_{t_h}^{t_I} dt\, \Delta_{\widetilde{ij}}(t_I, t)\, \mathcal{K}_{\widetilde{ij}\to \widetilde{ij}\,g}(t, z)\, \Theta\left(p_{T,\,h} - p_T(t, z)\right) &\\ \times\, \mathcal{S}^T_{\widetilde{ij}}(z\, t, t_h;\, p_{T,\,h})\, \mathcal{S}^V_g((1-z)\, t;\, p_{T,\,h})\,. &\end{aligned} \tag{5.31}$$

Note that as discussed before, in the truncated shower the splittings can only correspond to gluon emission[7], with the soft gluon itself proceeding to a vetoed shower. Note also that unlike the previous shower equations, the first term lacks a factor of $\mathcal{S}_{\widetilde{ij}}(t_h)$ as even if there is no emission before the hardest one (this term corresponds to the probability of no emission) the truncated shower must proceed to the hardest emission followed by the vetoed shower, which is given by

$$\begin{aligned}\mathcal{S}^V_{\widetilde{ij}}(t_h;\, p_{T,\,h}) = \Delta_{\widetilde{ij}}(t_h, t_0)\, \mathcal{S}_{\widetilde{ij}}(t_0) &\\ + \int_{t_0}^{t_h} dt\, \Delta_{\widetilde{ij}}(t_h, t)\, \sum_{ij} \left(\mathcal{K}_{\widetilde{ij}\to ij}(t, z) \right)\, \Theta\left(p_{T,\,h} - p_T(t, z)\right) &\\ \times\, \mathcal{S}^V_i(z\, t;\, p_{T,\,h})\, \mathcal{S}^V_j((1-z)\, t;\, p_{T,\,h})\,. &\end{aligned} \tag{5.32}$$

Unfortunately, in both the truncated and the vetoed showers as given by equations 5.31 and 5.32 the presence of the Heaviside step function imposing the transverse momentum veto here but not in the integrand of the standard Sudakov form factor (as shown in equation 5.16) violates unitarity and implies that the functional form in equation 5.28 required for the veto algorithm to work no longer holds.

Using the property $\Theta\left(p_{T,\,h} - p_T(t, z)\right) + \Theta\left(p_T(t, z) - p_{T,\,h}\right) = 1$ of the Heaviside step function the Sudakov can be written as the product

$$\Delta_i(t_1, t_2) = \Delta^V_i(t_1,\, t_2;\, p_{T,\,h})\, \Delta^R_i(t_1,\, t_2;\, p_{T,\,h})\,, \tag{5.33}$$

of the newly defined *vetoed Sudakov* and *remnant Sudakov*, respectively.

It can be shown (see derivation of equation 6.21 within [206]) that the product of remnant Sudakovs

[6] Shower lines not containing the hardest emission proceed according to equation 5.28, as usual.

[7] Since with angular ordering the first emissions are wide angle ones, and only gluon emission has a singular soft, non-collinear limit.

obtained by recursive use of the shower equations above may be combined into a single remnant Sudakov as

$$\begin{aligned}\Delta_i^R(t_I,\, t_0;\, p_{T,\,h}) &\approx \prod_i \Delta_i^R(t_i,\, t_{i+1};\, p_{T,\,h}) \\ &= \exp\left(-\sum_{\widetilde{ij}\to ij}\int_{t_0}^{t_I} \mathcal{K}_{\widetilde{ij}\to ij}(t,z)\,\Theta\left(p_T(t,z)-p_{T,\,h}\right)\right). \end{aligned} \tag{5.34}$$

Noting that the standard Sudakov form factor is related to the remnant Sudakov by

$$\Delta_i(t_I,t_0) = \Delta_i^R(t_I,t_0;\,0)\,, \tag{5.35}$$

and factorising all the remnant Sudakov factors from 5.30 using 5.34 we obtain the final expression for the hardest emission from the POWHEG-rearranged shower as

$$\begin{aligned}\mathcal{S}_{\widetilde{ij}}(t_I) &= \Delta_{\widetilde{ij}}^R(t_I,t_0;\,0)\;\mathcal{S}_{\widetilde{ij}}(t_0) \\ &+ \int_{t_0}^{t_I} dt\;\mathcal{S}_{\widetilde{ij}}^T(t_I,t_h;\,p_{T,\,h})\;\Delta_{\widetilde{ij}}^R(t_I,t_0;\,p_{T,\,h})\;\sum_{ij}\left(\mathcal{K}_{\widetilde{ij}\to ij}(t_h,z_h)\right) \\ &\times \mathcal{S}_i^V(z_h\,t_h;\,p_{T,\,h})\;\mathcal{S}_j^V\left((1-z_h)\,t_h;\,p_{T,\,h}\right). \end{aligned} \tag{5.36}$$

Here the truncated and vetoed showers are analogous to equations 5.31 and 5.32 but with the Sudakovs now being vetoed Sudakovs whose argument now correctly matches with the Heaviside step function after having factored out the remnant Sudakovs.

The new vetoed shower is given by

$$\begin{aligned}\mathcal{S}_{\widetilde{ij}}^V(t_h;\,p_{T,\,h}) &= \Delta_{\widetilde{ij}}^V(t_h,t_0)\;\mathcal{S}_{\widetilde{ij}}(t_0) \\ &+ \int_{t_0}^{t_h} dt\;\Delta_{\widetilde{ij}}^V(t_h,t)\;\sum_{ij}\left(\mathcal{K}_{\widetilde{ij}\to ij}(t,z)\right)\;\Theta\left(p_{T,\,h}-p_T(t,z)\right) \\ &\times \mathcal{S}_i^V(z\,t;\,p_{T,\,h})\;\mathcal{S}_j^V\left((1-z)\,t;\,p_{T,\,h}\right). \end{aligned} \tag{5.37}$$

With the corresponding truncated shower also being obtained from the previous one by replacing Sudakovs by vetoed Sudakovs, yielding

$$\begin{aligned}\mathcal{S}_{\widetilde{ij}}^T(t_I,t_h;\,p_{T,\,h}) &= \Delta_{\widetilde{ij}}^V(t_I,t_h) \\ &+ \int_{t_h}^{t_I} dt\;\Delta_{\widetilde{ij}}^V(t_I,t)\;\mathcal{K}_{\widetilde{ij}\to\widetilde{ij}\,g}(t,z)\;\Theta\left(p_{T,\,h}-p_T(t,z)\right) \\ &\times \mathcal{S}_{\widetilde{ij}}^T(z\,t,t_h;\,p_{T,\,h})\;\mathcal{S}_g^V\left((1-z)\,t;\,p_{T,\,h}\right). \end{aligned} \tag{5.38}$$

The required shower modifications for initial-state (spacelike) showers are analogous (see [204] for details).

The algorithmic implementation of equation 5.36 is as follows:

1. following equation 5.36 generate the hardest emission variables $(t_h,\, z_h,\, \phi_h)$ according to

$$\Delta^R_{\widetilde{ij}}(t_I, t_0;\, p_{T,\,h}) \sum_{ij} \left(\mathcal{K}_{\widetilde{ij}\to ij}(t_h, z_h)\right)$$

   using the veto algorithm;

2. following equation 5.37 generate the truncated shower from t_I to t_h allowing only gluon emission with $p_T < p_{T,\,h}$ by generating shower variables according to

$$\Delta^V_{\widetilde{ij}}(t_I, t)\; \mathcal{K}_{\widetilde{ij}\to \widetilde{ij}\; g}(t, z)$$

   using the veto method;

3. when the scale t_h is reached insert the hardest emission as generated in step 1;

4. continue shower to the hadronisation scale according to the vetoed shower, using

$$\Delta^V_{\widetilde{ij}}(t_h, t) \sum_{ij} \left(\mathcal{K}_{\widetilde{ij}\to ij}(t, z)\right)$$

   and allowing only emissions with $p_T < p_{T,\,h}$.

Note that the contribution from the truncated shower is purely from soft gluons (as (anti)quark emission is finite in the soft limit), and that even then their singly-logarithmic contribution is subleading relative to the dominant double-logarithmic contributions from LL Sudakov resummation in the collinear regions.

Nonetheless, if the coherence and proper treatment of soft wide-angle emissions of the HERWIG++ parton shower is to be preserved these contributions must be accounted for. This requires a slight reorganisation of the parton shower to consistently include the truncated shower whilst preserving the current shower's structure which allows for efficient numerical sampling. We describe the necessary modifications to the shower in section 5.3.2 and assume the presence and proper introduction of the truncated shower from here on.

Generation of the Hardest Emission

We now wish to find the POWHEG NLO+LL equivalent of equation 5.10. Expanding this expression to $\mathcal{O}(\alpha_S)$ and replacing these terms with the NLO fixed order contribution from equation 3.107 should provide us exactly with the NLO-accurate generation of the hardest emission matched to a parton shower which we desire.

Restating the relation for the hardest emission from the parton shower for convenience and proceeding to

expand it about $\alpha_S = 0$ yields

$$\begin{aligned} d\sigma &= B\,[\Delta(t_I,t_0)\;+\;\Delta(t,t_0)\,\mathcal{K}(t,z)\,dt\,dz]\;d\mathbf{\Phi}_n \\ &= B\,\left[\left(1-\int_{t_0}^{t_I}\mathcal{K}(t,z)\,dt\,dz+\ldots\right)\;+\;\left(1-\int_{t_0}^{t}\mathcal{K}(t,z)\,dt\,dz+\ldots\right)\,\mathcal{K}(t,z)\,dt\,dz\right]\;d\mathbf{\Phi}_n\,, \end{aligned}$$

so that to $\mathcal{O}(\alpha_S)$

$$d\sigma\Big|_{\mathcal{O}(\alpha_S)} = B\,\left[\left(1-\int_{t_0}^{t_I}\mathcal{K}(t,z)\,dt\,dz\right)+\mathcal{K}(t,z)\,dt\,dz\right]\;d\mathbf{\Phi}_n\,. \tag{5.39}$$

Neglecting for now the collinear remnant terms due to ISR, the NLO result from equation 3.107 can be written (using the singular real-emission contribution as a local subtraction term) as

$$\begin{aligned} d\sigma_{NLO} &= \left[V+\int_1 R\right]\;d\mathbf{\Phi}_n+\left[B-\int_1 R+R\,d\mathbf{\Phi}_1\right]\;d\mathbf{\Phi}_n \\ &= \left[V+\int_1 R\right]\;d\mathbf{\Phi}_n+B\,\left[1-\frac{\int_1 R}{B}+\frac{R\,d\mathbf{\Phi}_1}{B}\right]\;d\mathbf{\Phi}_n\,. \end{aligned} \tag{5.40}$$

The second set of square brackets now has precisely the same form as the square brackets in the expansion of the parton shower result, suggesting that with the replacements

$$\mathcal{K}(t,z)\longrightarrow\frac{R\,d\mathbf{\Phi}_1}{B}\,,\quad dt\,dz\longrightarrow d\mathbf{\Phi}_1\,, \tag{5.41}$$

both here and in the remnant Sudakov (equation 5.34) such that the remnant Sudakov is now

$$\Delta^R(p_T)=\Delta_i^R(t_I,\,t_0;\,p_T)=\exp\left(-\sum_{\widetilde{ij}\to ij}\int\frac{[R\;d\mathbf{\Phi}_1\;\Theta\left(p_T(\mathbf{\Phi}_{n+1})-p_T\right)]}{B}\right) \tag{5.42}$$

a NLO-accurate version of equation 5.10 (which avoids double-counting $\mathcal{O}(\alpha_S)$ contributions) may be obtained in the form of

$$d\sigma_{NLO}=\left[V+\int_1 R\right]\;d\mathbf{\Phi}_n+B\,d\mathbf{\Phi}_n\;\left[\Delta^R(p_T^{\min})+\Delta^R(p_T)\,\frac{R}{B}\;d\mathbf{\Phi}_1\right]\,. \tag{5.43}$$

This works but has the unfortunate feature of potentially yielding events with negative weights, spoiling the probabilistic interpretation of the events, posing a problem for detector simulation studies and potentially slowing down the convergence of the numerical result if large individual positive and negative weights result.

In POWHEG this is remedied by absorbing the terms in the first square brackets into the Born, B, contribution, which now becomes

$$\overline{B}=B+V+\int R\,d\mathbf{\Phi}_1\,. \tag{5.44}$$

When multiplied by the term in the second square brackets this introduces spurious terms of $\mathcal{O}(\alpha_S^2)$ and higher, but these are beyond the formal accuracy we aim for and can formally be neglected (though their numerical significance is not necessarily negligible).

Note also that this $\overline{B}$ function is positive definite as the Born is positive and the radiative corrections should not exceed it as long as perturbativity is preserved.

We therefore have the final POWHEG formula for the hardest emission from a NLO amplitude matched to a LL-accurate parton shower,

$$d\sigma_{\text{NLO}}^{\text{POWHEG}} = \overline{B}\, d\mathbf{\Phi}_n \left[\Delta^R(p_T^{\min}) + \Delta^R(p_T)\, \frac{R}{B}\, d\mathbf{\Phi}_1\right]. \tag{5.45}$$

Note however that a subtraction method is necessarily involved, which implies we must separate the real contribution into contributions where only a single dipole and its corresponding kinematic mapping (or singular region in the case of FKS subtraction) labelled α is relevant. This can be done by defining

$$\mathcal{R}_\alpha = \frac{|\mathcal{D}_\alpha|}{\sum_\alpha |\mathcal{D}_\alpha|}\, \mathcal{R}\,, \tag{5.46}$$

such that

$$\mathcal{R} = \sum_\alpha \mathcal{R}_\alpha\,. \tag{5.47}$$

This separation of the real emission contribution is also required since the POWHEG method relies on the construction of n-body underlying configurations from the real emission contribution to build the $\overline{B}$ function, and this is possible (by merging collinear partons or removing soft ones) only near a single collinear or soft region, as defined by a single dipole.

We must also account for the fact that the term in square brackets in equation 5.45 as well as the contribution in square brackets within the Sudakov in equation 5.42 must in fact be evaluated with their underlying Born kinematics[8] (which we denote using barred variables) at the same kinematic points as the Born contribution. This is possible thanks to the factorisations

$$d\mathbf{\Phi}_{n+1} = d\overline{\mathbf{\Phi}}_n^\alpha\, d\Phi_1^\alpha\,, \tag{5.48a}$$

$$d\mathbf{\Phi}_{n,\,z}^{a(b)} = \frac{dz}{z}\, d\overline{\mathbf{\Phi}}_n\,, \tag{5.48b}$$

of the phase space.

We denote this restriction on the phase-space evaluation as

$$[\ldots]^{\overline{\mathbf{\Phi}}_n = \mathbf{\Phi}_n}\,, \tag{5.49}$$

which applies to all the relevant quantities in the brackets ($\mathcal{R}$, $\mathbf{\Phi}_{n,\,z}^{a(b)}$, $k_T(\mathbf{\Phi}_{n+1})$, etc). This restriction on the phase space is crucial so that the $\overline{B}$ function provides n-body kinematic events with NLO normalisation, to which the POWHEG Sudakov can be used to add the hardest emission via the veto algorithm.

[8] This is obtained by deleting the soft or collinear parton from the event and absorbing its energy fraction into the incoming parton momenta for initial-state collinear configurations.

The underlying Born configurations as well as each of the regions where dipoles contribute must also have the same flavour structure as the Born contribution to be added consistently to the final result. Therefore the flavour structure of the Born contribution will be labelled f and this label is appended to relevant variables.

Taking into account these subtleties and including contributions from ISR the final results for the hardest emission in the POWHEG method is given by

$$d\sigma_{\mathrm{NLO}}^{\mathsf{POWHEG}} = \sum_f \overline{B}^f \, d\mathbf{\Phi}_n \left\{ \Delta^f(p_T^{\min}) + \sum_{\alpha_f} \frac{\left[R \, \Delta^f(k_T) \, \Theta(k_T(\mathbf{\Phi}_{n+1}) - p_T^{\min}) \, d\mathbf{\Phi}_1\right]_\alpha^{\overline{\mathbf{\Phi}}_n = \mathbf{\Phi}_n}}{B^f} \right\}, \tag{5.50}$$

its $\overline{B}$ function is given by

$$\overline{B} = B + \left(V + \int d\mathbf{\Phi}_1 \, C \right) + \left[\int d\mathbf{\Phi}_1 [R - C] \; + \; \int \frac{dz}{z} \, [G^a_{n,\,z} + G^b_{n,\,z}] \right]^{\overline{\mathbf{\Phi}}_n = \mathbf{\Phi}_n}, \tag{5.51}$$

and the corresponding POWHEG Sudakov is

$$\Delta(p_T) = \exp\left\{ - \int_{t_0}^{S/4} \sum_{\alpha_f} \frac{\left[R \, \Theta(k_T(\mathbf{\Phi}_{n+1}) - p_T^{\min}) \, d\mathbf{\Phi}_1\right]_\alpha^{\overline{\mathbf{\Phi}}_n = \mathbf{\Phi}_n}}{B^f} \right\}, \tag{5.52}$$

where the upper limit corresponds to the $\sqrt{S}/2 = E_{\mathrm{CM}}/2$ phase space limit for real emission, and the lower integration limit, $t_0 \approx 2^2\,\mathrm{GeV}^2$, corresponds to the parton shower cut-off where hadronisation and non-perturbative evolution is deemed to take over.

That these relations do indeed reproduce the NLO expectation value for IR-safe observables (equation 3.107) is proven in section 4.2 of [188].

Chapter 6

POWHEG Implementations

In this chapter we present the novel implementations of matching of the NLO corrections for the Z', slepton pairs, and gaugino pair production to the HERWIG++ parton shower via the POWHEG method.

6.1 Z' POWHEG Implementation

We now describe the POWHEG implementation (as overviewed in chapter 5) merging the NLO QCD corrections to Drell-Yan production of lepton pairs via a Z, γ or Z' as computed in chapter 3[1] with the HERWIG++ parton shower algorithm (as overviewed in chapter 4). This yields a novel[2] NLO+(N)LL-accurate event generation for Z' observables inclusive in jets.

The present implementation of the NLO QCD corrections to Drell-Yan for Z' production as described here is built on the SM Drell-Yan POWHEG implementation published in [209] and described in detail in [204], which can be consulted for more details.

The crucial ingredient for the implementation of any process in POWHEG (once the methods for the generation of the truncated shower and the hardest emission have been established, as done in sections 5.3.2 and 5.3.2, respectively) is the construction of the $\overline{B}$ function as defined in equation 5.51. The construction of the hardest emission according to the defining relation of the POWHEG method of equation 5.50 is then possible and follows more or less straightforwardly.

[1] The QCD radiative corrections for the SM Drell-Yan production are identical to those now including the Z', as the coloured content of the process is unaltered.

[2] This implementation went unpublished and was later carried out in [2]. We later also became aware of an earlier implementation using MC@NLO [208].

6.1.1 Generation of the $\overline{B}$ Function

The procedure used to numerically deal with the IR singularities of the NLO cross section is not limited to Catani-Seymour dipole subtraction and can in fact be performed by whichever method is most convenient, provided the real and virtual matrix elements are rendered individually finite and numerically integrable.

For the implementation of the NLO radiative corrections to Drell-Yan we use the results of [204]. This allows the Born contribution to be factorised from the real emission contributions (thereby simplifying the computation of R/B required by the POWHEG relation into a rescaling of the Born contribution), and where the IR singularities are isolated (and afterwards mutually cancelled) by use of the plus prescription defined in equation 3.51.

The Born and virtual contributions can be straightforwardly generated by HERWIG++ and taken from equation 3.75, respectively.

We therefore focus on the (singular) real emission contribution which (using the definitions from section 3.4) is given by

$$R_{0\,ab}(\mathbf{\Phi}_{n+1}) = d\mathbf{\Phi}_n\, d\mathbf{\Phi}_1\, \frac{D(\epsilon)}{4\pi^2}\, \frac{t\,u}{Q^2}\, J(z,\,y)\, \mathcal{R}_{ab}\, \mathcal{L}(x_a,\,x_b)\,, \tag{6.1}$$

where we have used the real emission 3-body phase space from equation 3.19, rewritten in $d = 4 - 2\epsilon$ as

$$d\mathbf{\Phi}_{n+1} = d\mathbf{\Phi}_n\, d\mathbf{\Phi}_1\, \frac{D(\epsilon)}{(4\pi)^2}\, \frac{t\,u}{Q^2}\, J(z,y)\,. \tag{6.2}$$

$D(\epsilon)$ is as defined in equation 3.45 and

$$J(z,\,y) = z^{\epsilon}\,(1-z)^{-1-2\epsilon}\,y^{-1-\epsilon}\,(1-y)^{-1-\epsilon}\,, \tag{6.3}$$

with the z, y variables defined in equations 3.35, 3.36 and 3.37.

The plus prescription can be used to rewrite $J(z,\,y)$ as

$$J(z,\,y) = S(\epsilon)\,\delta(1-z)\;+\;C(z,\,\epsilon)\,[\delta(y)\;+\;\delta(1-y)]\;+\;H(z,\,y)\,, \tag{6.4}$$

where the singular soft, singular collinear, and finite non-soft, non-collinear contributions are given by the $S(\epsilon)$, $C(z,\,\epsilon)$ and $H(z,\,y)$ functions, respectively.

Taking the soft and collinear limits of the real emission matrix element one obtains the limits

$$\lim_{z\to 1} |\mathcal{M}^{n+1}_{ab}|^2 = 16\pi\,\alpha_S\,C_{ab}\,\frac{s}{t\,u}\,|\mathcal{M}^{n}_{ab}(p_a,p_b)|^2 \tag{6.5}$$

in the soft limit[3] and

$$\lim_{y\to 0} |\mathcal{M}_{ab}^{n+1}|^2 = 8\pi\,\alpha_S\,\frac{s}{t\,u}\,\frac{1-z}{z}\,\hat{P}_{cd}(z,\epsilon)\,|\mathcal{M}_{ab}^{n}(p_a,\,z\,p_b)|^2 \tag{6.6a}$$

$$\lim_{y\to 1} |\mathcal{M}_{ab}^{n+1}|^2 = 8\pi\,\alpha_S\,\frac{s}{t\,u}\,\frac{1-z}{z}\,\hat{P}_{cd}(z,\epsilon)\,|\mathcal{M}_{ab}^{n}(z\,p_a,\,p_b)|^2 \tag{6.6b}$$

in the collinear limits from each initial-state leg. The splitting functions $\hat{P}_{cd}(z,\epsilon)$ are the unregularised Altarelli-Parisi splitting functions in $d = 4-2\epsilon$, which are as defined in figure 4.1 but with the added dependence on the dimensional regularisation parameter ϵ as

$$\hat{P}_{qq}(z,\,\epsilon) = C_F\,\left[\frac{1+z^2}{1-z}\;-\;\epsilon\,(1-z)\right] \tag{6.7a}$$

$$\hat{P}_{qg}(z,\,\epsilon) = C_F\,\left[\frac{1+(1-z)^2}{z}\;-\;\epsilon\,z\right] \tag{6.7b}$$

$$\hat{P}_{gq}(z,\,\epsilon) = T_R\,\left[1\;-\;\frac{2\,z\,(1-z)}{1-\epsilon}\right] \tag{6.7c}$$

$$\hat{P}_{gg}(z,\,\epsilon) = 2\,C_A\,\left[\frac{z}{1-z}\;+\;\frac{1-z}{z}\;+\;z\,(1-z)\right] \tag{6.7d}$$

Multiplying them by the soft and collinear contributions of $J(z,\,y)$, respectively, gives a function of the form

$$R_{0\;ab} = S_{0\;ab}\,\delta(1-z)\;+\;C_{0\;ab}\,[\delta(y)\;+\;\delta(1-y)]\;+\;H_{ab}\,, \tag{6.8}$$

where the singular soft, singular collinear, and finite non-soft and non-collinear contributions have been separated.

Summing the soft-singular contributions of the real contribution with those from the virtual yields a finite virtual contribution of the form

$$V(\mathbf{\Phi}_n) = \frac{\alpha_S}{2\pi}\,C_F\,V(Q^2)\,B(\mathbf{\Phi}_n)\,, \tag{6.9}$$

where

$$V(Q^2) = \frac{2\pi^2}{3}\;-\;8\;-\;3\,\log\frac{\mu^2}{Q^2}\,, \tag{6.10}$$

and Q^2 as usual is the invariant mass of the vector boson.

With the remaining collinear singularities in $R_{0\;ab}$ being cancelled by the parton distribution functions via mass factorisation as described in section 3.3.3 the real emission contribution is now finite and of the form

$$R_{ab} = C_{ab}\,[\delta(y)\;+\;\delta(1-y)]\;+\;H_{ab}\,, \tag{6.11}$$

[3]The colour factor is C_F for the $q\bar{q}$ initial state and C_A for the qg and $\bar{q}g$ initial states.

with

$$C_{q\bar{q}} = (1+z)^2 \left[\frac{1}{(1-z)_+} \log \frac{Q^2}{x\,\mu^2} \;+\; 2 \left(\frac{\log(1-z)}{1-z} \right)_+ \right] \;+\; (1-z)\,, \tag{6.12}$$

$$H_{q\bar{q}} = \frac{1}{(1-x)_+} \left(\frac{1}{y_+} \;+\; \frac{1}{(1-y)_+} \right) \left[(1-z)^2 \,(1 - 2\,y\,(1-y)) \;+\; 2\,z \right], \tag{6.13}$$

for $q\bar{q}$,

$$C_{qg} = (z^2 \;+\; (1-z)^2) \left[\log \frac{Q^2}{x\,\mu^2} \;+\; 2\,\log(1-z) \right] \;+\; 2\,z\,(1-z)\,, \tag{6.14}$$

$$H_{qg} = \frac{1}{y_+} \left[2\,z\,(1-z)\,y \;+\; (1-z)^2\,y^2 \;+\; z^2 \;+\; (1-z)^2 \right], \tag{6.15}$$

for qg, and $C_{g\bar{q}} = C_{gq}(y \leftrightarrow 1-y)$, $H_{g\bar{q}} = H_{gq}(y \leftrightarrow 1-y)$ for $\bar{q}g$.

The final form of the finite real contribution is then

$$R(\mathbf{\Phi}_{n+1}) = \frac{\alpha_S}{2\pi} \sum_{a,b} C_{F(A)} \frac{R_{ab}}{z} \hat{\mathcal{L}}_{ab}(x_a,\, x_b)\,, \tag{6.16}$$

where R_{ab} are given by

$$R_{q\bar{q}} = C_{q\bar{q}}[\delta(1-y) \;+\; \delta(y)] \;+\; H_{q\bar{q}}\,, \tag{6.17a}$$

$$R_{qg} = C_{qg}\,\delta(y) \;+\; H_{qg}\,, \tag{6.17b}$$

$$R_{\bar{q}g} = C_{\bar{q}g}\,\delta(1-y) \;+\; H_{\bar{q}g}\,, \tag{6.17c}$$

and

$$\hat{\mathcal{L}}_{ab}(x_a,\, x_b) = \frac{\mathcal{L}_{ab}(x_a,\, x_b)}{\mathcal{L}_{q\bar{q}}(\bar{x}_a,\, \bar{x}_b)}\,, \tag{6.18}$$

the $\bar{x}$ variables being the incoming parton momentum fractions in the Born configuration, and their unbarred counterparts the corresponding being the incoming partonic momentum fractions after an emission (with a factor of z folded into the emitting momentum fraction).

The $\overline{B}$ function is now given by

$$\overline{B}(\mathbf{\Phi}_n) = B(\mathbf{\Phi}_n) \left[1 \;+\; \frac{\alpha_S}{2\pi}\,C_F\,V(Q^2) \;+\; \sum_{a,b} \int d\mathbf{\Phi}_1 \frac{\alpha_S}{2\pi}\,C_{F(A)}\,\frac{R_{ab}}{z}\,\hat{\mathcal{L}}_{ab}(x_a,\, x_b) \right]. \tag{6.19}$$

The integral over the emission's phase space can then be performed by mapping the radiative variables $\{y,\, z,\, \phi\}$ (where ϕ is the azimuthal angle) to a unit cube (so that each takes values $[0,1]$) as

$$\phi \to \tilde{\phi} = \frac{\phi}{2\pi}\,, \tag{6.20a}$$

$$z(\tilde{z}, y) = z_{\min}(y) + (1 - z_{\min}(y))\,\tilde{z}\,, \tag{6.20b}$$

where $\tilde{z}$ is a variable generated uniformly in $[0,1]$. The variables $\{y,\, \tilde{z}, \tilde{\phi}\}$ can then be generated independently

and uniformly in $[0,1]$ to perform the required integral over $d\mathbf{\Phi}_1$.

The integration proceeds using the criteria[4]

$$(1-z) > \epsilon,\ y > \epsilon,\ 1-y > \epsilon \tag{6.21}$$

to decide whether a given emission phase space point is evaluated using H_{ab}, or otherwise evaluated by C_{ab}.

The numerical implementation of the plus prescriptions used in R_{ab} is performed as described in appendix B.2 of [204].

6.1.2 Generation of the Hardest Emission

The only additional ingredient required for the generation of the hardest emission to be attached to the n-body configuration is the singular form of the real emission contribution, $R_0(\mathbf{\Phi}_{n+1})$, required for the exponent of the POWHEG Sudakov to ensure the resummation of the corresponding logarithmic structure.

This is simply obtained from the H_{ab} function by removing the plus prescriptions from it. This new form is denoted with a caret. The kernel of the POWHEG Sudakov for the hardest emission is then

$$\frac{R_0(\mathbf{\Phi}_{n+1})}{B(\mathbf{\Phi}_n)} = \sum_{a,b} \frac{\alpha_S}{2\pi}\, C_{F(A)}\, \frac{\hat{H}_{ab}}{z}\, \hat{\mathcal{L}}_{ab}(x_a,\, x_b)\,. \tag{6.22}$$

A further Jacobian factor gets absorbed into this kernel whilst transforming the radiative variables into the p_T, y basis to facilitate the application of the p_T cut imposed by the step function also in the kernel, which now takes the form

$$\Delta^R_{ab}(p_T) = \exp\left(- \int_{p_T^{\min}\approx 2\,\mathrm{GeV}}^{p_T^{\max}=\sqrt{S}/2} dp_T\, dy\, W_{ab} \right)\,, \tag{6.23}$$

where

$$W_{ab} = \frac{R_0(\mathbf{\Phi}_{n+1})}{B(\mathbf{\Phi}_n)} = \frac{\alpha_S}{\pi}\, C_{F(A)}\, \frac{p_T}{s\,(1-z)}\, \frac{\hat{H}_{ab}}{z}\, \hat{\mathcal{L}}_{ab}(x_a,\, x_b)\,, \tag{6.24}$$

and $\sqrt{S}$ is the hadronic centre-of-mass energy.

The channel ($ab = q\bar{q}, qg, \bar{q}g$) through which the hardest emission proceeds and its transverse momentum and rapidity are chosen by using the veto algorithm and the highest-bid method, as described in section A.6.

The bivariant veto algorithm from section A.6 is applied using

$$\begin{aligned} b_1(p_T) &= \frac{1}{p_T^2} \\ b_2(y_k) &= c_{ab}\,, \end{aligned} \tag{6.25}$$

[4] In practice the value $\epsilon = 10^{-10}$ is used, ϵ here is a cut-off parameter unrelated to that of dimensional regularisation.

as the bounding functions for the generation of p_T and the rapidity of the emission y_k, respectively ($c_{ab} = \text{constant}$ is the overestimate of the rapidity integral for channel ab).

The generation of the hardest emission then proceeds as follows:

1. set $p_T = p_{T\,\max} = \frac{E_{\text{CM}}}{2}$;

2. Generate the emission's rapidity uniformly using one random number, $\mathcal{R}_i$. Generate the transverse momentum using another random number, $\mathcal{R}_j$, and the bounding functions in equation 6.25 as specified in step 2 of the bivariant veto algorithm of section A.6. This gives

$$y_k = y_{k\,\min} + \mathcal{R}_i \left(y_{k\,\max} - y_{k\,\min}\right)$$
$$p_{T,\,i+1} = \left(\frac{1}{p_{T,\,i}} - \frac{1}{c_{ab}\left(y_{k\,\max} - y_{k\,\min}\right)} \log \mathcal{R}_j \,.\right)^{-1}$$

3. If $p_T < p_{T\,\min}$ do not generate any hard emission.

4. For another random number, $\mathcal{R}_k$, and the generated transverse momentum, $p_{T,\,i+1}$, if

$$\mathcal{R}_k < \frac{W_{ab}}{b_1(p_{T,\,i+1})}$$

accept and insert the emission. Otherwise return to step 2 using the rejected scale as the input scale for the next iteration.

This algorithm consistently inserts the hardest emission generated from the NLO amplitude real emission kernel in equation 6.22.

This emission from the fixed-order matrix element along with the locally NLO-normalised configuration, $\overline{B}$, from equation 6.19 together complete the POWHEG matching of the NLO QCD corrections to Drell-Yan Z' production and the HERWIG++ parton shower.

6.2 Slepton Pair Production POWHEG Implementation

In this section we describe the POWHEG implementation of the matching of the NLO SQCD corrections to Drell-Yan slepton pair production within HERWIG++, giving event generation accurate to NLO for observables inclusive in jets.

6.2.1 Next-to-Leading Order Supersymmetric Quantum Chromodynamics Corrections

The NLO SQCD corrections to Drell-Yan slepton pair production are known [210] and arise from the contributions shown in figure 6.1.

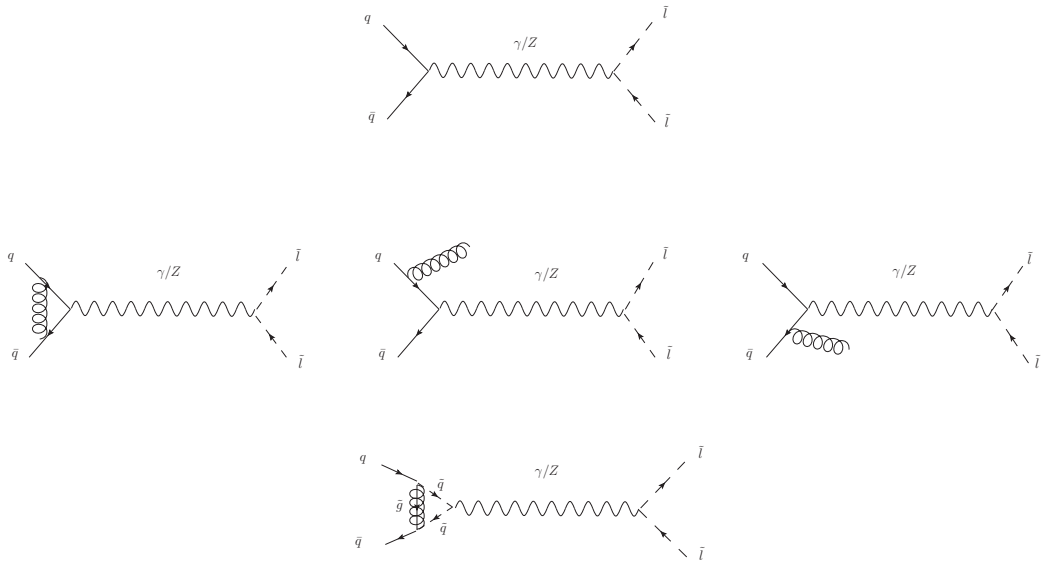

Figure 6.1: The LO (first row), NLO QCD (second row), and NLO SQCD (bottom row) radiative corrections to Drell-Yan slepton pair production. Together they form the full set of NLO SQCD corrections.

For our implementation the Born and real emission contributions were generated numerically within HERWIG++ by ThePEG's built-in helicity library. The virtual contribution, which is of the form[5]

$$2\,\mathrm{Re}\left[\mathcal{V}_{\mathrm{SQCD}}\,\mathcal{B}^{*}\right], \tag{6.26}$$

however can be more difficult to generate and will generally require the use of an external, specialised software package such as OPENLOOPS, GOLEM, LOOPTOOLS or MADLOOP. For our implementation we use the original result of Beenakker et al. [210], as coded in `X_matrix_ll_v.f` in the PROSPINO2 distribution.

[5]Here each of the virtual contributions denotes the (unsquared) amplitude of the vertex corrections shown in figure 6.1, such that the overall virtual contribution after multiplying by the Born amplitude is of order $\mathcal{O}(\alpha_S)$ as required at NLO, and not higher.

Their lengthy expression for the virtual contribution reduces to[6]

$$
\begin{aligned}
2\,\mathrm{Re}\left[\mathcal{V}_{\mathrm{SQCD}}\,\mathcal{B}^{*}\right]\Big|_{\mathrm{finite}} = \Bigg[& \frac{2\pi^2}{3} \;-\; 1 \;-\; 3\,\log\left(\frac{s}{\langle m_{\tilde{l}}\rangle^2}\right) \;+\; \log^2\left(\frac{s}{\langle m_{\tilde{l}}\rangle^2}\right) \;-\; \log^2\left(\frac{s}{\mu_R^2}\right) \\
& + \left(1 + 2\frac{m_{\tilde{g}}^2 - m_{\tilde{q}}^2}{s}\right)\left(B_0(s, m_{\tilde{q}}, m_{\tilde{q}}, \mu_R^2) \;-\; B_0(0, m_{\tilde{g}}, m_{\tilde{q}}, \mu_R^2)\right) \\
& - \; 3B_0(s, 0, 0, \mu_R^2) \;-\; (m_{\tilde{g}}^2 - m_{\tilde{q}}^2)\, B_{0\,P}(0, m_{\tilde{g}}, m_{\tilde{q}}, \mu_R^2) \\
& + \; 2\,\mathrm{Re}(C_0(\delta, \delta, s, m_{\tilde{q}}, m_{\tilde{g}}, m_{\tilde{q}}))\left(\frac{(m_{\tilde{q}}^2 - m_{\tilde{g}}^2)^2}{s^2} + m_{\tilde{g}}^2\right)\Bigg]\,\mathcal{B}\,, \qquad (6.27)
\end{aligned}
$$

where $\langle m_{\tilde{l}}\rangle = (m_{\tilde{l}_1} + m_{\tilde{l}_2})/2$ is the average mass of the final state sleptons, μ_R is the renormalisation scale and the B_0, $B_{0\,P}$ and C_0 are the analytic forms of scalar (no Lorentz index structure) integrals resulting from the Passarino-Veltman tensor reduction of loop diagrams with two (B_0) and three (C_0) internal legs, respectively. The parameter δ corresponds to an infrared numerical cutoff on the C_0 function (which was set to $0.1\ \mathrm{MeV}^2$ for all runs). The parameter $m_{\tilde{q}}$ denotes the average squark mass for all active flavours,

$$
m_{\tilde{q}} = \frac{1}{2\,n_f}\sum_{i=1}^{n_f}\left(m_{\tilde{q}_{L\,f}} \;+\; m_{\tilde{q}_{R\,f}}\right)\,. \qquad (6.28)
$$

For large slepton masses the (higher-order) vector boson fusion (VBF) channel may the dominant production channel [211] however we do not consider this channel and focus on Drell-Yan type production which is dominant and most relevant for initial LHC searches.

6.2.2 POWHEG Implementation

Generation of the $\overline{B}$ Function

The generation of the n-body, NLO-normalised POWHEG $\overline{B}$ function proceeds as follows:

1. A Born configuration is generated by ThePEG and its weight is computed.
2. Given this Born weight the corresponding finite virtual weight can be computed from equation 6.27.
3. The calculation of the collinear remnants requires the Born weight already obtained, as well as an integration over the collinear splitting momentum fraction, z. The collinear remnant functions peak at $z = 1$ such that a function of the form

$$
b(z) = \frac{1}{(1-z)^{\nu}}\,,
$$

(where $\nu \in [0, 1]$ is a constant whose value can be chosen to improve the efficiency[7]) can be used to generate values of z efficiently and used to perform the integration by importance sampling as set out

[6] The required factor of $1/2$ to account for the symmetry of the final state is already included here.
[7] We set $\nu = 0.6$ by default.

in appendix A.3. Generating points according to this bounding function as

$$\begin{aligned} z_i &= B^{-1}\left[B(z_{\min}) \;+\; \mathcal{R}_i\;(B(z_{\max}) \;-\; B(z_{\min}))\right] \\ &= 1 \;-\; \left[\mathcal{R}_i\,(1 \;-\; z_{\max})^{1-\nu} \;+\; (1 \;-\; \mathcal{R}_i)(1 \;-\; z_{\min})^{1-\nu}\right]^{\frac{1}{1-\nu}} \;. \end{aligned} \tag{6.29}$$

where $\mathcal{R}_i$ is a random number. Noting that $z_{\max} = 1$, replacing $(1 - \mathcal{R}) \to \mathcal{R}$ and defining $\rho = 1 - z$ such that $\rho_{\max} = 1 - z_{\min}$ gives

$$z_i = 1 \;-\; \left[\mathcal{R}_i\,\rho_{\max}\right]^{\frac{1}{1-\nu}} \;. \tag{6.30}$$

Sampling and accepting or rejecting 100 points (values of z) for each phase space point the collinear remnant contribution is thus obtained[8].

4. The real emission configurations from figure 6.1 have been coded so that these are numerically generated by ThePEG using the HELAS method. A real emission configuration with its corresponding weight is generated in this way.

   Flavour and colour configurations (in the leading colour approximation for gluons) are automatically assigned by ThePEG with probability

$$p_{\{f_i\},\{c_i\}} = \frac{\left|\mathcal{M}_{\{f_i\},\{c_i\}}\right|^2}{\sum_j \left|\mathcal{M}_{\{f_j\},\{c_j\}}\right|^2} \,. \tag{6.31}$$

5. Perform the dipole kinematic mapping on the final-state momenta of the real emission configuration as defined in equation 3.113. This is done by computing the two incoming and the emitted partons' momenta (which together fully specify the kinematics by momentum conservation) in the hadronic centre-of-mass frame where they can be computed simply as

$$\begin{aligned} p_a &= \left(\frac{1}{2}\sqrt{s}\,\frac{x_a}{z},\; 0,\; 0,\; \frac{1}{2}\sqrt{s}\,\frac{x_a}{z}\right) \\ p_b &= \left(\frac{1}{2}\sqrt{s}\,x_b,\; 0,\; 0,\; -\frac{1}{2}\sqrt{s}\,x_b\right) \\ p_k &= (p_T\cosh y,\; p_T\,\cos\phi,\; p_T\,\sin\phi,\; p_T\sinh y) \end{aligned} \tag{6.32}$$

   where the emission is here assumed to be from parton a (analogous expressions for emission from parton b hold) and all 4-momenta are on shell.

   The transverse momentum is computed as

$$p_T \;=\; \sqrt{\frac{s}{z}\,(1-z)^2\,y\,(1-y)} \;=\; \sqrt{\frac{s}{z}\,\tilde{v}\,(1-\tilde{v}-z)}\,, \tag{6.33}$$

[8] The number of sampled points used to estimate the collinear remnant, n_{coll}, can be increased to improve accuracy but such an increase will increase the computational requirements of the generation of an n-event sample (and hence also the required computation time) as n^n_{coll} and is therefore undesirable.

where we have used the kinematic variables defined in equations 3.35, 3.36, 3.37, the transverse momentum as defined in equation 4.14, and we have defined the variable $\tilde{v} = y\,(1-z)$.

The rapidity in this frame is likewise given (from the definition $x_{a,b} = \sqrt{\frac{p^2}{s}}\,e^{\pm y}$ and the relations 4.16 and 4.17) as

$$y_k \;=\; \log\left(\tilde{v}\,x_a\,\frac{\sqrt{s}}{p_T}\right) \;=\; -\log\left(\tilde{v}\,x_b\,\frac{\sqrt{s}}{p_T}\right). \tag{6.34}$$

The dipole kinematic mapping on the final-state momenta is then applied according to equation 3.113 and the resulting momenta are boosted to the lab frame, and the initial-state momentum mapping (equation 3.110) is also performed.

6. Perform the dipole subtraction using the momenta just computed, using equations 3.118a, 3.119a and 3.118b, 3.119b for $q(\bar{q}) \to g\,q(\bar{q})$ and $g \to q\,\bar{q}$ hard initial-state splittings, respectively.

   This must be done respecting the POWHEG separation of the real emission contribution into regions where only a single dipole is required, as described by equation 5.46.

   Furthermore, a *suppression function* of the form[9]

$$\begin{aligned}\mathcal{R} \;&=\; \frac{\Lambda^2}{p_T^2+\Lambda^2}\,\mathcal{R} \quad + \quad \frac{p_T^2}{p_T^2+\Lambda^2}\,\mathcal{R}\,,\\ &=\quad \mathcal{R}_S \quad + \quad \mathcal{R}_F\,,\end{aligned} \tag{6.35}$$

   is introduced to separate the real emission contribution into the IR-singular low transverse momentum $\left(\frac{p_T^2}{\Lambda^2} \ll 1\right)$ region, R_S, and the finite high transverse momentum $\left(\frac{\Lambda^2}{p_T^2} \ll 1\right)$ region, R_F. This is done for reasons which relate to which contributions one wishes to include (or rather, not include) in the POWHEG Sudakov to be exponentiated and resummed.

   The dipole subtraction is therefore performed as

$$\begin{aligned}\mathcal{R}_{S,\,\alpha}^{\text{finite}} &= \frac{|\mathcal{D}_\alpha|}{\sum_\alpha |\mathcal{D}_\alpha|}\,\frac{\Lambda^2}{p_T^2+\Lambda^2}\,\mathcal{R} \;-\; \mathcal{D}_\alpha\,\mathcal{B}\,,\\ &= \mathcal{R}_{S,\,\alpha} \;-\; \mathcal{D}_\alpha\,\mathcal{B}\,,\end{aligned} \tag{6.36}$$

   with $\alpha = \{qg,\, gq,\, \bar{q}g,\, g\bar{q}\}$ chosen as relevant for the configuration at hand, and the sum over all relevant dipoles and flavour configurations giving the full dipole-subtracted finite contribution from R_S,

$$R_S^{\text{finite}} = \sum_\alpha \mathcal{R}_{S,\,\alpha}^{\text{finite}}\,. \tag{6.37}$$

[9] By default the standard POWHEG approach was used, with $\Lambda^2 \to \infty$ such that the entire real emission contribution is exponentiated.

The finite part of the real emission contribution is similarly divided as

$$\mathcal{R}_F \;=\; \sum_\alpha \mathcal{R}_{F,\,\alpha} \;=\; \sum_\alpha \frac{|\mathcal{D}_\alpha|}{\sum_\alpha |\mathcal{D}_\alpha|}\,\frac{p_T^2}{p_T^2+\Lambda^2}\,\mathcal{R}\,. \tag{6.38}$$

7. Compute the required luminosity functions. These include the ones with Born kinematics

$$\overline{\mathcal{L}}(\bar{x}_a,\;\bar{x}_b;\;\mu_F) = f_a(\bar{x}_a,\;\mu_F)\,f_b(\bar{x}_b,\;\mu_F)\,, \tag{6.39}$$

the ones with with real emission kinematics,

$$\mathcal{L}\,(x_a,\;x_b;\;\mu_F) = f_a\,(x_a,\;\mu_F)\;f_b(x_b,\;\mu_F)\,, \tag{6.40}$$

and the ones with collinear remnant kinematics as defined in equation 3.134[10],

$$\tilde{\mathcal{L}}_a\left(\frac{x_a}{z},\;x_b;\;\mu_F\right) = f_a\left(\frac{x_a}{z},\;\mu_F\right)\;f_b(x_b,\;\mu_F)\,. \tag{6.41}$$

All contributions to the cross section are in fact initially computed using the Born kinematics luminosity function, $\overline{\mathcal{L}}$, and are subsequently multiplied by the luminosity weight $\frac{\mathcal{L}'}{\overline{\mathcal{L}}}$, where $\mathcal{L}'$ is the desired luminosity function for that contribution.

8. All the ingredients of the NLO-accurate amplitude have now been obtained and the $\overline{B}$ can be computed using equation 5.51 as

$$\overline{B} \;=\; \overline{\mathcal{L}}\,\mathcal{B} \;+\; \overline{\mathcal{L}}\,[\mathcal{V} \;+\; I(\epsilon)] \tag{6.42}$$
$$+\;\left[\int d\mathbf{\Phi}_1 \sum_\alpha \mathcal{L}\;[(\mathcal{R}_{S,\,\alpha} \;-\; \mathcal{D}_\alpha\,\mathcal{B}) \;+\; R_{F,\,\alpha}] \;+\; \int \frac{dz}{z}\sum_{ai,\,b}[\tilde{\mathcal{L}}_a\,\mathcal{G}_a^{ai,\,b}(z) \;+\; \tilde{\mathcal{L}}_b\,\mathcal{G}_b^{bi,\,a}(z)]\,\mathcal{B}\right]^{\overline{\mathbf{\Phi}}_n=\mathbf{\Phi}_n}\,,$$

where $[\mathcal{V} \;+\; I(\epsilon)]$ is given by equation 6.27, the dipoles $\mathcal{D}_\alpha$ are given by equations 3.118a-3.119b, the collinear remnants $\int \frac{dz}{z}\,\tilde{\mathcal{L}}_a\mathcal{G}_a^{ai,\,b}(z)$ are given by equations 3.143 and 3.144, and the Born and real emission configurations are generated numerically by ThePEG.

Generation of the Hardest Emission

Given the $\overline{B}$ function which provides the NLO normalisation, it remains to generate the hardest emission accurately from the NLO amplitude (though it must be emphasised that any observable dependent on the hardest emission itself is only accurate to LO).

This emission is generated using the NLO contributions computed in the previous section to construct the

[10] That for emission from parton a shown, similar expression for parton b holds.

POWHEG Sudakov (using equations 5.14 and 5.52) as

$$\Delta(p_T) = \exp\left\{ -\int_{t_0}^{S/4} \sum_{\alpha} \frac{f_{\widetilde{ai}}(x/z,\, Q^2 + p_T^2)}{z\, f_a(x,\, \mu_F^2)} \frac{\left[R_{S,\,\alpha}\, \Theta(k_T(\mathbf{\Phi}_{n+1}) - p_T^{\min})\, d\mathbf{\Phi}_1\right]^{\overline{\mathbf{\Phi}}_n = \mathbf{\Phi}_n}}{B} \right\}, \tag{6.43}$$

where S is the hadronic centre-of-mass energy, and $t_0 \approx 2^2\,\mathrm{GeV}^2$.

The bivariant veto algorithm is then applied to generate the hardest emission's scale in the shower, as well as its transverse momentum and rapidity (with its azimuthal angle being generated uniformly).

The procedure to achieve this as as follows:

While $p_T > p_T^{\min}$,

1. Compute the total high-p_T (finite) real emission weight

$$\mathcal{R}_F \;=\; \mathcal{R}_F^{qg,\,q} \;+\; \mathcal{R}_F^{\bar{q}g,\,\bar{q}} \;+\; \mathcal{R}_F^{gq,\,q} \;+\; \mathcal{R}_F^{g\bar{q},\,\bar{q}}\,. \tag{6.44}$$

2. Generate a random number, r_i, and if

$$r_i \;<\; \frac{\mathcal{R}_F}{\mathcal{B} \;+\; \mathcal{R}_F}\,, \tag{6.45}$$

   generate a hard emission. If this condition is not met proceed to generate the event without any hard emission.

3. Select the channel of the hardest emission by competition (the highest-bid method described in section A.6). Generate another random number, r_j. For the emission channels of $\mathcal{R}_F$, if the weight of the first channel satisfies

$$\mathcal{R}_F^{ai,\,b} \;\geqslant\; r_j\, \mathcal{R}_F\,, \tag{6.46}$$

   select this channel for the hard emission.

   Otherwise subtract this channel's weight from the right-hand side and test the next channel,

$$\mathcal{R}_F^{a'i',\,b'} \;\geqslant\; (r_j\, \mathcal{R}_F \;-\; \mathcal{R}_F^{ai,\,b})\,, \tag{6.47}$$

   if this assertion holds select the channel $a'i'$, b'. Repeat until a channel is selected.

Once the emission channel is selected its radiative variables $(p_T,\, y_k,\, \phi)$ can be generated from the POWHEG Sudakov as follows:

1. Set the phase space for the emission to be rectangular, within the ranges

$$p_T^{\min} \;<\; p_T \;<\; p_T^{\max}\,, \qquad\qquad y_k^{\min} \;<\; y_k \;<\; y_k^{\max}\,, \tag{6.48}$$

   where $p_T^{\min}$ is the cut chosen to define resolvable emission, $p_T^{\max}$ is set to the maximum kinematically allowed value $p_T^{\max} = \frac{\sqrt{S}}{2}$, and the rapidity limits are set symmetrically to $(y_k^{\min},\, y_k^{\max}) = (-10,\, 10)$.

2. Set the initial trial value of the transverse momentum to the maximum value,

$$p_{T\,\text{initial}} = p_T^{\max} = \frac{\sqrt{S}}{2}\,, \tag{6.49}$$

where $\sqrt{S}$ is the hadronic centre-of-mass energy.

3. Generate a transverse momentum as[11]

$$p_{T,\,i+1} = p_{T,\,i}\; r^{\frac{1}{k_{ab}}}\,, \tag{6.51}$$

and the emission's rapidity and azimuthal angle uniformly as

$$y_k \;=\; y_k^{\min} \;+\; r'\,(y_k^{\max} \;-\; y_k^{\min})\,, \tag{6.52}$$

$$\phi \;= 2\pi\, r'' \tag{6.53}$$

where we have defined $k_{ab} = \frac{\alpha_S^{\max}}{2\pi}\, C_{ab}\,(y_k^{\max} \;-\; y_k^{\min})$, the prefactors were set as $C_{q\bar{q}} = 5\,\text{GeV},$, $C_{qg} = C_{\bar{q}g} = 3\,\text{GeV}$, and r, r', r'' are random numbers.

4. Generate a real emission configuration by attaching this emission to an underlying Born configuration generated by ThePEG.

5. Convert the transverse momentum and rapidity to shower variables to give

$$\tilde{v} = \frac{p_T}{\sqrt{s}}\,\frac{1}{x_a}\,e^{y} \tag{6.54}$$

$$z = \frac{1 \;-\; \frac{p_T}{\sqrt{s}}\,\frac{1}{x_a}\,e^{y}}{1 \;+\; \frac{p_T}{\sqrt{s}}\,\frac{1}{x_b}\,e^{-y}} \tag{6.55}$$

for emission from parton a, and similarly with the replacements $y \leftrightarrow -y,\; x_a \leftrightarrow x_b$ for emission from parton b.

6. Compute the required kinematic configuration by rescaling the incoming emitting momentum by a factor $1/z$, and computing the emission's 4-momentum using equation 6.33.

7. Perform the dipole kinematic mapping from equations 3.110 and 3.113 as well as the separation into dipole regions and singular and finite regions from equations 5.46 and 6.35, but do not perform the dipole subtraction[12]. After dividing by the Born contribution this gives the weight of the emission event

[11] Use the bivariant veto algorithm set out in section A.6 with the bounding functions

$$b_1(p_T) \;=\; \frac{\alpha_S^{\max}}{2\pi}\,\frac{C_{ab}}{p_T}\,, \tag{6.50a}$$

$$b_2(y) \;=\; 1\,, \tag{6.50b}$$

where $\alpha_S^{\max}$ is a fixed value of α_S which provides an overestimate of the running α_S used to generate the hardest emission, and C_{ab} is constant used to ensure the bounding function lies above the integrand for each specific channel ab.Note that the bounding function over the rapidity is chosen to be flat and set to unity for simplicity, but its normalisation is implicitly also set and manually adjusted by the prefactor C_{ab} as both bounding functions always appear multiplied together in the algorithm.

[12] The singularity structure from the Sudakov kernel must be preserved, as it yields the required logarithmic structure of the shower and is finite with the imposition of the the $p_T^{\min}$ constraint seen explicitly as the step function in equation 5.52.

as generated by the veto algorithm from the second term of the POWHEG relation (equation 5.45).

8. Backwards evolution of the shower as required here for initial-state splittings requires a re-weighting to restore the shower evolution's consistency with the DGLAP equation (see equation 5.14), consistency which was shown in section 4.8 for final-state showers. More specifically, equation 4.50 holds for final- and initial-state showers alike, however if backwards evolution is to be used, at the hard interaction the PDF factor of $f_a(x, Q^2)$ already includes the DGLAP resummation of logarithms from from the lower scale Q_0^2 up to the hard scale Q^2. This evolution must be step-wise reversed as the parton shower will now be performing this evolution, and this is achieved via the re-weighting factor we effectively introduce in the Sudakov here. The weight generated in the previous step must therefore be re-weighted by a PDF-dependent factor[13]

$$\frac{f_{\widetilde{ai}}(x/z,\, \mu_F^2)}{z\, f_a(x,\, \mu_F^2)}\,. \tag{6.56}$$

A further rescaling of the factorisation scale from a fixed scale to a dynamical scale governed by the hardness of the emission can be used, as

$$\frac{f_{\widetilde{ai}}(x/z,\, Q^2+p_T^2)}{z\, f_a(x,\, \mu_F^2)}\,, \tag{6.57}$$

where $\widetilde{ai}$ denotes the emitter.

This turns the factorisation scale into a dynamical scale[14], $\mu_F^2 = Q^2 + p_T^2$ and shifts logarithms of the form $\alpha_S \log\left(\frac{Q^2}{\mu_F^2}\right)$ which arise for each emission (as derived in equation 4.1), and $\alpha_S \log\left(\frac{g(Q^2,\, p_T^2)}{\mu_F^2}\right)$ for multiple emissions to the form $\alpha_S \log\left(\frac{g(Q^2,\, p_T^2)}{Q^2+p_T^2}\right)$. This form of scale-setting better reflects the multi-scale (Q^2, p_T^2) nature of the process once multiple emissions are included and is expected to lead to improved control of large logarithms and smaller scale variation.

9. Using the PDF-dependent factor just computed and the momenta (after the dipole kinematic mapping) computed from the emission variables for the selected emission process, accept the emission if

$$\frac{f_{\widetilde{ai}}(x/z,\, Q^2+p_T^2)}{z\, f_a(x,\, \mu_F^2)}\, \frac{\mathcal{R}_{S,\,\alpha}^{ai,\,b}(p_T,\, y_k,\, \phi)}{\mathcal{B}} \;<\; r'''\,, \tag{6.58}$$

where r''' is yet another random number. Otherwise return to step 2 using the rejected p_T as input into the new iteration. Repeat until either an emission is generated, or $p_T < p_T^{\min}$, where $p_T^{\min}$ is the threshold chosen for resolvable emission ($p_T^{\min} = 2\,\mathrm{GeV}$ was used throughout).

Inserting this emission into the standard HERWIG++ shower as detailed in section 5.3.2 then yields the completes the insertion of the fixed-order hardest emission into the shower (the terms in square brackets

[13] See the discussion around equation 1.122 of [204] for a derivation of this result.
[14] Where Q^2 is the hard-interaction scale of a Born process with a single scale.

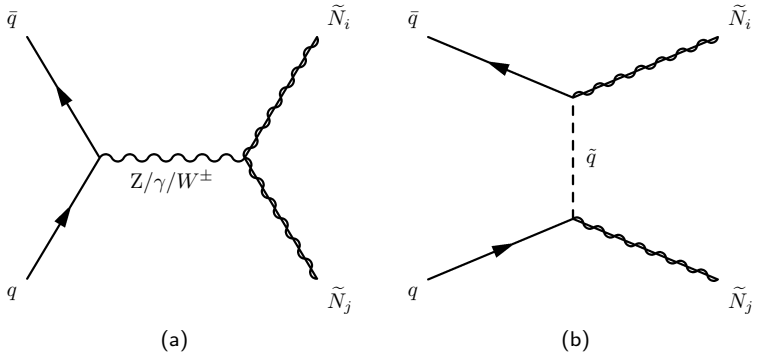

Figure 6.2: The leading-order contributions to gaugino pair production.

in equation 5.45) and together with the NLO-accurate normalisation from the $\overline{B}$ function constructed in section 6.2.2 completes the implementation of the POWHEG method and the NLO+LL matching.

6.3 Gaugino Pair Production POWHEG Implementation

In this section we present the NLO corrections to gaugino pair production, the issues they present regarding the presence of resonant states within them, the on-shell contributions from these, and the complications arising from the necessary introduction of the resonant state's width. Following these the method by which the POWHEG implementation was carried out is presented.

6.3.1 Next-to-Leading Order Supersymmetric Quantum Chromodynamics Corrections

The SQCD NLO corrections to gauginos are long known [210] and have been implemented in PROSPINO2 which computes the corresponding total inclusive cross section. There are some subtleties involved in consistently regularising SUSY radiative corrections without explicitly (non-softly) breaking SUSY in the process, we discuss these in appendix B.2 but we will not give much attention to them as we do not perform any such computation and these issues have properly been accounted for in the PROSPINO2 results we use.

The leading-order gaugino pair production diagrams at a hadron collider are shown in figure 6.2. The one-loop diagrams which form the virtual contribution term as $2\mathrm{Re}(\mathcal{V}\mathcal{B}^*)$ are shown in figure 6.3.

The $q\bar{q}$ real emission diagrams are shown in figure 6.4, where it is understood that the qg and $\bar{q}g$ initial-state contributions obtained from these diagrams via crossing symmetry are included as well[15].

[15]Though the amplitudes obtained by crossing are identical to the original ones they require convolution with different PDFs and hence give different hadronic rates, as well as giving rise to new potentially resonant configurations which require special

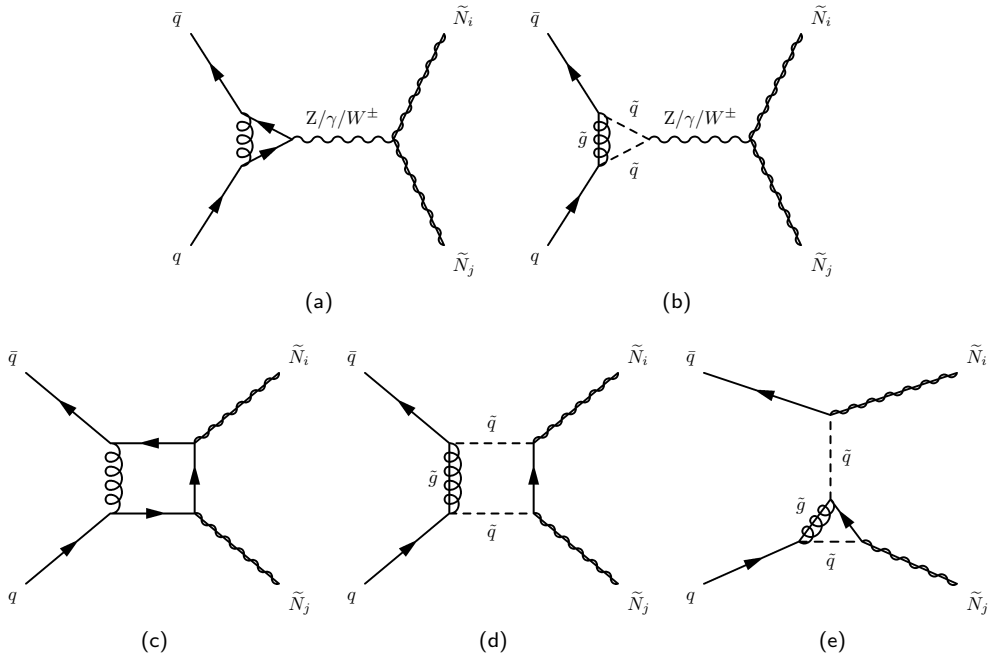

Figure 6.3: The virtual one-loop radiative corrections to gaugino pair production.

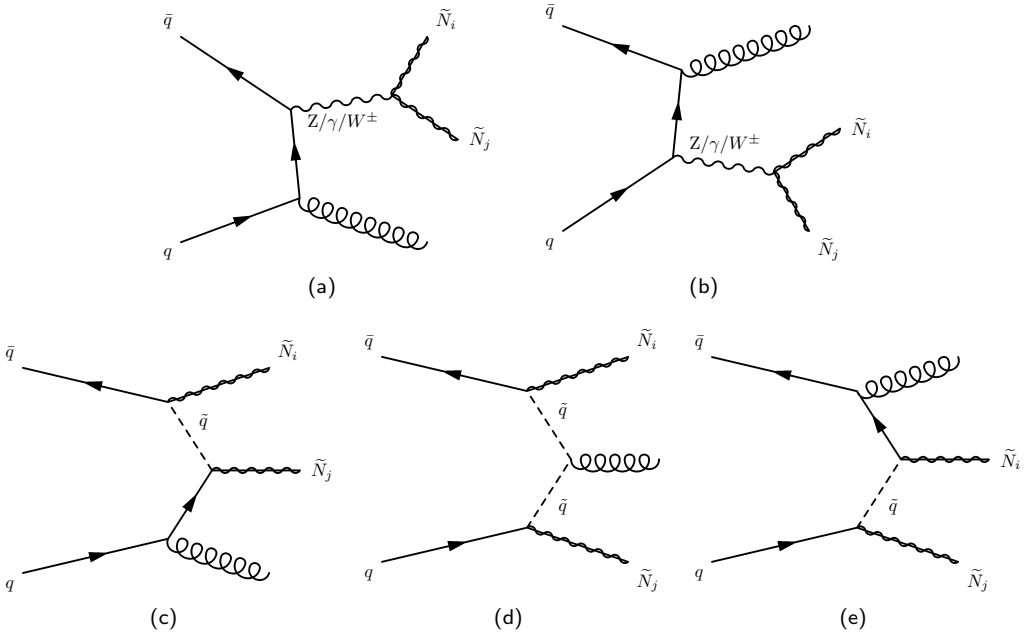

Figure 6.4: The real emission contribution to NLO gaugino pair production.

We have shown only the neutralino pair production diagrams but diagrams with $\widetilde{C}_i^{\pm}\,\widetilde{C}_j^{\mp}$ and $\widetilde{C}_i^{\pm}\,\widetilde{N}_j^{0}$ final states are identical and understood to be included as well. Configurations with the final state gauginos swapped and symmetry factors of $1/2$ for identical pairs in the final state are understood as well.

Note that for all the Drell-Yan-type diagrams there is in principle a contribution with an s-channel Higgs which must be included. However given that we deal with light-quarks only (as the non-valence heavy quark contribution is heavily PDF-suppressed) and the Higgs couplings are proportional to the mass of the fermion they couple to, the contribution from these diagrams should be negligible. Nonetheless it has been included in other studies [212].

Within the PROSPINO2 distribution the analytic forms for the real emission and virtual contributions are contained in `X_matrix_nn_r.f` and `X_matrix_nn_v.f` respectively, and it is the latter from which we take the required one-loop contribution to our POWHEG implementation. The real emission contribution we generate numerically using ThePEG's built-in HELAS helicity amplitude libraries.

6.3.2 The Treatment of Resonant Diagrams

When computing the rate for gaugino pair production at NLO one must sum over all possible incoming parton configurations as indicated in definition of hadron-level cross sections via the factorisation theorem (equation 2.22). This includes qg and $\bar{q}g$ initial-state configurations as shown in figure 6.5 obtained from the real emission contributions (figure 6.4) by crossing symmetry.

attention. We will deal with these in the next section.

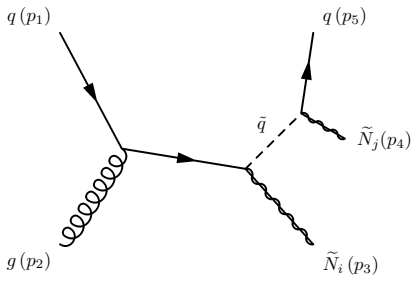

(a) Resonant qg initial-state diagram 1.

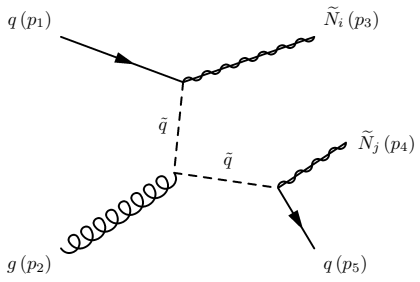

(b) Resonant qg initial-state diagram 2.

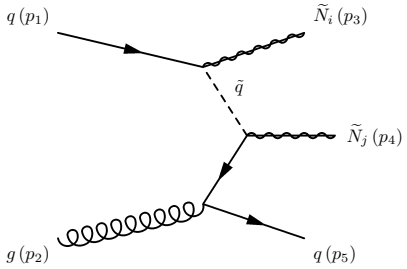

(c) Non-resonant qg initial-state diagram.

Figure 6.5: The $q(\bar{q})g$ initial-state contributions to real emission. This subset of diagrams includes two diagrams with resonant regions, (a) and (b), as well as a non-resonant contribution, (c), which will not necessarily be negligible in the resonant regions.

These diagrams form a gauge-invariant subset of the total amplitude and two of the diagrams, (a) and (b), include an internal squark line attached to two on-shell external legs at one end, hence allowing for kinematic configurations where $p_{\tilde{q}}^2 \sim m_{\tilde{q}}^2$ and the squark can be resonant.

Explicitly, using the labelling in figure 6.5, in the kinematic region[16]

$$\begin{aligned} \sqrt{s} \;&\geq\; m_{\widetilde{N}_i} \;+\; m_{\tilde{q}}\,, \\ p_{\tilde{q}}^2 \;&\geq\; m_{\widetilde{N}_j}^2 \;+\; m_q^2\,, \end{aligned} \tag{6.59}$$

a resonant contribution to the qg and $\bar{q}g$ initial-state amplitude exists. The permutation $m_{\widetilde{N}_i} \leftrightarrow m_{\widetilde{N}_j}$ and the resonant regions around both left- and right-handed squark masses must be considered, or a single average squark mass defined as in equation 6.28 may be used. We consistently consider all the individual flavour and left- and right-handed squark masses.

These resonant contributions present a problem for several reasons:

- if squark widths are not included the squark propagators become singular in the on-shell regions, such

[16]We include the quark mass term for completeness but we always work with massless quarks.

that the width must be included;

- however including the width is formally incorrect for spacelike propagators (that is, for the non-resonant t- or u-channel squark propagators) which cannot go on mass shell, and may also potentially break gauge invariance;
- even if the widths can be inserted to render the resonant regions finite and this is done without violating gauge invariance, the resonant regions give large contributions which may be of the order of the Born contribution or larger, bringing into question the validity of the entire perturbative expansion.

These issues are symptomatic of the inherent ambiguities and unresolved issues in dealing with unstable particles in QFT, from the inapplicability of the Lehmann-Symanzik-Zimmermann (LSZ) reduction formula to them as required to construct an S-matrix from correlation functions (the issue being that they are not asymptotic states)[17], through to the fact that width in different renormalisation schemes may become ill-defined or gauge-dependent beyond a given order or for particular unstable particles.

6.3.3 The Introduction of Width

The NLO radiative corrections for gaugino pair production introduce extra complications due to the fact that they contain intermediate, potentially resonant states, which introduce a divergence if their width is not included, but the inclusion of the width itself presents issues regarding gauge invariance. We must tackle these first.

Gauge Invariance

Since the diagrams shown in figure 6.5 form a (statistically, but not individually) physically distinguishable observable and are added incoherently to the total hadronic contribution (as indicated in equation 2.22) one expects they must form a gauge-invariant subset of diagrams. This is indeed the case with squark propagators of the form $1/(p_{\tilde{q}}^2 - m_{\tilde{q}}^2)$ but one must verify that the naïve introduction of width as

$$\frac{1}{p_{\tilde{q}}^2 - m_{\tilde{q}}^2} \longrightarrow \frac{1}{p_{\tilde{q}}^2 - m_{\tilde{q}}^2 + i m_{\tilde{q}} \Gamma_{\tilde{q}}}\,, \tag{6.60}$$

does not spoil the gauge invariance under the SM gauge groups which must hold order by order for physical observables to be insensitive to arbitrarily chosen gauge parameters.

[17] This is an issue when the unstable particle enters the calculation as an external leg of a diagram, such as the calculation of decay rates by multiplication of the production cross section times a branching fraction.

Width is effectively a higher order correction, it is not a parameter of the Lagrangian or the Feynman rules, which are an expansion about a free theory for stable particles. Gauge invariance (and unitarity) hold order-by-order in perturbation theory. Therefore introduction of an all-orders Dyson-resummed width comes with potential loss of gauge invariance as we are mixing radiative corrections of different orders. However we introduce it out of necessity, to turn squark singularities into resonances. We give a treatment of some of the subtleties in consistently defining and implementing unstable particle widths in appendix B.1.

The check for gauge invariance, which constitutes a non-trivial consistency check, is performed by verifying that the Ward identity

$$k_\mu \sum_i \mathcal{M}_i^\mu \;=\; 0\,, \tag{6.61}$$

holds, where $\mathcal{M}_i$ are the individual amplitudes contributing to the total amplitude and k_μ is the 4-momentum of an external boson line. Here we have obtained $\mathcal{M}^\mu$ from the total amplitude $\mathcal{M}$ by omitting a polarisation tensor for an external boson, $\epsilon_\mu(k)$ or $\epsilon^*_\mu(k)$, and this amplitude is then contracted with the boson's 4-momentum, k_μ.

For gauge invariance to hold in the presence of width this Ward identity must be verified for the diagrams in figure 6.5 with the width introduced as in equation 6.60 in all the propagators, and we prove this here[18].

As labelled in figure 6.5, diagram (a) gives an amplitude

$$\begin{aligned}\mathcal{M}_a \;&= (-1)\,\bar{u}(p_5)\,C_j\,v(p_4)\,\frac{-i}{(p_1+p_2-p_3)^2-m^2+im\Gamma}\,\bar{u}(p_3)\,C_i \\ &\quad\times\;\frac{i(\not{p}_1+\not{p}_2)}{(p_1+p_2)^2}\,(-ig_S\,t^a\,\gamma^\mu)\,\epsilon_\mu(p_2)\,u(p_1)\,,\end{aligned} \tag{6.62}$$

where the factor of -1 arises from the permutation of final-state fermions of this diagram with respect to the ordering in the other two diagrams. Here the masses and widths in propagators implicitly refer to the squark, $m = m_{\tilde{q}}$ and $\Gamma = \Gamma_{\tilde{q}}$, and C_i refer to gaugino-quark-squark couplings for gaugino $\widetilde{N}_i$, which can be found in [122] which is also where the squark-squark-gluon coupling used was taken from (figure 72a). The gaugino couplings contain no explicit momentum dependence so do not need to be written out explicitly.

Performing the replacement $\epsilon_\mu(p_2) \to p_{2\,\mu}$ to check the Ward identity for this amplitude gives

$$\mathcal{M}_a^{\text{W.I.}} \;=\; ig_S\,t^a\,\bar{u}(p_5)\,C_j\,v(p_4)\,\frac{1}{(p_1+p_2-p_3)^2-m^2+im\Gamma}\,\bar{u}(p_3)\,C_i\,\frac{(\not{p}_1+\not{p}_2)}{(p_1+p_2)^2}\,\not{p}_2\,u(p_1)\,.$$

[18] This is a crucial check as there are known cases where the gauge-invariance violation created by the introduction of width is disastrous [213]

Using the anti-commutation relation[19] of the gamma matrices $\{\gamma^\mu,\,\gamma^\nu\} = 2g^{\mu\nu}$ to derive

$$\not{p}_2^2 \,=\, 0\,, \qquad \not{p}_1\not{p}_2 \,=\, 2p_1\cdot p_2 \,-\, \not{p}_2\not{p}_1\,,$$

and the massless Dirac equation $\not{p}_1\, u(p_1) = 0$ this equation becomes

$$\mathcal{M}_a^{\rm W.I.} \;=\; i g_S\, t^a\, \bar{u}(p_5)\, C_j\, v(p_4)\, \frac{1}{(p_1+p_2-p_3)^2 - m^2 + im\Gamma}\, \bar{u}(p_3)\, C_i\, u(p_1)\,. \tag{6.63}$$

Diagram (b) gives a contribution

$$\begin{aligned}\mathcal{M}_b = \bar{u}(p_5)\, C_j\, v(p_4)\, \frac{-i}{(p_1+p_2-p_3)^2 - m^2 + im\Gamma}\; (-ig_S\, t^a\,(2p_1+p_2-2p_3)^\mu)\; \epsilon_\mu(p_2) \\ \times\; \frac{-i}{(p_1-p_3)^2 - m^2 + im\Gamma}\, \bar{u}(p_3)\, C_i\, u(p_1)\,.\end{aligned} \tag{6.64}$$

Computing the Ward identity for this term gives

$$\begin{aligned}\mathcal{M}_b^{\rm W.I.} \;&= i\, g_S\, t^a\, \bar{u}(p_5)\, C_j\, v(p_4)\, \frac{1}{(p_1+p_2-p_3)^2 \,-\, m^2 \,+\, im\Gamma}\, 2\,(p_1\cdot p_2 - p_2\cdot p_3) \\ &\quad\times \frac{1}{(p_1-p_3)^2 \,-\, m^2 \,+\, im\Gamma}\, \bar{u}(p_3)\, C_i\, u(p_1)\,.\end{aligned} \tag{6.65}$$

Lastly, diagram (c) of figure 6.5 gives

$$\mathcal{M}_c \;= \bar{u}(p_5)\,(-ig_S\, t^a\,\gamma^\mu)\,\epsilon_\mu(p_2)\, \frac{i(\not{p}_2 - \not{p}_5)}{(p_2-p_5)^2}\, C_j\, v(p_4)\, \frac{-i}{(p_1-p_3)^2 - m^2 + im\Gamma}\, \bar{u}(p_3)\, C_i\, u(p_1)\,, \tag{6.66}$$

which gives a contribution to the Ward identity of the form

$$\mathcal{M}_c^{\rm W.I.} \;=\; -\,i\, g_S\, t^a\, \bar{u}(p_5)\, \not{p}_2\, \frac{(\not{p}_2 - \not{p}_5)}{(p_2-p_5)^2}\, C_j\, v(p_4)\, \frac{1}{(p_1-p_3)^2 - m^2 + im\Gamma}\, \bar{u}(p_3)\, C_i\, u(p_1)\,.$$

Using the relations $\not{p}_2\not{p}_5 \,=\, 2p_2\cdot p_5 \,-\, \not{p}_5\not{p}_2$, the massless condition, $\not{p}_2^2 \,=\, 0$, and the massless Dirac equation, $\bar{u}(p_5)\,\not{p}_5 = 0$, this gives

$$\mathcal{M}_c^{\rm W.I.} \;=\; -\,i\, g_S\, t^a\, \bar{u}(p_5)\, C_j\, v(p_4)\, \frac{1}{(p_1-p_3)^2 - m^2 + im\Gamma}\, \bar{u}(p_3)\, C_i\, u(p_1)\,. \tag{6.67}$$

Using the partial-fraction decomposition

$$\begin{aligned}\frac{2p_1\cdot p_2 \,-\, 2p_2\cdot p_3}{[(p_1+p_2-p_3)^2 - m^2 + im\Gamma]\,[(p_1-p_3)^2 - m^2 + im\Gamma]} \;=& \\ \frac{1}{(p_1-p_3)^2 - m^2 + im\Gamma} \;-\; \frac{1}{(p_1+p_2-p_3)^2 - m^2 + im\Gamma}\,,&\end{aligned} \tag{6.68}$$

[19] In this work we use the signature $g^{\mu\nu} = \mathrm{diag}(+1,\,-1,\,-1,\,-1)$ for the metric. Use of the $(-,\,+,\,+,\,+)$ signature would lead to a minus sign in this many other relations.

the contribution from diagram (b) to the Ward identity (equation 6.65) can be rewritten as

$$\mathcal{M}_b^{\text{W.I.}} \;=\; i\, g_S\, t^a\, \bar{u}(p_5)\, C_j\, v(p_4) \left[\frac{1}{(p_1-p_3)^2 - m^2 + im\Gamma} \right. \\ \left. -\; \frac{1}{(p_1+p_2-p_3)^2 - m^2 + im\Gamma} \right] \bar{u}(p_3)\, C_i\, u(p_1)\,. \tag{6.69}$$

Here the first term can be seen to cancel the contribution from diagram (c) (equation 6.67) and the second term cancels the contribution from diagram (a) (equation 6.63). Thus the relation

$$\mathcal{M}_a^{\text{W.I.}} \;+\; \mathcal{M}_b^{\text{W.I.}} \;+\; \mathcal{M}_c^{\text{W.I.}} \;=\; 0\,, \tag{6.70}$$

holds, and completes the proof that the subset of diagrams in figure 6.5 with the width naïvely inserted in all squark propagators as defined in equation 6.60 satisfies the Ward identity in equation 6.61 and gauge invariance has therefore been preserved.

6.3.4 Treatment of On-shell Contributions

Given that the width is a correction of order $\mathcal{O}(\alpha)$

$$\frac{1}{p^2 - m^2 + im\Gamma} \;\sim\; \begin{cases} \mathcal{O}(1) & |p^2 - m^2| \;\gg\; m\Gamma\,, \\ \mathcal{O}(\alpha^{-1}) & |p^2 - m^2| \;\lessapprox\; m\Gamma\,, \end{cases} \tag{6.71}$$

the non-resonant region is of order $\mathcal{O}(\alpha)$ with respect to the resonant region, where the non-resonant region is of the same order as the Born process under consideration.

The resonant contribution can therefore be argued to belong to a perturbative expansion of a different process, of one order lower. This also gives some indication of why resonant contributions can be numerically of the order of the Born contribution thereby spoiling our perturbative expansion. Both of these arguments indicate that the resonant contributions must be removed and included in a separate perturbative series.

This series is naturally defined by the the one where the potentially resonant on-shell legs are defined to be the final state, in our case by defining squark-gaugino pair production to be the desired final state. A separate simulation for such a final state must be included for realistic event simulation for a SUSY search, and since the Born contribution to this final state will be precisely the on-shell resonant contribution which must be subtracted from the NLO gaugino pair production perturbative series, such a subtraction must be performed to avoid double-counting.

To achieve this so-called *on-shell subtraction* requires the resonant contributions to be removed from the perturbative expansion, either by subtracting the exactly on-shell contribution from phase space points

above the squark-neutralino threshold *(diagram subtraction)*, or by omitting the potentially resonant diagrams altogether *(diagram removal)*.

The contribution from the potentially resonant $q(\bar{q})g$ initial-state diagrams of figure 6.5 has the form

$$\left|\mathcal{M}_{qg\to\widetilde{N}_i\widetilde{N}_j q}\right|^2 = |\mathcal{M}_{\rm res}|^2 \;+\; 2\,{\rm Re}\left(\mathcal{M}_{\rm res}\mathcal{M}^*_{\rm non-res}\right) \;+\; |\mathcal{M}_{\rm non-res}|^2 \;, \tag{6.72}$$

where with the diagram labelling from figure 6.5, $\mathcal{M}_{\rm res} = \mathcal{M}_{(a)} + \mathcal{M}_{(b)}$ are the resonant diagrams, and $\mathcal{M}_{\rm non-res} = \mathcal{M}_{(c)}$ is the non-resonant one.

In this context the diagram subtraction scheme can be schematically defined as

$$\left|\mathcal{M}_{qg\to\widetilde{N}_i\widetilde{N}_j q}\right|^2_{\rm DS} = \left(|\mathcal{M}_{\rm res}|^2 \;+\; 2\,{\rm Re}\left(\mathcal{M}_{\rm res}\mathcal{M}^*_{\rm non-res}\right) \;+\; |\mathcal{M}_{\rm non-res}|^2\right) \;-\; \left|\mathcal{M}_{\rm res}(\widetilde{\phi})\right|^2 \;, \tag{6.73}$$

where $\widetilde{\phi}$ denotes that the phase space is mapped to the on-shell region by a suitable kinematic mapping.

The diagram removal scheme can be similarly defined as

$$\left|\mathcal{M}_{qg\to\widetilde{N}_i\widetilde{N}_j q}\right|^2_{\rm DR} \;=\; \begin{cases} 2\,{\rm Re}\left(\mathcal{M}_{\rm res}\mathcal{M}^*_{\rm non-res}\right) \;+\; |\mathcal{M}_{\rm non-res}|^2 \;, \\ |\mathcal{M}_{\rm non-res}|^2 \;, \end{cases} \tag{6.74}$$

where there is the option of removing just the resonant diagrams, or removing them and their interference with the non-resonant diagrams as well.

The stronger form of diagram removal which removes all diagrams except the purely non-resonant ones has the disadvantage of neglecting the interference of the resonant and the non-resonant diagrams, which would not be double-counted by the squark-neutralino pair event generation and which there is no reason to remove, except for added simplicity of implementation (this interference contribution would have to be put in by hand in the squark-neutralino process if it is to be accounted for, or one can choose to recklessly neglect it altogether).

However, whichever form diagram removal takes, arbitrarily omitting diagrams from a gauge invariant subset will spoil the gauge invariance we have fought to preserve and can in principle lead to arbitrary, meaningless results. The trade-off for this is a significantly easier implementation and that it is considerably less computationally taxing, as it requires no kinematic mapping, subtraction, or potentially difficult phase space integration over the resonant (subtraction) region. However the consequences of violating gauge invariance and also possibly neglecting interference terms must be studied (most likely by validating against the diagram subtraction scheme) before any diagram removal implementation can be meaningfully used (this has been done for squark pair production in [5]). We therefore choose diagram subtraction over the alternatives.

The On-shell Subtraction Terms

To construct the on-shell (OS) subtraction terms we make use of the *pole approximation* (also known as *resonant scheme* [214]). In this approximation two amplitudes squared with on-shell external legs are stitched together with a Breit-Wigner propagator factor, and used with off-shell kinematics. This approximation is commonly used in studies of SM diboson production (see for example [215, 216]).

In our case this gives a contribution of the form[20]

$$\mathcal{D}^{\mathrm{OSsub}}_{i,\,j;\,\lambda} \;=\; \frac{\overline{\left|\mathcal{M}_{qg\to\widetilde{N}_i\tilde{q}_\lambda}\right|^2}\;\overline{\left|\mathcal{M}_{\tilde{q}_\lambda\to\widetilde{N}_j q}(\widetilde{\phi})\right|^2}}{(p^2_{\tilde{q}_\lambda}-m_{\tilde{q}_\lambda})^2 \;+\; m^2_{\tilde{q}_\lambda}\Gamma^2_{\tilde{q}_\lambda}}\,, \tag{6.75}$$

for squarks of handedness λ, where to obtain the total subtraction term the gaugino mass eigenstates from the production and decay process must also be swapped, and the contribution from both left- and right-handed squarks must be included,

$$\mathcal{D}^{\mathrm{OSsub}} = \left(\mathcal{D}^{\mathrm{OSsub}}_{i,\,j;\,L} \;+\; \mathcal{D}^{\mathrm{OSsub}}_{i,\,j;\,R}\right) \;+\; \left(\mathcal{D}^{\mathrm{OSsub}}_{j,\,i;\,L} \;+\; \mathcal{D}^{\mathrm{OSsub}}_{j,\,i;\,R}\right)\,. \tag{6.76}$$

This method has the advantage of encapsulating only the desired resonant contributions that need to be subtracted, at the price of using on-shell matrix elements to compute the weights of off-shell kinematic points. The kinematic conditions for the subtraction stated in equation 6.59 are now not only required for proper OS subtraction, but are also required as the on-shell amplitude used in the numerator of the OS subtraction term are ill-defined below their threshold.

Both the problem of resonant regions and the need for on-shell subtraction are in fact issues already well known from SM processes, namely single top production, where the NLO QCD corrections to single top production in the tW final-state have resonant contributions which overlap with the Born contribution of top pair production where the decay of one of the tops is considered at the matrix-element level (and therefore includes off-shell effects, the other top is left as an on-shell external leg and decayed using its branching fraction). These issues for single-top production were studied in [217–220].

Construction of the On-shell Subtraction Terms

We now compute the on-shell amplitudes required to construct the on-shell subtraction term in equation 6.75. The production contribution is given by the diagrams in figure 6.6.

[20] The bar over the amplitudes indicates that they are summed and averaged over both spin and colour.

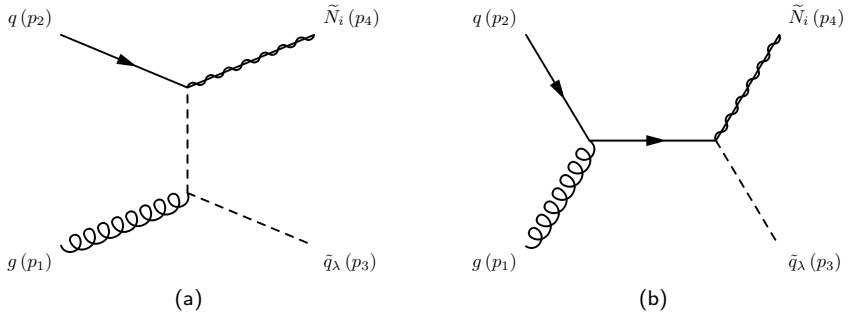

Figure 6.6: Diagrams for on-shell squark-gaugino pair production.

These diagrams give an amplitude of the form

$$i\,\mathcal{M}_{(a)} = \bar{u}(p_4)\,(ig_\lambda P_\lambda)\,u(p_2)\,\frac{i}{t_3}\,(-ig_S\,t^a)\,(2p_3 - p_1)\cdot\epsilon(p_1)\,, \tag{6.77a}$$

$$i\,\mathcal{M}_{(b)} = \bar{u}(p_4)\,(ig_\lambda P_\lambda)\,\left(\frac{i(\not{p}_1 + \not{p}_2)}{s}\right)\,(-ig_S\,t^a)\,\not{\epsilon}(p_1)\,u(p_2)\,, \tag{6.77b}$$

such that the on-shell squark-gaugino amplitude squared is given by

$$\begin{aligned}\overline{\left|\mathcal{M}_{qg\to\widetilde{N}_i\tilde{q}_\lambda}\right|^2} &= \overline{\left|\mathcal{M}_{(a)} + \mathcal{M}_{(b)}\right|^2} \\ &= \frac{1}{2}\frac{1}{N_c}\frac{1}{N_c^2-1}N_c\,\frac{N_c^2-1}{2N_c}\left\{2\,g_S^2\,|g_\lambda|^2\left[-\frac{u_4}{s} - \frac{2(m_3^2-m_4^2)}{s\,t_3}\,u_4\,\left(1+\frac{m_4}{u_4}+\frac{m_3^2}{t_3}\right)\right]\right\} \\ &= \frac{g_S^2\,|g_\lambda|^2}{2\,N_c}\,\left[-\frac{u_4}{s} - \frac{2(m_3^2-m_4^2)}{s\,t_3}\,u_4\,\left(1+\frac{m_4}{u_4}+\frac{m_3^2}{t_3}\right)\right]\,,\end{aligned} \tag{6.78}$$

where we have defined

$$s = (p_1+p_2)^2 \quad\Rightarrow\quad p_1\cdot p_2 = \frac{s}{2} \tag{6.79a}$$

$$t_3 = t - m_3^2 = (p_1-p_3)^2 - m_3^2 \quad\Rightarrow\quad p_1\cdot p_3 = -\frac{t_3}{2} \tag{6.79b}$$

$$u_4 = u - m_4^2 = (p_1-p_4)^2 - m_4^2 \quad\Rightarrow\quad p_1\cdot p_4 = -\frac{u_4}{2} \tag{6.79c}$$

which also imply $t = (p_2-p_4)^2 \;\Rightarrow\; p_2\cdot p_4 = 1/2\,(m_4^2 - m_3^2 - t_3)$ and $u = (p_2-p_3)^2 \;\Rightarrow\; 1/2\,(m_3^2 - m_4^2 - u_4)$, and we have made use of the relations

$$\gamma^\mu\gamma^\nu\gamma_\mu = -2\,\gamma^\nu \tag{6.80a}$$

$$\mathrm{tr}\,[\gamma^\mu\gamma^\nu\gamma^\rho\gamma^\sigma] = 4\,(g^{\mu\nu}g^{\rho\sigma} \;-\; g^{\mu\rho}g^{\nu\sigma} \;+\; g^{\mu\sigma}g^{\nu\rho}) \tag{6.80b}$$

$$s+t+u = m_3^2 + m_4^2 \quad\Rightarrow\quad s = -t_3 - u_4\,. \tag{6.80c}$$

This result (equation 6.78) has been checked against equation 3.25 of [221] and both expressions are identical.

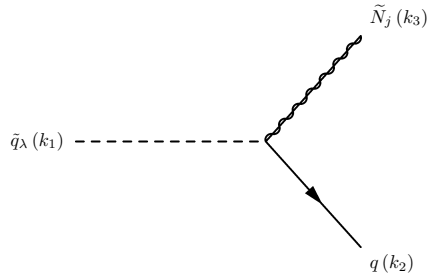

Figure 6.7: Diagram for on-shell squark decay.

Similarly the decay amplitude can be straightforwardly computed from the diagram in figure 6.7 as

$$i\,\mathcal{M}_{\text{decay}} = \bar{u}(k_2)\,(ig_\lambda P_\lambda)\,v(k_3)\,, \tag{6.81}$$

so that

$$\overline{\left|\mathcal{M}_{\tilde{q}_\lambda \to \tilde{N}_j q}\right|^2} = 4\,|g_\lambda|^2\;k_2 \cdot k_3\,, \tag{6.82}$$

where we have used $\text{tr}\,(\gamma^\mu\gamma^\nu) = 4\,g^{\mu\nu}$.

These on-shell production and decay amplitudes fully specify the individual on-shell subtraction terms, and via equation 6.76 give the total on-shell term which must be subtracted from the weight of any phase space point which satisfies the constraints of equation 6.59.

The On-shell Kinematic Projection

The definition of the diagram subtraction on-shell subtraction scheme given in equation 6.73 also requires the definition of a kinematic mapping from the full two-body phase space of the decay products, to the subset of on-shell points. The method chosen to achieve this is not uniquely defined and various kinematic mappings may suffice equally well. The requirements of this mapping are only that the mapping respect energy-momentum conservation, fulfil the on-shell conditions for the final state decay products, and that it correctly generates momenta where the parent particle is on mass shell[21]. The dipole kinematic mappings presented in section 3.5.2 satisfy similar requirements and therefore mappings analogous to (massive, final-final) dipole kinematic mappings can be used, as was done for example in [5].

However a significant simplification can be made if the decaying particle satisfies $\Gamma/m \ll 1$ (as is generally the case for squarks) such that points within $\mathcal{O}(\Gamma)$ of its pole can be deemed on shell and therefore appropriate for on-shell subtraction. In this case instead of generating the full 3-body phase space and mapping to the

[21] The issues, requirements and ambiguities surrounding the construction of such a kinematic mapping are discussed in detail in [5, 215]

on-shell point one may simply generate the decaying particle's momentum using the Breit-Wigner mapping described in appendix A.5, so that in our case the invariant mass of the squark is generated to always be approximately on shell via equation A.20 and the momenta of its decay products can then be generated from it and on-shell configurations are in this way generated. This was the approach taken here and is how the on shell configurations were generated in this work.

6.3.5 POWHEG Implementation

The POWHEG implementation of NLO gaugino pair production proceeds exactly in the same way as described for slepton pair production in section 6.2.2, with the only difference being the need to implement the on-shell subtraction (and its required kinematic mapping), as well as implementing multi-channel sampling to try to improve the integration over such subtracted real emission $q(\bar{q})g$ initial-state contributions.

The implementation is otherwise identical, with the Born and real emission being hard-coded and generated numerically by ThePEG, the collinear remnant terms being identical, and the finite virtual contribution being taken from `Xmatrix_nn_v.f` in PROSPINO2 (the expression for this virtual contribution is quite lengthy and unwieldy so we do not reproduce it here).

Generation of the On-shell Subtraction Term

The procedure to generate the on-shell subtraction term which will be subtracted from the real emission contribution both in the $\overline{B}$ function and in the kernel of the Sudakov POWHEG is performed as follows:

For each real emission configuration generated:

1. choose a possible resonance channel uniformly using a random number. Each channel consists of a specific choice for quark/anti-quark initial-state, squark left- or right-handedness, and choice of gaugino mass eigenstate attachment to either the production diagram or the decay one.

2. For the chosen channel generate the squark invariant mass using another random number according to equation A.20.

3. Given $\sqrt{s}$, the invariant mass of the squark which we have just generated, $p_{\tilde{q}}^2$, and the rest mass of the neutralino produced with the squark, $m_{\widetilde{N}_i}$, compute the magnitude of the first gaugino's 3-momentum in the rest frame of the incoming quark by solving

$$s = (p_{\tilde{q}} + p_{\widetilde{N}_i})^2 = p_{\tilde{q}}^2 + 2p_{\tilde{q}} \cdot p_{\widetilde{N}_i} + m_{\widetilde{N}_i}^2$$

for $|\mathbf{p}_{\widetilde{N}_i}|$.

4. Generate the polar angle of this gaugino as

$$\frac{d\sigma}{d\cos\theta_i} \propto 1 + \left(\frac{E^2_{\widetilde{N}_i} - m^2_{\widetilde{N}_i}}{E^2_{\widetilde{N}_i} + m^2_{\widetilde{N}_i}}\right)\cos^2\theta_i\,, \tag{6.83}$$

as expected for a fermion in the CM frame [222], using $\cos\theta = 1 - \left(\frac{p_T^{\min}}{|\mathbf{p}_{\tilde{q}}|}\right)$ as a minimum angle.

5. Compute the gaugino transverse momentum as

$$p_{T,\,i} = |\mathbf{p}_{\widetilde{N}_i}|\,\sqrt{1-\cos^2\theta_i}\,, \tag{6.84}$$

and generate its azimuthal angle uniformly, $\phi_i = 2\,\pi\,r$.

6. Using the $(p_T,\,\theta,\,\phi)$ just computed generate the squark and the gaugino at its vertex back-to back as

$$\mathbf{p}_{\tilde{q}} \;=\; (-p_{T,\,i}\,\sin\phi_i,\; -p_{T,\,i}\,\cos\phi_i,\; -|\mathbf{p}_{\tilde{q}}|\,\cos\theta_i)\;, \tag{6.85a}$$

$$\mathbf{p}_{\widetilde{N}_i} \;=\; (p_{T,\,i}\,\sin\phi_i,\; p_{T,\,i}\,\cos\phi_i,\; |\mathbf{p}_{\tilde{q}}|\,\cos\theta_i)\;. \tag{6.85b}$$

7. Using the invariant mass of the squark and the rest masses of the outgoing particles from the squark decay, that is, the quark mass (zero) and the rest mass of its associated gaugino compute the magnitude 3-momentum in the squark's rest frame.

8. Generate the squark's azimuthal angle uniformly in $\cos\theta$ (so that $d\sigma/d\cos\theta = 0$ as expected for pure phase space or a scalar) and generate the azimuthal angle uniformly, $\phi_j = 2\,\pi\,r$.

9. Compute the transverse momentum in this frame as

$$p_{T,\,j} = |\mathbf{p}_{\widetilde{N}_j}|\,\sqrt{1-\cos^2\theta_j}\,. \tag{6.86}$$

10. Compute the 3-momenta of this gaugino and quark as

$$\mathbf{p}_q \;=\; \left(-p_{T,\,j}\,\sin\phi_j,\; -p_{T,\,j}\,\cos\phi_j,\; -|\mathbf{p}_{\widetilde{N}_j}|\,\cos\theta_j\right)\;, \tag{6.87a}$$

$$\mathbf{p}_{\widetilde{N}_j} \;=\; \left(p_{T,\,j}\,\sin\phi_j,\; p_{T,\,j}\,\cos\phi_j,\; |\mathbf{p}_{\widetilde{N}_j}|\,\cos\theta_j\right)\;, \tag{6.87b}$$

and set them on-shell.

11. Boost this gaugino and quark to the lab frame.

12. Compute the weight for this on-shell term as

$$\frac{1}{n_{\text{channels}}}\,\frac{1}{(p^2_{\tilde{q}} - m^2_{\tilde{q}})^2 + m^2_{\tilde{q}}\Gamma^2_{\tilde{q}}}\,, \tag{6.88}$$

such that we have effectively implemented the multichannel-sampling described in appendix A.4, with each possible resonant configuration as a channel.

If the weight generated for the on-shell subtraction term is less than a given random number then this subtraction term is chosen and the procedure for generating the $\overline{B}$ function from section 6.2.2 is simply obtained by modifying step 6 such that if the configuration is a qg or $\bar{q}g$ initial-state one, the on-shell contribution just calculated is subtracted as

$$\mathcal{R}^{\text{finite}}_{S,\,\alpha} = \frac{\sum_{i,j;\,\lambda} \mathcal{D}^{OSsub}_{i,\,j;\,\lambda}}{\sum_{\alpha} |\mathcal{D}_{\alpha}| + \sum_{i,j;\,\lambda} \mathcal{D}^{OSsub}_{i,\,j;\,\lambda}} \frac{\Lambda^2}{p_T^2 + \Lambda^2} \mathcal{R} \; - \; \sum_{i,j;\,\lambda} \mathcal{D}^{OSsub}_{i,\,j;\,\lambda} \,. \tag{6.89}$$

The validation of this implementation is shown in section 7.3.1.

Chapter 7

Results

In this chapter we present the novel NLO-accurate differential distributions obtained from the POWHEG implementations for BSM models described in the previous chapter.

7.1 NLO Z' Results

In the following we present the NLO-accurate lepton observables for Z' models obtained from our POWHEG implementation.

7.1.1 NLO-accurate Differential Distributions

Figures 7.1 and 7.1 show the a set of NLO-accurate (jet-inclusive) observables for a χ-model Z' of mass $m_{Z'_\chi}$ at a $\sqrt{s} = 13\ \mathrm{TeV}$ LHC.

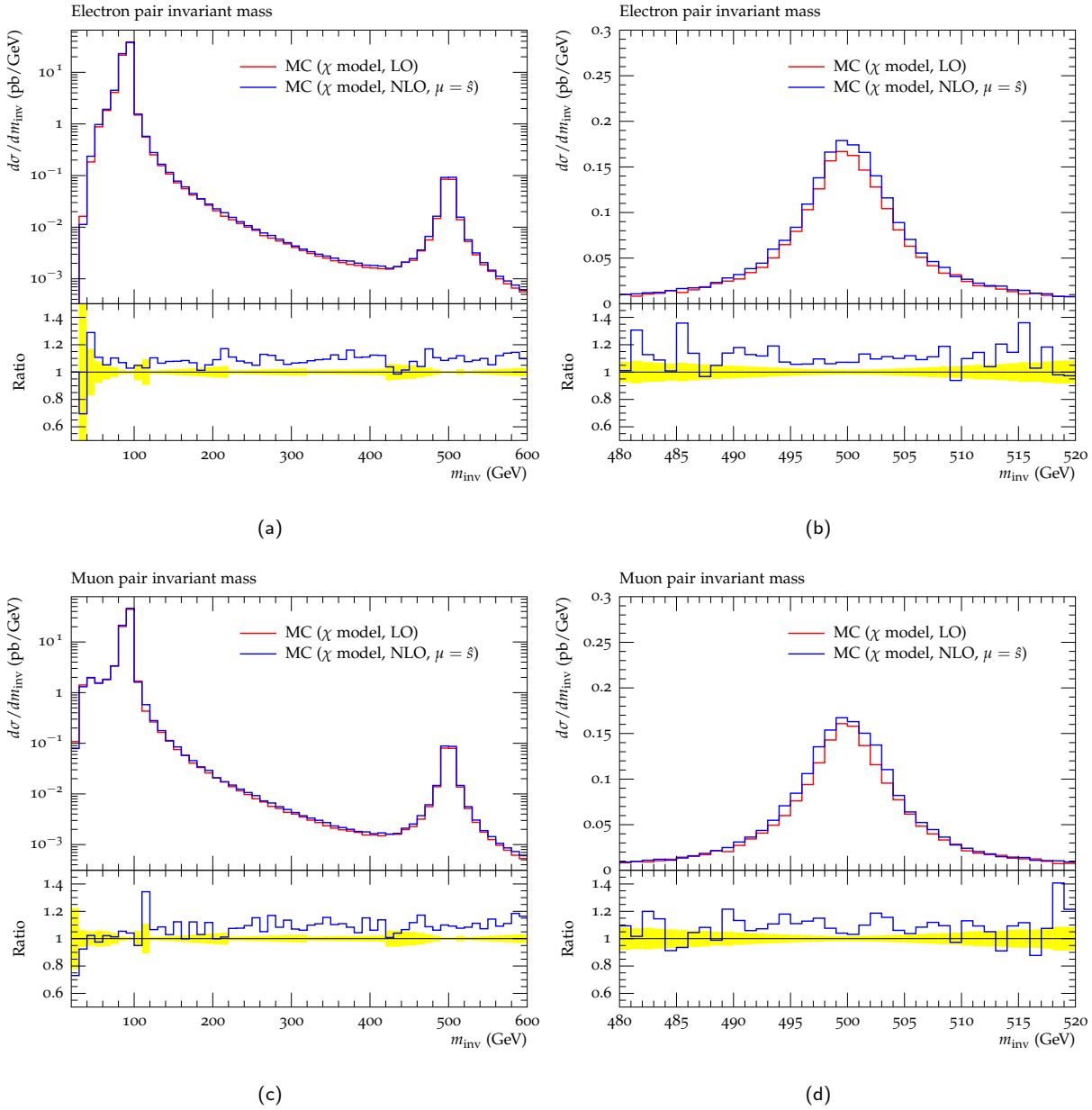

Figure 7.1: Comparison of the invariant mass of electron and muon produced by LO and NLO event generation for a Z'_χ with $m_{Z'} = 500$ GeV (at the LHC for a centre-of-mass energy of $\sqrt{s} = 13$ TeV) both up to, and focussed on, the Z' resonance.

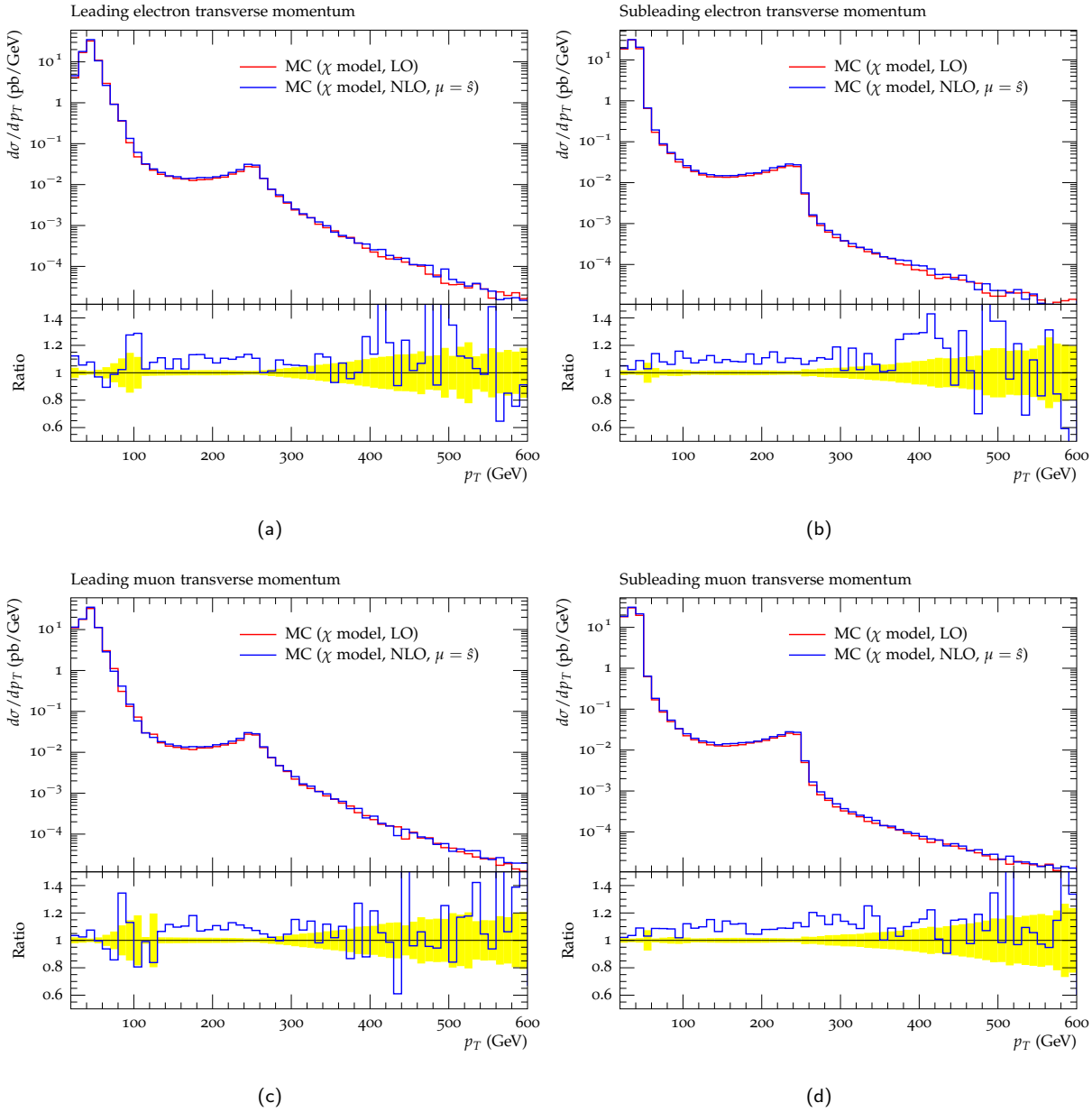

Figure 7.2: Comparison of leading and sub-leading lepton transverse momenta produced by LO and NLO event generation for a Z'_χ with $m_{Z'} = 500$ GeV at the LHC for a centre-of-mass energy of $\sqrt{s} = 13$ TeV.

Figures 7.3 and 7.4 show these same observables, also at NLO, comparing between the χ, ψ and Sequential Standard Model (SSM)[1] models.

[1]This is a benchmark scenario where the Z' is considered to have exactly the same couplings as the SM Z boson.

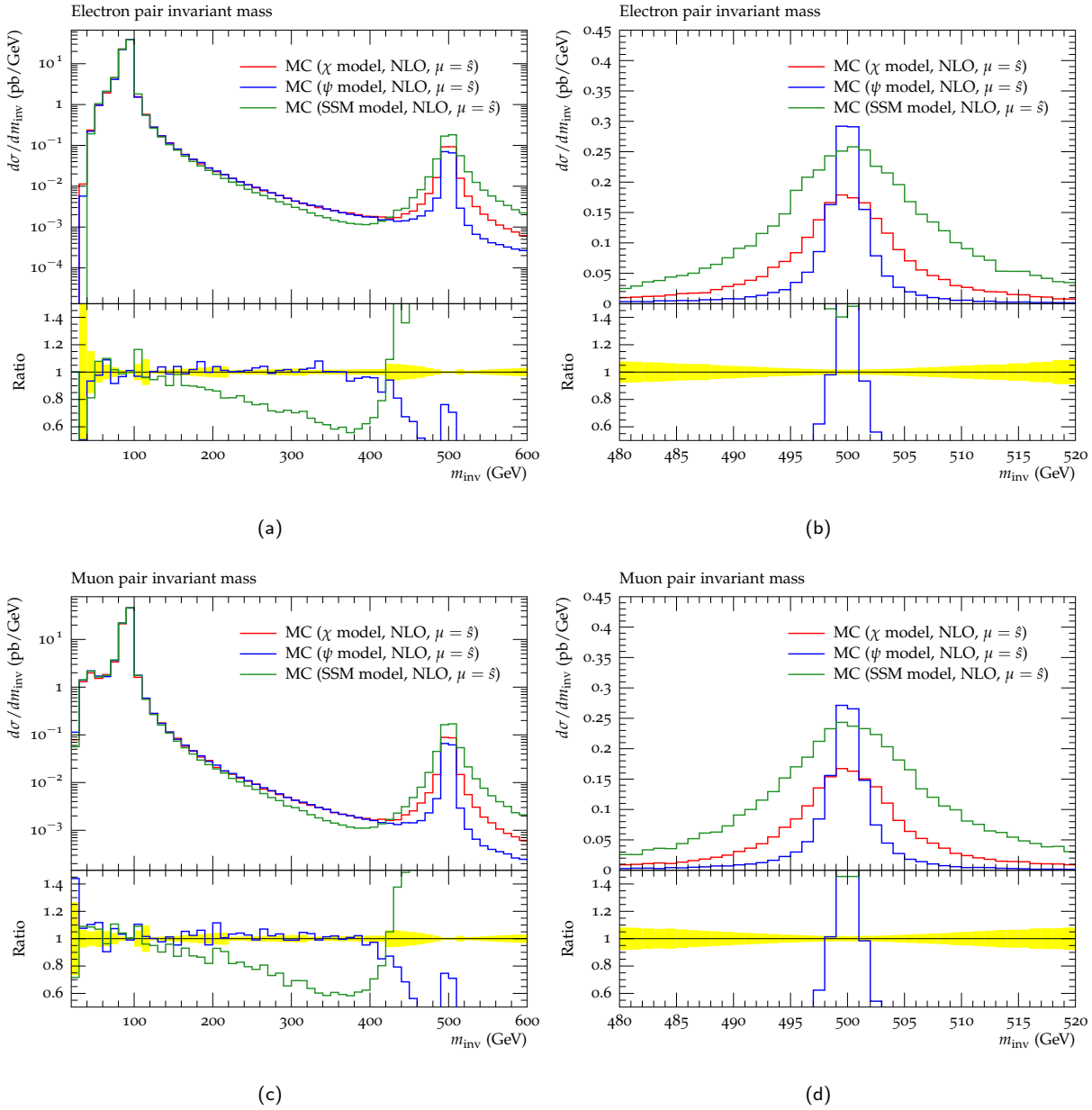

Figure 7.3: Comparison of the invariant mass of electron and muon produced by LO and NLO event generation for the χ, ψ and the SSM models with a Z'_χ with $m_{Z'} = 500\ \text{GeV}$ (at the LHC for a centre-of-mass energy of $\sqrt{s} = 13\ \text{TeV}$) both up to, and focussed on, the Z' resonance.

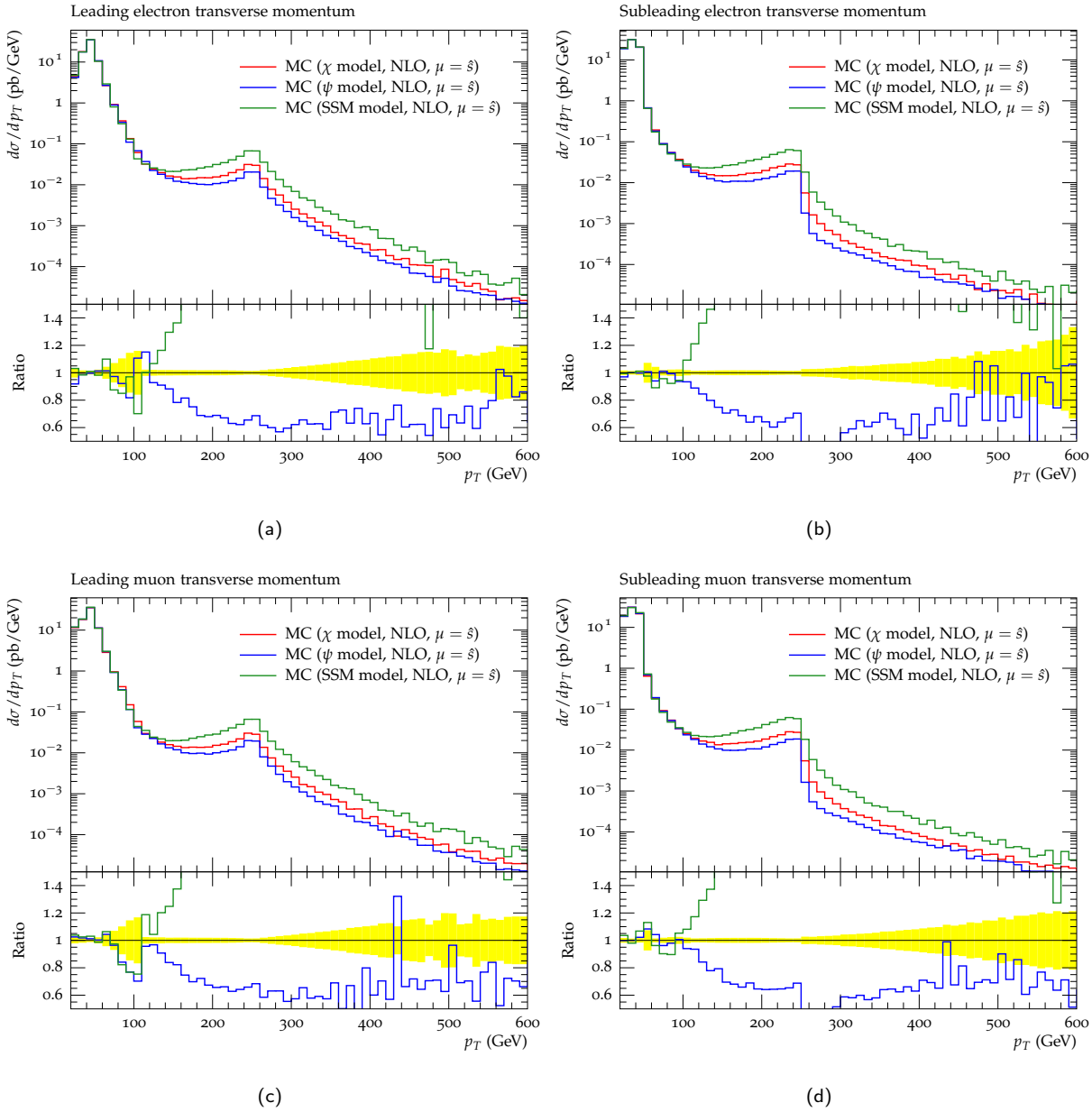

Figure 7.4: Comparison of leading and sub-leading lepton transverse momenta produced by LO and NLO event generation for the χ, ψ and the SSM models with $m_{Z'} = 500$ GeV at the LHC for a centre-of-mass energy of $\sqrt{s} = 13$ TeV.

Figures 7.5 and 7.6 show the scale dependence of the leptonic NLO-accurate observables under scale variations $\frac{1}{2}\,\mu \leftrightarrow \mu \leftrightarrow 2\,\mu$, where $\mu := \mu_F = \mu_R = \sqrt{s}$.

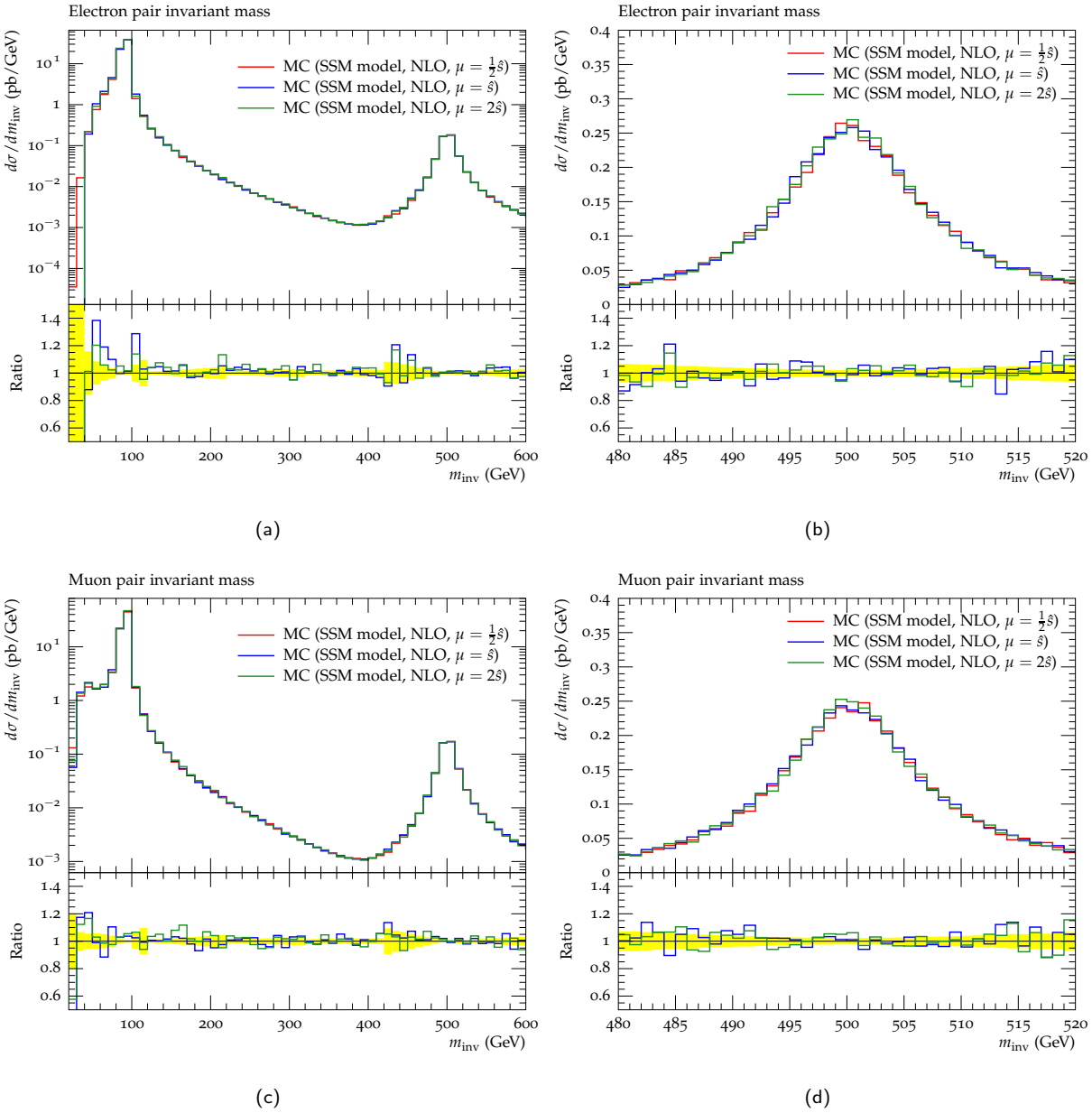

Figure 7.5: The invariant mass distributions of electron and muon produced at NLO under the scale variation $\frac{1}{2}\,\mu \leftrightarrow \mu \leftrightarrow 2\,\mu$ (where $\mu := \mu_F = \mu_R = \sqrt{\hat{s}}$) for the SSM model with a Z'_{SSM} with $m_{Z'} = 500$ GeV (at the LHC for a centre-of-mass energy of $\sqrt{s} = 13$ TeV).

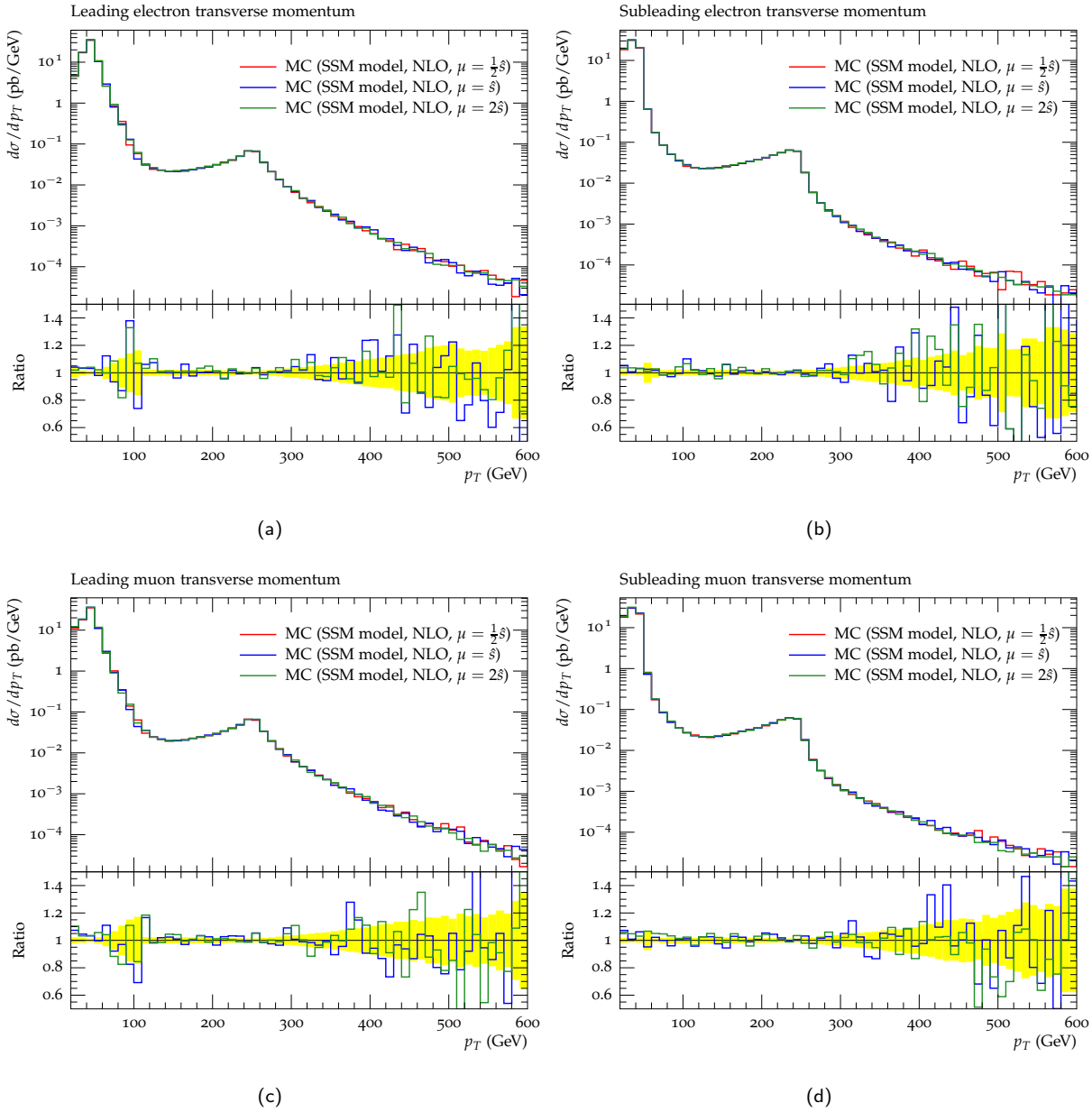

Figure 7.6: The leading and sub-leading lepton transverse momentum distributions for NLO event generation under the scale variation $\frac{1}{2}\,\mu \;\leftrightarrow\; \mu \;\leftrightarrow\; 2\,\mu$ (where $\mu := \mu_F = \mu_R = \sqrt{s}$) for the SSM model with $m_{Z'} = 500$ GeV at the LHC for a centre-of-mass energy of $\sqrt{s} = 13$ TeV.

7.1.2 Discussion

As expected the inclusion of NLO corrections to the event generation slightly increases both the total fully-inclusive cross section and impacts the transverse momentum distributions of the leptons. However the effect of the increased rates on acceptances of largely inclusive observables for which the event generation is NLO-accurate is most likely negligible.

Nonetheless, the effect of scale variation at the event generation level with NLO corrections included has been shown to be small[2] and for all the observables examined it has a negligible effect. If taken as a proxy for the theoretical error due to the missing higher orders[3] and the truncation of the perturbative expansion at $\mathcal{O}(\alpha^2\,\alpha_S)$, this would indicate that the theory uncertainties are now well under control for any foreseeable observable at a hadron collider.

The PDF uncertainty[4] is not included, however this lies beyond the scope of this thesis as it is inherent to the use of the factorisation theorem and exists independently of the improvement obtained by calculating fixed-order amplitudes to higher order or matching NLO amplitudes to parton showers.

In general, the NLO corrections to the differential distributions examined are unlikely to substantially impact the reach of Z' searches within the context of E_6 models, though the implementation presented can be used for any $m_{Z'}$ and any (perturbative) couplings, and for models with a lighter mass and smaller couplings the NLO corrections may be (relatively) more significant. For masses $m_{Z'} \gtrsim 1\,\mathrm{TeV}$ however the SM dilepton rate is negligible at these invariant masses such that any statistically significant signal found in this region would yield an observation/discovery, and for the purpose of discovery searches in these high-mass regions LO event generator predictions are likely to suffice. However, regardless of the minimal impact of the NLO corrections on the discovery potential at high invariant masses, their inclusion in event generation is nonetheless warranted to provide added theoretical control and minimisation of uncertainties in the signal predictions, and their inclusion is therefore a necessity given that the NLO corrections are well known and their inclusion within event generation is now possible.

Alternative NLO+parton shower implementations of Drell-Yan Z' production can be found in [2,208,224]. The NNLO corrections for Drell-Yan Z' production have been implemented in [225], though for phenomenology purposes at a hadron collider as we have shown here, they have already been shown to be largely irrelevant

[2] The scale variation at LO is not included in the comparisons as there it corresponds only to variation in μ_F as the Born process is $\mathcal{O}(\alpha_S^0)$.

[3] This belief is based on the tendency for higher order computations of highly inclusive observables to lie within the scale variation of the previous order. However, exceptions to this trend are not hard to find and in fact this applies to SM Drell-Yan [223]. A more solid case can be made for this expectation, as shown in [158].

[4] As estimated for example by using the envelope of the cross section prediction from several different PDF sets as recommended by the PDF4LHC working group. This uncertainty comes from the uncertainty in the data used for extraction of the PDFs and its propagation to the corresponding PDF set, and has nothing to do with the truncation of the perturbative series.

(see also [226]).

7.2 NLO Slepton Pair Production Results

7.2.1 Validation of NLO Slepton Pair Total Cross Sections

For slepton pair production a parameter space point in the pMSSM which is still not excluded but should be within reach of the LHC Run 2 ($\sqrt{s} = 14\,\mathrm{TeV}$ was assumed) was chosen, with electroweak masses $m_{\tilde{l}_L} = 350\,\mathrm{GeV}$, $m_{\tilde{l}_R} = 300\,\mathrm{GeV}$, $m_{\tilde{N}_1} = 150\,\mathrm{GeV}$ and strong sector masses $m_{\tilde{q}_{L,\,R}} = 1\,\mathrm{TeV}$ and $m_{\tilde{g}} = 1.4\,\mathrm{TeV}$.

Tables 7.1, 7.2, 7.3, 7.4 shows the validation of the total inclusive cross section agains PROSPINO2, with agreement $\mathcal{O}(0.1\%)$ found everywhere. All cross sections are computed in the $\overline{\mathrm{MS}}$ scheme. Further validation and results can be found in our preprint [227].

Mass eigenstates	Herwig++ (pb)	Prospino (pb)	F.D.
$\tilde{e}_L^+\tilde{\nu}_L$	5.6470e-03	5.6403e-03	-0.00119
$\tilde{e}_L^-\tilde{\nu}_e$	2.4300e-03	2.4291e-03	-0.00037
$\tilde{\tau}_1^+\tilde{\nu}_\tau$	4.7340e-05	4.7308e-05	-0.00067
$\tilde{\tau}_1^-\tilde{\nu}_\tau$	2.0370e-05	2.0374e-05	0.00021
$\tilde{\tau}_2^+\tilde{\nu}_\tau$	7.4400e-03	7.4430e-03	0.00040
$\tilde{\tau}_2^-\tilde{\nu}_\tau$	3.2910e-03	3.2902e-03	-0.00023

Table 7.1: Validation of the LO total cross section for $\tilde{l}\tilde{\nu}$ pair production.

Mass eigenstates	Herwig++ (pb)	Prospino (pb)	F.D.
$\tilde{e}_L^+\tilde{\nu}_L$	6.6640e-03	6.6987e-03	0.00519
$\tilde{e}_L^-\tilde{\nu}_e$	2.9480e-03	2.9652e-03	0.00580
$\tilde{\tau}_1^+\tilde{\nu}_\tau$	5.5930e-05	5.6186e-05	0.00455
$\tilde{\tau}_1^-\tilde{\nu}_\tau$	2.4760e-05	2.4871e-05	0.00445
$\tilde{\tau}_2^+\tilde{\nu}_\tau$	8.8700e-03	8.9107e-03	0.00457
$\tilde{\tau}_2^-\tilde{\nu}_\tau$	4.0160e-03	4.0356e-03	0.00485

Table 7.2: Validation of the NLO total cross section for $\tilde{l}\tilde{\nu}$ pair production.

Mass eigenstates	Herwig++ (pb)	Prospino (pb)	F.D.
$\tilde{e}_L\tilde{e}_L$	2.2260e-03	2.2283e-03	0.00102
$\tilde{e}_R\tilde{e}_R$	1.5980e-03	1.5989e-03	0.00058
$\tilde{\tau}_1\tilde{\tau}_1$	8.5800e-04	8.5780e-04	-0.00024
$\tilde{\tau}_2\tilde{\tau}_2$	4.0880e-03	4.0861e-03	-0.00047
$\tilde{\tau}_1\tilde{\tau}_2$	4.6650e-05	4.6640e-05	-0.00021
$\tilde{\nu}_e\tilde{\nu}_e$	2.0780e-03	2.0788e-03	0.00037
$\tilde{\nu}_\tau\tilde{\nu}_\tau$	2.0780e-03	2.0788e-03	0.00037

Table 7.3: Validation of the LO total cross section for $\tilde{l}\tilde{l}$, $\tilde{l}\tilde{\nu}$ pair production.

Mass eigenstates	Herwig++ (pb)	Prospino (pb)	F.D.
$\tilde{e}_L\tilde{e}_L$	2.6610e-03	2.6754e-03	0.00538
$\tilde{e}_R\tilde{e}_R$	1.9290e-03	1.9397e-03	0.00550
$\tilde{\tau}_1\tilde{\tau}_1$	1.0240e-03	1.0290e-03	0.00483
$\tilde{\tau}_2\tilde{\tau}_2$	4.9390e-03	4.9676e-03	0.00576
$\tilde{\tau}_1\tilde{\tau}_2$	5.6130e-05	5.6442e-05	0.00553
$\tilde{\nu}_e\tilde{\nu}_e$	2.4870e-03	2.4986e-03	0.00465
$\tilde{\nu}_\tau\tilde{\nu}_\tau$	2.4870e-03	2.4986e-03	0.00465

Table 7.4: Validation of the NLO total cross section for $\tilde{l}\tilde{l}$, $\tilde{l}\tilde{\nu}$ pair production.

7.2.2 NLO-accurate Differential Distributions

Figures 7.7, 7.8 and 7.9 show the $\sqrt{s} = 14\,\text{TeV}$ LHC invariant mass and transverse momenta observables obtained for $\tilde{e}_L\tilde{e}_L$ production, where $m_{\tilde{e}_L} = 350\,\text{GeV}$, $m_{\widetilde{N}_1} = 150\,\text{GeV}$ $\text{Br}(\tilde{l} \to \widetilde{N}_1\, l) = 1$ was used for all slepton decays.

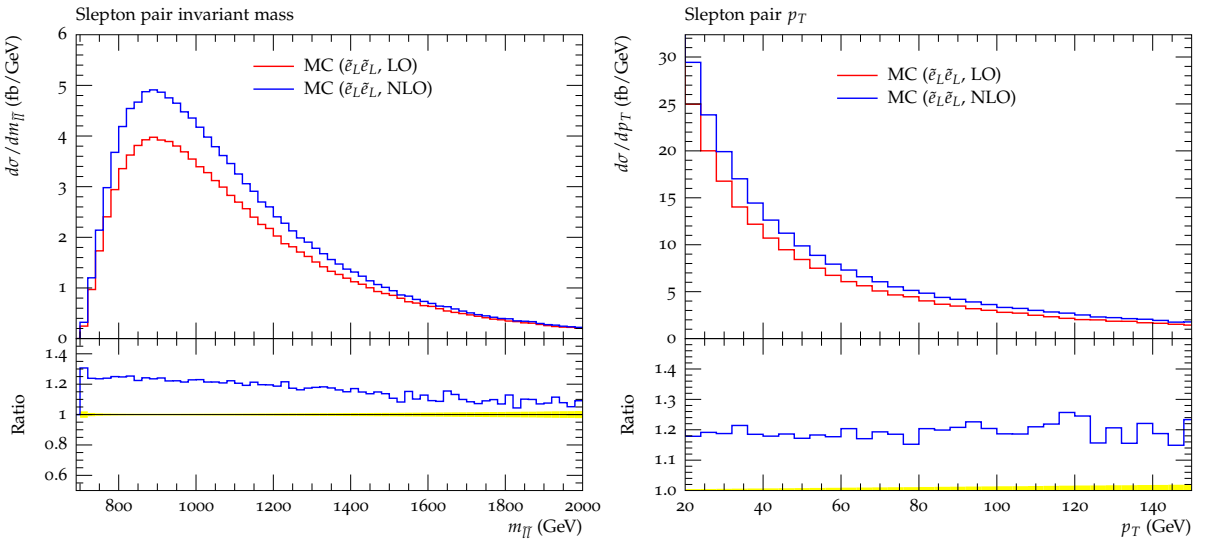

(a) (b)

Figure 7.7: The LO+PS and NLO+PS invariant mass and transverse momentum distributions of the slepton pair, $\tilde{e}_L\tilde{e}_L$, for a $\sqrt{s} = 14\,\text{TeV}$ LHC, with masses $m_{\tilde{e}_L} = 350\,\text{GeV}$ and $m_{\widetilde{N}_1} = 150\,\text{GeV}$.

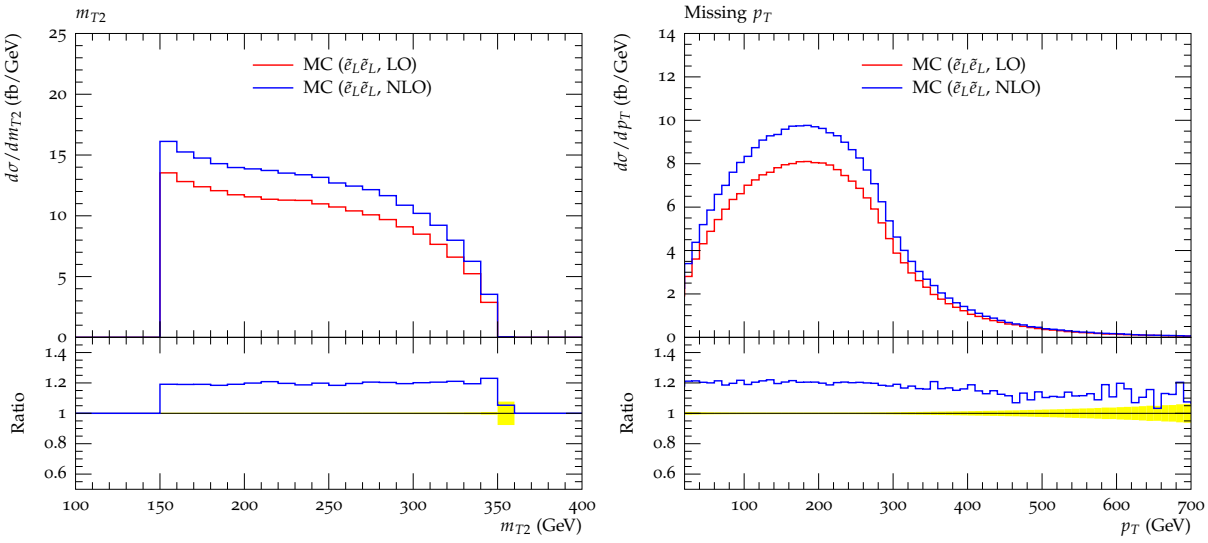

(a) (b)

Figure 7.8: The LO+PS and NLO+PS stransverse mass and missing transverse momentum distributions produced by the decay of the $\tilde{e}_L\tilde{e}_L$ slepton pairs, for a $\sqrt{s} = 14\,\mathrm{TeV}$ LHC, with masses $m_{\tilde{e}_L} = 350\,\mathrm{GeV}$ and $m_{\widetilde{N}_1} = 150\,\mathrm{GeV}$. The actual neutralino mass, $m_{\widetilde{N}_1} = 150\,\mathrm{GeV}$ was used as the trial mass in the stransverse momentum computation.

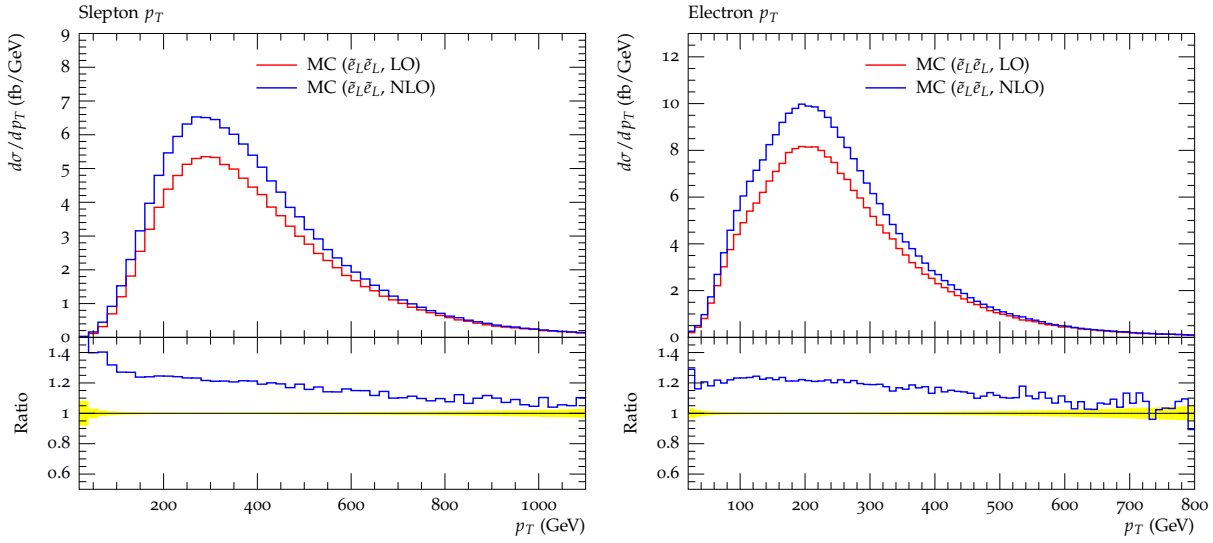

(a) (b)

Figure 7.9: The LO+PS and NLO+PS leading slepton and electron transverse momentum distributions for $\tilde{e}_L\tilde{e}_L$ production, for a $\sqrt{s} = 14\,\text{TeV}$ LHC, with masses $m_{\tilde{e}_L} = 350\,\text{GeV}$ and $m_{\widetilde{N}_1} = 150\,\text{GeV}$.

Leptons and jets within pseudorapidity $[-2.5, 2.5]$ were considered, with a p_T cut of $20\ \text{GeV}$ on the leptons, and jet clustering via the anti-k_t algorithm with a cone size of 0.4.

From both of the examples shown one can see that NLO contributions are significant. In particular they increase the number of signal events which would pass a p_T cut on the leptons or a $\not{p}_T$ cut on the event in a non-trivial way, which will depend on the exact position of the cut. This difference may be negligible in some regions, but could be significant if the signal constitutes only a few events.

7.2.3 Suppression Scale Dependence of Observables

Figures 7.10, 7.11 and 7.12 show the corresponding invariant mass and transverse momenta observables obtained for $\tilde{e}_L\tilde{e}_L$ production, where $\text{Br}(\tilde{l} \to \widetilde{N}_1\, l) = 1$ was used for all slepton decays, and the Λ^2 scale of the suppression function defined in equation 6.35 was varied. This therefore varied the transverse momentum region of the real emission weights which is used in the POWHEG Sudakov and therefore exponentiated, with $\Lambda^2 \to p_T^{\text{min}}$ (where $p_T^{\text{min}} = 5\,\text{GeV}$ is the threshold chosen for resolvable emission) corresponding to exponentiating only the low-p_T nearly-soft and/or collinear limit of the $\mathcal{R}/\mathcal{B}$ kernel, and $\Lambda^2 \to \infty$ corresponds to using the full real emission matrix element in the Sudakov, including both its singular low-p_T region and contributions from its finite high-p_T region, as is done in the original POWHEG implementations.

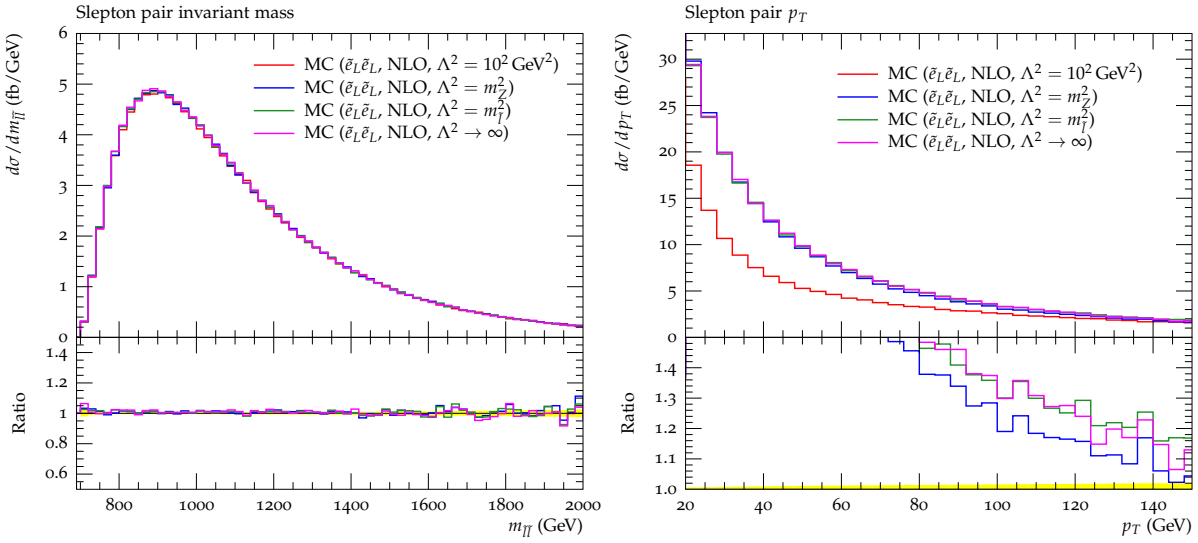

(a) (b)

Figure 7.10: The invariant mass and transverse momentum distributions of the slepton pair, $\tilde{e}_L\tilde{e}_L$, as a function of varying suppression scale, Λ^2, for a $\sqrt{s} = 14\,\mathrm{TeV}$ LHC, with masses $m_{\tilde{e}_L} = 350\,\mathrm{GeV}$ and $m_{\widetilde{N}_1} = 150\,\mathrm{GeV}$.

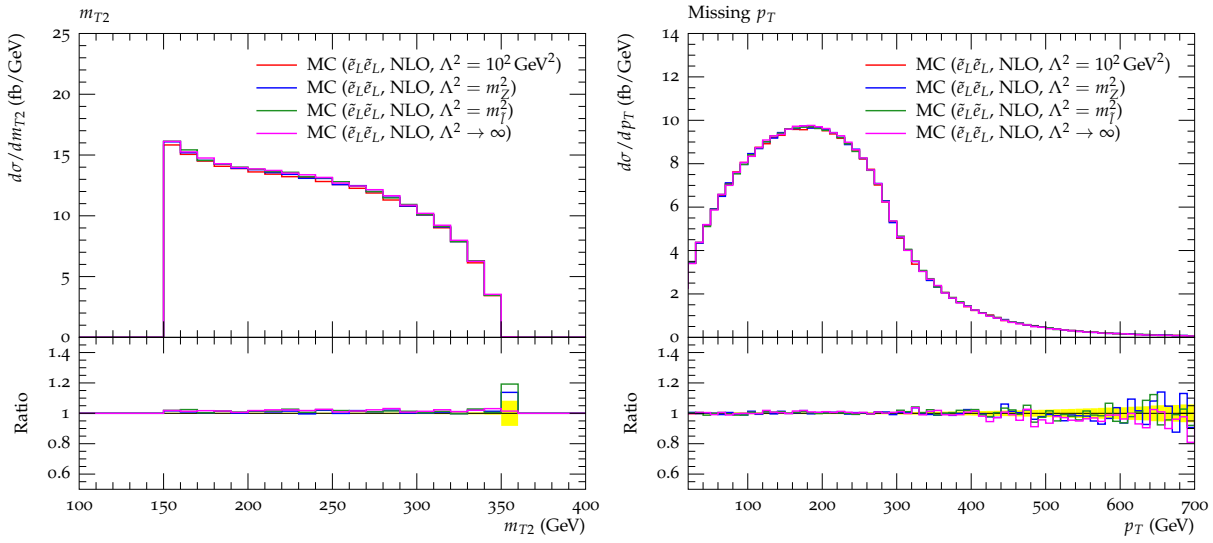

(a) (b)

Figure 7.11: The stransverse mass and missing transverse momentum distributions produced by the decay of the $\tilde{e}_L\tilde{e}_L$ slepton pairs, as a function of varying suppression scale, Λ^2, for a $\sqrt{s} = 14\,\mathrm{TeV}$ LHC, with masses $m_{\tilde{e}_L} = 350\,\mathrm{GeV}$ and $m_{\widetilde{N}_1} = 150\,\mathrm{GeV}$. The actual neutralino mass, $m_{\widetilde{N}_1} = 150\,\mathrm{GeV}$ was used as the trial mass in the stransverse momentum computation.

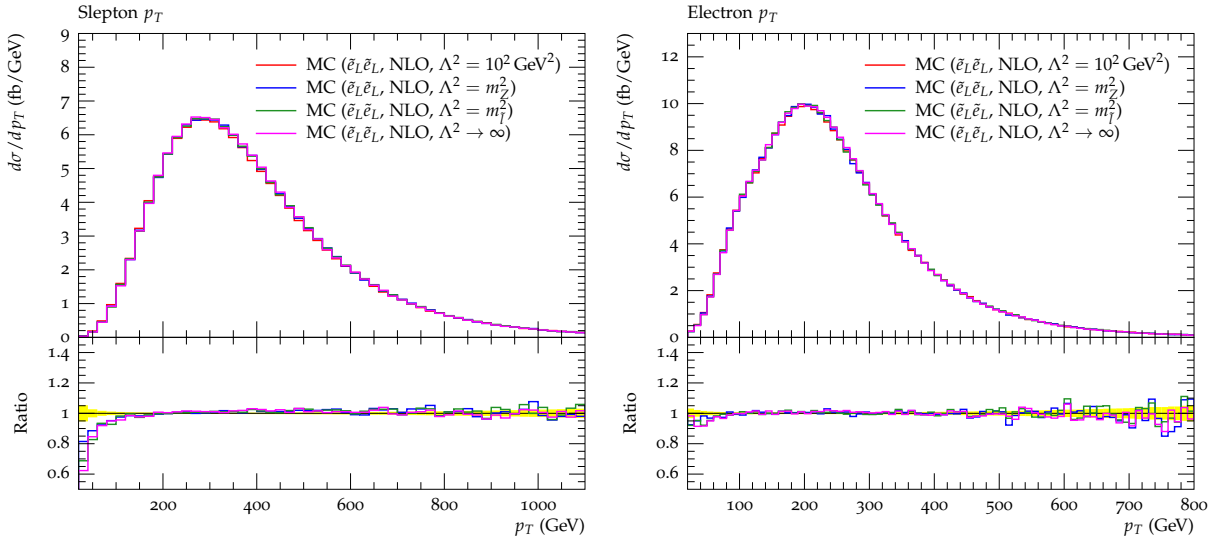

(a) (b)

Figure 7.12: The leading slepton and electron transverse momentum distributions for $\tilde{e}_L\tilde{e}_L$ production, as a function of varying suppression scale, Λ^2, for a $\sqrt{s} = 14\,\mathrm{TeV}$ LHC, with masses $m_{\tilde{e}_L} = 350\,\mathrm{GeV}$ and $m_{\widetilde{N}_1} = 150\,\mathrm{GeV}$.

Figure 7.10b shows that the suppression scale, and therefore the exponentiation of the finite part of the real emission weights has a strong impact on the (unobservable) slepton pair transverse momentum in the limit where the suppression scale approaches the low-p_T soft and collinear region which is crucial for correct resummation in the parton shower, and corresponding emission in the soft and collinear limits. This is to be expected since introducing the suppression down to the enhanced soft and collinear emission scales is bound to suppress the low p_T region these emissions populate.

However, more interesting is whether or not exponentiating the finite part of the real emission as the suppression scale moves away from the soft and collinear limit has any significant impact on kinematic distributions and observables[5]. Here we see that for the slepton pair transverse momentum once the suppression scale moves above the very low $p_T \ll m_Z$ region the transverse momentum distribution stabilises by the time it reaches $\Lambda^2 = m_Z^2$ and the inclusion of further portions of the finite part of the real emission contribution in the POWHEG Sudakov kernel has no impact. One may surmise from this that the standard POWHEG procedure of using the full real emission weights including their finite parts in the Sudakov is, in this particular case,

[5]It is worth noting that the use of the suppression function in no way modifies the correct NLO normalisation of the distributions as both the singular, low p_T and the finite, high p_T components of the real emission get added as usual within the POWHEG $\overline{B}$ function.

not numerically worrisome. Indeed as can be seen in all the (actually measurable) observables in figures 7.8a,b and 7.12b, the suppression scale seems to be of no consequence and the LL accuracy of the shower can be argued to not have been compromised, neither formally nor numerically, by the exponentiation of the finite regions of the real emission weights. This is not entirely unexpected since the K-factor (and therefore the typical real emission weights) for these processes are mild to small, and given that the addition of the finite real part in the exponential of the Sudakov amounts by a trivial algrabraic manipulation to a multiplication by an exponential of this finite contribution, for small real emission weights this will amount to a factor of approximately unity.

Exactly the same behaviour and suppression scale (non)dependence of observables were seen for the gaugino pair production parameter space points explored.

7.2.4 Discussion

The assessment of the accuracy of the NLO-accurate implementation of event generation of slepton pair production we have presented can be approached from several different angles. One perspective is that of the formal correctness of the matching implementation and the approximations used in it. Another is of the checks of the correctness of the NLO calculation and the logarithmic accuracy of the shower, and lastly there is the aspect of the theoretical uncertainty as estimated from scale variation of the total cross section or differential distributions computed. We now address these in order.

The POWHEG implementation is by construction NLO+LL-accurate. However, also by construction it involves exponentiating not only the singular contribution from one emission, but also the non-singular parts of the real emission contribution. These finite contributions do not impact on the logarithmic accuracy, but they are not constrained to be numerically small by any obvious argument. This characteristic of the POWHEG method is known since the *matrix-element correction* methods were formulated[6]. However these finite contributions will be sub-dominant and negligible in low transverse momentum regions (as expected since they are finite, and as required if logarithmic accuracy is to be preserved) and will impact the large transverse momentum regions where they are dominant, but these regions are in any case sensitive to NNLO and higher order fixed-order (non-singular) contributions which we do not include. These finite terms are therefore formally of higher order, though they will affect any observable sensitive to high transverse momentum regions of phase space (the most obvious example being the high p_T tail of transverse momentum distributions inclusive in jets).

[6]These are effectively the POWHEG equation (equation 5.50) with the POWHEG Sudakov but with replacement $\overline{B} \to B$ such that the hardest emission is generated correctly according to the real emission matrix element but the overall normalisation is only LO-accurate.

This is the reason why we have partitioned the real emission contribution into singular and finite contributions in equation 6.35 and have chosen to exponentiate only the former in the Sudakov (equation 6.43).

A similar further issue is that for the POWHEG formula to faithfully reproduce the NLO cross section the integral over the scale in the POWHEG Sudakov must run from the lower cut-off, $t_0 \sim 1\ \mathrm{GeV}$, to the hadronic centre-of-mass energy, $S = E^2_{\mathrm{C.M.}}$, as opposed to the the factorisation scale μ_F as required by the consistent use of DGLAP-resummed PDFs and the constraint that the phase space for resummation in the collinear limit be limited to only the approximately collinear region. These issues are discussed at length in [228], however they are well understood and do not compromise the NLO+LL accuracy claimed.

Regarding the correctness of the NLO matrix elements used, the Born, virtual and real emission contributions have been extensively validated against those in $\mathrm{PROSPINO2}$. The Born has also been checked against the corresponding standard implementation of SUSY processes in HERWIG++. The basic consistency check that the virtual contribution must satisfy $\mathcal{V}_{\mathrm{SQCD}} \underset{m_{\tilde{g}},\, m_{\tilde{q}} \gg \sqrt{s}}{\longrightarrow} \mathcal{V}_{\mathrm{QCD}}$ (as can be seen from the loop diagrams in figure 6.1) has been verified. Both the real emission and the virtual contributions have also been independently computed in a similar NLO+LL matching implementation for slepton pair production [3] and good agreement with $\mathrm{PROSPINO2}$ was found there as well, thereby providing a cross check. We are therefore confident that the NLO matrix elements used are correct.

Note that for $m_{\tilde{q}},\, m_{\tilde{g}} \gg \sqrt{s}$ the SQCD radiative corrections have a small impact on the total cross section, and for any squark or gluino mass have negligible impact on bins which cannot be populated by events with Born kinematics. Current exclusions in the coloured SUSY sector are generally at the level of $m_{\tilde{g}} \gtrsim 1\ \mathrm{TeV}$, $m_{\tilde{q}} \gtrsim 700\ \mathrm{GeV}$ for $m_{\tilde{g}} \gg m_{\tilde{N}_1}$ (and $m_{\tilde{g}} \gtrsim 700\ \mathrm{GeV}$, $m_{\tilde{q}} \gtrsim 500\ \mathrm{GeV}$ for $m_{\tilde{g}} \gtrsim m_{\tilde{N}_1}$) with reasonable assumptions (see figure 2.11, and see [154] for an example of how to combine fairly inclusive searches to obtain reasonably universal[7] mass limits). However, it will always be the case that $m^{\mathrm{excluded}}_{\tilde{q},\,\tilde{g}} \lesssim \sqrt{S}$ and therefore the full SQCD corrections are relevant and worth including, if known.

Figures 7.9 and 7.8 show that the K-factor from the NLO corrections is approximately uniform, such that the global K-factor used by experimental collaborations is in fact a good approximation to the true NLO local K-factor implemented here. It is nonetheless desirable for the known LHC exclusion plots to be produced with the local K-factor produced here to include the signal process at truly NLO accuracy.

Also note that as expected the ISR contributions implemented affect the normalisation of the distributions everywhere (in contrast to FSR corrections which only affect distributions beyond the mass peak and into the high invariant mass tail, as below the peak they are kinematically suppressed).

[7] 'Universal' here meaning relatively independent of the sparticle spectrum (and admixtures for sleptons, gauginos and third generation squarks) and therefore the assumed dominant production channel and viable decay chains.

The scale variation of differential distributions and the total cross section may also be analysed with the implementation presented here (as was done in figures 7.5 and 7.6 for Z' models), however results for such scale variation have not been included here as they are not necessarily meaningful given that one of the scales to be varied (the renormalisation scale) was not present at all at leading order. Hence the scale variation here is rather an indicator of the estimated expected region for the NNLO prediction rather than for comparison with the LO results, and would be more meaningful in that context.

Aside from the present POWHEG implementation, a later independent implementation within POWHEG BOX exists [3], as do equivalent analytically resummed and matched NLO+NLL results [229, 230].

In future works the present implementation can be used to verify and potentially improve LHC slepton search bounds and the impact of the NLO corrections on studies such as [222] can be considered.

7.3 NLO Gaugino Pair Production Results

We now present the validation of our NLO POWHEG implementation for gaugino pair production, followed by novel NLO-accurate results for differential distributions.

7.3.1 Validation of NLO Gaugino Pair Total Cross Sections

The total cross sections produced by our POWHEG-merged NLO code were extensively validated against Prospino, with good agreement found everywhere.

Validation Using SPS1a

For this sample point the high-scale SUSY-breaking parameter values are $m_0 = 100\ \mathrm{GeV}$, $m_{1/2} = 250\ \mathrm{GeV}$, $\tan\beta = 10$, $\mu > 0$ and $A_0 = -100$. The relevant electroweak-scale pole masses are $m_{\tilde{q}_{L\,i=1,2}} \approx 570\ \mathrm{GeV}$, $m_{\tilde{q}_{R\,i=1,2}} \approx 550\ \mathrm{GeV}$, $m_{\widetilde{N}_1} \approx 97\ \mathrm{GeV}$, $m_{\widetilde{N}_2} \approx 180\ \mathrm{GeV}$, $m_{\widetilde{N}_3} \approx 363\ \mathrm{GeV}$, $m_{\widetilde{N}_4} \approx 381\ \mathrm{GeV}$, $m_{\widetilde{C}_1} \approx 180\ \mathrm{GeV}$ and $m_{\widetilde{C}_2} \approx 381\ \mathrm{GeV}$.

Mass eigenstates	HERWIG++ (pb)	Prospino (pb)	F.D.
11	0.01285710	0.01259831	-0.02054
12	0.00150420	0.00142067	-0.05879
13	0.00269270	0.00269149	-0.00045
14	0.00058540	0.00058109	-0.00741
22	0.02730000	0.02616919	-0.04321
23	0.00767600	0.00767186	-0.00054
24	0.00242100	0.00235385	-0.02853
33	0.00000269	0.00000266	-0.01178
34	0.02119700	0.02119585	-0.00005
44	0.00005943	0.00005503	-0.08002

Table 7.5: Validation of the NLO total cross section for neutralino pair production for SPS1a.

Mass eigenstates	HERWIG++ (pb)	Prospino (pb)	F.D.
11	0.72840000	0.72677468	-0.00224
12	0.00435714	0.00431568	-0.00961
21	0.00435187	0.00421654	-0.03210
22	0.02035600	0.02039374	0.00185

Table 7.6: Validation of the NLO total cross section for chargino pair production for SPS1a.

Mass eigenstates	HERWIG++ (pb)	Prospino (pb)	F.D.
11	0.01329300	0.01316599	-0.00965
12	0.47840000	0.47971818	0.00275
13	0.00515500	0.00521775	0.01203
14	0.00048178	0.00044706	-0.07768
21	0.00138270	0.00137966	-0.00220
22	0.00034780	0.00032688	-0.06401
23	0.01285800	0.01313664	0.02121
24	0.01172500	0.01198883	0.02201

Table 7.7: Validation of the NLO total cross section for (negatively charged) chargino-neutralino pair production for SPS1a.

Mass eigenstates	HERWIG++ (pb)	Prospino (pb)	F.D.
11	0.02271200	0.02226654	-0.02001
12	0.84760000	0.85008985	0.00293
13	0.01030100	0.01041014	0.01048
14	0.00095032	0.00098761	0.03776
21	0.00274350	0.00272333	-0.00741
22	0.00072902	0.00069985	-0.04168
23	0.02815000	0.02865564	0.01765
24	0.02579800	0.02634914	0.02092

Table 7.8: Validation of the NLO total cross section for (positively charged) chargino-neutralino pair production for SPS1a.

Validation Using the Parameter Point $m_0 = 500$ GeV, $m_{1/2} = 200$ GeV

For this sample point the high-scale SUSY-breaking parameter values are $m_0 = 500$ GeV, $m_{1/2} = 200$ GeV, $\tan\beta = 10$, $\mu > 0$ and $A_0 = 0$. The relevant electroweak-scale pole masses are $m_{\tilde{q}_{L\,i=1,2}} \approx 660$ GeV, $m_{\tilde{q}_{R\,i=1,2}} \approx 650$ GeV, $m_{\widetilde{N}_1} \approx 77$ GeV, $m_{\widetilde{N}_2} \approx 142$ GeV, $m_{\widetilde{N}_3} \approx 303$ GeV, $m_{\widetilde{N}_4} \approx 323$ GeV, $m_{\widetilde{C}_1} \approx 141$ GeV and $m_{\widetilde{C}_2} \approx 323$ GeV.

Mass eigenstates	HERWIG++ (pb)	Prospino (pb)	F.D.
11	1.1160e-02	1.1372e-02	0.01865
12	1.0510e-03	9.8930e-04	-0.06237
13	7.7260e-03	7.7202e-03	-0.00076
14	1.1240e-03	1.1201e-03	-0.00347
22	2.5400e-02	2.4947e-02	-0.01816
23	1.8750e-02	1.8746e-02	-0.00020
24	3.2895e-03	3.2212e-03	-0.02122
33	1.0900e-05	1.0867e-05	-0.00305
34	4.0570e-02	4.0555e-02	-0.00038
44	1.2818e-04	1.2066e-04	-0.06234

Table 7.9: Validation of the NLO total cross section for neutralino pair production for $m_0 = 500$ GeV, $m_{1/2} = 200$ GeV.

Mass eigenstates	HERWIG++ (pb)	Prospino (pb)	F.D.
11	2.2820e+00	2.2825e+00	0.00021
12	7.2440e-03	7.1841e-03	-0.00834
21	7.2190e-03	7.1929e-03	-0.00364
22	4.2570e-02	4.2624e-02	0.00127

Table 7.10: Validation of the NLO total cross section for chargino pair production for $m_0 = 500$ GeV, $m_{1/2} = 200$ GeV.

Mass eigenstates	HERWIG++ (pb)	Prospino (pb)	F.D.
11	6.9660e-02	6.8546e-02	-0.01625
12	1.6020e+00	1.5961e+00	-0.00368
13	1.3830e-02	1.3919e-02	0.00638
14	1.9390e-03	1.9646e-03	0.01302
21	2.6970e-03	2.6805e-03	-0.00615
22	1.8081e-03	1.8119e-03	0.00211
23	2.5700e-02	2.6112e-02	0.01577
24	2.5250e-02	2.5803e-02	0.02143

Table 7.11: Validation of the NLO total cross section for (negatively charged) chargino-neutralino pair production for $m_0 = 500$ GeV, $m_{1/2} = 200$ GeV.

Mass eigenstates	HERWIG++ (pb)	Prospino (pb)	F.D.
11	1.1280e-01	1.1059e-01	-0.01999
12	2.7070e+00	2.6859e+00	-0.00784
13	2.6270e-02	2.6359e-02	0.00337
14	3.6776e-03	3.6904e-03	0.00344
21	5.1330e-03	5.0846e-03	-0.00953
22	3.3840e-03	3.4892e-03	0.03014
23	5.3340e-02	5.4093e-02	0.01393
24	5.2770e-02	5.3603e-02	0.01555

Table 7.12: Validation of the NLO total cross section for (positively charged) chargino-neutralino pair production for $m_0 = 500$ GeV, $m_{1/2} = 200$ GeV.

7.3.2 NLO-accurate Differential Distributions

The results for our POWHEG implementation for $C_1^+ N_2^0$ pair production (targeting the $3l + \not{p}_T$ signal are shown in figures 7.13, 7.14 and 7.15.

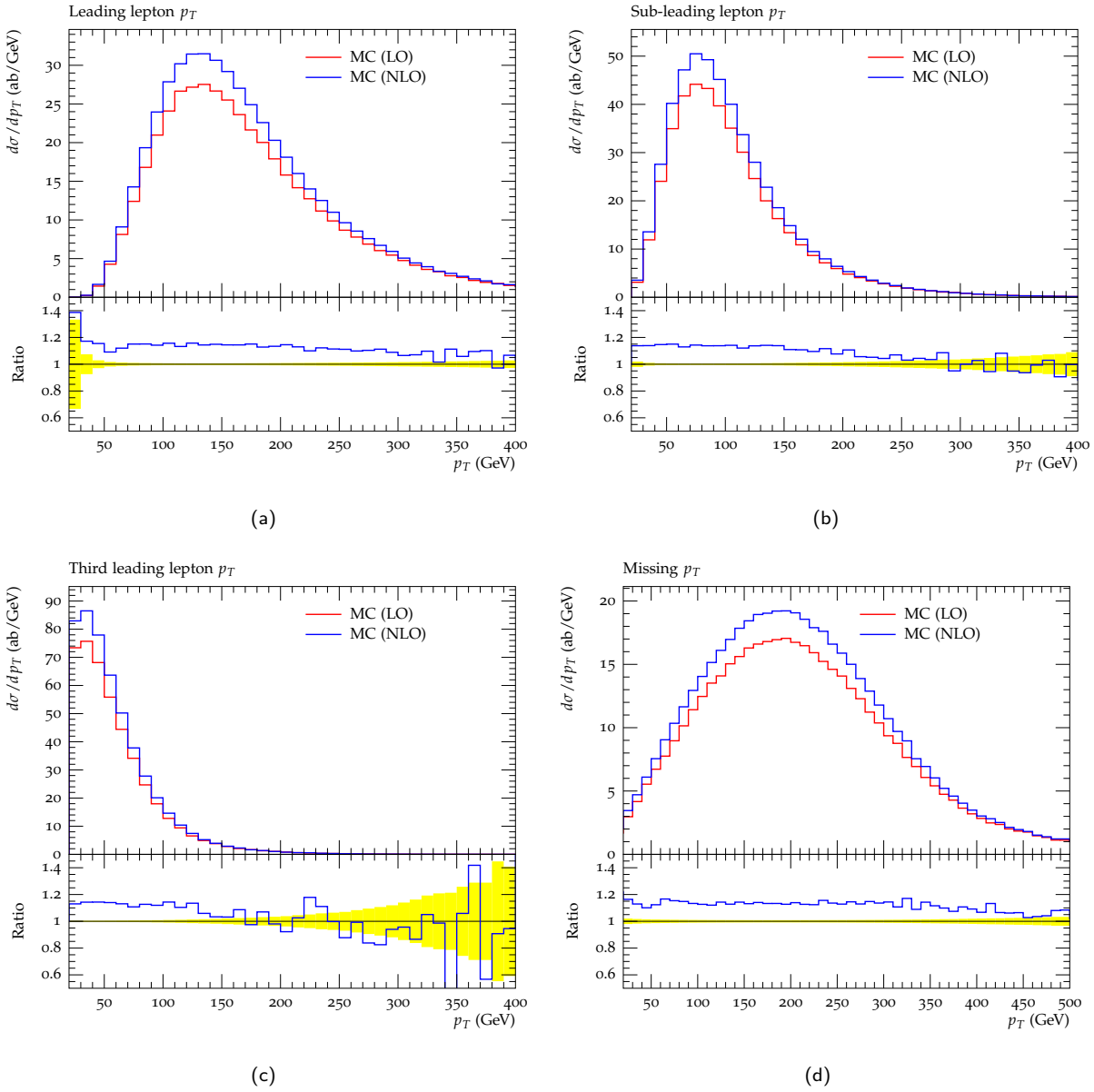

Figure 7.13: Sample transversve momentum distributions for LO and NLO-accurate leptonic observables, as produced by our implementation, for an arbitrary point in the SUSY parameter space in the channel $\widetilde{C}_1^+\widetilde{N}_2$ with W- and Z-mediated decays with branching fraction 1.

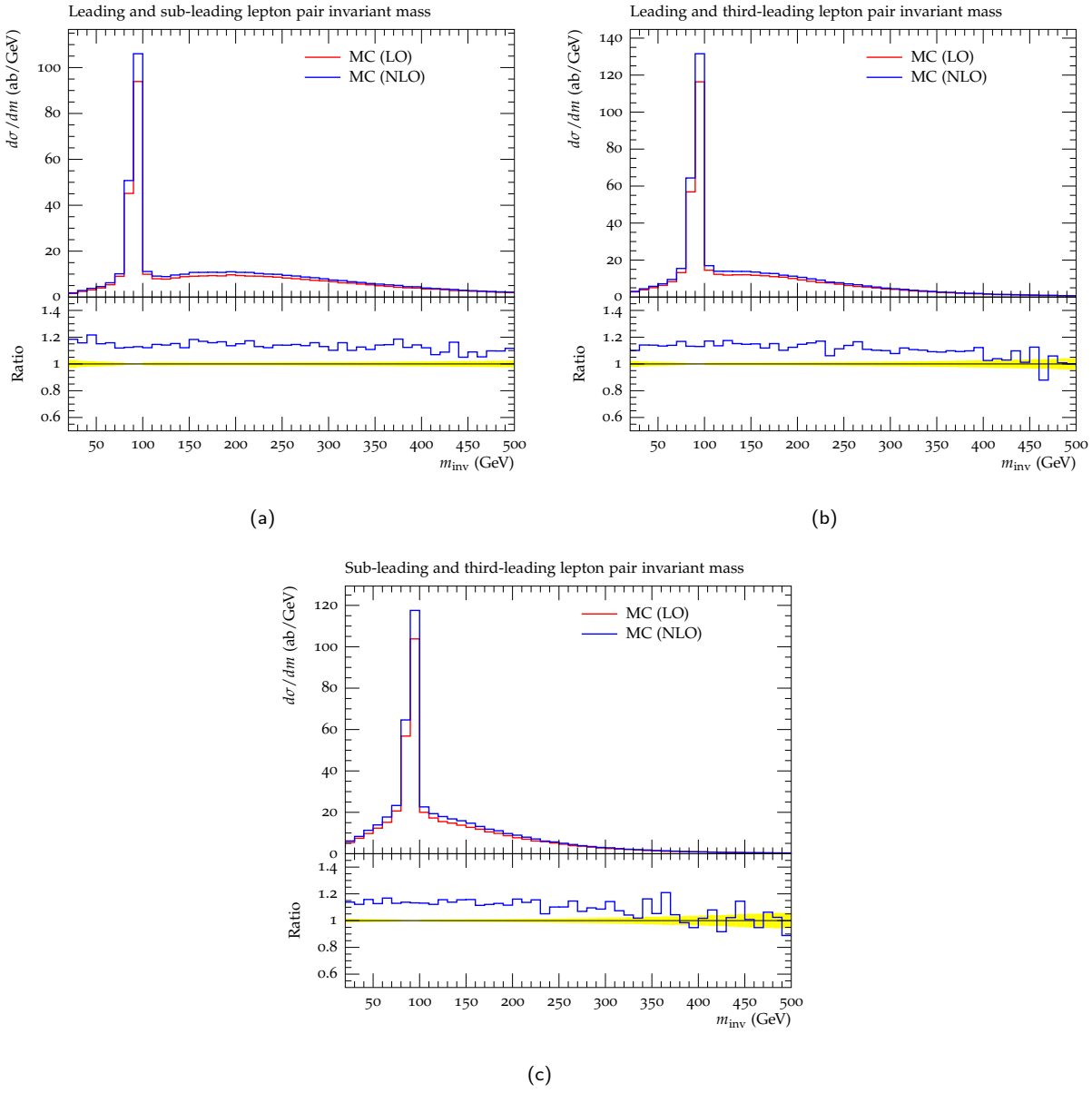

Figure 7.14: Sample invariant mass distributions for LO and NLO-accurate leptonic observables, as produced by our implementation, for an arbitrary point in the SUSY parameter space in the channel $\widetilde{C}_1^+\widetilde{N}_2$ with W- and Z-mediated decays with branching fraction 1. The stransverse mass trial mass is set exactly to $m_{\widetilde{N}_1}$.

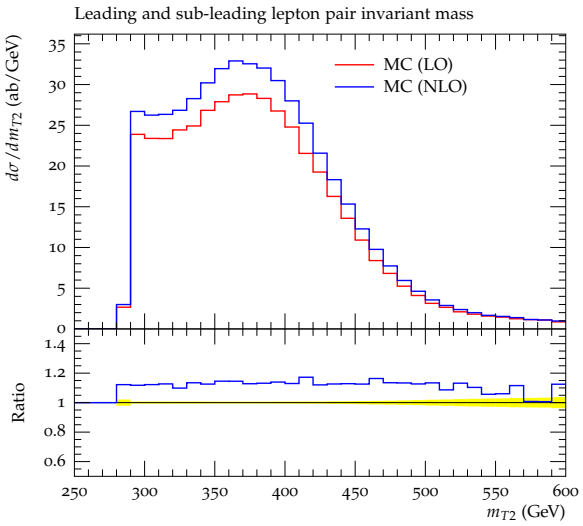

(a)

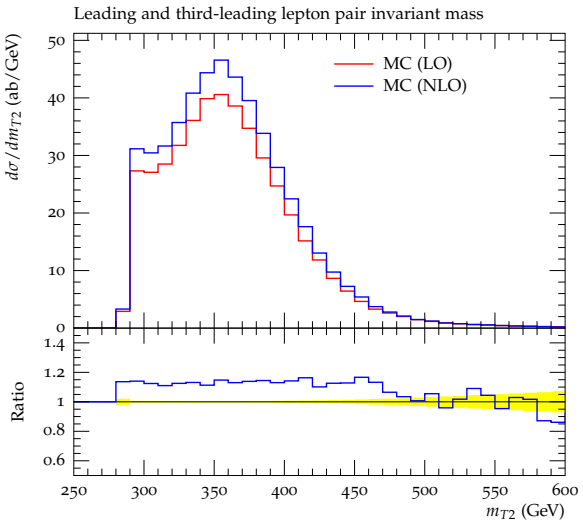

(b)

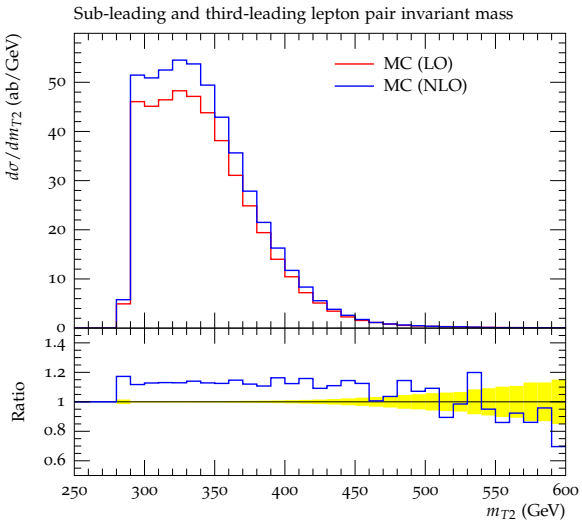

(c)

Figure 7.15: Sample stransverse mass distributions for LO and NLO-accurate leptonic observables, as produced by our implementation, for an arbitrary point in the SUSY parameter space in the channel $\widetilde{C}_1^+\widetilde{N}_2$ with W- and Z-mediated decays with branching fraction 1. The stransverse mass trial mass is set exactly to $m_{\widetilde{N}_1}$.

7.3.3 Width-Dependence of the Total Cross Sections

By including the width in *all* the squark propagators to preserve gauge invariance we have introduced a formally incorrect contribution. Defining width via equation B.4 the width of a spacelike particle is formally zero as the self-energy contribution only acquires an absorptive contribution (and therefore a width) at threshold.

The width on the (spacelike and never on-shell) propagator joining the two neutralino vertices in diagram (c), as well as the one joining the incoming gluon and quark in diagram (b) of figure 6.5 are therefore formally spurious (but necessary to preserve gauge invariance). However the inclusion of squark width in the NLO diagrams is itself a higher-order effect (by two powers in the strong coupling) this contribution does not spoil our desired NLO fixed-order accuracy, though it may be numerically significant and this must be checked.

The numerical size of this spurious contribution, and of the introduction of width in general, can be assessed by computing the dependence of the total cross section on the width. This dependence for an arbitrary point in SUSY parameter space is shown in figure 7.16.

The total cross section is seen to be largely independent of the width over many orders of magnitude. This is a valuable verification that higher-order width-related effects, either legitimate or spurious, are not globally numerically important (though they may well become relevant for other points in parameter space which we have not inspected, and certainly define behaviour in the squark resonant region).

Other similar works [5] treat the width purely as an unphysical regularisation parameter. For treatments of that type width-independence checks of the form shown in figure 7.16 are performed as a consistency check that the cross section is independent of an arbitrary regularistion parameter.

However given that the width is observable (at least in principle), and we aim for accurate event generation, we treat it as a calculable and physically meaningful parameter and use the computed width where available.

7.3.4 Discussion

The single most troublesome issue with the POWHEG implementation of NLO corrections for gaugino pair production was the subtraction of the on-shell contribution, and more specifically, the integration of the subtracted amplitude. Here, even with the appropriate Breit-Wigner mapping about the squark pole to efficiently generate the on-shell contribution[8] and then subtract it (as indicated in equation 6.73), the integration over the subtracted matrix element proved problematic.

The reason for this is most likely that it involves the subtraction of a potentially large on-shell contribution with a sharp step-function onset, precisely at or above a resonant region (which by itself can already be challenging to efficiently sample over) both at the pre-sampling and the event generation stages. Where the on-shell contribution happens to be moderate (relative to the real emission contribution it is being subtracted from) the integration can proceed unhindered, but if it happens to be sizeable (of the order of the matrix element it is being subtracted from or larger) the accuracy and efficiency of the phase space sampling can

[8] It is argued in [5] that this Breit-Wigner mapping is unsuitable for on-shell subtraction purposes but no argument is given and it is not apparent to us why this may be the case. They also argue the need for a Jacobian factor which is not clear to us.

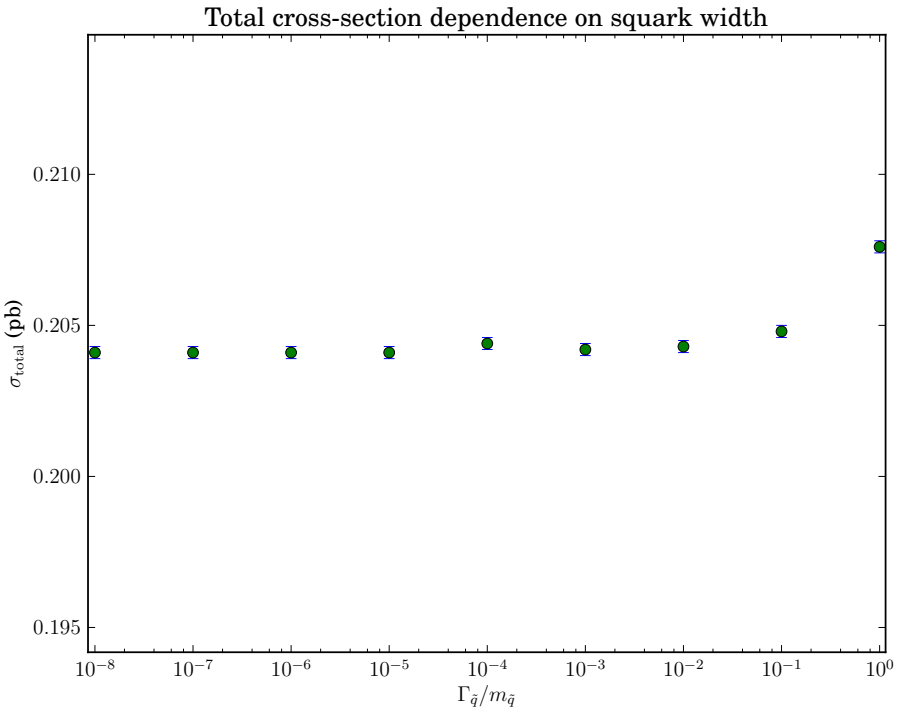

(a) The squark width-dependence of the NLO total cross section for $\widetilde{N}_1\widetilde{N}_1$ production, for the SPS1a benchmark parameter space point.

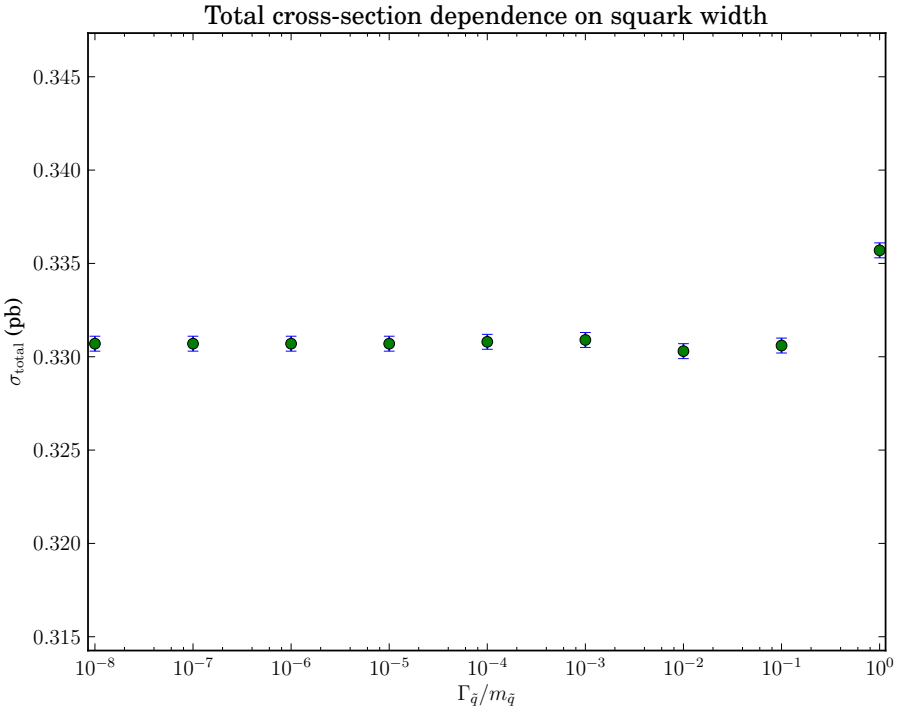

(b) The squark width-dependence of the NLO total cross section for $\widetilde{N}_1\widetilde{N}_1$ production, for the CMSSM $m_0 = 500$, $m_{1/2} = 200$ parameter space point.

Figure 7.16: Proof of the relative independence of the total cross section on the squark width, for spectra where on-shell subtraction is relevant.

suffer significantly.

Furthermore if this region happens to be poorly described at the pre-sampling stage where the bounding functions are set, the integration over the event generation stage will be no better and can produce unreliable and inaccurate results. This inaccuracy is surmised from discrepancies between our implementation and the PROSPINO2 result where we have good agreement in other contributions which don't involve on-shell subtraction (for example in $B+R_{\bar{q}q}$, or $B+R_{gq(\bar{q})}$ but with $m_{\widetilde{N}_i} > m_{\tilde{q}}$ such that on-shell subtraction doesn't apply) but where the agreement can disappear where on-shell subtraction becomes relevant.

We have validated our on-shell subtraction term (equation 6.75) to be correct by ensuring that it matches the weight from the full $2 \to 3$ matrix element for phase space points where the squark is very close to its mass shell. Note however that the ratio of the on-shell subtraction term and the full matrix element evaluated close to the squark pole can differ significantly from unity for some phase space points since the non-resonant contribution (see equation 6.72) is not guaranteed to be small in the resonant region. Nonetheless their ratio being approximately unity for most resonant points tested is enough to convince us of the correctness of the on-shell subtraction terms.

Given the correctness of the actual subtraction terms, the simplicity of the implementation of the conditions under which the subtraction should take place (equation 6.59), and the fact that we do in fact see agreement with PROSPINO2 on processes which do involve on-shell subtraction but albeit of presumably smaller on-shell subtraction contributions (for example due to a smaller $\tilde{q}\widetilde{N}_i$ production matrix element due to smaller couplings of the gaugino resulting from its particular mixing composition) suggests that it is not the subtraction itself but rather the integration of the subtracted amplitude where the problem lies. Further evidence of this is that when using an alternative phase-space sampler (namely ExSample [231]) for these cases the integrated cross section can vary by more than the variance of their respective Monte Carlo integrations.

We can only conclude from this that for parameter space points which involve on-shell subtraction of large on-shell contributions (that is, that satisfy both the on-shell subtraction condition in equation 6.59 and for which the squark-neutralino production on-shell amplitude is relatively large due to the gaugino composition) the phase space integration can be unreliable, and though we are reasonably confident of the correctness our implementation, we urge the user to be aware of these issues when considering these points. This is still very much an open issue which, in the absence of any obvious further integration techniques to tackle it, remains an open area for potential improvement in the phase-space sampling.

It is this also this issue alone which can motivate one to choose diagram removal techniques over the diagram subtraction method we have chosen at the price of losing gauge invariance, whose loss if proven

numerically irrelevant for the parameter points considered, is compensated by a significantly reduced computational workload and diminished unreliable integration hazards.

This integration issue arises already at the level of sampling over the (possibly on-shell subtracted) NLO matrix elements, without yet considering the details of an explicit matching procedure such as POWHEG. As it happens the required on-shell subtraction introduces a further problem for the matching, this being that it may spoil the generation of strictly positive weights built into the POWHEG method, and which is arguably its main strength against MC@NLO for event generation purposes.

Intuitively it is clear how this may happen: the subtraction of a potentially large on-shell weight from the dipole-subtracted real emission contribution may render the $\overline{B}$ function no longer positive definite. This is in contrast to the standard POWHEG formulation where, for the full integral over the radiative phase space of this contribution, $\int (R-C)\, d\mathbf{\Phi}_1$ (which must be performed for each Born-type $\overline{\Phi}_n = \Phi_n$ configuration sampled in the $\overline{B}$ function) is in principle guaranteed to be positive, though in practice sampling over a limited number of points of $(R-C)$ may yield a negative weight large enough to give an overall negative weight for $\overline{B}$. This means that the POWHEG method will in practice give a small fraction of events with negative weights[9], though these can be reduced using folding techniques and in principle can be made negligible by increasing the number of points used to sample $(R-C)$.

Including on-shell subtraction however makes the situation more akin to that of MC@NLO where the $\mathbb{H}$-type events (as defined in equation 5.26) arising from $\int (\mathcal{R}_0 - \mathcal{R}^{\mathrm{MC}})\, d\mathbf{\Phi}_{n+1}$ involve a subtraction which is never guaranteed to be positive for any number of points sampled, and where therefore negative-weighted events unavoidably arise and cannot be easily suppressed.

This would appear to nullify the advantage of using the POWHEG scheme for event generation purposes, however in practice we found that for most of the SUSY parameter space points we tested, the contribution from negative weights was still negligible. However, this must be checked for each spectrum and beam energy considered, as this is not guaranteed to be generally the case, and failure to account for[10] non-negligible negative weights can overestimate the signal cross section and in principle produce spurious signal events or overestimate exclusion regions. From the testing performed by us this seems unlikely, but it must be checked if the cross section seems suspiciously large or doesn't match the total cross section given by PROSPINO2, for example[11].

[9] Negative weights can also be generated by points where spurious higher order contributions become large, for example when they involve terms in the strong coupling (evaluated at the p_T scale preferred to get NLL resummation from the shower), $\alpha_S(p_T^2)$, at low transverse momenta where the coupling approaches the Landau pole.

[10] It is not known how to best account for these negative weights, a subtraction from the signal cross section is a possibility but the source of the large negative contribution and its kinematics may give better indication which bins this contribution must be subtracted from.

[11] Given that we have event generation purposes in mind our implementation by default discards negative weights unless one

Another problem which affects the POWHEG method for the present implementation is that of radiation zeroes. The well-known phenomenon of radiation zeroes [232, 233] originally discovered in the amplitude of the SM process $q\bar{q}' \to W\gamma$ and expected to give a dip in the charged-sign rapidity difference (more precisely, at $Q_l \times \Delta y = 0$) between the photon and the lepton from the W decay and was observed both at the Tevatron [234] and LHC [235] are inherited to the MSSM (by way the fact that the gauge charges carried by the SM fields and their corresponding SUSY partners are identical) to chargino-neutralino, $\widetilde{C}_i\widetilde{N}_j$, pair production. The large gaugino masses, the averaging over the couplings from each of the chiralities of the incoming quarks, the negligible mass-suppressed coupling of the Higgs/Higgsino-component of the gauginos to light quarks and the summing over colour states when a final-state gluon is involved [236] strongly suppress radiation zeroes in chargino-neutralino pair production. However, a radiation zero dip still persists if the neutralino produced is wino-like [237][12]. This potential radiation zero may affect the matching procedure as the R/B factor in the POWHEG formula may become numerically unstable if the Born contribution becomes strongly suppressed and finding a bounding function to efficiently generate it becomes problematic. Techniques to tackle this issue are known[13] [238] however for the many SUSY parameter points we tested we found no evidence of this being an issue so we have not addressed it. Nonetheless if scenarios with wino-like neutralinos are being considered this point may be worth keeping in mind if integration problems were to arise.

A slight inconsistency in our implementation must also be mentioned. The virtual contribution taken from PROSPINO2 is computed using an average over the squark masses as defined in equation 6.28 considering 4 squark flavours. The real contributions however we have generated considering the individual mass values of each flavour and handedness of squarks. The squark masses used for the real emission matrix element can be reset to an average value from the SLHA file or the HERWIG++ input file, though in CMSSM scenarios the mass splitting between left- or right-handed squarks, or squarks of different flavours of the first two generations is negligible.

To the best of our knowledge the present implementation is the first NLO+parton shower matching performed for NLO gaugino pair production, with previous analytic NLO+NLL matching implementations capable of producing the total cross section and leptonic invariant mass and transverse momentum distributions first computed in [239] and implemented in the RESUMMINO [240] software package. The NLO SQCD corrections to $\widetilde{N}_i\widetilde{N}_j + j$ (where all gaugino pair combinations are understood) have now also been computed [241].

In a future work we plan to compare the results of the analytic matching as performed by RESUMMINO

asks it to compute only the negative weights.

[12]This would in principle give a handle on measuring the wino component of the neutralino if it were discovered.

[13]These amount to the use of a suppression function similar to equation 6.35, where $\Lambda^2 = \frac{\mathcal{B}}{\mathcal{B}_{\max}} p_T^{\max}$ and the real emission contribution is assumed to have the same radiation zero behaviour as the Born such that the ratio R/B is well-behaved at the Born zero.

with the present parton shower implementation, as both should agree up to differences in higher order terms. It is also desirable to replicate current multilepton+p_T analyses from ATLAS and CMS to include the effect of the local K-factor which may have a slight impact on acceptances and the signal cross section in the fiducial region, and therefore may have an small effect on current exclusion bounds. Such effects are expected to be very modest, but insofar as they correspond to a more faithful implementation of the NLO corrections they are therefore desirable.

Other analyses may also benefit from the present implementation, as for example the implemented matrix element for $\widetilde{N}_1\widetilde{N}_1 + j$ corresponds to a potential LO contribution to monojet searches. This will be the subject of a future work.

Chapter 8

Summary and Outlook

In the present work we have presented novel implementations of known NLO corrections into the HERWIG++ event generator employing the POWHEG framework to consistently matching the additional jet from the NLO matrix element with the parton shower.

Our results show that for the BSM processes examined, namely E_6 Z' models and the MSSM, their colour-singlet final states are subject to K-factors which are largely uniform through the phase space. Though for both of these BSM models the NLO total cross sections have long been known, the absence of their implementation into an event generator had meant the phase-space dependence of their K factors was assumed to be approximately uniform, and this work confirms as much. The approximation made in previous experimental searches where the signal was modelled via LO+PS event generation multiplied by a global K factor is hence validated by this work as a reasonable, but improvable, approximation.

Nonetheless, given that the NLO corrections for the processes here treated have been known for some time, and NLO corrections for further BSM processes are likely to become available in the near future, their correct implementation within an event generator and a parton shower are a necessity for accurate and reliable searches in LHC data, particularly in the view of the increased cross section and reduced theoretical (scale variation) error they provide. It cannot be assumed, even for the processes studied here, that the K factor will be exactly uniform for all points in the model's parameter space, and indeed small variations in the K factors distribution may prove crucial in computing the signal cross section within the experimental acceptances when the signal sought constitutes a very low number of events. Hence where the radiative corrections are known –since the tools for matching them with a parton shower are known and now mature– they must be consistently included in the event generation if the experimental searches for the corresponding model are to be carried

out to the best of our ability.

In this work we have focussed on colour-singlet final states which correspond to extensions of the leptonic and electroweak sectors of the SM due to their simpler colour structure and therefore considerably simpler radiative corrections and IR singularity structure. However the tools used in the present implementations can in principle be extended to colour-charged final state processes, properly accounting for the more complex real emission and virtual matrix elements, with the implementation of the required additional dipoles, and the on-shell subtraction performed where an overlap with the perturbative expansion of another process occurs. The first of these implementations has now been performed in [5] and both the present colour-singlet tools and it form a starting point and direction in which high-accuracy (with scale variation uncertainties of the order or smaller than experimental uncertainties) direct searches for BSM physics must proceed. Multi-jet merging techniques must also be brought to bear (as has begun to be done in [242] and [239]) and present a complementary search tool to exploit multi-jet final states to probe and increase the sensitivity to potential BSM models with compressed mass spectra where decays of the BSM states will by themselves not yield sufficient transverse momenta for their SM decay products to pass experimental cuts. However outside these compressed mass-spectra scenarios accurate signal predictions require the normalisation of their cross section to be properly accounted for in the event generation, and this may only be obtained from the full NLO radiative corrections which include the one loop matrix element. Matching tools such as those presented here are therefore steps in this direction, with many more implementations for other BSM final states (and the possible automation of the construction of these implementations) surely to follow.

The present implementations of E_6 Z' models, slepton pairs and gaugino pairs are yet to be applied to bring to bear their effect on current ATLAS and CMS search results and on those still to come in Run 2 of the LHC. These will form part of future works.

Appendix A

Monte Carlo Integration

Monte Carlo integration is based on the definition of the mean value of a function in its discrete -and therefore numerically tractable- form

$$\begin{aligned} \langle f(x) \rangle_{x_{\min}, x_{\max}} &= \frac{1}{x_{\max} - x_{\min}} \int_{x_{\min}}^{x_{\max}} f(x)\, dx \\ &\approx \frac{1}{N} \sum_{i=1}^{N} f(x_i)\,. \end{aligned} \tag{A.1}$$

So to numerically solve an integral of the function $f(x)$ we can rewrite this relation as

$$\begin{aligned} \int_{x_{\min}}^{x_{\max}} f(x)\, dx &= (x_{\max} - x_{\min})\, \langle f(x) \rangle_{x_{\min}, x_{\max}} \\ &\approx \frac{x_{\max} - x_{\min}}{N} \sum_{i=1}^{N} f(x_i)\,. \end{aligned} \tag{A.2}$$

No assumption has so far been made about how the values of x_i are chosen and indeed they can be chosen with any desired distribution within the integration range and this will affect the only the rate of convergence and the size of the numerical integration error, but convergence to the correct integral value[1] is guaranteed by the law of large numbers[2].

The values of x_i can most simply be generated uniformly as

$$x_i = x_{\min} + \mathcal{R}\,(x_{\max} - x_{\min})\,, \tag{A.3}$$

where $\mathcal{R}$ is a random number chosen from a flat distribution.

[1] Provided the integrand is everywhere finite (and indeed square-integrable for the numerical error in the form of the standard deviation to be well defined) within the integration range of course.

[2] This is roughly speaking the theorem in probability theory that guarantees that over a large number of random trials, the average value of the outcome of the trials will tend towards the expectation value computed from the weighted average of the possible outcomes, such that $\lim_{N\to\infty} \frac{x_{\max}-x_{\min}}{N} \sum_{i=1}^{N} f(x_i) = \int_{x_{\min}}^{x_{\max}} f(x)\, dx$, where the x_i are randomly selected.

It can be shown (see [243]) that the error on integrals computed in this fashion can be estimated by

$$\sigma_{\mathrm{MC}} = \frac{\sigma_N}{\sqrt{N}} \tag{A.4}$$

where σ_N is the standard deviation (the square root of the variance) of the integrand function $f(x)$ in the region of integration (here taken to be $[a, b]$), computed as

$$\begin{aligned}\sigma_N &= \sqrt{\frac{1}{N}\sum_i^N \Big(f(x_i) \; - \; \langle f\rangle_{a,\,b}\Big)^2} \\ &= \sqrt{\langle f^2\rangle_{a,\,b} \; - \; \langle f\rangle_{a,\,b}^2} \\ &= \sqrt{\frac{1}{N}\sum_{i=1}^N f^2(x_i) - \left(\frac{1}{N}\sum_{i=1}^N f(x_i)\right)^2}\,.\end{aligned} \tag{A.5}$$

The error from Monte Carlo integration is then given by

$$\sigma_{\mathrm{MC}}(f_{a,\,b}(N)) = \sqrt{\frac{\langle f^2\rangle_{a,\,b} \; - \; \langle f\rangle_{a,\,b}^2}{N}}\,, \tag{A.6}$$

so that our final result for the Monte Carlo integration of a function $f(x)$ is:

$$\int_{x_{\min}}^{x_{\max}} f(x)\,dx = \left[\frac{x_{\max} - x_{\min}}{N}\sum_{i=1}^N f(x_i)\right] \; \pm \; \frac{\sigma_N}{\sqrt{N}}\,. \tag{A.7}$$

Note that the error in Monte Carlo integration scales as $1/\sqrt{N}$ regardless of how many dimensions the integral is performed over. Herein lies one of the main strengths of Monte Carlo integration and why it is chosen for event generation (for a full discussion of the advantages of Monte Carlo integration over alternative numerical integration methods for event generation purposes see section 3.2 of [244]).

In the following sections we will overview the Monte Carlo integration and variance reduction techniques used in this work to efficiently perform the integration and event generation (especially over the real emission amplitudes with on-shell subtraction which are particularly challenging), for a full treatment of Monte Carlo methods see for example [243].

A.1 Selection from a Distribution

If we generate values, x_i, using a random, flat distribution, we can then accept each value with a probability proportional to a function $f(x)\,dx$ and then produce a histogram of number of x values accepted within each step in Δx. This is a numerical way of producing a histogram which approximates the distribution $f(x)$.

Replicating a distribution using a numerical algorithm can come in very handy for numerical integration purposes. In the previous section we outlined a numerical method to compute integrals, but this method's

speed of convergence can be increased drastically by choosing our values of x_i in a way which resembles the distribution of the integrand. In this manner the values of x_i for which $f(x_i)$ is largest and makes the dominant contributions to the total integral are sampled more often, yielding a more rapidly converging estimate of the integral.

In general if we have a function $f(x)$ which is analytically integrable so that we can solve the result of the indefinite integration for x then we can use randomly generated numbers from a flat distribution, $\mathcal{R}_i$ to generate values of x_i which emulate the distribution $f(x)$ between $x_{\min}$ and $x_{\max}$, as follows:

$$x_i = F^{-1}\left(F(x_{\min}) + \mathcal{R}_i(F(x_{\max}) - F(x_{\min}))\right) \ . \tag{A.8}$$

This is a generalization of equation A.3, where $f(x) = 1$ so that $F(x) = x$.

Unfortunately one is rarely so lucky that $f(x)$ is nice enough that $F(x)$ can be computed analytically (let alone $F^{-1}(x)$). This method of phase space sampling is therefore usually not directly applicable but is usually instead applied to an analytically tractable function used as a bounding function on the integrand, and then an accept-or-reject (also known as hit-or-miss) method is applied.

A.2 Hit-or-Miss Method

This method is based on the observation that an n-dimensional integral is equivalent to the calcution of an $n+1$-dimensional volume

$$\begin{aligned} \int f(x)\, dx &= \int dx \int_0^{f(x)} 1\, dy \\ &\approx \sum_i \{y_i \mid y_i \leqslant f(x_i),\ x \in [x_{\min}, x_{\max}]\} \ , \end{aligned} \tag{A.9}$$

such that flat sampling simultaneously along the x and y axes by generating x_i randomly and y_i according to $y_i = \mathcal{R}\, f_{\max}$ (where $f_{\max} = \text{constant} \ \geqslant f(x) \ \ \forall\ x \in [x_{\min}, x_{\max}]$) whilst accepting only points for which $y_i \leqslant f(x_i)$ (that is, those which land below the integrand function) can yield the desired integral.

However this method samples uniformly over a (hyper)cube, and is thus ill-suited (inefficient and slowly convergent) for anything but fairly flat (approximately constant) integrands.

A.3 Importance Sampling

If the integrand function $f(x)$ is not analytically integrable but its functional form is roughly known then one can construct a bounding function $b(x)$ for which

$$b(x) \geqslant f(x) \qquad \forall\, x \in [x_{\min}, x_{\max}]\,, \tag{A.10}$$

and which (unlike $f(x)$ itself) is analytically integrable and whose integral is invertible, so that equation A.8 can be used to generate points according to it[3].

The integration then proceeds by the following steps:

1. generate a value x_i from $b(x)$ equation A.8 using a random number;

2. using this x_i evaluate $f(x_i)/b(x_i)$ and generate another random number $\mathcal{R}_j$. If

$$\mathcal{R}_j < \frac{f(x_i)}{b(x_i)} \tag{A.11}$$

   keep the weight $w_i = f(x_i)$, otherwise return to step 1.

3. Repeat N times, each time summing the weights to yield the desired integral (the observable's cross section in the cases of interest to us), and using each weight to generate (or not) an event according to the kinematics corresponding to the (phase space) point sampled[4]. The result produced this way will be of the form of equation A.7, as desired.

A.4 Multi-channel Integration

However, often the form of the integrand cannot be well fitted by a single bounding function (for example, if contains two or more resonant regions as is the case for gaugino pair production in the present work[5]), such that more than one bounding function may be required, with each one being referred to as an integration *channel*.

[3] A function $b(x)$ such that $f(x)/b(x) \sim \text{constant}$ is desirable to minimise the variance and optimise the convergence of the estimate of the integral, but it is not required.

[4] *Unweighted* events can be generated by accepting or rejecting each weight (using yet another random number) with a probability $w_i/w_{\max}$, where $w_{\max}$ is the largest weight found during a previous *pre-sampling* of the integrand (amplitude) over the integration region (phase space).

[5] Here there are not two separate internal legs which can become resonant, as is the case for example for WZ vector boson pair production, but rather for the resonant diagrams there are two squark masses (left- and right-handed) which contribute, each with a potentially distinct mass and therefore resonant region as well.

We therefore define a total bounding function[6]

$$b(x) = \sum_i b_i(x)\,, \tag{A.12}$$

and then proceed as with importance sampling, but selecting an appropriate integration channel for each point.

The algorithm proceeds as follows:

1. select an integration channel with relative probability[7] $\alpha_i = \int_{x_{\min}}^{x_{\max}} b_i(x)\,dx$, that is, accept the channel $b_i(x)$ if

$$\mathcal{R}_i \leqslant \frac{\int_{x_{\min}}^{x_{\max}} b_i(x)\,dx}{\int_{x_{\min}}^{x_{\max}} b(x)\,dx} \tag{A.13}$$

   where $\mathcal{R}_i$ is a random number. If this condition is satisfied for more than one channel accept the one with smaller α_i.

2. Generate x_i according to $b_i(x)$ using equation A.8.

3. Generate another random number $\mathcal{R}_j$ and check that

$$\mathcal{R}_j \leqslant \frac{f(x_i)}{b(x_i)}\,. \tag{A.14}$$

   If so, accept this weight $w_i = f(x_i)$, otherwise return to step 1.

This can be seen to work as we may rewrite the integral as

$$\begin{aligned}\int_{x_{\min}}^{x_{\max}} f(x)\,dx \;&=\; \int_{x_{\min}}^{x_{\max}} \frac{f(x)}{b(x)} \sum_i b_i(x)\,dx \;=\; \int_{x_{\min}}^{x_{\max}} \frac{f(x)}{b(x)} \sum_i \alpha_i \frac{b_i(x)}{\alpha_i}\,dx \\ &= \sum_i \alpha_i \int_{x_{\min}}^{x_{\max}} \frac{f(x)}{b(x)}\,\frac{b_i(x)}{\alpha_i}\,dx\,,\end{aligned} \tag{A.15}$$

such that the integral becomes a weighted sum of probability distributions, with each distribution given by the product of the probability of choosing a given channel times the probability of accepting the weight generated according to this channel, as shown in equations A.13 and A.14, respectively.

A.5 Variable Transformation

For a select few integrand functions, $f(x)$, there are variable transformations which may be found under which the integrand becomes flat and the numerical integration can proceed straightforwardly by generating

[6] Here each bounding function is analytically integrable and with an invertible integral, though the total bounding function may not fulfil the latter condition.

[7] The weights, α_i of each channel can be normalised to $\int_{x_{\min}}^{x_{\max}} b(x)\,dx$ such that $\sum_i \alpha_i = 1$. Provided this holds so they can be interpreted as probabilities, the individual weights can be assigned arbitrarily or evenly, if desired. This will affect the integration efficiency but not the result of the integral.

random numbers and directly sampling uniformly over the transformed integration range. This will have the added benefit of providing a mapping under which sampled points will all be mapped to the region where the integrand is largest (strongly clustered on a resonance, for example).

This is indeed the case for the Breit-Wigner mapping we have employed in this work to focus the sampling of phase space points about the resonance regions in contributions with potentially on-shell squarks.

Such resonant contributions are determined by the Breit-Wigner functional form and give the integral[8]

$$\int_{-\infty}^{\infty} \frac{ds}{(s-m^2)^2 \; + \; m^2\Gamma^2} \,. \tag{A.16}$$

Using the variable change of variables

$$\tan\theta = \frac{s-m^2}{m\,\Gamma} \,, \tag{A.17}$$

this integral can be shown to give[9]

$$\int_{-\infty}^{\infty} \frac{dp^2}{(p^2-m^2)^2 \; + \; m^2\Gamma^2} = \frac{1}{m\,\Gamma} \int_{-\pi/2}^{\pi/2} d\theta \,, \tag{A.19}$$

where it is now clear we may now sample uniformly in $\theta \in [-\pi/2,\, \pi/2]$ to perform the integral, which yields[10] $\frac{\pi}{m\,\Gamma}$.

This transformation also allows for the efficient integration of an amplitude with a resonant region, as points can be sampled as

$$s_i = m^2 \; + \; m\,\Gamma \, \tan\theta_i \,, \tag{A.20}$$

using a flat distribution in θ within the integration range, and thereby producing sampling clustered around the dominant region $s \approx m^2$.

[8] Here, as with the narrow-width approximation, we make the approximation that the momentum dependence from the amplitude factor, $|\mathcal{M}|^2$, and the phase space is subdominant and negligible. This may not necessarily be the case and the error incurred from this assumption may be larger than the expected $\mathcal{O}(\Gamma/m)$, see [245].

[9] Note that for simplicity we neglect the finite phase space we are working with here and integrate over the full $(-\infty, \infty)$ invariant mass range. The contributions from the tails should be heavily suppressed and negligible but the integration region can (and indeed has been in the present implementation) appropriately confined to the kinematically available phase space as

$$\int_{-S}^{S} \frac{dp^2}{(p^2-m^2)^2 \; + \; m^2\Gamma^2} = \frac{1}{m\,\Gamma} \int_{\arctan\frac{-S-m^2}{m\,\Gamma}}^{\arctan\frac{S-m^2}{m\,\Gamma}} d\theta \,, \tag{A.18}$$

where $S = E^2_{\mathrm{C.M.}}$ is the hadronic centre-of-mass energy squared.

[10] The value of this integral gives the prefactor used in the narrow-width approximation (equation 2.86), as expected.

A.6 The Veto Algorithm

Parton shower evolution consists of the iterative generation of emission variables t and z according to the distribution

$$\mathcal{P}(t,z) = \mathcal{K}(t,z)\,\Delta(t,t_0)\,. \tag{A.21}$$

For an analytically integrable distribution of a single variable, $f(t)$, with primitive integral $F(t)$ and with an invertible integral, $F^{-1}(t)$, the task of generating values according to it can be performed by generating random numbers, $\mathcal{R}_i$, and computing

$$t_i = F^{-1}\left(F(t_{\min}) + \mathcal{R}_i\left(F(t_{\max}) - F(t_{\min})\right)\right) \tag{A.22}$$

as many times as desired.

However if the integral of $f(t)$ and its inverse are not analytically tractable, as is the case for $\mathcal{K}(t,z)$ in equation 5.21, a numerical algorithm must be employed. The method used in this work is known as the *veto algorithm*.

This algorithm consists of finding a bounding function, $b(t)$, which is everywhere larger than $f(t)$, and is also (unlike $f(t)$ itself), analytically integrable and with an invertible integral. Values of t can then be generated according to this bounding function using equation A.22, and accepted or rejected according to $\frac{f(t)}{b(t)}$. This can be proven (see [188, 202, 204, 246]) to generate values of t exactly according to equation 5.21.

Once the bounding function $b(t)$ has been found, the algorithm proceeds as follows:

1. start with the highest allowed value for t, $t_i = t_I$;

2. generate a random number, $\mathcal{R}$, and compute the next scale as[11]

$$t_{i+1} = B^{-1}[\log\mathcal{R} + B(t_i)]\,,$$

   where $B(t)$ is the primitive integral of $b(t)$;

[11] Given that the Sudakov form factor represents the inclusive probability of no resolvable emission between two scales, by unitarity the probability of emission between a high initial scale t_I and a lower scale t is given by

$$\mathcal{P}(t) = 1 - \Delta(t_I,t) \;=\; 1 - \exp[F(t) - F(t_I)]\,.$$

Equating this expression to a random number and solving for t gives

$$t = F^{-1}(\log\mathcal{R} + F(t_I))\,,$$

where we have made the replacement $(1-\mathcal{R}) \to \mathcal{R}$ which is valid for $\mathcal{R} \in [0,1]$, which we will always assume. This is therefore the form of equation A.22 required here.

3. using another random number accept t_{i+1} as the scale of the next emission if

$$\mathcal{R} < \frac{f(t_{i+1})}{b(t_{i+1})}\,;$$

4. if this value of t_{i+1} has been rejected return to step 2.

However, in the case at hand the function being considered is a function not only of the scale t but also of the energy fraction of the splitting, z. This requires the use of an extended form of the veto algorithm known as the *bivariant veto algorithm* to generate values of both t and z according to equation 5.21.

In this case we must choose a bounding function, $b(t,z)$, such that

$$b(t,z) = b_1(t)\,b_2(z) > \mathcal{K}(t,z) \quad \forall\ (t,z) \in \mathbf{\Phi}_1\,.$$

The algorithm then proceeds by

1. starting with $t_i = t_I$;

2. generate a scale as

$$t_{i+1} = B^{-1}[\log\mathcal{R} + B(t_i)]\,,$$

where

$$b(t) = b_1(t)\int dz\, b_2(z)\,;$$

3. generate z for this scale as

$$z_{i+1} = B_2^{-1}\left(B_2(z_{\min}) + \mathcal{R}\left(B_2(z_{\max}) - B_2(z_{\min})\right)\right)\,;$$

4. accept (t_{i+1}, z_{i+1}) if

$$\mathcal{R} < \frac{f(t_{i+1}, z_{i+1})}{b(t_{i+1}, z_{i+1})}\,;$$

5. otherwise return to step 2 and use the rejected scale as input to generate the next trial scale.

The scale, t, at which each emission emission occurs and the energy fraction, z, of the splitting are therefore correctly generated according to equation 5.21. The remaining third variable to fully specify a splitting is its azimuthal angle, which is generated uniformly as $\phi = 2\,\pi\,\mathcal{R}$ using another random number.

In order to correctly account for all the possible splittings from a given parent parton as expressed as the sum over parton flavours in the Sudakov form factor one must proceed by generating values according to each configuration and accepting them by *competition* (otherwise known as the *highest-bid method*). This consists

of accepting the emission from the subprocess which occurs at the highest scale t, as this is the one which will have happened first and therefore the one which must be accepted (see [188, 202, 204]).

Note that for both the simple and the bivariant veto method to work the factor multiplying the Sudakov in the second term of equation 5.10 must be identical to the integrand in the argument of the Sudakov. This requirement strongly constrains extensions of the fixed order and parton shower merging method and must be respected to facilitate the numerical treatment.

Appendix B

Technical Remarks

B.1 The Definition of Width

The necessary introduction of width to regulate squark propagators and render them physical resonances instead of singularities is fraught with subtleties and intrinsic ambiguities stemming from the fact that width is higher-order effect[1] which requires a form of resummation as well as the introduction of a renormalisation scheme, and it is only in the context of a given renormalisation scheme that quantities such as width (and mass) are consistently defined.

The concept of width arises and can be defined in at least two different but related contexts:

- as a fixed-order $1 \to 2$ calculation of a decay rate of the form

$$\Gamma = \frac{1}{2m} \sum_{f_1\, f_2} \int \mathbf{\Phi}_2 \, |\mathcal{M}_{i \to f_1\, f_2}|^2 \,, \tag{B.1}$$

  which is formally ill-defined as it falls foul of the LSZ reduction formula since the unstable state i is not an asymptotic, free stable state from which an S-matrix can be computed;

- as the imaginary component of an all-orders resummation of loop corrections to the unstable particle's propagator.

The first definition can be better motivated through the optical theorem

$$2\mathrm{Im}\, \mathcal{M}_{a \to b} = \sum_{f_i} \int d\mathbf{\Phi}_2 \mathcal{M}^*_{b \to \{f_i\}} \mathcal{M}_{a \to \{f_i\}} \,, \tag{B.2}$$

[1] A particle's width is not a parameter of the Lagrangian, or indeed the Feynman rules as these are are perturbatively defined as an expansion of a free theory with stable particles.

where f_i runs over all possible final states both a and b couple to. Using this to consider the $1 \to 1$ process within which the amplitudes for all possible splittings $i \to f_1\, f_2$ are considered as self-energy corrections, as

$$\operatorname{Im} \mathcal{M}_{a\to a} = \frac{1}{2} \sum_{f_i} \int d\mathbf{\Phi}_2 \mathcal{M}^*_{a\to\{f_i\}} \mathcal{M}_{a\to\{f_i\}} \,, \tag{B.3}$$

the left-hand side can be identified[2] to be equal to the imaginary part of the 1-loop self-energy correction, $\Sigma(p^2)$, (where p^2 is the virtuality of the external legs of the loop) and the right-hand side can be seen to be equal to the right-hand side of equation B.1 up to a factor of $1/m$.

The conventional definition of the width is then

$$\Gamma_{\text{conv}} = \frac{1}{m_{\text{conv}}} \operatorname{Im} \Sigma(p^2) \,, \tag{B.4}$$

where we assume wavefunction renormalisation has already taken place and omitted the corresponding factor[3] of Z_A.

Alternatively, using the all-orders formulation the infinite series of 1-loop insertions on a scalar/vector propagator gives a contribution of the form[4]

$$\frac{1}{p^2 - m_0^2} \sum_{n=0}^{\infty} \left(\frac{-\Sigma(p^2)}{p^2 - m_0^2} \right)^n \tag{B.5}$$

which is a geometric series which can be summed[5] to give the *Dyson-resummed* propagator

$$P(p^2) \;=\; \frac{1}{p^2 - m_0^2 + \Sigma(p^2)} \,, \tag{B.6}$$

which includes 1-loop self-energy contributions to all orders.

Constraining this propagator to be of the form[6]

$$\frac{1}{p^2 - m_0^2 + im\Gamma} \,, \tag{B.7}$$

which is required to give the relativistic Breit-Wigner resonance shape which we expect upon computing the squared amplitude gives the relation

$$m\Gamma = \operatorname{Im} \Sigma(p^2) \,, \tag{B.8}$$

which is of the same form as the width defined in equation B.4. This is therefore the canonical definition of

[2] Here $\Sigma(p^2)$ denotes the fermionic 1-loop corrections to a scalar propagator, or the transverse part (proportional to $g^{\mu\nu}$) of such corrections for a vector propagator.

[3] This factor is singular and within perturbation theory can be written as $A_0 = Z_A^{\frac{1}{2}} A = (1 + \delta Z) A$ for a scalar/vector field A, where the singular contribution δZ_A, can be written separately as part of a renormalisation counterterm Lagrangian which we have so far omitted. It is precisely the scale-dependence of these renormalisation factors (namely Z_g which renormalises the coupling) which gives the running of the coupling (see section 6 of [179] for derivation)

[4] Here we have made explicit that the mass is the as of yet unrenormalised bare mass.

[5] Using the relation $a \sum_{n=0}^{\infty} r^n = \frac{a}{1-r}$ which holds provided $r \in (-1, 1)$.

[6] Both here and in equation B.6 we omit a wavefunction renormalisation factor of Z from the numerator.

width, which different renormalisation schemes can be applied to to produce observable quantities.

Defining the mass in the *on-shell scheme* to be the value of p^2 such that the real part of the denominator of the Dyson-resummed propagator is zero, $P^{-1}(m^2_{\rm os}) = 0$, we have

$$m^2_{\rm os} - m^2_0 + {\rm Re}\Sigma(m^2_{\rm os}) = 0 \qquad \Rightarrow \qquad m^2_{\rm os} = m^2_0 - {\rm Re}\Sigma(m^2_{\rm os})\,. \tag{B.9}$$

Rewriting $P^{-1}(p^2)$ in terms of the on-shell mass, separating the self-energy contribution into real and imaginary parts and rewriting the real part using the Taylor expansion

$$\Sigma(p^2) \approx \Sigma(p^2 - m^2_{\rm os})\Big|_{\rm T.E.(m^2_{os}=0)}\,, \tag{B.10}$$

we have

$$\begin{aligned} P^{-1}(p^2) &= p^2 - m^2_{\rm os} + \Sigma(p^2) - {\rm Re}\,\Sigma(m^2_{\rm os}) \\ &= i{\rm Im}\,\Sigma(p^2) + (p^2 - m^2_{\rm os})(1 + {\rm Re}\,\Sigma'(m^2_{\rm os})) \;+\; \mathcal{O}\left((p^2 - m^2_{\rm os})^2\right) \\ &= Z^{-1}\left[p^2 - m^2_{\rm os} + i\,Z{\rm Im}\,\Sigma(p^2)\right] \;+\; \mathcal{O}\left((p^2 - m^2_{\rm os})^2\right)\,, \end{aligned} \tag{B.11}$$

where we have defined $Z = \frac{1}{1+{\rm Re}\,\Sigma'(p^2)}$. Setting this propagator equal to the Breit-Wigner propagator and evaluating the self-energy at $m^2_{\rm os}$ gives the definition of width in the on-shell scheme as

$$m_{\rm os}\Gamma_{\rm os} = Z{\rm Im}\,(m^2_{\rm os}) = \frac{{\rm Im}\,\Sigma(m^2_{\rm os})}{1 + {\rm Re}\,\Sigma'(m^2_{\rm os})}\,. \tag{B.12}$$

Equations B.9 and B.12 together define the mass and width in the on-shell scheme, respectively.

The *pole scheme* is defined such that the renormalised pole mass, m, and pole scheme width, Γ, correspond to the position of the pole in the propagator of the corresponding propagator, such that a complex, renormalised mass can be defined as

$$\mu^2 = m^2 - im\Gamma\,. \tag{B.13}$$

This finite complex mass must be equal to the sum of the bare mass with the Dyson-resummed contribution, $\mu^2 = m^2_0 - \Sigma(\mu^2)$ (note the argument of the self-energy correction), such that we have the relation

$$\begin{aligned} m^2_0 - im\Gamma &= m^2_0 - \Sigma(m^2 - im\Gamma) \\ &= m^2_0 - \Sigma(m^2) + im\Gamma\Sigma'(m^2) + \frac{1}{2}(m\Gamma)^2\Sigma''(m^2) + \mathcal{O}(\alpha^4)\,, \end{aligned} \tag{B.14}$$

where we have expanded the self-energy contribution around m^2 (or rather about $im\Gamma \approx 0$) and α corresponds to the coupling of the 1-loop self-energy diagram (for the case of squark width which we are concerned with, $\alpha = \alpha_S$).

Taking the real and imaginary parts of equation B.14 yields

$$m^2 = m_0^2 - \mathrm{Re}\,\Sigma(m^2) - m\Gamma \mathrm{Im}\,\Sigma'(m^2) + \mathcal{O}(\alpha^2)\,, \tag{B.15a}$$

$$m\Gamma = \mathrm{Im}\,\Sigma(m^2) - m\Gamma \mathrm{Re}\,\Sigma'(m^2) - \frac{1}{2}(m\Gamma)^2 \mathrm{Im}\,\Sigma''(m^2) + \mathcal{O}(\alpha^4)\,, \tag{B.15b}$$

respectively, where iteratively inserting the expression for $m\Gamma$ gives

$$m^2 = m_0^2 - \mathrm{Re}\,\Sigma(m^2) - \mathrm{Im}\,\Sigma(m^2)\mathrm{Im}\,\Sigma'(m^2) + \mathcal{O}(\alpha^3)\,, \tag{B.16}$$

$$m\Gamma = \mathrm{Im}\,\Sigma(m^2)\left[1 - \mathrm{Re}\,\Sigma'(m^2) + (\mathrm{Re}\,\Sigma'(m^2))^2 - \frac{1}{2}\mathrm{Im}\,\Sigma(m^2)\mathrm{Im}\,\Sigma''(m^2) + \mathcal{O}(\alpha^3)\right], \tag{B.17}$$

which are the perturbative definitions of the pole mass and width, respectively.

A perturbative expansion of this type can be obtained for any mass and scheme width, and their differences and conversion formulas to a given order can thereby be found.

The on-shell and pole schemes are the most commonly used, with the masses and widths for the SM gauge bosons, top quark[7] and tau lepton (including the values quoted by the Particle Data Group and used by the ATLAS and CMS collaborations) typically being quoted in the pole scheme. Numerical differences between schemes are often comparable to the experimental mass resolution possible, as is the case for the W and Z bosons where $m_{W,\,\mathrm{os}} - m_W \approx 27\ \mathrm{MeV}$ and $m_{Z,\,\mathrm{os}} - m_Z \approx 34\ \mathrm{MeV}$, or the top quark where $m_{t,\,\overline{\mathrm{MS}}}(m_t^2) - m_t \approx 1\ \mathrm{GeV}$ [248].

There is a further scheme introduced in [249] known as the *complex-mass scheme* which is guaranteed to preserve gauge invariance to all orders, however we will not discuss it here as we do not use it.

Each scheme has its own strengths and weaknesses and must be chosen appropriately. The pole scheme is sensitive to non-perturbative $\mathcal{O}(\Lambda_{\mathrm{QCD}})$ renormalon[8] corrections [247], the on-shell scheme is subject to threshold singularities [250] and becomes gauge dependent beyond 1-loop order [251], etc. The scheme used for any given unstable particle must be chosen as the one with the best convergence properties. For heavy coloured particles such as heavy quarks (namely the top quark, or the squarks which we deal with) where precision measurements are possible but the pole mass is sensitive to soft corrections (the renormalon corrections just mentioned) *short-distance* schemes such as the $\overline{\mathrm{MS}}$ scheme can be defined such that that insensitivity to long-distance soft corrections is precisely their defining characteristic. Many such schemes can be defined (see [252] for more) and it is the $\overline{\mathrm{MS}}$ scheme which is used for squarks.

It is worth noting that particle masses and widths are often experimentally determined by one of two methods. The first and theoretically best defined is by measuring the signal cross section, extrapolating out of

[7] Even though the pole mass is ill-defined for any coloured particle due to confinement, and even for the unconfined top quark due to colour conservation considerations [247].

[8] Soft singularities in the 1-loop self-energy insertions on a line which is itself a loop in a self-energy correction.

the detector's geometric acceptance and fitting to it a given mass value in an analytic calculation of the total cross section, consistently performed in a given renormalisation sheme so that the scheme of the measurement is well defined, but often the error of the fit is sizeable. The other more popular method is to fit measured invariant mass distributions to Monte Carlo-generated *templates* with different mass values. This yields very precise results but their accuracy is questionable given that in the presence of a parton shower required to generate realistic distributions the mass and width schemes are ill-defined (or are in the ill-defined so-called *Monte Carlo scheme*) given that it is not clear which scheme the mass factorisation implicitly performed by the parton shower corresponds to (or resembles), if any[9]. For a discussion of how this scheme ambiguity in the commonly used top quark mass impacts for example the SM electroweak vacuum stability see [253].

We use squark masses widths in the $\overline{\rm MS}$ scheme, with fixed width (the width can be be allowed to run as $m\Gamma \to p^2 \frac{\Gamma}{m}$ but schemes with running width violate gauge invariance and as a consequence have been found to produce erratic behaviour [249]). Though we do include the width out of necessity, we do not include real emission radiative corrections from the squark, as is done for example in the case of squark pair production in [254].

The squark 1-loop self-energy corrections relevant to us, along with explicit expressions for the required renormalisation factors Z_i in the $\overline{MS}$ scheme can be found in [255] and are included in the SPHENO and SOFTSUSY packages we use[10].

Further discussion of the various possible treatments of finite width can be found in [214, 257–260].

B.2 Renormalisation of SUSY Radiative Corrections

There are interesting issues concerning the use of dimensional regularisation in calculations of radiative corrections to SUSY processes which we will only briefly comment on, as they turn out to be effectively higher order for our purposes, and we assume they have been appropriately accounted for in the virtual contribution we take from PROSPINO2.

One is the issue that in the $d = 4 - 2\epsilon$ dimensions that dimensional regularisation requires the gluon and the gluino no longer have the same number of helicity degrees of freedom, even in the energy regime where SUSY is assumed to be unbroken. The gluon has the $d - 2$ degrees of freedom of a massless vector field in d dimensions, whilst the gluino has 2 polarisations in d dimensions. The regularisation procedure has therefore broken SUSY and this is a highly undesirable and accidental feature of dimensional regularisation.

[9] A perturbative expansion relating the Monte Carlo scheme to any of the known schemes has yet to be constructed.
[10] The 2-loop contributions are known but negligible [256].

The Dirac algebra is also complicated by dimensional regularisation as the γ^5 matrix required to describe chiral fermions can be defined from the other gamma matrices for example as $\gamma^5 = -i\gamma^0\gamma^1\gamma^2\gamma^3$ and it therefore anti-commutes with the other gamma matrices in 4 dimensions, $\{\gamma^5, \gamma^\mu\} = 0$, as required. However there is no known definition of γ^5 which has this property in a general d-dimensional representation (see section 3 of [261]).

A commonly used technique to deal with this problem is *dimensional reduction* (DRED) [262, 263] which consists of computing the loop integrals in d dimensions as required for regularisation, but keeping the fields and the gamma matrices in 4 dimensions, such that SUSY is preserved (at least at the 1-loop level, it is known to break down at higher orders) and γ^5 is well defined. Conventional $\overline{\text{MS}}$ PDF sets can be used with DRED amplitudes but additional dipoles are required for the dipole subtraction [264]. DRED also introduces issues with mass factorisation which require special treatment [264, 265].

Alternatively the radiative corrections can be computed using the standard $\overline{\text{MS}}$ scheme, and a finite shift of the quark-squark-gluino coupling, $\hat{g_S}$, from being equal to the gauge coupling of the quark-quark-gluon vertex (by SUSY), g_S, to the value

$$\hat{g_S} = g_S \left[1 + \frac{\alpha_S}{3\pi}\right], \tag{B.18}$$

can be used to restore SUSY at 1 loop [125, 266]. This correction impacts the calculation of the virtual contribution diagrams of figure 6.3 and is indeed how the virtual contribution we take from PROSPINO2 (for both slepton and gaugino pair production) is computed [210].

Note that a SUSY-breaking modification of a Yukawa/trilinear coupling, as is effectively introduced by using dimensional regularisation constitutes an explicit hard (non-soft) breaking of SUSY of the type that breaks relations of the form of equation 2.109 and therefore impairs its ability to solve the hierarchy problem. This contribution therefore cannot be simply reabsorbed into a soft-SUSY breaking parameter of equation 2.149 and must instead be cancelled by using a counterterm as given in equation B.18 if SUSY is to be only softly broken, as required.

Bibliography

[1] W. de Boer and C. Sander, *Global electroweak fits and gauge coupling unification*, *Phys.Lett.* **B585** (2004) 276–286 [hep-ph/0307049].

[2] A. Papaefstathiou and O. Latunde-Dada, *NLO production of W ' bosons at hadron colliders using the MC@NLO and POWHEG methods*, *JHEP* **0907** (2009) 044 [0901.3685].

[3] B. Jager, A. von Manteuffel and S. Thier, *Slepton pair production in the POWHEG BOX*, *JHEP* **1210** (2012) 130 [1208.2953].

[4] B. Jager, A. von Manteuffel and S. Thier, *Slepton pair production in association with a jet: NLO-QCD corrections and parton-shower effects*, 1410.3802.

[5] R. Gavin, C. Hangst, M. Krmer, M. Mhlleitner, M. Pellen *et. al.*, *Matching Squark Pair Production at NLO with Parton Showers*, *JHEP* **10** (2013) 187 [1305.4061].

[6] **High Resolution Fly's Eye Collaboration** Collaboration, R. U. Abbasi *et. al.*, *First Observation of the Greisen-Zatsepin-Kuzmin Suppression*, *Phys. Rev. Lett.* **100** (Mar, 2008) 101101.

[7] **IceCube Collaboration** Collaboration, M. Aartsen *et. al.*, *First observation of PeV-energy neutrinos with IceCube*, 1304.5356.

[8] M. Melles, *Electroweak radiative corrections in high-energy processes*, *Phys.Rept.* **375** (2003) 219–326 [hep-ph/0104232].

[9] S. A. Abel, J. R. Ellis, J. Jaeckel and V. V. Khoze, *Will the LHC Look into the Fate of the Universe?*, 0807.2601.

[10] G. Degrassi, S. Di Vita, J. Elias-Miro, J. R. Espinosa, G. F. Giudice *et. al.*, *Higgs mass and vacuum stability in the Standard Model at NNLO*, *JHEP* **1208** (2012) 098 [1205.6497].

[11] L. N. Mihaila, J. Salomon and M. Steinhauser, *Gauge Coupling Beta Functions in the Standard Model to Three Loops*, *Phys.Rev.Lett.* **108** (2012) 151602 [1201.5868].

[12] **CTEQ Collaboration** Collaboration, R. Brock *et. al.*, *Handbook of perturbative QCD; Version 1.1: September 1994*, *Rev. Mod. Phys.* (1994).

[13] N. Vandersickel and D. Zwanziger, *The Gribov problem and QCD dynamics*, *Phys.Rept.* **520** (2012) 175–251 [1202.1491].

[14] K. Ottnad, B. Kubis, U.-G. Meissner and F.-K. Guo, *New insights into the neutron electric dipole moment*, *Phys.Lett.* **B687** (2010) 42–47 [0911.3981].

[15] A. Anselm and A. Johansen, *Can electroweak theta term be observable?*, *Nucl.Phys.* **B412** (1994) 553–573 [hep-ph/9305271].

[16] S. D. Hsu, *Physical consequences of the QED theta angle*, 1012.2906.

[17] M. Bahr, S. Gieseke, M. Gigg, D. Grellscheid, K. Hamilton *et. al.*, *Herwig++ Physics and Manual*, *Eur.Phys.J.* **C58** (2008) 639–707 [0803.0883].

[18] H. Murayama, I. Watanabe and K. Hagiwara, *HELAS: HELicity amplitude subroutines for Feynman diagram evaluations*, .

[19] P. Richardson, *Simulations of R-parity violating SUSY models*, hep-ph/0101105.

[20] S. Catani, D. de Florian and G. Rodrigo, *Space-like (versus time-like) collinear limits in QCD: Is factorization violated?*, *JHEP* **1207** (2012) 026 [1112.4405].

[21] J. R. Forshaw, M. H. Seymour and A. Siodmok, *On the Breaking of Collinear Factorization in QCD*, *JHEP* **1211** (2012) 066 [1206.6363].

[22] B. Kors and P. Nath, *Aspects of the Stueckelberg extension*, *JHEP* **0507** (2005) 069 [hep-ph/0503208].

[23] J. Jaeckel, *A force beyond the Standard Model - Status of the quest for hidden photons*, *Frascati Phys.Ser.* **56** (2013) 172–192 [1303.1821].

[24] **ATLAS** Collaboration, G. Aad *et. al.*, *Observation of a new particle in the search for the Standard Model Higgs boson with the ATLAS detector at the LHC*, *Phys.Lett.* **B716** (2012) 1–29 [1207.7214].

[25] **CMS Collaboration** Collaboration, S. Chatrchyan *et. al.*, *Observation of a new boson at a mass of 125 GeV with the CMS experiment at the LHC*, *Phys.Lett.* **B716** (2012) 30–61 [1207.7235].

[26] **ATLAS Collaboration** Collaboration, *Combined coupling measurements of the Higgs-like boson with the ATLAS detector using up to 25 fb^{-1} of proton-proton collision data*, Tech. Rep. ATLAS-CONF-2013-034, CERN, Geneva, Mar, 2013.

[27] **CMS Collaboration** Collaboration, *Combination of standard model Higgs boson searches and measurements of the properties of the new boson with a mass near 125 GeV*, Tech. Rep. CMS-PAS-HIG-13-005, CERN, Geneva, 2013.

[28] **ATLAS Collaboration** Collaboration, *Combined measurements of the mass and signal strength of the Higgs-like boson with the ATLAS detector using up to 25 fb^{-1} of proton-proton collision data*, Tech. Rep. ATLAS-CONF-2013-014, CERN, Geneva, Mar, 2013.

[29] **CMS Collaboration** Collaboration, S. Chatrchyan *et. al.*, *Study of the Mass and Spin-Parity of the Higgs Boson Candidate Via Its Decays to Z Boson Pairs*, *Phys.Rev.Lett.* **110** (2013) 081803 [1212.6639].

[30] **ATLAS Collaboration** Collaboration, *Study of the spin of the new boson with up to 25 fb^{-1} of ATLAS data*, Tech. Rep. ATLAS-CONF-2013-040, CERN, Geneva, Apr, 2013.

[31] L. Landau, *On the angular momentum of a two-photon system*, *Dokl.Akad.Nauk Ser.Fiz.* **60** (1948) 207–209.

[32] C.-N. Yang, *Selection Rules for the Dematerialization of a Particle Into Two Photons*, *Phys.Rev.* **77** (1950) 242–245.

[33] H. E. Haber, *Nonminimal Higgs sectors: The Decoupling limit and its phenomenological implications*, hep-ph/9501320.

[34] M. S. Carena and H. E. Haber, *Higgs boson theory and phenomenology*, *Prog.Part.Nucl.Phys.* **50** (2003) 63–152 [hep-ph/0208209].

[35] F. Jegerlehner, *Comment on $H \to \gamma\gamma$ and the Role of the Decoupling theorem and the Equivalence Theorem*, 1110.0869.

[36] T. Appelquist and J. Carazzone, *Infrared Singularities and Massive Fields*, *Phys.Rev.* **D11** (1975) 2856.

[37] F. Jegerlehner, *The hierarchy problem of the electroweak Standard Model revisited*, 1305.6652.

[38] D. Choudhury, A. Kundu and P. Saha, *Z-pole observables in an effective theory*, 1305.7199.

[39] M. Baak, M. Goebel, J. Haller, A. Hoecker, D. Kennedy *et. al.*, *The Electroweak Fit of the Standard Model after the Discovery of a New Boson at the LHC*, *Eur.Phys.J.* **C72** (2012) 2205 [1209.2716].

[40] **Particle Data Group** Collaboration, J. Beringer *et. al.*, *Review of Particle Physics (RPP)*, *Phys.Rev.* **D86** (2012) 010001.

[41] K. Melnikov, *On the theoretical uncertainties in the muon anomalous magnetic moment*, *Int.J.Mod.Phys.* **A16** (2001) 4591–4612 [hep-ph/0105267].

[42] K. Hagiwara, R. Liao, A. D. Martin, D. Nomura and T. Teubner, $(g-2)_m u$ *and* $\alpha(M_Z^2)$ *re-evaluated using new precise data*, *J.Phys.* **G38** (2011) 085003 [1105.3149].

[43] M. Bohm, A. Denner and H. Joos, *Gauge theories of the strong and electroweak interaction*. 2001.

[44] H. Georgi and S. Glashow, *Unity of All Elementary Particle Forces*, *Phys.Rev.Lett.* **32** (1974) 438–441.

[45] C. Itzykson and M. Nauenberg, *UNITARY GROUPS: REPRESENTATION AND DECOMPOSITIONS*, *Rev.Mod.Phys.* **38** (1966) 95–120.

[46] R. Robinett and J. L. Rosner, *Mass Scales in Grand Unified Theories*, *Phys.Rev.* **D26** (1982) 2396.

[47] H. Murayama and A. Pierce, *Not even decoupling can save minimal supersymmetric SU(5)*, *Phys.Rev.* **D65** (2002) 055009 [hep-ph/0108104].

[48] **Super-Kamiokande Collaboration** Collaboration, Y. Hayato *et. al.*, *Search for proton decay through p —¿ anti-neutrino K+ in a large water Cherenkov detector*, *Phys.Rev.Lett.* **83** (1999) 1529–1533 [hep-ex/9904020].

[49] J. L. Hewett and T. G. Rizzo, *Low-Energy Phenomenology of Superstring Inspired E(6) Models*, *Phys.Rept.* **183** (1989) 193.

[50] A. Font, L. E. Ibanez and F. Quevedo, *Does Proton Stability Imply the Existence of an Extra Z0?*, *Phys.Lett.* **B228** (1989) 79.

[51] P. Langacker, R. W. Robinett and J. L. Rosner, *New Heavy Gauge Bosons in p p and p anti-p Collisions*, *Phys.Rev.* **D30** (1984) 1470.

[52] S. L. Adler and W. A. Bardeen, *Absence of higher order corrections in the anomalous axial vector divergence equation*, *Phys.Rev.* **182** (1969) 1517–1536.

[53] L. Alvarez-Gaume and M. A. Vazquez-Mozo, *Introductory lectures on quantum field theory*, hep-th/0510040.

[54] J. Erler, P. Langacker, S. Munir and E. Rojas, *Z' Bosons at Colliders: a Bayesian Viewpoint*, *JHEP* **1111** (2011) 076 [1103.2659].

[55] B. Holdom, *Two U(1)'s and Epsilon Charge Shifts*, *Phys.Lett.* **B166** (1986) 196.

[56] P. Langacker and J. Wang, *U(1)-prime symmetry breaking in supersymmetric E(6) models*, *Phys.Rev.* **D58** (1998) 115010 [hep-ph/9804428].

[57] D. Feldman, Z. Liu and P. Nath, *The Stueckelberg Z Prime at the LHC: Discovery Potential, Signature Spaces and Model Discrimination*, *JHEP* **0611** (2006) 007 [hep-ph/0606294].

[58] D. Feldman, Z. Liu and P. Nath, *The Stueckelberg Z-prime Extension with Kinetic Mixing and Milli-Charged Dark Matter From the Hidden Sector*, *Phys.Rev.* **D75** (2007) 115001 [hep-ph/0702123].

[59] A. Dueck and W. Rodejohann, *Fits to SO(10) Grand Unified Models*, 1306.4468.

[60] E. Dudas, L. Heurtier, Y. Mambrini and B. Zaldivar, *Extra U(1), effective operators, anomalies and dark matter*, 1307.0005.

[61] M. Dittmar, A.-S. Nicollerat and A. Djouadi, *Z-prime studies at the LHC: An Update*, *Phys.Lett.* **B583** (2004) 111–120 [hep-ph/0307020].

[62] F. Del Aguila, *The Physics of z-prime bosons*, *Acta Phys.Polon.* **B25** (1994) 1317–1336 [hep-ph/9404323].

[63] L. Durkin and P. Langacker, *Neutral Current Constraints on Heavy Z Bosons*, *Phys.Lett.* **B166** (1986) 436.

[64] F. D. Aguila, G. Coughlan and M. Quirs, *Gauge coupling renormalisation with several u(1) factors*, *Nuclear Physics B* **307** (1988), no. 3 633 – 648.

[65] K. Babu, C. F. Kolda and J. March-Russell, *Implications of generalized Z - Z-prime mixing*, *Phys.Rev.* **D57** (1998) 6788–6792 [hep-ph/9710441].

[66] T. G. Rizzo, *Gauge Kinetic Mixing in the E_6SSM*, *Phys.Rev.* **D85** (2012) 055010 [1201.2898].

[67] J. Heeck and W. Rodejohann, *Kinetic and mass mixing with three abelian groups*, *Phys.Lett.* **B705** (2011) 369–374 [1109.1508].

[68] J. Erler and P. Langacker, *Constraints on extended neutral gauge structures*, *Phys.Lett.* **B456** (1999) 68–76 [hep-ph/9903476].

[69] J. Erler, P. Langacker, S. Munir and E. Rojas, *Improved constraints on z ' bosons from electroweak precision data*, *Journal of High Energy Physics* **2009** (2009), no. 08 017.

[70] N. Kauer and G. Passarino, *Inadequacy of zero-width approximation for a light Higgs boson signal*, *JHEP* **1208** (2012) 116 [1206.4803].

[71] P. Langacker, *The Physics of Heavy Z' Gauge Bosons*, *Rev.Mod.Phys.* **81** (2009) 1199–1228 [0801.1345].

[72] **ATLAS** Collaboration, *Search for high-mass dilepton resonances in 20 fb^{-1} of pp collisions at $\sqrt{s} = 8$ tev with the atlas experiment*, Tech. Rep. ATLAS-CONF-2013-017, CERN, Geneva, Mar, 2013.

[73] **CMS** Collaboration, S. Chatrchyan *et. al.*, *Search for heavy narrow dilepton resonances in pp collisions at $\sqrt{s} = 7$ TeV and $\sqrt{s} = 8$ TeV*, *Phys.Lett.* **B720** (2013) 63–82 [1212.6175].

[74] M. Cvetic and S. Godfrey, *Discovery and identification of extra gauge bosons*, hep-ph/9504216.

[75] A. Gulov and A. Kozhushko, *Model-Independent Estimates for the Couplings of the Abelian Z' Boson in the Drell-Yan Process at the LHC*, 1307.2393.

[76] **ATLAS** Collaboration, *A search for $t\bar{t}$ resonances in the lepton plus jets final state with atlas using 14 fb^{-1} of pp collisions at $\sqrt{s} = 8$ tev*, Tech. Rep. ATLAS-CONF-2013-052, CERN, Geneva, May, 2013.

[77] J. Gao, C. S. Li, B. H. Li, C.-P. Yuan and H. X. Zhu, *Next-to-leading order QCD corrections to the heavy resonance production and decay into top quark pair at the LHC*, *Phys.Rev.* **D82** (2010) 014020 [1004.0876].

[78] F. Caola, K. Melnikov and M. Schulze, *A complete next-to-leading order QCD description of resonant Z' production and decay into $t\bar{t}$ final states*, *Phys.Rev.* **D87** (2013) 034015 [1211.6387].

[79] J. de Blas, *Electroweak limits on physics beyond the Standard Model*, 1307.6173.

[80] S. R. Coleman and J. Mandula, *All Possible Symmetries of the S Matrix*, *Phys.Rev.* **159** (1967) 1251–1256.

[81] R. Haag, J. T. Lopuszanski and M. Sohnius, *All Possible Generators of Supersymmetries of the s Matrix*, *Nucl.Phys.* **B88** (1975) 257.

[82] H. Muller-Kirsten and A. Wiedemann, *SUPERSYMMETRY: AN INTRODUCTION WITH CONCEPTUAL AND CALCULATIONAL DETAILS*. 1986.

[83] B. Allanach, "Supersymmetry (Cambridge Part III Lecture Notes)." http://www.damtp.cam.ac.uk/user/examples/indexP3.html, Apr, 2013. Accessed: 2013-11-25.

[84] E. Diehl, G. L. Kane, C. F. Kolda and J. D. Wells, *Theory, phenomenology, and prospects for detection of supersymmetric dark matter*, *Phys.Rev.* **D52** (1995) 4223–4239 [hep-ph/9502399].

[85] H. Baer, V. Barger and A. Mustafayev, *Neutralino dark matter in mSUGRA/CMSSM with a 125 GeV light Higgs scalar*, *JHEP* **1205** (2012) 091 [1202.4038].

[86] J. Ellis and K. A. Olive, *Revisiting the Higgs Mass and Dark Matter in the CMSSM*, *Eur.Phys.J.* **C72** (2012) 2005 [1202.3262].

[87] G. Blanger, G. Drieu La Rochelle, B. Dumont, R. M. Godbole, S. Kraml *et. al.*, *LHC constraints on light neutralino dark matter in the MSSM*, *Phys.Lett.* **B726** (2013) 773–780 [1308.3735].

[88] **BayesFITS Group** Collaboration, A. Fowlie, K. Kowalska, L. Roszkowski, E. M. Sessolo and Y.-L. S. Tsai, *Dark matter and collider signatures of the MSSM*, *Phys.Rev.* **D88** (2013), no. 5 055012 [1306.1567].

[89] C. Boehm, P. S. B. Dev, A. Mazumdar and E. Pukartas, *Naturalness of Light Neutralino Dark Matter in pMSSM after LHC, XENON100 and Planck Data*, *JHEP* **1306** (2013) 113 [1303.5386].

[90] A. Arbey, M. Battaglia and F. Mahmoudi, *Supersymmetry with Light Dark Matter confronting the recent CDMS and LHC Results*, *Phys.Rev.* **D88** (2013) 095001 [1308.2153].

[91] M. Cahill-Rowley, R. Cotta, A. Drlica-Wagner, S. Funk, J. Hewett *et. al.*, *Complementarity of Dark Matter Searches in the pMSSM*, 1405.6716.

[92] H. Baer, A. D. Box and H. Summy, *Neutralino versus axion/axino cold dark matter in the 19 parameter SUGRA model*, *JHEP* **1010** (2010) 023 [1005.2215].

[93] H. Baer, V. Barger, P. Huang, D. Mickelson, A. Mustafayev *et. al.*, *Naturalness, Supersymmetry and Light Higgsinos: A Snowmass Whitepaper*, 1306.2926.

[94] H. Baer, V. Barger and D. Mickelson, *Direct and indirect detection of higgsino-like WIMPs: concluding the story of electroweak naturalness*, *Phys.Lett.* **B726** (2013) 330–336 [1303.3816].

[95] G. Belanger, F. Boudjema, A. Pukhov and A. Semenov, $\mathrm{micrOMEGAs}_3$*: A program for calculating dark matter observables*, *Comput.Phys.Commun.* **185** (2014) 960–985 [1305.0237].

[96] **Planck Collaboration** Collaboration, P. Ade *et. al.*, *Planck 2013 results. XVI. Cosmological parameters*, 1303.5076.

[97] K. A. Olive, *Introduction to supersymmetry: Astrophysical and phenomenological constraints*, hep-ph/9911307.

[98] L. E. Ibanez and G. G. Ross, *SU(2)-L x U(1) Symmetry Breaking as a Radiative Effect of Supersymmetry Breaking in Guts*, *Phys.Lett.* **B110** (1982) 215–220.

[99] M. A. Luty, *2004 TASI lectures on supersymmetry breaking*, hep-th/0509029.

[100] M. Pospelov and A. Ritz, *Electric dipole moments as probes of new physics*, *Annals Phys.* **318** (2005) 119–169 [hep-ph/0504231].

[101] H. Fargnoli, C. Gnendiger, S. Passehr, D. Stckinger and H. Stckinger-Kim, *Non-decoupling two-loop corrections to $(g-2)_\mu$ from fermion/sfermion loops in the MSSM*, 1309.0980.

[102] M. Drees, *An Introduction to supersymmetry*, hep-ph/9611409.

[103] R. Argurio, "Introduction to Supersymmetry (PHYS-F-417) Lecture Notes." http://homepages.ulb.ac.be/~rargurio/susycourse.pdf, Nov, 2011. Accessed: 2013-12-01.

[104] J. Terning, *Modern supersymmetry: Dynamics and duality*, .

[105] S. P. Martin, *A Supersymmetry primer*, hep-ph/9709356.

[106] A. Signer, *ABC of SUSY*, *J.Phys.* **G36** (2009) 073002 [0905.4630].

[107] M. E. Peskin, *Supersymmetry in Elementary Particle Physics*, 0801.1928.

[108] A. Bilal, *Introduction to supersymmetry*, hep-th/0101055.

[109] F. Quevedo, S. Krippendorf and O. Schlotterer, *Cambridge Lectures on Supersymmetry and Extra Dimensions*, 1011.1491.

[110] Y. Shirman, *TASI 2008 Lectures: Introduction to Supersymmetry and Supersymmetry Breaking*, 0907.0039.

[111] G. L. Kane, *TASI lectures on weak scale supersymmetry: A Top motivated bottom up approach*, hep-ph/0202185.

[112] I. J. Aitchison, *Supersymmetry and the MSSM: An Elementary introduction*, hep-ph/0505105.

[113] D. Bertolini, J. Thaler and Z. Thomas, *TASI 2012: Super-Tricks for Superspace*, 1302.6229.

[114] J. D. Lykken, *Introduction to supersymmetry*, hep-th/9612114.

[115] H. Murayama, *Supersymmetry phenomenology*, hep-ph/0002232.

[116] M. Dine, *Supersymmetry Breaking at Low Energies*, *Nucl.Phys.Proc.Suppl.* **192-193** (2009) 40–60 [0901.1713].

[117] K. A. Intriligator and N. Seiberg, *Lectures on Supersymmetry Breaking*, *Class.Quant.Grav.* **24** (2007) S741–S772 [hep-ph/0702069].

[118] L. Girardello and M. T. Grisaru, *Soft Breaking of Supersymmetry*, *Nucl.Phys.* **B194** (1982) 65.

[119] D. Chung, L. Everett, G. Kane, S. King, J. D. Lykken *et. al.*, *The Soft supersymmetry breaking Lagrangian: Theory and applications*, *Phys.Rept.* **407** (2005) 1–203 [hep-ph/0312378].

[120] P. Z. Skands, B. Allanach, H. Baer, C. Balazs, G. Belanger *et. al.*, *SUSY Les Houches accord: Interfacing SUSY spectrum calculators, decay packages, and event generators*, *JHEP* **0407** (2004) 036 [hep-ph/0311123].

[121] J. Bellm, S. Gieseke, D. Grellscheid, A. Papaefstathiou, S. Platzer *et. al.*, *Herwig++ 2.7 Release Note*, 1310.6877.

[122] H. E. Haber and G. L. Kane, *The Search for Supersymmetry: Probing Physics Beyond the Standard Model*, *Phys.Rept.* **117** (1985) 75–263.

[123] J. Rosiek, *Complete Set of Feynman Rules for the Minimal Supersymmetric Extension of the Standard Model*, *Phys.Rev.* **D41** (1990) 3464.

[124] J. Gunion and H. E. Haber, *Higgs Bosons in Supersymmetric Models. 1.*, *Nucl.Phys.* **B272** (1986) 1.

[125] W. Hollik and D. Stockinger, *Regularization and supersymmetry restoring counterterms in supersymmetric QCD*, *Eur.Phys.J.* **C20** (2001) 105–119 [hep-ph/0103009].

[126] E. Dudas, Y. Mambrini, A. Mustafayev and K. A. Olive, *Relating the CMSSM and SUGRA Models with GUT Scale and Super-GUT Scale Supersymmetry Breaking*, *Eur.Phys.J.* **C72** (2012) 2138 [1205.5988].

[127] G. Giudice and A. Masiero, *A Natural Solution to the mu Problem in Supergravity Theories*, *Phys.Lett.* **B206** (1988) 480–484.

[128] B. Allanach, *SOFTSUSY: a program for calculating supersymmetric spectra*, *Comput.Phys.Commun.* **143** (2002) 305–331 [hep-ph/0104145].

[129] W. Porod, *SPheno, a program for calculating supersymmetric spectra, SUSY particle decays and SUSY particle production at e+ e- colliders*, *Comput.Phys.Commun.* **153** (2003) 275–315 [hep-ph/0301101].

[130] G.-C. Cho, K. Hagiwara, Y. Matsumoto and D. Nomura, *The MSSM confronts the precision electroweak data and the muon g-2*, *JHEP* **1111** (2011) 068 [1104.1769].

[131] A. Arbey, M. Battaglia, A. Djouadi, F. Mahmoudi and J. Quevillon, *Implications of a 125 GeV Higgs for supersymmetric models*, *Phys.Lett.* **B708** (2012) 162–169 [1112.3028].

[132] **MSSM Working Group** Collaboration, A. Djouadi *et. al.*, *The Minimal supersymmetric standard model: Group summary report*, hep-ph/9901246.

[133] C. F. Berger, J. S. Gainer, J. L. Hewett and T. G. Rizzo, *Supersymmetry Without Prejudice*, *JHEP* **0902** (2009) 023 [0812.0980].

[134] **ATLAS Collaboration** Collaboration, *Search for direct production of charginos and neutralinos in events with three leptons and missing transverse momentum in 21 fb^{-1} of pp collisions at $\sqrt{s} = 8$ TeV with the ATLAS detector*, Tech. Rep. ATLAS-CONF-2013-035, CERN, Geneva, Mar, 2013.

[135] **MEG Collaboration** Collaboration, J. Adam *et. al.*, *New constraint on the existence of the $\mu^+ \to e^+\gamma$ decay*, *Phys.Rev.Lett.* **110** (2013) 201801 [1303.0754].

[136] J. Hisano, T. Moroi, K. Tobe and M. Yamaguchi, *Lepton flavor violation via right-handed neutrino Yukawa couplings in supersymmetric standard model*, *Phys.Rev.* **D53** (1996) 2442–2459 [hep-ph/9510309].

[137] A. Masiero, S. K. Vempati and O. Vives, *Seesaw and lepton flavor violation in SUSY SO(10)*, *Nucl.Phys.* **B649** (2003) 189–204 [hep-ph/0209303].

[138] A. Bartl, W. Majerotto, W. Porod and D. Wyler, *Effect of supersymmetric phases on lepton dipole moments and rare lepton decays*, *Phys.Rev.* **D68** (2003) 053005 [hep-ph/0306050].

[139] B. Allanach, S. Kraml and W. Porod, *Theoretical uncertainties in sparticle mass predictions from computational tools*, *JHEP* **0303** (2003) 016 [hep-ph/0302102].

[140] H. Baer and X. Tata, *Weak scale supersymmetry: From superfields to scattering events*. 2006.

[141] S. Choi, M. Guchait, J. Kalinowski and P. Zerwas, *Chargino pair production at e+ e- colliders with polarized beams*, *Phys.Lett.* **B479** (2000) 235–244 [hep-ph/0001175].

[142] S. Choi, H. Haber, J. Kalinowski and P. Zerwas, *The Neutralino sector in the U(1)-extended supersymmetric standard model*, *Nucl.Phys.* **B778** (2007) 85–128 [hep-ph/0612218].

[143] D. M. Pierce, J. A. Bagger, K. T. Matchev and R.-j. Zhang, *Precision corrections in the minimal supersymmetric standard model*, *Nucl.Phys.* **B491** (1997) 3–67 [hep-ph/9606211].

[144] R. Barbieri and G. Giudice, *Upper Bounds on Supersymmetric Particle Masses*, *Nucl.Phys.* **B306** (1988) 63.

[145] J. D. Wells, *The Utility of Naturalness, and how its Application to Quantum Electrodynamics envisages the Standard Model and Higgs Boson*, 1305.3434.

[146] D. Ghilencea, *Fixing the EW scale in supersymmetric models after the Higgs discovery*, 1302.5262.

[147] J. L. Feng, *Naturalness and the Status of Supersymmetry*, *Ann.Rev.Nucl.Part.Sci.* **63** (2013) 351–382 [1302.6587].

[148] H. Baer, V. Barger and M. Padeffke-Kirkland, *Electroweak versus high scale finetuning in the 19-parameter SUGRA model*, *Phys.Rev.* **D88** (2013) 055026 [1304.6732].

[149] E. Hardy, *Is Natural SUSY Natural?*, *JHEP* **1310** (2013) 133 [1306.1534].

[150] K. R. Dienes, M. Lennek, D. Senechal and V. Wasnik, *Is SUSY Natural?*, *New J.Phys.* **10** (2008) 085003 [0804.4718].

[151] G. F. Giudice, *Naturally Speaking: The Naturalness Criterion and Physics at the LHC*, 0801.2562.

[152] A. Mustafayev and X. Tata, *Supersymmetry, Naturalness, and Light Higgsinos*, 1404.1386.

[153] N. Craig, *The State of Supersymmetry after Run I of the LHC*, 1309.0528.

[154] O. Buchmueller and J. Marrouche, *Universal mass limits on gluino and third-generation squarks in the context of Natural-like SUSY spectra*, 1304.2185.

[155] S. Kraml, S. Kulkarni, U. Laa, A. Lessa, W. Magerl *et. al.*, *SModelS: a tool for interpreting simplified-model results from the LHC and its application to supersymmetry*, 1312.4175.

[156] M. W. Cahill-Rowley, J. L. Hewett, A. Ismail and T. G. Rizzo, *More Energy, More Searches, but the pMSSM Lives On*, *Phys.Rev.* **D88** (2013) 035002 [1211.1981].

[157] J. Ellis, *Supersymmetric Fits after the Higgs Discovery and Implications for Model Building*, 1312.5426.

[158] M. Cacciari and N. Houdeau, *Meaningful characterisation of perturbative theoretical uncertainties*, *JHEP* **1109** (2011) 039 [1105.5152].

[159] S. Drell and T.-M. Yan, *Massive Lepton Pair Production in Hadron-Hadron Collisions at High-Energies*, *Phys.Rev.Lett.* **25** (1970) 316–320.

[160] G. Altarelli, R. K. Ellis and G. Martinelli, *Large Perturbative Corrections to the Drell-Yan Process in QCD*, *Nucl.Phys.* **B157** (1979) 461.

[161] J. Kubar-Andre and F. E. Paige, *Gluon Corrections to the Drell-Yan Model*, *Phys.Rev.* **D19** (1979) 221.

[162] J. C. Collins, D. E. Soper and G. Sterman, *Factorization for short distance hadron-hadron scattering*, *Nuclear Physics B* **261** (1985), no. 0 104 – 142.

[163] J. C. Collins, D. E. Soper and G. Sterman, *Factorization for one-loop corrections in the drell-yan process*, *Nuclear Physics B* **223** (1983), no. 2 381 – 421.

[164] R. Hamberg, W. van Neerven and T. Matsuura, *A Complete calculation of the order $\alpha - s^2$ correction to the Drell-Yan K factor*, *Nucl.Phys.* **B359** (1991) 343–405.

[165] C. Anastasiou, L. J. Dixon, K. Melnikov and F. Petriello, *Dilepton rapidity distribution in the Drell-Yan process at NNLO in QCD*, *Phys.Rev.Lett.* **91** (2003) 182002 [hep-ph/0306192].

[166] M. Huber, *Radiative corrections to the neutral-current Drell-Yan process*. PhD thesis, Albert-Ludwigs-Universität Freiburg im Breisgau, 2010.

[167] M. Bonvini, S. Forte and G. Ridolfi, *Soft gluon resummation of Drell-Yan rapidity distributions: Theory and phenomenology*, *Nucl.Phys.* **B847** (2011) 93–159 [1009.5691].

[168] G. Bozzi, S. Catani, G. Ferrera, D. de Florian and M. Grazzini, *Production of drell-yan lepton pairs in hadron collisions: Transverse-momentum resummation at next-to-next-to-leading logarithmic accuracy*, *Physics Letters B* **696** (2011), no. 3 207 – 213.

[169] S. Marzani and R. D. Ball, *High Energy Resummation of Drell-Yan Processes*, *Nucl.Phys.* **B814** (2009) 246–264 [0812.3602].

[170] R. Gavin, Y. Li, F. Petriello and S. Quackenbush, *FEWZ 2.0: A code for hadronic Z production at next-to-next-to-leading order*, *Comput.Phys.Commun.* **182** (2011) 2388–2403 [1011.3540].

[171] S. Catani, L. Cieri, G. Ferrera, D. de Florian and M. Grazzini, *Vector boson production at hadron colliders: A Fully exclusive QCD calculation at NNLO*, *Phys.Rev.Lett.* **103** (2009) 082001 [0903.2120].

[172] C. Balazs and C. Yuan, *Soft gluon effects on lepton pairs at hadron colliders*, *Phys.Rev.* **D56** (1997) 5558–5583 [hep-ph/9704258].

[173] B. Potter, *Calculational Techniques in Perturbative QCD: The Drell-Yan Process*, .

[174] Yuan, C.-P., *A NLO Calculation of pQCD: Total Cross Section of $PP \to W^+ + X$*, 2002.

[175] S. Willenbrock, *QCD CORRECTIONS TO p anti-p to $W^+ + X$: A CASE STUDY*, .

[176] R. Field, *Applications of Perturbative QCD*, *Front.Phys.* **77** (1989) 1–366.

[177] S. Becker, C. Reuschle and S. Weinzierl, *Numerical NLO QCD calculations*, *JHEP* **1012** (2010) 013 [1010.4187].

[178] O. Yudilevich, *Calculating One-Loop Massive Amplitudes in QCD)*, Master's thesis, Institute of Theoretical Physics, Utrecht University, Theory Group, Nikhef, 2009.

[179] S. Weinzierl, *Introduction to Feynman Integrals*, 1005.1855.

[180] F. Bloch and A. Nordsieck, *Note on the Radiation Field of the electron*, *Phys.Rev.* **52** (1937) 54–59.

[181] T. Kinoshita, *Mass singularities of Feynman amplitudes*, *J.Math.Phys.* **3** (1962) 650–677.

[182] T. Lee and M. Nauenberg, *Degenerate Systems and Mass Singularities*, *Phys.Rev.* **133** (1964) B1549–B1562.

[183] S. Catani and M. Seymour, *A General algorithm for calculating jet cross-sections in NLO QCD*, *Nucl.Phys.* **B485** (1997) 291–419 [hep-ph/9605323].

[184] T. Gleisberg and F. Krauss, *Automating dipole subtraction for QCD NLO calculations*, *Eur.Phys.J.* **C53** (2008) 501–523 [0709.2881].

[185] S. Frixione, Z. Kunszt and A. Signer, *Three jet cross-sections to next-to-leading order*, *Nucl.Phys.* **B467** (1996) 399–442 [hep-ph/9512328].

[186] S. Frixione, *A General approach to jet cross-sections in QCD*, *Nucl.Phys.* **B507** (1997) 295–314 [hep-ph/9706545].

[187] S. Alioli, *Matching Next-to-Leading-Order QCD Calculations with Shower Monte Carlo Simulations: Single Vector Boson and Higgs Boson Productions in POWHEG*. PhD thesis, Universita degli Studi di Milano-Bicocca, 2009.

[188] S. Frixione, P. Nason and C. Oleari, *Matching NLO QCD computations with Parton Shower simulations: the POWHEG method*, *JHEP* **0711** (2007) 070 [0709.2092].

[189] T. Plehn, *Lectures on LHC Physics*, *Lect.Notes Phys.* **844** (2012) 1–193 [0910.4182].

[190] S. Catani, "Introduction to QCD." http://cds.cern.ch/record/377090?ln=en, 1998. CERN, Geneva, 23 - 27 Nov 1998.

[191] **CMS Collaboration** Collaboration, S. Chatrchyan *et. al.*, *Probing color coherence effects in pp collisions at $\sqrt{s} = 7$ TeV*, 1311.5815.

[192] F. Ambroglini, R. Armillis, P. Azzi, G. Bagliesi, A. Ballestrero *et. al.*, *Proceedings of the Workshop on Monte Carlo's, Physics and Simulations at the LHC. Part I*, 0902.0293.

[193] R. Bonciani, S. Catani, M. L. Mangano and P. Nason, *Sudakov resummation of multiparton QCD cross-sections*, *Phys.Lett.* **B575** (2003) 268–278 [hep-ph/0307035].

[194] C. Balazs, J.-w. Qiu and C. Yuan, *Effects of QCD resummation on distributions of leptons from the decay of electroweak vector bosons*, *Phys.Lett.* **B355** (1995) 548–554 [hep-ph/9505203].

[195] C. Balazs, J. Huston and I. Puljak, *Higgs production: A Comparison of parton showers and resummation*, *Phys.Rev.* **D63** (2001) 014021 [hep-ph/0002032].

[196] L. G. Almeida, S. D. Ellis, C. Lee, G. Sterman, I. Sung *et. al.*, *Comparing and Counting Logs in Direct and Effective Methods of Resummation*, 1401.4460.

[197] Y. L. Dokshitzer, D. Diakonov and S. Troian, *Hard Processes in Quantum Chromodynamics*, *Phys.Rept.* **58** (1980) 269–395.

[198] G. Parisi and R. Petronzio, *Small Transverse Momentum Distributions in Hard Processes*, *Nucl.Phys.* **B154** (1979) 427.

[199] J. C. Collins, D. E. Soper and G. F. Sterman, *Transverse Momentum Distribution in Drell-Yan Pair and W and Z Boson Production*, *Nucl.Phys.* **B250** (1985) 199.

[200] S. Catani and L. Trentadue, *Resummation of the QCD Perturbative Series for Hard Processes*, *Nucl.Phys.* **B327** (1989) 323.

[201] S. Catani, L. Trentadue, G. Turnock and B. Webber, *Resummation of large logarithms in e+ e- event shape distributions*, *Nucl.Phys.* **B407** (1993) 3–42.

[202] M. H. Seymour, *Matrix element corrections to parton shower algorithms*, *Comput.Phys.Commun.* **90** (1995) 95–101 [hep-ph/9410414].

[203] S. Gieseke, P. Stephens and B. Webber, *New formalism for QCD parton showers*, *JHEP* **0312** (2003) 045 [hep-ph/0310083].

[204] J. Tully, *Monte Carlo simulations of hard QCD radiation*. PhD thesis, Durham University, 2009.

[205] S. Frixione and B. R. Webber, *Matching NLO QCD computations and parton shower simulations*, *JHEP* **0206** (2002) 029 [hep-ph/0204244].

[206] P. Nason, *A New method for combining NLO QCD with shower Monte Carlo algorithms*, *JHEP* **0411** (2004) 040 [hep-ph/0409146].

[207] S. Alioli, P. Nason, C. Oleari and E. Re, *A general framework for implementing NLO calculations in shower Monte Carlo programs: the POWHEG BOX*, *JHEP* **1006** (2010) 043 [1002.2581].

[208] B. Fuks, *Precision predictions for Z-prime production at the LHC*, 0805.2004.

[209] K. Hamilton, P. Richardson and J. Tully, *A Positive-Weight Next-to-Leading Order Monte Carlo Simulation of Drell-Yan Vector Boson Production*, *JHEP* **0810** (2008) 015 [0806.0290].

[210] W. Beenakker, M. Klasen, M. Kramer, T. Plehn, M. Spira *et. al.*, *The Production of charginos / neutralinos and sleptons at hadron colliders*, *Phys.Rev.Lett.* **83** (1999) 3780–3783 [hep-ph/9906298].

[211] D. Choudhury, A. Datta, K. Huitu, P. Konar, S. Moretti *et. al.*, *Slepton production from gauge boson fusion*, *Phys.Rev.* **D68** (2003) 075007 [hep-ph/0304192].

[212] A. Arhrib, R. Benbrik, M. Chabab and C.-H. Chen, *Pair production of neutralinos and charginos at the LHC: the role of Higgs bosons exchange*, *Phys.Rev.* **D84** (2011) 115012 [1109.0518].

[213] Y. Kurihara, D. Perret-Gallix and Y. Shimizu, $e^+e^- \to e^-\bar{\nu}_e u\bar{d}$ *from LEP to linear collider energies*, *Phys.Lett.* **B349** (1995) 367–374 [hep-ph/9412215].

[214] A. Aeppli, F. Cuypers and G. J. van Oldenborgh, *O(Gamma) corrections to W pair production in e+ e- and gamma gamma collisions*, *Phys.Lett.* **B314** (1993) 413–420 [hep-ph/9303236].

[215] A. Denner, S. Dittmaier, M. Roth and D. Wackeroth, *Electroweak radiative corrections to* $e^+e^- \to WW \to 4$ *fermions in double pole approximation: The RACOONWW approach*, *Nucl.Phys.* **B587** (2000) 67–117 [hep-ph/0006307].

[216] S. Gieseke, T. Kasprzik and J. H. Khn, *Vector-boson pair production and electroweak corrections in HERWIG++*, 1401.3964.

[217] T. M. Tait, *The* tW^- *mode of single top production*, *Phys.Rev.* **D61** (2000) 034001 [hep-ph/9909352].

[218] S. Frixione, E. Laenen, P. Motylinski, B. R. Webber and C. D. White, *Single-top hadroproduction in association with a W boson*, *JHEP* **0807** (2008) 029 [0805.3067].

[219] C. D. White, S. Frixione, E. Laenen and F. Maltoni, *Isolating Wt production at the LHC*, *JHEP* **0911** (2009) 074 [0908.0631].

[220] E. Re, *Single-top Wt-channel production matched with parton showers using the POWHEG method*, *Eur.Phys.J.* **C71** (2011) 1547 [1009.2450].

[221] S. Moretti, K. Odagiri, P. Richardson, M. H. Seymour and B. R. Webber, *Implementation of supersymmetric processes in the HERWIG event generator*, *JHEP* **0204** (2002) 028 [hep-ph/0204123].

[222] A. Barr, *Measuring slepton spin at the LHC*, *JHEP* **0602** (2006) 042 [hep-ph/0511115].

[223] C. Anastasiou, L. J. Dixon, K. Melnikov and F. Petriello, *High precision QCD at hadron colliders: Electroweak gauge boson rapidity distributions at NNLO*, *Phys.Rev.* **D69** (2004) 094008 [hep-ph/0312266].

[224] B. Fuks, M. Klasen, F. Ledroit, Q. Li and J. Morel, *Precision predictions for Z' - production at the CERN LHC: QCD matrix elements, parton showers, and joint resummation*, *Nucl.Phys.* **B797** (2008) 322–339 [0711.0749].

[225] V. Barger, D. Marfatia and A. Peterson, *LHC and Dark Matter Signals of Z' Bosons*, *Phys.Rev.* **D87** (2013) 015026 [1206.6649].

[226] F. Petriello and S. Quackenbush, *Measuring Z' couplings at the CERN LHC*, *Phys.Rev.* **D77** (2008) 115004 [0801.4389].

[227] I. Fridman-Rojas and P. Richardson, *Next-to-Leading Order Simulation of Slepton Pair Production*, 1208.0279.

[228] S. Hoeche, F. Krauss, M. Schonherr and F. Siegert, *A critical appraisal of NLO+PS matching methods*, *JHEP* **1209** (2012) 049 [1111.1220].

[229] G. Bozzi, B. Fuks and M. Klasen, *Transverse-momentum resummation for slepton-pair production at the CERN LHC*, *Phys.Rev.* **D74** (2006) 015001 [hep-ph/0603074].

[230] A. Broggio, M. Neubert and L. Vernazza, *Soft-gluon resummation for slepton-pair production at hadron colliders*, *JHEP* **1205** (2012) 151 [1111.6624].

[231] S. Platzer, *ExSample: A Library for Sampling Sudakov-Type Distributions*, *Eur.Phys.J.* **C72** (2012) 1929 [1108.6182].

[232] S. J. Brodsky and R. W. Brown, *Zeros in Amplitudes: Gauge Theory and Radiation Interference*, *Phys.Rev.Lett.* **49** (1982) 966.

[233] R. W. Brown, K. Kowalski and S. J. Brodsky, *Classical Radiation Zeros in Gauge Theory Amplitudes*, *Phys.Rev.* **D28** (1983) 624.

[234] **D0 Collaboration** Collaboration, V. Abazov *et. al.*, *First study of the radiation-amplitude zero in $W\gamma$ production and limits on anomalous $WW\gamma$ couplings at $\sqrt{s} = 1.96$- TeV*, *Phys.Rev.Lett.* **100** (2008) 241805 [0803.0030].

[235] **CMS Collaboration** Collaboration, S. Chatrchyan *et. al.*, *Measurement of $W\gamma$ and $Z\gamma$ production in pp collisions at $\sqrt{s} = 7$ TeV*, *Phys.Lett.* **B701** (2011) 535–555 [1105.2758].

[236] N. Deshpande, X.-G. He and S. Oh, *Amplitude zeros in radiative decays of scalar particles*, *Phys.Rev.* **D51** (1995) 2295–2301 [hep-ph/9410373].

[237] J. L. Hewett, A. Ismail and T. G. Rizzo, *Zeroing in on Supersymmetric Radiation Amplitude Zeros*, *Phys.Rev.* **D84** (2011) 115015 [1110.4144].

[238] S. Alioli, P. Nason, C. Oleari and E. Re, *NLO vector-boson production matched with shower in POWHEG*, *JHEP* **0807** (2008) 060 [0805.4802].

[239] B. Fuks, M. Klasen, D. R. Lamprea and M. Rothering, *Gaugino production in proton-proton collisions at a center-of-mass energy of 8 TeV*, *JHEP* **1210** (2012) 081 [1207.2159].

[240] B. Fuks, M. Klasen, D. R. Lamprea and M. Rothering, *Precision predictions for electroweak superpartner production at hadron colliders with Resummino*, *Eur.Phys.J.* **C73** (2013) 2480 [1304.0790].

[241] G. Cullen, N. Greiner and G. Heinrich, *Susy-QCD corrections to neutralino pair production in association with a jet*, *Eur.Phys.J.* **C73** (2013) 2388 [1212.5154].

[242] D. Goncalves-Netto, D. Lopez-Val, K. Mawatari, T. Plehn and I. Wigmore, *Sgluon Pair Production to Next-to-Leading Order*, *Phys.Rev.* **D85** (2012) 114024 [1203.6358].

[243] S. Weinzierl, *Introduction to Monte Carlo methods*, hep-ph/0006269.

[244] M. H. Seymour, *Predictions for Higgs and Electroweak Boson Production*. PhD thesis, University of Cambridge, 1992.

[245] C. Uhlemann and N. Kauer, *Narrow-width approximation accuracy*, *Nucl.Phys.* **B814** (2009) 195–211 [0807.4112].

[246] T. Sjostrand, S. Mrenna and P. Z. Skands, *PYTHIA 6.4 Physics and Manual*, *JHEP* **0605** (2006) 026 [hep-ph/0603175].

[247] M. C. Smith and S. S. Willenbrock, *Top quark pole mass*, *Phys.Rev.Lett.* **79** (1997) 3825–3828 [hep-ph/9612329].

[248] F. Jegerlehner, M. Y. Kalmykov and B. A. Kniehl, *On the difference between the pole and the MSbar masses of the top quark at the electroweak scale*, *Phys.Lett.* **B722** (2013) 123–129 [1212.4319].

[249] A. Denner, S. Dittmaier, M. Roth and D. Wackeroth, *Predictions for all processes $e^+e^- \to 4\,\mathrm{fermions} + \gamma$*, *Nucl.Phys.* **B560** (1999) 33–65 [hep-ph/9904472].

[250] B. A. Kniehl, C. P. Palisoc and A. Sirlin, *Higgs boson production and decay close to thresholds*, *Nucl.Phys.* **B591** (2000) 296–310 [hep-ph/0007002].

[251] A. Sirlin, *Theoretical considerations concerning the Z0 mass*, *Phys.Rev.Lett.* **67** (1991) 2127–2130.

[252] A. H. Hoang, A. Jain, I. Scimemi and I. W. Stewart, *Infrared Renormalization Group Flow for Heavy Quark Masses*, *Phys.Rev.Lett.* **101** (2008) 151602 [0803.4214].

[253] G. Degrassi, *The role of the top quark in the stability of the SM Higgs potential*, 1405.6852.

[254] W. Hollik, J. M. Lindert and D. Pagani, *NLO corrections to squark-squark production and decay at the LHC*, *JHEP* **1303** (2013) 139 [1207.1071].

[255] W. Beenakker, R. Hopker and P. Zerwas, *SUSY QCD decays of squarks and gluinos*, *Phys.Lett.* **B378** (1996) 159–166 [hep-ph/9602378].

[256] S. P. Martin, *Two-loop scalar self-energies and pole masses in a general renormalizable theory with massless gauge bosons*, *Phys.Rev.* **D71** (2005) 116004 [hep-ph/0502168].

[257] H. G. Veltman, *Mass and width of unstable gauge bosons*, *Z.Phys.* **C62** (1994) 35–52.

[258] R. G. Stuart, *Gauge invariance, analyticity and physical observables at the Z0 resonance*, *Phys.Lett.* **B262** (1991) 113–119.

[259] A. Aeppli, G. J. van Oldenborgh and D. Wyler, *Unstable particles in one loop calculations*, *Nucl.Phys.* **B428** (1994) 126–146 [hep-ph/9312212].

[260] C. Schwinn, *Gauge checks, consistency of approximation schemes and numerical evaluation of realistic scattering amplitudes*, hep-ph/0307057.

[261] P. Pascual and R. Tarrach, *QCD: RENORMALIZATION FOR THE PRACTITIONER*, *Lect.Notes Phys.* **194** (1984) 1–277.

[262] W. Siegel, *Supersymmetric Dimensional Regularization via Dimensional Reduction*, *Phys.Lett.* **B84** (1979) 193.

[263] D. Stockinger, *Regularization by dimensional reduction: consistency, quantum action principle, and supersymmetry*, *JHEP* **0503** (2005) 076 [hep-ph/0503129].

[264] A. Signer and D. Stockinger, *Using Dimensional Reduction for Hadronic Collisions*, *Nucl.Phys.* **B808** (2009) 88–120 [0807.4424].

[265] L. Edelhaeuser, *Mass Factorization of SUSY QCD Processes in Dimensional Reduction*. PhD thesis, Würzburg University, 2007.

[266] S. P. Martin and M. T. Vaughn, *Regularization dependence of running couplings in softly broken supersymmetry*, *Phys.Lett.* **B318** (1993) 331–337 [hep-ph/9308222].